Spin-wave calculations for Heisenberg magnets with reduced symmetry

Dissertation
zur Erlangung des Doktorgrades
der Naturwissenschaften

vorgelegt beim Fachbereich Physik der
Johann Wolfgang Goethe-Universität
in Frankfurt am Main

von
Andreas Kreisel
aus
Hanau

Frankfurt (2011)
(D30)

vom Fachbereich Physik der

Johann Wolfgang Goethe - Universität

als Dissertation angenommen.

Dekan: Prof. Dr. Michael Huth

Gutachter: Prof. Dr. Peter Kopietz
Prof. Dr. Sebastian Eggert

Datum der Disputation: 14.07.2011

Contents

Abstract of the thesis

The phenomenon of magnetism is a pure quantum effect and has been studied since the beginning of civilization. The practical use of magnetic materials for technical purposes was well established in the 19th century; still nowadays there is no lack of new high-tech applications based on magnetism for example in information technology to store and process data.

This thesis does not focus on the development of new applications of magnetism in technology, nor enhancement of known fields of application. Instead, the intention is to use a quantum theory of magnetism for obtaining new insights on physical effects that accompany the phenomenon of magnetism. Therefore three different model systems, each of which are believed to describe a class of real compounds, are considered. Starting from the idea that magnetism can be understood by use of the so-called Heisenberg model that microscopically characterizes the interaction between localized magnetic moments, we restrict ourselves to the case where a long-range magnetic order is present. In order to deduce consequences resulting from this microscopic picture we use the spin-wave theory that is introduced in the first chapter. Central objects of this theory are the magnons which are elementary quantum excitations in ordered magnets.

An application of these mathematical techniques to a model that describes an antiferromagnet in an external magnetic field is presented in the second chapter. Quantities like the spin-wave velocity and the damping of magnons are calculated using a Hermitian operator approach in the framework of spin-wave theory. A strong renormalization of the magnetic excitations arises because the symmetry of the system is reduced due to the external magnetic field.

In the second model system, that describes thin films of a ferromagnet, concepts of classical physics meet quantum physics: The magnetic dipole-dipole interaction that is also known in everyday life from the magnetic forces between magnets and was initially formulated in the theory of electromagnetism, is included in the microscopic model. Having a special compound in mind where the magnetic excitations are directly accessible in experiments, the energy dispersions of magnon modes in thin-film ferromagnets are deduced. Our approach is essentially a basis for further investigations beyond this thesis to describe strong correlations and condensation of magnons. A recent

realization of data processing devices with spin waves puts the understanding of physical processes in these ferromagnetic films in the focus of upcoming research.

The third model system brings in the so-called frustration where the interactions between the spins are such that the total energy cannot be minimized by an appropriate alignment of the magnetic moments in the classical picture. In the simplest case this appears because the antiferromagnetically coupled spins are located on a triangular lattice. This situation will lead to strong quantum fluctuations which make this model system interesting. Finally the overall symmetry is reduced by inclusion of spin anisotropies and an external magnetic field. Instead of focusing on the properties of the magnetic excitations, the effect of the magnetic field on the properties of the lattice vibrations is subject to the investigation. This is interesting because the characteristics of lattice vibrations can be measured experimentally using the supersonic technique.

Inhaltsangabe

Magnetismus ist ein Naturphänomen, das schon vor Jahrtausenden beschrieben und diskutiert wurde. Eine physikalische Erklärung ist jedoch erst auf der Basis der Anfang des 20. Jahrhunderts entwickelten Quantentheorie möglich. Schon vorher spielten magnetische Werkstoffe in technischen Anwendungen eine wichtige Rolle. Auch in jüngster Zeit finden sich immer neue Anwendungsmöglichkeiten für magnetische Materialien, zum Beispiel in der Informationstechnologie.

Die vorliegende Arbeit beschäftigt sich weder mit neuen Anwendungsgebieten von magnetischen Effekten, noch mit der gezielten Optimierung bekannter Einsatzgebiete. Vielmehr wollen wir mit Hilfe der Quantentheorie neue Erkenntnisse über physikalische Effekte gewinnen, die mit dem Phänomen des Magnetismus zusammenhängen. Dazu starten wir nacheinander mit drei verschiedenen mikroskopischen Modellen, die jeweils eine Klasse magnetischer Materialien beschreiben. Das sogenannte Heisenberg-Modell, das die Wechselwirkungen zwischen lokalisierten Spins beschreibt, ist der Ausgangspunkt für die drei Untersuchungen. Wir beschränken uns weiterhin auf geordnete Magnete, in denen eine langreichweitige magnetische Ordnung vorliegt, um die Methode der Spinwellentheorie anzuwenden. Im ersten Kapitel werden die Grundzüge der Spinwellentheorie sowie einige für die späteren Ausführungen wichtige Besonderheiten beschrieben. Die sogenannten Magnonen oder Spinwellen stellen in dieser Herangehensweise die elementaren Anregungen in geordneten Magneten dar.

Im zweiten Kapitel wenden wir die Spinwellentheorie auf ein Modellsystem an, das einen Antiferromagneten in einem externen Magnetfeld beschreibt. Unter Verwendung einer sogenannten hermiteschen Parametrisierung werden physikalische Größen wie die Spinwellengeschwindigkeit sowie die Dämpfung der Spinwellen berechnet. Wir sind dabei insbesondere am Einfluss des Magnetfeldes interessiert, welches die Symmetrie des Systems reduziert und die magnetischen Anregungen wesentlich renormiert.

Im zweiten Modellsystem, welches zur Beschreibung dünner Filme von Ferromagneten geeignet ist, werden Konzepte der klassischen Magnetostatik mit denen der Quantenphysik vereinigt: Wir betrachten zusätzlich die Dipol-Dipol

Wechselwirkungen zwischen den mikroskopischen magnetischen Momenten. Diese Wechselwirkung ist als magnetische Kraft zwischen zwei Magneten auch aus unserem Alltag bekannt. Unter Verwendung der Spinwellentheorie berechnen wir die Energie-Impuls-Beziehung, die sogenannte Dispersion, der magnetischen Anregungen in dünnen Filmen eines experimentell untersuchten Ferromagneten. Dieser theoretische Ansatz ist schließlich der Ausgangspunkt für weitere Untersuchungen im Hinblick auf starke Korrelationen und Kondensationsphänomene von Magnonen. Das physikalische Verständnis der Vorgänge in dünnen ferromagnetischen Filmen ist auch von technologischem Interesse, da kürzlich Bauteile zur Datenverarbeitung auf der Basis von Spinwellen realisiert wurden.

Das dritte Modellsystem enthält schließlich zusätzlich die sogenannte magnetische Frustration. In diesem Fall sind die Wechselwirkungen zwischen benachbarten Spins derart, dass nicht alle Wechselwirkungsenergien gleichzeitig durch Ausrichtung der Spins minimiert werden können und starke Quantenfluktuationen auftreten. Ein Beispiel dafür ist der Antiferromagnet auf dem Dreiecksgitter, den wir in der vorliegenden Arbeit behandeln. Wir reduzieren die Symmetrie weiter durch Hinzunahme von Anisotropien, um mit unseren Ergebnissen auch an experimentelle Untersuchungen anknüpfen zu können. Der Schwerpunkt liegt jedoch nicht auf Einsichten in die magnetischen Anregungen, sondern auf dem Verständnis der Änderung der Gitterschwingungen in Anwesenheit der magnetischen Wechselwirkungen. Wir berechnen schließlich die Verschiebung der Schallgeschwindigkeit und die Dämpfung des Schalls als Funktion des angelegten Magnetfeldes und vergleichen die Ergebnisse mit experimentellen Daten aus Ultraschallmessungen.

Chapter 1

Introduction

1.1 Basic models

1.1.1 Exchange interaction and Heisenberg model

Most of the collective magnetic phenomena are not due to classical dipole-dipole interactions between magnetic moments present in a material, since the relevant energy scales for these interactions are far too small to cause for example magnetic ordering at room temperature. Instead, magnetism is a result of the interplay between the Coulomb interactions of electrons and the Pauli principle.

In a simplified model consisting of two electrons located at different, neighboring atoms, one can use the antisymmetry of the total multi-particle state with respect to permutation of the electrons to build up a Hamiltonian on a four-dimensional Hilbert space. The spectrum of this Hamiltonian is, apart from a constant, identical to the spectrum of the Heisenberg Hamiltonian,

$$\hat{H} = J\boldsymbol{S}_1 \cdot \boldsymbol{S}_2 \ , \tag{1.1}$$

where J is the exchange constant and $\boldsymbol{S}_1$, $\boldsymbol{S}_2$ are spin operators with total spin $S = \frac{1}{2}$. The Hamiltonian Eq. (1.1) was first derived by Heisenberg [93] more than 80 years ago, and has later been generalized to the model

$$\hat{H} = \frac{1}{2}\sum_{ij} J_{ij}\boldsymbol{S}_i \cdot \boldsymbol{S}_j \ , \tag{1.2}$$

where J_{ij} are the exchange energies that mediate the interaction between the spin $\boldsymbol{S}_i$ at the position i and that at the position j. The sum in Eq. (1.2) over the indices i and j runs over all N sites of the lattice. In general, the sign of the exchange couplings J_{ij} can be positive (antiferromagnetic coupling) or negative (ferromagnetic coupling). Although the physical principles that lead to this effective model, antisymmetry of multi-particle state and Coulomb interactions, are always the same, the order of magnitude of the exchange couplings spans

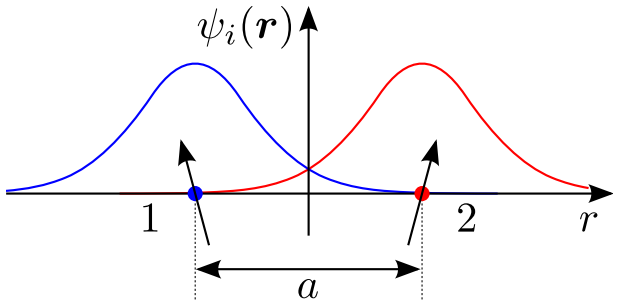

Figure 1.1: *In the easiest picture the exchange interactions between the spins at the lattice points 1 and 2 arise from the interplay of the Coulomb interaction between two electrons and the Pauli principle. The value of the exchange constant in Eq. (1.1) is then given as an integral over the product of the two wave functions and the Coulomb interaction. The wave functions $\psi_i(\boldsymbol{r})$ of the electrons usually drop exponentially for large distances, which leads to the exponential behavior given in Eq. (1.3).*

quite a wide range, because the details of how the effective model comes about can be quite different. One should mention that the exchange constants between spins located close to each other are in most cases the largest, and therefore the majority of theoretical investigations, including this work, only consider interactions between nearest neighbors. Models on different lattice types can be mapped into each other by a proper choice of nearest-neighbor and next nearest-neighbor interactions.

Up to now, the Heisenberg model had great success in explaining magnetic phenomena and related physical observables. It has even been applied to model systems where itinerant magnetism is dominant [B21]. But its central application is to describe magnetic insulators.

The mechanism how the effective exchange interaction between the spins is generated can differ a lot depending on the structure of the material considered. Instead of a direct exchange interaction due to two involved electrons (see Fig. 1.1), in insulating compounds one usually deals with super-exchange interactions [2]. Nonmagnetic anions between the cations allow a virtual exchange of electrons and therefore lead to a splitting of the energies of different multiplets which is again the equivalent of the Heisenberg model. A qualitative description of the mechanism then includes processes where a total of four electron hoppings to neighboring orbitals take place. A more detailed calculation shows that two processes are involved [173]: In the antiparallel spin configuration both electrons of the anion in between the localized spins can hop to the outer positions which will lower the energy and lead to an effective antiferromagnetic superexchange contribution. In the second process an electron in a localized state hops through the anion to the orbital where

the neighbored localized electron is sitting, and then back to the original state. Depending on the effective on-site repulsion energy of the electrons occupying states on the same cation, this mechanism can create an effective ferromagnetic or antiferromagnetic exchange interaction. The sum of both contributions is then the total superexchange coupling used as parameter in the following chapters [B5]. In practice, this simple picture of one anion whose electrons mediate the exchange interaction is not sufficient to describe quantitatively the exchange couplings in real compounds because essentially all electrons of the atoms in the elementary cell contribute to the effective exchange interaction. Moreover one has to consider so-called exchange paths consisting of a set of non-magnetic atoms to explain exchange effects. This is for example the case in the more complicated structures of the compound Cs_2CuCl_4 which is also considered in this work [68, 69]. In general, the exchange constants decrease with the length of the exchange path. The exchange interaction strength $J(x)$ from Eq. (1.1), being a pure quantum mechanical effect, usually obeys the law[1]

$$J(x) = J(x_0)e^{-\kappa(x-x_0)/x_0} \,, \tag{1.3}$$

where $J(x_0)$ is the exchange coupling at the equilibrium bond length x_0 and x is the actual bond length [13]. The dimensionless constant κ is usually of the order of 10. In a simplified picture this law can be justified by the fact that the exchange coupling is basically given by the value of overlap integrals between electron states, and that the corresponding wave functions decay exponentially in the contributing intervals in real space, see Fig. 1.1. An extended description also includes bond angles to estimate the order of magnitude of the exchange interactions [B9, B39]. Nowadays it is also possible to extract the exchange couplings from *ab initio* calculations by fitting the electronic band structure to a Hubbard model

$$\hat{H} = \sum_{ij\,\sigma} t_{ij} c^\dagger_{i\sigma} c_{j\sigma} + U \sum_i c^\dagger_{i,\uparrow} c_{i\uparrow} c^\dagger_{i,\downarrow} c_{i\downarrow} \,, \tag{1.4}$$

where $c^\dagger_{i\sigma}$ and $c_{i\sigma}$ are creation and annihilation operators at the position i of fermions with the spin σ. The Hubbard model at half filling and small hopping $t_{ij} \ll U$ corresponds to a Heisenberg model of Eq. (1.1) with the exchange couplings $J_{ij} = 4|t_{ij}|^2/U$. This procedure will not be elucidated in more detail, as it is not used in this work, but one should mention that it is subject to a large number of studies that fill the gap between the exploration of model systems as the Heisenberg model and the application of the results to explain experiments on real materials [123].

1.1.2 Anisotropies

In real compounds the isotropic Heisenberg model is only realized approximately. The original Heisenberg model Eq. (1.2) has a full $SU(2)$ spin rotation symmetry

[1] M. Kulic, private communication.

that can be broken for example by anisotropies. Due to the fact that the elementary cell, and also the environment of the magnetic ions has no rotational symmetry, the Heisenberg model has to be generalized to

$$\hat{H} = \sum_{\alpha,\beta=1}^{3} \sum_{ij} J_{ij}^{\alpha\beta} S_i^{\alpha} S_j^{\beta} \ , \tag{1.5}$$

where S_i^{α} is the α-component of the spin operator on the site i and $J_{ij}^{\alpha\beta}$ is a tensor. Luckily, the crystal symmetry reduces the number of nonzero elements of $J_{ij}^{\alpha\beta}$. Therefore in many cases the number of relevant parameters is small. For example, if one direction is favored or disfavored the model modifies to

$$\hat{H} = \sum_{ij} J_{ij} \left[S_i^x S_j^x + S_i^y S_j^y + (1+\lambda) S_i^z S_j^z \right] \ , \tag{1.6}$$

where λ is an additional parameter describing this anisotropy in one axis. A special anisotropy, which emerges only in materials where no inversion symmetry is present, is the Dzyaloshinsky-Moriya (DM) anisotropy. It leads to the following additional term in the Hamiltonian [56, 144, 145],

$$\hat{H}_{\mathrm{DM}} = \sum_{ij} \boldsymbol{D}_{ij} \cdot (\boldsymbol{S}_i \times \boldsymbol{S}_j) \ . \tag{1.7}$$

Since the components of the anisotropy vector $\boldsymbol{D}_{ij}$ are related to the value of the corresponding exchange couplings, one usually considers the anisotropy along the bonds with the largest exchange coupling [193].

1.1.3 Dipole-dipole interactions

As mentioned above, the dipole-dipole interactions are rather weak and typically do not dominate the behavior of magnetic ordering and related physical observables [B21]. Deduced from the classical energy between magnetic moments, known from electrodynamics, the dipole-dipole interaction can be written as

$$\hat{H}_{\mathrm{dd}} = -\frac{1}{2} \sum_{ij, i\neq j} \frac{\mu^2}{|\boldsymbol{R}_{ij}|^3} \left[3(\boldsymbol{S}_i \cdot \hat{\boldsymbol{R}}_{ij})(\boldsymbol{S}_j \cdot \hat{\boldsymbol{R}}_{ij}) - \boldsymbol{S}_i \cdot \boldsymbol{S}_j \right] \ , \tag{1.8}$$

where the sums are over the sites $\boldsymbol{R}_i$ of the lattice and $\hat{\boldsymbol{R}}_{ij} = \boldsymbol{R}_{ij}/|\boldsymbol{R}_{ij}|$ are unit vectors in the direction of $\boldsymbol{R}_{ij} = \boldsymbol{R}_i - \boldsymbol{R}_j$. Here, $\mu = g\mu_B$ is the magnetic moment associated with the spins, where g is the effective g-factor and $\mu_B = e\hbar/(2mc)$ is the Bohr magneton.

However, this contribution to the energy will matter if the isotropic exchange Hamiltonian does not allow ordering at finite temperature. For example in two-dimensional Heisenberg magnets the Mermin-Wagner theorem guarantees that in the presence of $SU(2)$ symmetry there is no magnetic long-range order

at any finite temperature [95, 141]. In addition the dipole-dipole interaction term has a lower symmetry and therefore opens the possibility of a nonzero gap in the excitation spectrum, because in that case the Goldstone theorem [76, 77] does not apply. But the term Eq. (1.8) includes interactions between spins at long distances, so-called long-range interactions and is quite challenging to deal with [194–197].

1.2 Techniques

Below, the main techniques used in this work are introduced whereas particularities in the application of them will be discussed later in the chapters 2–4. We will restrict ourselves to a brief introduction as most of the content presented below can be found in common textbooks [B19, B21].

1.2.1 Mapping to bosonic degrees of freedom

A model Hamiltonian like the Heisenberg model containing spin operators is quite challenging to deal with. Without mapping to other degrees of freedom the Heisenberg equations of motion and spin correlators (Green functions) are used in the literature [B24]. Another ansatz is the mapping to fermionic degrees of freedom for the special case of the total spin $S = \frac{1}{2}$ [B21]. Instead of calculating physical observables or studying properties of the Heisenberg model and its extension directly in terms of the spin operators, we concentrate on the mapping to bosonic degrees of freedom. Advantages of this approach are the well known statistics of the bosonic degrees of freedom and a more direct insight to the relevant excitations in the system. Within this work we mainly focus on the so-called spin waves which are the elementary excitations in ordered quantum magnets.

The relevant Hilbert space of the Hamiltonian, Eq. (1.2), is given by the direct product of the Hilbert spaces at all N lattice points

$$\mathcal{H}_N = \prod_{i=1}^{N} \mathcal{H}_i \ , \tag{1.9}$$

because the Heisenberg model is a sum over the spin operators. Since the Hamiltonian only contains the components of the spin operators at all lattice points which fulfill the general commutation relation

$$\left[S_i^\alpha, S_j^\beta\right] = i\epsilon_{\alpha\beta\gamma} S_i^\gamma \delta_{ij} \ , \tag{1.10}$$

we conclude that the individual Hilbert spaces can be constructed from the eigenbasis of the set

$$\left\{\boldsymbol{S}_i^2, S_i^z\right\} \tag{1.11}$$

of the operators, i.e. a basis of the Hilbert space at one lattice point is

$$\{|S, m_i\rangle\} \ . \tag{1.12}$$

Here $S = \frac{1}{2}, 1, \frac{3}{2} \ldots$ is the total spin and $m = -S, \cdots, S$ is the discrete quantum number of the operator S_i^z at the lattice point i. For completeness we also quote the eigenvalue equations

$$\boldsymbol{S}_i^2 \, |S, m_i\rangle = S(S+1) \, |S, m_i\rangle \ , \tag{1.13a}$$

$$S_i^z \, |S, m_i\rangle = m_i \, |S, m_i\rangle \ . \tag{1.13b}$$

For a fixed total spin at each site the individual Hilbert spaces have the dimension

$$\dim \mathcal{H}_i = 2S + 1 \ , \tag{1.14}$$

and the total Hilbert space is of dimension

$$\dim \mathcal{H}_N = (2S+1)^N \ , \tag{1.15}$$

which results in a hardly solvable mathematical problem for large N since the Hamiltonian is not diagonal. For small system sizes it is possible to explore symmetries of the Hamiltonian to obtain block-diagonal matrices and then directly diagonalize the Hamiltonian applying the numerical method of exact diagonalization [120, 215]. In the next step we want to map the states of the Hilbert space and the corresponding spin operators to bosonic degrees of freedom. Considering the Hilbert space for the bosonic operators $b_i^\dagger$ and b_i with the commutation relation

$$\left[b_i, b_j^\dagger\right] = \delta_{ij} \ , \tag{1.16a}$$

$$[b_i, b_j] = 0 \ , \tag{1.16b}$$

we have to restrict the Hilbert space to a space with the same dimension, namely use the basis

$$\{|n_i\rangle\}_S = \{|0_i\rangle \, , \ldots , |2S_i\rangle\} \tag{1.17}$$

with the eigenvalue equation for the number operator

$$b_i^\dagger b_i \, |n_i\rangle = n_i \, |n_i\rangle \, , \quad n_i = 0, 1, \ldots, 2S \ . \tag{1.18}$$

In principle this can be done formally by help of projection operators. In an early work Dyson has shown that the restriction $n_i \leq 2S$ leads to additional interactions, so-called kinematic interactions in the spin-wave approach. For the pure ferromagnet in three dimensions the effect of these terms can be neglected [54, 55]. Referring to other works which have studied possible projection schemes and their impact on physical observables [115] we will not further consider this problem and continue with the standard technique to build up the spin-wave theory.

1.2.2 General transformation

The spin algebra Eq. (1.10) still holds if one uses the parametrization [9]

$$S_i^z = S - n_i \ , \quad n_i = b_i^\dagger b_i \ , \tag{1.19a}$$

$$S_i^+ = \sqrt{2S}\left(1 - \frac{n_i}{2S}\right)^{\frac{1+\eta}{2}} b_i \ , \tag{1.19b}$$

$$S_i^- = \sqrt{2S} b_i^\dagger \left(1 - \frac{n_i}{2S}\right)^{\frac{1-\eta}{2}} \ , \tag{1.19c}$$

where $S_i^\pm = S_i^x \pm i S_i^y$ are the ladder operators and $\eta \in \mathbb{R}$ is an arbitrary constant. The bosonic creation and annihilation operators $b_i^\dagger$ and b_i fulfill the algebra Eqs. (1.16a) and (1.16b). This transformation will map all terms discussed in the last section (Eqs. (1.1), (1.8) and (1.5)) to terms with a definite power of bosonic operators, so that the Hamiltonian reads

$$\hat{H} = \sum_{n=0}^{\infty} \hat{H}_n \ , \tag{1.20}$$

where $\hat{H}_n$ is a term which contains n powers of the bosonic operators.

1.2.3 Holstein-Primakoff transformation

Setting $\eta = 0$ yields the well known Holstein-Primakoff (HP) transformation [96],

$$S_i^z = S - n_i \ , \quad n_i = b_i^\dagger b_i \ , \tag{1.21a}$$

$$S_i^+ = \sqrt{2S}\sqrt{1 - \frac{n_i}{2S}} b_i \ , \tag{1.21b}$$

$$S_i^- = \sqrt{2S} b_i^\dagger \sqrt{1 - \frac{n_i}{2S}} \ , \tag{1.21c}$$

which additionally to Eq. (1.10) also implements the Hermiticity condition

$$\left(S_i^+\right)^\dagger = S_i^- \ , \tag{1.22}$$

and therefore transforms a naturally Hermitian Hamiltonian to its Hermitian counterpart in the bosonic representation. Now we expand the square roots in the transformation of Eqs. (1.21b) and (1.21c) in powers of $1/S$ to obtain

$$S_i^+ = \sqrt{2S}\left(b_i - \frac{n_i b_i}{4S} + \ldots\right) , \tag{1.23a}$$

$$S_i^- = \sqrt{2S}\left(b_i^\dagger - \frac{b_i^\dagger n_i}{4S} + \ldots\right) . \tag{1.23b}$$

Since this expansion yields an infinite series, the HP transformation has the disadvantage that the expansion Eq. (1.20) is an infinite sum which must be truncated to perform any calculation.

1.2.4 Dyson-Maleyev transformation

Choosing any $\eta \neq 0$ violates the Hermiticity condition Eq. (1.22), such that the transformation results in a non Hermitian effective Boson Hamiltonian. Nevertheless, the case $\eta = 1$ is often used because it generates a simpler transformation [135, 136]

$$S_i^z = S - n_i \ , \tag{1.24a}$$

$$S_i^+ = \sqrt{2S}\left(1 - \frac{n_i}{2S}\right) b_i \ , \tag{1.24b}$$

$$S_i^- = \sqrt{2S} b_i^\dagger \ , \tag{1.24c}$$

which directly restricts the sum Eq. (1.20) to terms up to $\hat{H}_6$. For a two sublattice quantum antiferromagnet a special choice of the transformation on the sublattices can essentially lead to $\hat{H}_6 = 0$, see section 1.4.3.

Note that the disadvantages of the two suitable transformations seem to be severe: In the case of the HP transformation one should keep infinite many terms whereas in the Dyson-Maleyev approach an important and basic principle of quantum mechanics is violated. However, following the usual steps to build up the interacting spin-wave theory explained in detail in the upcoming section, the differences are marginal and the results for physical quantities do not depend on the type of transformation used. For practical applications to model systems only the HP transformation will be used within this work.

1.3 Transformations in quantum mechanics

As the concept of transformations is already introduced at the beginning of the quantum mechanics lecture for undergraduate students, the reader should be quite familiar with the basic idea of expressing the Hamiltonian in terms of different operators to facilitate calculations. However, we will quote the most important transformation schemes for later reference in this work, and briefly discuss the specialties upon application to the model systems.

1.3.1 Bogoliubov transformation

A key transformation in the theory of Bose systems is the Bogoliubov transformation [B6] which can also be used in the context of fermions with appropriate changes. This case will not be discussed here since we restrict ourselves to the mapping of the Heisenberg model to bosonic degrees of freedom. The starting point for the transformation is a general many-particle Hamiltonian whose quadratic part reads in momentum space

$$H_2 = \sum_{\boldsymbol{k}} \left[A_{\boldsymbol{k}} b_{\boldsymbol{k}}^\dagger b_{\boldsymbol{k}} + \frac{B_{\boldsymbol{k}}}{2} \left(b_{\boldsymbol{k}} b_{-\boldsymbol{k}} + b_{-\boldsymbol{k}}^\dagger b_{\boldsymbol{k}}^\dagger \right) \right] \ , \tag{1.25}$$

where the coefficient

$$A_{\boldsymbol{k}} = A^{+}_{\boldsymbol{k}} + A^{-}_{\boldsymbol{k}} \tag{1.26}$$

contains symmetric and antisymmetric terms with respect to inversion of momenta i.e.

$$A^{\pm}_{\boldsymbol{k}} = \pm A^{\pm}_{-\boldsymbol{k}} \, . \tag{1.27}$$

Without loss of generality the non-diagonal part has a symmetric coefficient,

$$B_{\boldsymbol{k}} = B_{-\boldsymbol{k}} \, . \tag{1.28}$$

The transformation

$$\begin{pmatrix} b_{\boldsymbol{k}} \\ b^{\dagger}_{-\boldsymbol{k}} \end{pmatrix} = \begin{pmatrix} u_{\boldsymbol{k}} & -v_{\boldsymbol{k}} \\ -v_{\boldsymbol{k}} & u_{\boldsymbol{k}} \end{pmatrix} \begin{pmatrix} \beta_{\boldsymbol{k}} \\ \beta^{\dagger}_{-\boldsymbol{k}} \end{pmatrix} \tag{1.29}$$

to new bosonic operators $\beta^{\dagger}_{\boldsymbol{k}}$ and $\beta_{\boldsymbol{k}}$ keeps the statistics Eqs. (1.16a) and (1.16b), i.e.

$$\left[\beta_{\boldsymbol{k}}, \beta^{\dagger}_{\boldsymbol{k}'}\right] = \delta_{\boldsymbol{k},\boldsymbol{k}'} \, , \tag{1.30a}$$

$$\left[\beta_{\boldsymbol{k}}, \beta_{\boldsymbol{k}'}\right] = 0 \, , \tag{1.30b}$$

if the coefficients fulfill

$$u^2_{\boldsymbol{k}} - v^2_{\boldsymbol{k}} = 1 \, . \tag{1.31}$$

In order to obtain a diagonal Hamiltonian in terms of the new operators we have to claim

$$u^2_{\boldsymbol{k}} + v^2_{\boldsymbol{k}} = \frac{A^{+}_{\boldsymbol{k}}}{\epsilon_{\boldsymbol{k}}} \, , \tag{1.32a}$$

$$2u_{\boldsymbol{k}} v_{\boldsymbol{k}} = \frac{B_{\boldsymbol{k}}}{\epsilon_{\boldsymbol{k}}} \, , \tag{1.32b}$$

where the energy is given by

$$\epsilon_{\boldsymbol{k}} = \sqrt{(A^{+}_{\boldsymbol{k}})^2 - B^2_{\boldsymbol{k}}} \, . \tag{1.33}$$

Choosing the coefficients as real quantities the following equations will solve Eqs. (1.32a) and (1.32b)

$$u_{\boldsymbol{k}} = \sqrt{\frac{A^{+}_{\boldsymbol{k}} + \epsilon_{\boldsymbol{k}}}{2\epsilon_{\boldsymbol{k}}}} \, , \tag{1.34a}$$

$$v_{\boldsymbol{k}} = \frac{B_{\boldsymbol{k}}}{|B_{\boldsymbol{k}}|} \sqrt{\frac{A^{+}_{\boldsymbol{k}} - \epsilon_{\boldsymbol{k}}}{2\epsilon_{\boldsymbol{k}}}} \, , \tag{1.34b}$$

and yield the Hamiltonian

$$\hat{H}_2 = \sum_{\boldsymbol{k}} \left[E_{\boldsymbol{k}} \beta^{\dagger}_{\boldsymbol{k}} \beta_{\boldsymbol{k}} + \frac{\epsilon_{\boldsymbol{k}} - A^{+}_{\boldsymbol{k}}}{2} \right] \tag{1.35}$$

with the new energy dispersion [213, B1]

$$E_{\boldsymbol{k}} = \epsilon_{\boldsymbol{k}} + A^{-}_{\boldsymbol{k}} \ , \tag{1.36}$$

and an additional shift of the ground-state energy due to the proper choice of the eigenstates. Note that the presence of a nonzero coefficient $A^{-}_{\boldsymbol{k}}$ is usually accompanied by a lack of inversion symmetry of the underlying lattice-spin model that leads to the Hamiltonian Eq. (1.25). For a complete discussion of the transformation we cite the following symmetries and properties,

$$u_{\boldsymbol{k}} = u_{-\boldsymbol{k}} \ , \tag{1.37a}$$

$$v_{\boldsymbol{k}} = v_{-\boldsymbol{k}} \ , \quad \text{sign } v_{\boldsymbol{k}} = \text{sign } B_{\boldsymbol{k}} \ , \tag{1.37b}$$

$$\epsilon_{\boldsymbol{k}} = \epsilon_{-\boldsymbol{k}} \ , \tag{1.37c}$$

which are easy to verify from the definitions above. We further mention the fact that both coefficients diverge in the limit of small momenta $\lim_{\boldsymbol{k}\to 0} u_{\boldsymbol{k}} = |\lim_{\boldsymbol{k}\to 0} v_{\boldsymbol{k}}| = \infty$ if the dispersion is gapless, $\epsilon_0 = 0$, and $A_0 = |B_0| \neq 0$. These properties make it tedious to work in the Bogoliubov basis in actual applications in the framework of spin-wave theory [86, 114, 213].

Later, we will see that general Bogoliubov transformations for quadratic Hamiltonians with $n > 1$ modes can also be useful. But the generalization of the transformation Eq. (1.29) will lead to the calculation of $n \times n$ matrix coefficients instead of the functions $u_{\boldsymbol{k}}$ and $v_{\boldsymbol{k}}$. If the mixing terms are not sufficiently easy to deal with, for example constant, or independent of the mode number, the general case is a quite difficult task [39, 40, 126, 182, B27]. Even for $n = 2$, in the absence of inversion symmetry there seems to be no direct way to analytically calculate the transformation matrices, so that we will avoid this calculation in chapter 4.

1.3.2 Hermitian operator parametrization

The basic idea to use Hermitian operators in describing a bosonic system should be quite familiar to the reader since in the discussion of the quantum harmonic oscillator a similar transformation is applied. Let us briefly recall the discussion that can be found in standard textbooks [B25]. The starting point is the Hamiltonian of the harmonic oscillator

$$\hat{H}(X, P) = \frac{\hat{P}^2}{2m} + \frac{1}{2} m\omega^2 \hat{X}^2 \ , \tag{1.38}$$

where m and ω are the mass and the oscillator frequency. The position operator $\hat{X}$ and the momentum operator $\hat{P}$ fulfill[2]

$$\left[\hat{X}, \hat{P}\right] = i \ . \tag{1.39}$$

[2]Throughout this work we use natural units, i.e. $\hbar = 1$ and $k_B = 1$, if not indicated otherwise.

To arrive at the number-operator representation of Eq. (1.38) we introduce the annihilation and creation operators,

$$a = \sqrt{\frac{m\omega}{2}}\left(\hat{X} + i\frac{\hat{P}}{m\omega}\right) , \tag{1.40a}$$

$$a^\dagger = \sqrt{\frac{m\omega}{2}}\left(\hat{X} - i\frac{\hat{P}}{m\omega}\right) , \tag{1.40b}$$

which obey the commutation relation

$$\left[a, a^\dagger\right] = 1 . \tag{1.41}$$

After substitution this yields the Hamiltonian

$$\hat{H} = \omega\Big(a^\dagger a + \frac{1}{2}\Big) , \tag{1.42}$$

whose spectrum is that of the quantum mechanical oscillator $E_n = \omega(n + \frac{1}{2})$, $n \in \mathbb{N}_0$. Any anharmonic perturbation of the potential energy will now lead to additional terms in the number representation where three or more powers of the creation operator $a^\dagger$ or the annihilation operator a are present.

Keeping in mind this idea of the transformation, we now apply it in the other direction: The starting point is the Hamiltonian introduced in Eq. (1.25) in the number representation, a generalization of Eq. (1.38) with many modes and non-diagonal terms. As discussed in the previous section, a Bogoliubov transformation removes the non-diagonal terms; here we will be more general to use the following formulas in several contexts. We introduce Hermitian field operators $\hat{\Phi}_{\boldsymbol{k}} = \hat{\Phi}^\dagger_{-\boldsymbol{k}}$ and $\hat{\Pi}_{\boldsymbol{k}} = \hat{\Pi}^\dagger_{-\boldsymbol{k}}$ as follows,

$$b_{\boldsymbol{k}} = \sqrt{\frac{\Delta_{\boldsymbol{k}}}{2}}\hat{\Phi}_{\boldsymbol{k}} + \frac{i}{\sqrt{2\Delta_{\boldsymbol{k}}}}\hat{\Pi}_{\boldsymbol{k}} , \tag{1.43a}$$

$$b^\dagger_{\boldsymbol{k}} = \sqrt{\frac{\Delta_{\boldsymbol{k}}}{2}}\hat{\Phi}_{-\boldsymbol{k}} - \frac{i}{\sqrt{2\Delta_{\boldsymbol{k}}}}\hat{\Pi}_{-\boldsymbol{k}} , \tag{1.43b}$$

where the energy $\Delta_{\boldsymbol{k}}$ is given by

$$\Delta_{\boldsymbol{k}} = A^+_{\boldsymbol{k}} + |B_{\boldsymbol{k}}| . \tag{1.44}$$

Requiring similar commutation relations as Eq. (1.39), i.e. in the discrete formulation

$$\left[\hat{\Phi}_{\boldsymbol{k}}, \hat{\Pi}_{\boldsymbol{k}'}\right] = i\delta_{\boldsymbol{k},-\boldsymbol{k}'} , \tag{1.45a}$$

$$\left[\hat{\Phi}_{\boldsymbol{k}}, \hat{\Phi}_{\boldsymbol{k}'}\right] = 0 , \qquad \left[\hat{\Pi}_{\boldsymbol{k}}, \hat{\Pi}_{\boldsymbol{k}'}\right] = 0 , \tag{1.45b}$$

the canonic commutators Eqs. (1.30a) and (1.30b) for the Bose operators are satisfied and the Hamiltonian of Eq. (1.25) transforms to

$$\hat{H}_2 = \frac{1}{2}\sum_{\boldsymbol{k}} \left\{ \hat{\Pi}_{-\boldsymbol{k}}\hat{\Pi}_{\boldsymbol{k}} + \epsilon_{\boldsymbol{k}}^2 \hat{\Phi}_{-\boldsymbol{k}}\hat{\Phi}_{\boldsymbol{k}} + iA_{\boldsymbol{k}}^{-}(\hat{\Phi}_{-\boldsymbol{k}}\hat{\Pi}_{\boldsymbol{k}} - \hat{\Phi}_{\boldsymbol{k}}\hat{\Pi}_{-\boldsymbol{k}}) - A_{\boldsymbol{k}}^{+} \right\} . \quad (1.46)$$

Again, also terms of the Hamiltonian containing more than two powers of the bosonic operators will have a counterpart in the Hermitian field operator representation. Contrary to the simple example of the anharmonic oscillator, mixed terms of the position type operator $\hat{\Phi}_{\boldsymbol{k}}$ and the momentum type operator $\hat{\Pi}_{\boldsymbol{k}}$ can occur. The helpfulness of the Hermitian parametrization in the theory of interacting Bose gases has been demonstrated in Refs. [23, 86, 156, P2, P8]. The connection of the field operators to physical observables in the context of spin-wave theory will be explained later upon application to model systems.

1.4 $1/S$ expansion and spin-wave theory

The main part of this thesis is about the study of low-energy excitations in magnetic insulators. Apart from the fact that also other types of quasiparticles are possible elementary excitations in low-dimensional Heisenberg magnets, we will focus our discussion on the spin-waves (magnons). The general steps to set up a spin-wave calculation in ordered magnets will be presented. Formally the spin-wave theory is an expansion in inverse powers of the total spin S ($1/S$ expansion), where S is assumed to be large. For more detailed discussions and explicit calculations the reader is referred to the explanations in the upcoming chapters, to original works [3, 96, 119], and to textbooks on quantum magnetism [B2, B3, B5, B20, B21, B26, B33, B38].

1.4.1 Classical ground state

In general, the spin-wave theory is an expansion in terms of excitations around the classical ground state where the spin operators are replaced by classical magnetic moments. For the Heisenberg ferromagnet one can show that the classical ground state, a saturated ferromagnet, is also the quantum ground state and that one-magnon states are also exact eigenstates of the Hamiltonian [54, B20, B21]. This rigorous statement is not true any more in the case of the antiferromagnet where the equivalent ground state, the Néel state, is not an eigenstate of the Hamiltonian. This is also the case if other terms like the dipole-dipole interactions Eq. (1.8) are present. Nevertheless, the spin-wave approach is still being considered a useful technique if an ordered state is observed [B21]. Even if the macroscopic ordering is forbidden due to large fluctuations[3], it is possible to keep a local order and set up a modified spin-wave

[3]For example the Mermin-Wagner theorem does not allow long range order at one- and two-dimensional isotropic Heisenberg magnets with finite range interactions at finite temperature [95, 141].

theory by a method introduced by Takahashi [202]. Not considering this in detail, let us assume a Heisenberg magnet with finite magnetic order described by the Hamiltonian

$$\hat{H}_{\text{spin}} = \frac{1}{2}\sum_{ij}\Big[J_{ij}\boldsymbol{S}_i \cdot \boldsymbol{S}_j + \boldsymbol{D}_{ij} \cdot (\boldsymbol{S}_i \times \boldsymbol{S}_j)\Big] - \boldsymbol{h} \cdot \sum_i \boldsymbol{S}_i \,, \tag{1.47}$$

that extends the model of Eq. (1.2) by DM anisotropies and the Zeeman term. The uniform magnetic field $\boldsymbol{h}$ is measured in units of energy and $\boldsymbol{S}_i$ are spin operators such that the operator $\boldsymbol{S}_i^2$ has the eigenvalue $S(S+1)$. Note that this model does not contain all terms discussed in section 1.1; the dipole-dipole interaction would significantly complicate the following general discussion. In this work the dipole-dipole interaction is only included in the model of the ferromagnet where the discussion of the ground state is done briefly in the corresponding chapter 3.

Let us now assume that the classical ground state is known and replace the spin operators by three-component classical vectors of length S, i.e.

$$\boldsymbol{S}_i = S\hat{\boldsymbol{m}}_i \,. \tag{1.48}$$

The unit vectors $\hat{\boldsymbol{m}}_i$ pointing in the direction of the local magnetization,

$$\hat{\boldsymbol{m}}_i = \frac{\langle \boldsymbol{S}_i \rangle}{|\langle \boldsymbol{S}_i \rangle|} \,, \tag{1.49}$$

will later be constructed explicitly and can be calculated, once the model system is fixed by the definition of the lattice and the exchange constants J_{ij} and $\boldsymbol{D}_{ij}$. Note that $\langle A \rangle$ denotes the expectation value of the operator A.

1.4.2 Local coordinate system and bosonization

In the next step we construct a right-handed triad,

$$\{\boldsymbol{e}_i^{(1)}, \boldsymbol{e}_i^{(2)}, \hat{\boldsymbol{m}}_i\} \,, \tag{1.50}$$

of orthogonal unit vectors for each site $\boldsymbol{R}_i$ of the lattice which form the basis vectors for a local coordinate system. Note that there is an $O(2)$-gauge freedom in the choice of the two vectors orthogonal to $\hat{\boldsymbol{m}}_i$ which might change some intermediate formulas, but will not change final results for the spin-wave theory [174]. In order to formally use the HP transformation we introduce spherical basis vectors via

$$\boldsymbol{e}_i^{\pm} = \boldsymbol{e}_i^{(1)} \pm i\boldsymbol{e}_i^{(2)} \,, \tag{1.51}$$

and decompose the spin operators in this basis,

$$\boldsymbol{S}_i = S_i^{\parallel}\hat{\boldsymbol{m}}_i + \boldsymbol{S}_i^{\perp} \,, \tag{1.52}$$

where the transverse part is given by

$$\boldsymbol{S}_i^{\perp} = \frac{1}{2}\sum_{p=\pm} S_i^{-p}\boldsymbol{e}_i^{p} \ . \tag{1.53}$$

Identifying the longitudinal part with the quantization axis of the spin operator we can directly use the HP transformation Eqs. (1.21a–1.21c) to bosonize the Heisenberg model. The Hamiltonian will then read [191]

$$\hat{H}_{\text{spin}} = E_0^{\text{cl}} + \hat{H}_2^{\parallel} + \hat{H}_4^{\parallel} + \hat{H}^{\perp} + \hat{H}^{\parallel\perp} \ , \tag{1.54}$$

where the individual terms are given by

$$E_0^{\text{cl}} = \frac{S^2}{2}\sum_{ij} J_{ij}^{\parallel} - S\sum_i \boldsymbol{h}\cdot\hat{\boldsymbol{m}}_i \ , \tag{1.55a}$$

$$\hat{H}_2^{\parallel} = -\frac{S}{2}\sum_{ij} J_{ij}^{\parallel}(n_i + n_j) + \sum_i \boldsymbol{h}\cdot\hat{\boldsymbol{m}}_i n_i \ , \tag{1.55b}$$

$$\hat{H}_4^{\parallel} = \frac{1}{2}\sum_{ij} J_{ij}^{\parallel} n_i n_j \ , \tag{1.55c}$$

$$\begin{aligned}\hat{H}^{\perp} &= \frac{1}{2}\sum_{ij}\left[J_{ij}\boldsymbol{S}_i^{\perp}\cdot\boldsymbol{S}_j^{\perp} + \boldsymbol{D}_{ij}\cdot(\boldsymbol{S}_i^{\perp}\times\boldsymbol{S}_j^{\perp})\right] \\ &= \frac{1}{8}\sum_{ij}\sum_{pp'} J_{ij}^{pp'} S_i^{-p} S_j^{-p'} \ ,\end{aligned} \tag{1.55d}$$

$$\hat{H}^{\parallel\perp} = \sum_{ij}\boldsymbol{S}_i^{\perp}\cdot\left[(J_{ij} - \boldsymbol{D}_{ij}\times)\,\hat{\boldsymbol{m}}_j(S - n_j) - \delta_{ij}\boldsymbol{h}\right] , \tag{1.55e}$$

and we have introduced some shorthand notations for the combinations of the exchange constants and the products of the basis vectors,

$$J_{ij}^{\parallel} = J_{ij}\hat{\boldsymbol{m}}_i\cdot\hat{\boldsymbol{m}}_j + \boldsymbol{D}_{ij}\cdot(\hat{\boldsymbol{m}}_i\times\hat{\boldsymbol{m}}_j) \ , \tag{1.56a}$$

$$J_{ij}^{pp'} = J_{ij}(\boldsymbol{e}_i^{p}\cdot\boldsymbol{e}_j^{p'}) + \boldsymbol{D}_{ij}\cdot(\boldsymbol{e}_i^{p}\times\boldsymbol{e}_j^{p'}) \ . \tag{1.56b}$$

From its definition the classical ground state minimizes the classical energy E_0^{cl} leading to the equation [175, 190, 191]

$$\hat{\boldsymbol{m}}_i\times\left[\boldsymbol{h} - S\sum_j (J_{ij} - \boldsymbol{D}_{ij}\times)\hat{\boldsymbol{m}}_j\right] = 0 \ . \tag{1.57}$$

The part Eq. (1.55e) of the Hamiltonian which mixes longitudinal and transverse spin fluctuations simplifies to

$$\hat{H}^{\parallel\perp} = -\sum_{ij}\boldsymbol{S}_i^{\perp}\cdot\left[(J_{ij} - \boldsymbol{D}_{ij}\times)\hat{\boldsymbol{m}}_j n_j\right] . \tag{1.58}$$

Now we use the expansion, Eqs. (1.23a) and (1.23b), to rewrite the transverse parts as

$$\hat{H}^{\perp} = \hat{H}_2^{\perp} + \hat{H}_4^{\perp} + \dots \ , \tag{1.59a}$$

$$\hat{H}^{\parallel\perp} = \hat{H}_1 + \hat{H}_3 + \dots \ . \tag{1.59b}$$

Note that the index of the individual terms of the Hamiltonian indicates the power of bosonic operators in the term, and that it is proportional to a specified power of the total spin, namely [190]

$$\hat{H}_n \propto S^{2-\frac{n}{2}} \; . \tag{1.60}$$

Once the classical ground state is chosen correctly, there is no contribution to the Hamiltonian containing one power of bosonic operators,

$$\hat{H}_1 = 0 \; . \tag{1.61}$$

For completeness and later reference we also cite the lowest-order terms of the transverse part,

$$\hat{H}_2^{\perp} = \frac{S}{4} \sum_{ij} \left(J_{ij}^{+-} b_i^{\dagger} b_j + J_{ij}^{-+} b_j^{\dagger} b_i + J_{ij}^{++} b_i^{\dagger} b_j^{\dagger} + J_{ij}^{--} b_i b_j \right) \; , \tag{1.62a}$$

$$\hat{H}_4^{\perp} = -\frac{1}{8} \sum_{ij} \left(J_{ij}^{++} b_i^{\dagger} b_j^{\dagger} n_j + J_{ij}^{--} n_i b_i b_j + J_{ij}^{+-} b_i^{\dagger} n_j b_j + J_{ij}^{-+} b_j^{\dagger} n_j b_i \right) \; , \tag{1.62b}$$

$$\hat{H}_1 = \frac{(2S)^{3/2}}{4} \sum_{ij} \left[b_i^{\dagger} \boldsymbol{e}_i^{+} + b_i \boldsymbol{e}_i^{-} \right] \cdot \left[\left(J_{ij} - \boldsymbol{D}_{ij} \times \right) \hat{\boldsymbol{m}}_j - \frac{\delta_{ij} \boldsymbol{h}}{S} \right] \; , \tag{1.62c}$$

$$\begin{aligned} \hat{H}_3 = -\frac{\sqrt{2S}}{8} \sum_{ij} \Bigg\{ & \left[b_i^{\dagger} n_i \boldsymbol{e}_i^{+} + n_i b_i \boldsymbol{e}_i^{-} \right] \cdot \left[\left(J_{ij} - \boldsymbol{D}_{ij} \times \right) \hat{\boldsymbol{m}}_j - \frac{\delta_{ij} \boldsymbol{h}}{S} \right] \\ & + 4 \left[b_i^{\dagger} \boldsymbol{e}_i^{+} + b_i \boldsymbol{e}_i^{-} \right] \cdot \left[\left(J_{ij} - \boldsymbol{D}_{ij} \times \right) \hat{\boldsymbol{m}}_j \right] \Bigg\} \; . \end{aligned} \tag{1.62d}$$

Depending on the actual model system the cubic terms might vanish, for example in the pure Heisenberg ferromagnet.

1.4.3 Specialties

At this point it is advantageous to already discuss some specialties about the setup of the spin-wave theory for a quantum antiferromagnet (QAFM).

Antiferromagnet on a bipartite lattice

In analogy to the ferromagnet, the classical ground state of an isotropic antiferromagnet with nearest-neighbor interaction on a hypercubic lattice is the so-called Néel ground state where every second spin is just flipped, see Figs. 1.2 and 1.3. If a magnetic field is applied, the spins are canted by an angle ϑ from this state, but still every second spin points in the same direction, i.e. a so-called collinear state is realized. For applying standard techniques of condensed-matter theory we now have to choose a different elementary cell to also yield a translational invariance of the classical ground state. This is accompanied by a smaller Brillouin zone in momentum space, and the occurrence

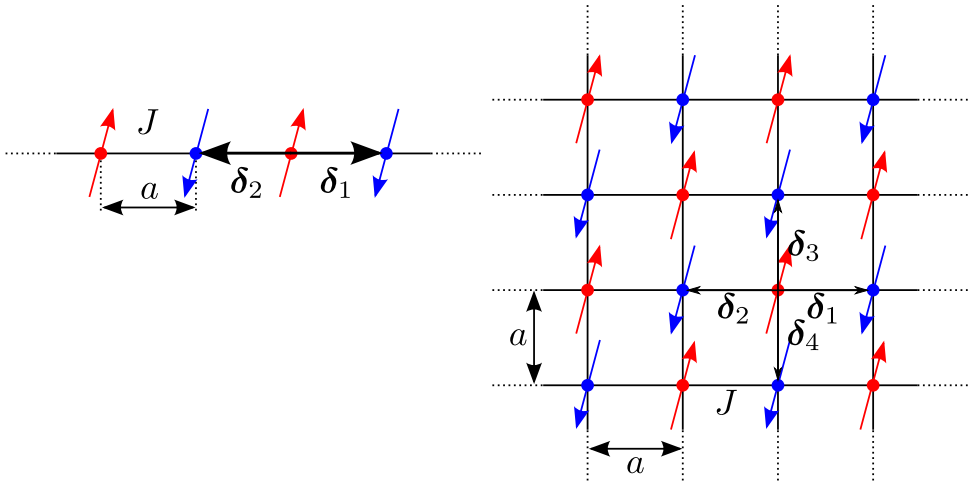

Figure 1.2: *Illustration of the classical ground state of an antiferromagnet in absence of external fields and anisotropies on a hypercubic lattice with lattice spacing a and nearest-neighbor interactions mediated along the bonds described by the vectors $\boldsymbol{\delta}_i$ (black arrows). The spins (blue and red arrows) on the two sublattices interact by the coupling J. In one dimension, i.e. for the antiferromagnetic spin chain, the sublattice magnetization vanishes in the quantum state [B8, B21]. An expansion around the Néel state therefore does not describe the physics of this system (left). Whereas the classical ground state is a good starting point for spin-wave theory in two dimensions, because the sublattice magnetization at zero temperature is only suppressed by quantum fluctuations, but does not vanish [137]. Note that in both cases the classical ground state is degenerate with respect to total rotations in spin space due to the $SU(2)$ symmetry.*

of two spin-wave modes since the elementary cell consists of two basis points, compare Fig. 1.4. This procedure is usually done by the introduction of two types of bosonic operators a_i and b_i. We divide the lattice into two sublattices A and B and use the HP transformation

$$S_i^{\parallel} = S - a_i^\dagger a_i \,, \tag{1.63a}$$

A lattice

$$S_i^{+} = \sqrt{2S}\sqrt{1 - \frac{a_i^\dagger a_i}{2S}}\, a_i \,, \tag{1.63b}$$

$$S_i^{-} = \sqrt{2S}\, a_i^\dagger \sqrt{1 - \frac{a_i^\dagger a_i}{2S}} \,, \tag{1.63c}$$

$$S_i^{\parallel} = S - b_i^\dagger b_i \,, \tag{1.64a}$$

B lattice

$$S_i^{+} = \sqrt{2S}\sqrt{1 - \frac{b_i^\dagger b_i}{2S}}\, b_i \,, \tag{1.64b}$$

$$S_i^{-} = \sqrt{2S}\, b_i^\dagger \sqrt{1 - \frac{b_i^\dagger b_i}{2S}} \,. \tag{1.64c}$$

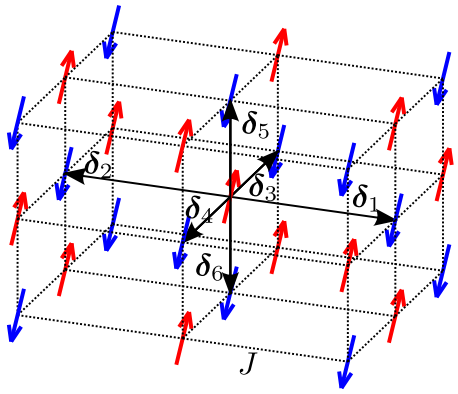

Figure 1.3: *Illustration of the classical ground state of a QAFM in three dimensions. As in Fig. 1.2 the sublattices are illustrated by the different colors of the arrows and the 6 directions to the nearest neighbors are indicated by the vectors* $\boldsymbol{\delta}_i$.

Further calculations for antiferromagnets on bipartite lattices are based on two different bosonic species. Besides, the following Dyson-Maleyev transformation for the two sublattices avoids terms with more than 4 bosonic operators [190]

$$S_i^{\parallel} = S - a_i^\dagger a_i \,, \tag{1.65a}$$

A lattice

$$S_i^{+} = \sqrt{2S}\left(1 - \frac{a_i^\dagger a_i}{2S}\right) a_i \,, \tag{1.65b}$$

$$S_i^{-} = \sqrt{2S}\, a_i^\dagger \,, \tag{1.65c}$$

$$S_i^{\parallel} = S - b_i^\dagger b_i \,, \tag{1.66a}$$

B lattice

$$S_i^{+} = \sqrt{2S}\, b_i \,, \tag{1.66b}$$

$$S_i^{-} = \sqrt{2S}\, b_i^\dagger \left(1 - \frac{b_i^\dagger b_i}{2S}\right) \,. \tag{1.66c}$$

1.4.4 Folding of the Brillouin zone, helimagnets

Using two or more sublattices in the case of frustrated spin systems like the QAFM on the triangular lattice [28, 29] may be cumbersome, and for magnets without translational symmetry in the ground state it is not possible to use the sublattice formalism directly. In the case of helimagnets, see Fig. 1.5, we parametrize the local coordinate system and the local magnetization with two rotation matrices A_ϑ and $B_{\boldsymbol{Q}\cdot\boldsymbol{R}_i}$ that rotate the laboratory reference frame

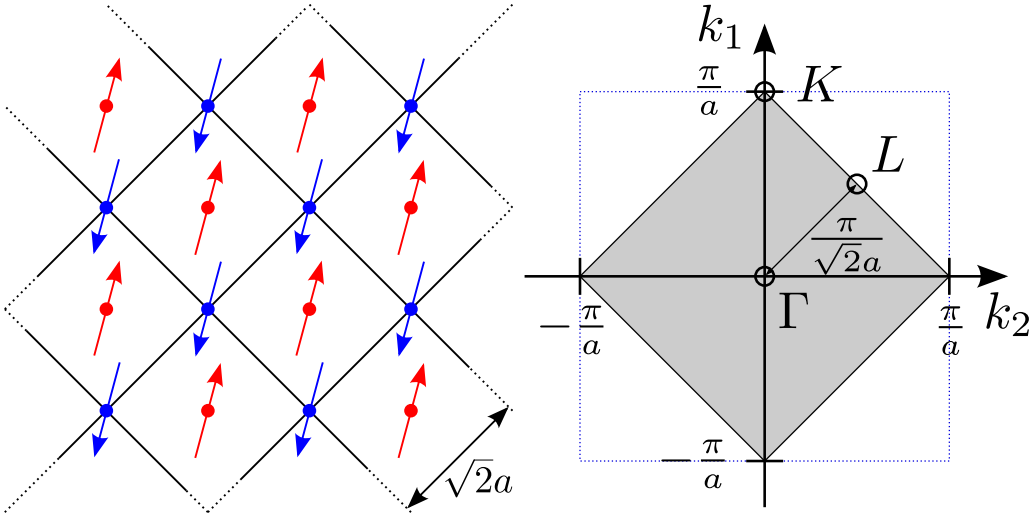

Figure 1.4: *In order to select an elementary cell which also respects the translational symmetry of the classical ground state of the QAFM on the square lattice one extends it to an elementary cell with two basis points, which is the area disclosed by the black solid line. One of the lattice points belongs to the A sublattice (red) and the other to the B sublattice (blue), (left). Since the effective lattice constant is now* $\sqrt{2}a$*, the corresponding Brillouin zone is downsized to the reduced Brillouin zone. The shaded area denotes the reduced (antiferromagnetic) Brillouin zone where the two magnon modes are defined. The area inside the dashed line is the full Brillouin zone (right).*

$\{\boldsymbol{e}_x, \boldsymbol{e}_y, \boldsymbol{e}_z\}$ to the local reference frame $\{\boldsymbol{e}_i^{(1)}, \boldsymbol{e}_i^{(2)}, \hat{\boldsymbol{m}}_i\}$ [152],

$$\begin{pmatrix} \boldsymbol{e}_i^{(1)} \\ \boldsymbol{e}_i^{(2)} \\ \boldsymbol{m}_i \end{pmatrix} = A_\vartheta B_{\boldsymbol{Q}\cdot\boldsymbol{R}_i} \begin{pmatrix} \boldsymbol{e}_x \\ \boldsymbol{e}_y \\ \boldsymbol{e}_z \end{pmatrix} , \tag{1.67}$$

where A_ϑ is a rotation matrix around the axis A and $B_{\boldsymbol{Q}\cdot\boldsymbol{R}_i}$ is a rotation matrix around the axis B which depend on the lattice vector $\boldsymbol{R}_i$ and the ordering vector $\boldsymbol{Q}$. A suitable choice for the QAFM subject to a magnetic field in the z-direction is

$$A_\vartheta = X_{\vartheta-\pi/2} = \begin{pmatrix} 1 & 0 & 0 \\ 0 & \sin\vartheta & -\cos\vartheta \\ 0 & \cos\vartheta & \sin\vartheta \end{pmatrix} , \tag{1.68a}$$

$$B_{\boldsymbol{Q}\cdot\boldsymbol{R}_i} = Z_{\boldsymbol{Q}\cdot\boldsymbol{R}_i-\pi/2} = \begin{pmatrix} \cos(\boldsymbol{Q}\cdot\boldsymbol{R}_i - \pi/2) & \sin(\boldsymbol{Q}\cdot\boldsymbol{R}_i - \pi/2) & 0 \\ \sin(\boldsymbol{Q}\cdot\boldsymbol{R}_i - \pi/2) & \cos(\boldsymbol{Q}\cdot\boldsymbol{R}_i - \pi/2) & 0 \\ 0 & 0 & 1 \end{pmatrix} . \tag{1.68b}$$

The additive constant $\pi/2$ in the rotation matrix around the x- and z-axis already incorporates the expected antiferromagnetic ground state. After checking

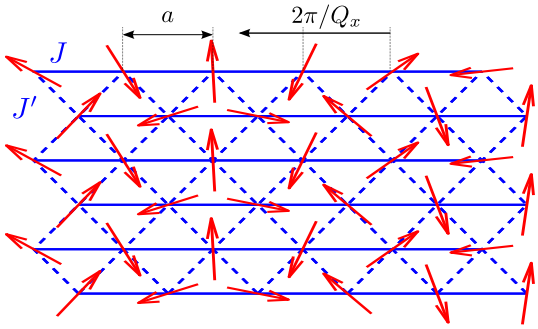

Figure 1.5: *Classical ground state of a frustrated QAFM on a triangular lattice. Spatial anisotropies, e.g. two different values of the exchange couplings $J/J' = 0.5$, lead to an ordering vector $\boldsymbol{Q}$ which results in a classical ground state without translational symmetry.*

whether the correct ground state can be parametrized by the opening angle ϑ and the ordering vector $\boldsymbol{Q}$, the explicit form of the rotation matrices has to be adapted to the actual problem. These can then formally be calculated by the minimization of the ground-state energy Eq. (1.55a). In the case of the QAFM on a hypercubic lattice the nesting vector $\boldsymbol{Q}$ directly points to the center of the second Brillouin zone in the bipartite lattice formulation. Hence, the bosonic states corresponding to the second species now belong to states in the extended Brillouin zone, compare Fig. 1.4. For general antiferromagnets, especially helimagnets, the vector $\boldsymbol{Q}$ is not on a point of high symmetry since the classical ground state does not have a precise translation symmetry. Instead, it obeys a combined symmetry of translation and rotation in real space, see Fig. 1.5.

1.4.5 Setup of spin-wave calculations

To finish the discussion we will briefly summarize the main steps to obtain spin-wave spectra in linear spin-wave theory and how to derive the nonlinear interaction terms. As already mentioned above one can use the translation symmetry of the lattice and transform to momentum space by

$$b_i = \frac{1}{\sqrt{N}} \sum_{\boldsymbol{k}} e^{i\boldsymbol{k}\cdot\boldsymbol{R}_i} b_{\boldsymbol{k}} \ , \tag{1.69}$$

where the sum runs over all reciprocal vectors in the first Brillouin zone. The quadratic part of the Hamiltonian is the sum of Eqs. (1.55b) and (1.62a),

$$\hat{H}_2 = \hat{H}_2^{\parallel} + \hat{H}_{2\perp} \ , \tag{1.70}$$

and has the form of Eq. (1.25). Diagonalization by a Bogoliubov transformation yields the magnon spectrum Eq. (1.33) in linear spin-wave theory. The interaction terms Eqs. (1.55c), (1.62b) and (1.62d) and also higher order interactions can be transformed to momentum space as well to accomplish the starting point for the application of many-body techniques.

1.4.6 Non-linear sigma model

In theoretical physics the non-linear sigma model (NLSM) is considered as a field theory whose fields are restricted to a Riemannian manifold. Apart from studies on renormalizability and beta functions of the NLSM [11, 20, 71], this model has been applied in the context supersymmetry [236] and quantum magnets [19, 25]. We will only consider the latter application to quantum magnets in our short overview. The NLSM considered here is an effective low-energy field theory and its connection to the microscopic Hamiltonian of the QAFM was first derived by Haldane [82, 83]. In that special case a three-component vector field $\mathbf{\Omega}$ with the constraint $|\mathbf{\Omega}| = 1$ is considered. The effective Euclidean action of the $O(3)$ symmetric theory in D dimensions can be written in the form [25, 82, 104]

$$S_{\text{eff}}\left[\mathbf{\Omega}\right] = \frac{\rho_s^0}{2} \int_0^\beta d\tau \int_{\Lambda^{-1}} d^D r \left[\sum_{\mu=1}^{D} \left(\partial_\mu \mathbf{\Omega}\right)^2 + \frac{1}{c_0^2} \left(\partial_\tau \mathbf{\Omega}\right)^2 \right] , \tag{1.71}$$

where the spatial integrations over r are constrained by a short-distance cutoff Λ^{-1}. Note that for the QAFM the unit vector $\mathbf{\Omega}(\tau, r)$ represents the slowly fluctuating staggered magnetization. The two parameters of this theory are the bare spin stiffness ρ_s^0 and the bare spin-wave velocity c_0 at $T = 0$. $\partial_\mu = \partial/\partial r_\mu$ is the spatial derivative in direction $\mu = 1, \ldots, D$. The partition function as fundamental quantity is then given by the functional integral

$$\mathcal{Z} = \int \mathcal{D}\left[\mathbf{\Omega}\right] \delta\left(|\mathbf{\Omega}| - 1\right) e^{-S_{\text{eff}}[\mathbf{\Omega}]} , \tag{1.72}$$

where the constraint is directly implemented. For a QAFM with total spin S on a two-dimensional quadratic lattice with spacing a the two parameters are given by [25]

$$\rho_s^0 = JS^2 , \tag{1.73a}$$

$$c_0 = 2\sqrt{2} JSa , \tag{1.73b}$$

where J is the nearest-neighbor exchange interaction. However, the NLSM contains two independent parameters which were studied as independent coupling constants in a momentum-space renormalization group analysis. Depending on the value of the physical spin stiffness,

$$\Delta\rho_s = \rho_s^0 - \rho_s^c , \tag{1.74}$$

where ρ_s^c is a critical value of the spin stiffness, there exist three different regimes [25]:

1. In the renormalized classical regime, where $\Delta\rho_s > 0$, an ordered antiferromagnetic phase at $T = 0$ is observed. In two dimensions the correlation length has the asymptotic behavior $\xi \propto e^{2\pi\Delta\rho_s/T}$ at low temperatures.

This is identical to the classical Heisenberg model [19]. An example of a system in this regime is the QAFM mentioned above. In this case the quantum fluctuations are not strong enough to destroy the magnetic order at $T = 0$ so that for example the spin-wave approach, requiring an ordered state, is well defined.

2. In the quantum disordered regime, $\Delta\rho_s < 0$, the magnetic order is destroyed even at $T = 0$ and the correlation length obeys a power law that is independent of the temperature T.

3. In between these regimes, at $|\rho_s^0 - \rho_s^c| \approx T$, the system behaves quantum critical. The correlation length is inversely proportional to the temperature, and physical quantities follow scaling relations known from the theory of critical phenomena.

The latter two phases might be realized in the QAFM with frustrating interactions beyond the nearest neighbors.

Although the NLSM has been quite successful in explaining magnetic phases and predicting the behavior of physical observables it needs the values of the two parameters ρ_s^0 and c_0 as input. The cutoff in the effective action Λ^{-1} has to be determined from microscopic calculations. Thus, the NLSM alone cannot predict physical observables in Heisenberg magnets quantitatively. Finally let us mention some recent applications of the NLSM in the context of QAFMs in Refs. [4, 58, 105].

NLSM at finite magnetic field

A generalization of the NLSM for a QAFM subject to a uniform magnetic field $\boldsymbol{h}$ can be obtained from the NLSM without field defined in Eq. (1.71) substituting the time derivative by a covariant derivative [66, B32],

$$\partial_\tau \to \partial_\tau - i\boldsymbol{h}\times \,, \tag{1.75}$$

to get

$$S_{\mathrm{NLSM}}[\boldsymbol{\Omega}] = \frac{\rho_s}{2}\int_0^\beta d\tau \int d^D r \Big[\sum_{\mu=1}^{D}(\partial_\mu \boldsymbol{\Omega})^2 + c^{-2}(\partial_\tau \boldsymbol{\Omega} - i\boldsymbol{h}\times\boldsymbol{\Omega})^2\Big]\,. \tag{1.76}$$

Knowing the studies on the NLSM without magnetic field [25] one usually argues that the parameters c and ρ_s are effective parameters also including the effect of the magnetic field. Since in the substitution procedure of Eq. (1.75) the number of parameters does not change, it is assumed that even in presence of a magnetic field the magnon dispersions can be characterized by a single (renormalized) spin-wave velocity $c(h)$. Using a spin-wave calculation to linear order we show in chapter 2 that this assumption is not justified any more, and that the number of relevant parameters has to be increased [87, P2].

1.5 Many-particle methods

This work focuses on the calculation of physical quantities that are related to the elementary excitations in magnetic insulators, the so-called magnons. In order to discuss the properties of these quantum mechanical objects we need the concept of quasiparticles that is mathematically formulated in the framework of functional methods. At this point we cannot give a self-contained introduction to all theoretical techniques which are used in this thesis. The reader is referred to textbooks introducing path integrals [B29, B34], and its generalization to functional integrals [B23, B28, B41]. Nevertheless the formulas needed to follow the calculations in the upcoming chapters will be cited and features that are important for our calculation will be discussed.

1.5.1 Phase-space path integral

Quantum mechanics can be formulated in terms of the phase-space path integral; this technique will be derived in the case of a one-particle system. In chapters 2 and 4 we will then use its generalization to many-particle systems to describe the elementary excitations in quantum magnets

The basic idea is the calculation of the time-evolution operator $U(t_f, \boldsymbol{x}_f; t_i, \boldsymbol{x}_i)$ which evolves the quantum state $|\boldsymbol{x}_i(t_i)\rangle$ from the initial time t_i in position representation to the quantum state $|\boldsymbol{x}_f(t_f)\rangle$ at some finial time t_f under the Hamiltonian $\hat{H}(\boldsymbol{x}, \boldsymbol{p})$. This Hamiltonian in the position and momentum representation describes for example a single particle in a potential. Applying the Trotter product formula [B34] one can evaluate the result in a discretized way by inserting complete sets of states,

$$\mathbb{1} = \int d\boldsymbol{x}_j \, |\boldsymbol{x}_j\rangle \, \langle \boldsymbol{x}_j| \ , \tag{1.77a}$$

in the position representation and

$$\mathbb{1} = \int d\boldsymbol{p}_j \, |\boldsymbol{p}_j\rangle \, \langle \boldsymbol{p}_j| \ , \tag{1.77b}$$

in the momentum representation at intermediate times $t_i < t_j < t_f$. We now formally insert infinitely many states so that the higher order terms of the Trotter product formula do not contribute to the final result. The time-evolution operator can be written as

$$\begin{aligned} U(t_f, \boldsymbol{x}_f; t_i, \boldsymbol{x}_i) &= \lim_{N\to\infty} \int d^D\boldsymbol{x}_1 \cdots \int d^D\boldsymbol{x}_{N-1} \int \frac{d^D\boldsymbol{p}_1}{(2\pi\hbar)^D} \cdots \int \frac{d^D\boldsymbol{p}_N}{(2\pi\hbar)^D} \\ &\times \exp\left\{ \frac{i}{\hbar} \sum_{j=0}^{N-1} \left[\frac{1}{2}\boldsymbol{p}_{j+1} \cdot (\boldsymbol{x}_{j+1} - \boldsymbol{x}_j) - \frac{1}{2}(\boldsymbol{p}_{j+1} - \boldsymbol{p}_j) \cdot \boldsymbol{x}_{j+1} - \frac{1}{N} H(\boldsymbol{x}_j, \boldsymbol{p}_{j+1}) \right] \right\} \\ &= \int_{\boldsymbol{x}(t_i)=\boldsymbol{x}_i}^{\boldsymbol{x}(t_f)=\boldsymbol{x}_f} \mathcal{D}[\boldsymbol{x}, \boldsymbol{p}] e^{\frac{i}{\hbar}\int_{t_i}^{t_f} [\boldsymbol{p}\cdot\partial_t\boldsymbol{x} - \{H(\boldsymbol{p},\boldsymbol{x})\}]} \ . \end{aligned} \tag{1.78}$$

Switching to imaginary time by the replacement $\tau = it$ this transforms to

$$U(\tau, \boldsymbol{x}_f; \tau', \boldsymbol{x}_i) = \int_{\boldsymbol{x}(\tau')=\boldsymbol{x}_i}^{\boldsymbol{x}(\tau)=\boldsymbol{x}_f} \mathcal{D}[\boldsymbol{x}, \boldsymbol{p}] e^{-S[\boldsymbol{x},\boldsymbol{p}]} \,, \tag{1.79}$$

where we have introduced the Euclidean action,

$$S[\boldsymbol{x}, \boldsymbol{p}] = \int_{\tau'}^{\tau} d\tau'' \Big(\frac{1}{2} (i\boldsymbol{p} \cdot \partial_{\tau''} \boldsymbol{x} - i(\partial_{\tau''} \boldsymbol{p}) \cdot \boldsymbol{x}) + \{H(\boldsymbol{x}, \boldsymbol{p})\} \Big) \,, \tag{1.80}$$

of the field variables $\boldsymbol{x}$ and $\boldsymbol{p}$ which have been replaced from the corresponding operators. The partition function is then the imaginary time-evolution operator with periodic boundary conditions at imaginary time $\tau = \beta$,

$$\mathcal{Z} = \mathrm{Tr}\; e^{-\beta \hat{H}} = \int_{\boldsymbol{x}(\beta\hbar)=\boldsymbol{x}(0)} \mathcal{D}[\boldsymbol{x}, \boldsymbol{p}] e^{-S[\boldsymbol{x},\boldsymbol{p}]} \,. \tag{1.81}$$

A precise investigation on the operator-ordering problem of quantum mechanics and the ambiguities appearing in the path-integral formalism is subject to recent research. Wilson and Galitski [222] for example showed that the coherent-state path integral in the time-continuous formulation breaks down in two simple examples. Neither the normal-ordering of operators, nor the Weyl-ordering always yield the correct result for the partition function. However, in the context of the interacting Bose gas it is believed that the symmetrized Hamiltonian $\big\{\hat{H}(\boldsymbol{x}, \boldsymbol{p})\big\}$ in conjunction with the phase-space path-integral formalism leads to correct results [78, 219]. To define symmetrized quantities we introduce the symmetrized product,

$$\big\{\hat{A}_1 \hat{A}_2 \cdots \hat{A}_n\big\} \equiv \frac{1}{n!} \sum_P \hat{A}_{P_1} \hat{A}_{P_2} \cdots \hat{A}_{P_n} \,, \tag{1.82}$$

of the operators $\hat{A}_1 \hat{A}_2 \cdots \hat{A}_n$ representing momentum or position operators. The sum on the right-hand side runs over all $n!$ permutations of the n-tuple $(1, \ldots, n)$. In the case of a quantum particle in a potential, where the Hamiltonian $H(\boldsymbol{x}, \boldsymbol{p}) = \frac{p^2}{2m} + V(\boldsymbol{q})$ is just the sum of the kinetic and potential energy, the symmetrization is trivially $\{\hat{H}\} = \hat{H}$ and usually ignored in the literature [B34]. Using the shifted Gaussian integral,

$$\int_{-\infty}^{\infty} e^{-\frac{\alpha}{2}x^2 - \beta p x} dx = e^{-\frac{\beta^2}{\alpha} p^2} \sqrt{\frac{2\pi}{\alpha}} \,, \tag{1.83}$$

the integration over the position fields is carried out to arrive at the Lagrangian path integral. Later in section 2.3.3 we will describe an interacting Bose gas in a position and momentum like representation (Hermitian parametrization) where the latter integration step cannot be performed exactly since the Hamiltonian also has terms of higher order in the momentum field.

The many-particle version of the partition function then simply includes an integration over all position and momentum field variables of all particles. Finally let us cite the multidimensional generalization of the Gaussian integral [B23],

$$\int_{-\infty}^{\infty} \frac{dx_1 \cdots dx_n}{(2\pi)^{n/2}} e^{-\frac{1}{2}\sum_{ij} x_i A_{ij} x_j} = \frac{1}{\sqrt{\mathrm{det}A}} \,, \tag{1.84}$$

where the matrix A has to be positive definite to guarantee convergence of the integrations.

1.5.2 Method of Green functions

In a quite general context Green functions are types of functions used to solve inhomogeneous differential equations, for example the Maxwell equations in classical electrodynamics. In this work we will refer to Green functions as correlation functions in the context of many-body theory. To be more precise we consider a system of (interacting) bosons described by a Hamiltonian $\hat{H}$ which is a function of the bosonic operators $b_j^\dagger$ and b_j in the Heisenberg picture satisfying the relations in Eqs. (1.16a) and (1.16b). The real time Green function of the state j is then given as

$$G(j,t,t') = -i \left\langle 0 \right| \hat{T}\Big(b_j(t) b_j^\dagger(t')\Big) \left| 0 \right\rangle \,, \tag{1.85}$$

where $|0\rangle$ is the exact ground state in the Heisenberg picture. We have defined the time-ordering operator,

$$\hat{T}\left(A(t_2)B(t_1)\right) = \begin{cases} B(t_1)A(t_2) & \text{if } t_1 > t_2 \\ A(t_2)B(t_1) & \text{if } t_2 > t_1 \end{cases} \,, \tag{1.86}$$

which orders the operators A and B according to their time argument putting the operator with the earliest time to the right. Considering a non-interacting Hamiltonian $\hat{H}_0$ where the multiple-particle state $|\alpha\rangle$ is an eigenstate with eigenenergy ϵ_α, i.e. $\hat{H}_0 |\alpha\rangle = \epsilon_\alpha |\alpha\rangle$, the free Green function at zero temperature is given by

$$G_0(\alpha,t,t') = -i \left\langle 0 \right| \hat{T} \left(b_\alpha(t) b_\alpha^\dagger(t')\right) \left| 0 \right\rangle \,, \tag{1.87}$$

and can be calculated for bosons as

$$G_0(\alpha,t,t') = -ie^{-\epsilon_\alpha(t-t')} \left[\Theta(t-t')(1+N_\alpha) + \Theta(t'-t)N_\alpha\right] \,, \tag{1.88}$$

where N_α is the number of bosons in the one-particle state $|\alpha\rangle$ in the ground state of the system. Noting that the free Green function only depends on the time difference $t-t'$ one can Fourier transform it to frequency space via

$$G_0(\alpha,t-t') = \int_{-\infty}^{\infty} \frac{d\omega}{2\pi} G_0(\alpha,\omega) e^{-i\omega(t-t')} \,, \tag{1.89}$$

where

$$G_0(\alpha,\omega) = \int_{-\infty}^{\infty} dt'\, G_0(\alpha,t') e^{i\omega t'} = \frac{1}{\omega - \epsilon_\alpha + i0^+} \,. \tag{1.90}$$

The notation $i0^+$ means that the limit has to be taken from above, i.e. for an arbitrary function f,

$$f(i0^+) \to \lim_{\epsilon \searrow 0} f(i\epsilon) \,. \tag{1.91}$$

1.5.3 Wick theorem and Feynman diagrams

The Gell-Mann Low theorem [73] allows to calculate the Green function in presence of an interaction $\hat{H}_1$ via the formula

$$G(\alpha,t,t') = \sum_{\nu=0}^{\infty} \frac{(-i)^{\nu+1}}{\nu!} \int_{-\infty}^{\infty} dt_1 \cdots dt_\nu \frac{{}_0\langle 0|\hat{T}\Big(\hat{H}_1(t_1)\cdots\hat{H}_1(t_\nu) b_\alpha(t) b_\alpha^\dagger(t')\Big)|0\rangle_0}{{}_0\langle 0|\hat{S}\,|0\rangle_0} \,, \tag{1.92}$$

where the interaction $\hat{H}_1(t)$ is given in the interaction picture of quantum mechanics, $|0\rangle_0$ is the ground state of the non-interacting Hamiltonian $\hat{H}_0$, and $\hat{S}$ is the S-matrix which connects the interacting ground state and the non-interacting one. Observing the structure of Eq. (1.92) it is obvious that the Green function is given as an expansion in terms of matrix elements of the bosonic operators. Dropping the factor of the interaction vertices all terms in the numerator are of the form

$${}_0\langle 0|\hat{T}\left((b^\dagger)^n b^m b_\alpha(t) b_\alpha^\dagger(t')\right)|0\rangle_0 \,. \tag{1.93}$$

$(b^\dagger)^n$ is shorthand notation for a product of n creation operators at different times, and b^m is its counterpart for m annihilation operators. The general calculation of these matrix elements is rather tedious, and the reader is referred to textbooks on many-particle theory for an explicit derivation [B1, B6, B22, B23, B24]. To avoid lengthy formulas we use graphical representations and cite the Feynman rules that advise how to translate the graphical representations to formulas:

1. *Vertex:* Points where lines meet represent the vertex function in the interaction part of the Hamiltonian. The shape or color of the points might facilitate to recognize the type of interaction. For directed lines we use the following convention: An outgoing line with index α corresponds to an operator $b_\alpha^\dagger$ whereas an ingoing line corresponds to an operator b_α in the Hamiltonian. Within this work we use symmetrized vertices so that the factorials in the denominators of the interaction terms always cancel.

2. *A directed line* with index α and times t and t' at the endpoints corresponds to a factor of a free Green function $iG_0(\alpha, t-t')$.

$$ {}_0\langle 0|\,\hat{T}(\hat{H}_1(t_1)b_\alpha(t)b^\dagger_\alpha(t'))\,|0\rangle_0 = $$

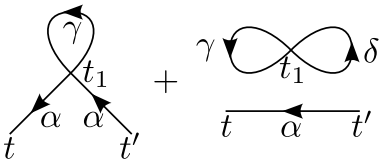

Figure 1.6: *Graphical representation of one matrix element needed to calculate the general expansion of the Green function Eq. (1.92). Directed lines represent free (bosonic) propagators, a point represents the interaction vertex and the Greek letters indicate the flavors of the involved particles. It is summed over internal flavor indices and integrated over intermediate times t_i.*

3. Summation or integration over all *internal degrees of freedom* which are visible as indices of the internal Green functions.

4. Multiplication with a *convergence factor* of $e^{-\epsilon|t_i|}$ (and the limit $\epsilon \to 0$) for all internal times t_i and integration $\int dt_i$ over all these times.

5. Multiplication with $(-i)^n$ for diagrams of order n.

Applying these rules, all matrix elements in the summation Eq. (1.92) have a graphical representation, for example ${}_0\langle 0|\hat{T}(\hat{H}_1(t_1)b_\alpha(t)b^\dagger_\alpha(t'))\,|0\rangle_0$ is shown in Fig. 1.6. In this example we assumed a quartic interaction term,

$$\hat{H}_1 = \frac{1}{(2!)^2}\sum_{\alpha\beta\gamma\delta} V_{\alpha,\beta;\gamma,\delta} b^\dagger_\alpha b^\dagger_\beta b_\gamma b_\delta \ . \tag{1.94}$$

Fig. 1.6 shows that the matrix element is a sum of a connected and a disconnected diagram. The latter contains at least one drawing that is not connected by lines to the rest of the diagram.

Upon evaluation of Eq. (1.92) it turns out that the denominator ${}_0\langle 0|\hat{S}\,|0\rangle_0$ is given by a sum of disconnected diagrams that cancel the disconnected ones in the numerator. Hence the full Green function simplifies to

$$G(\alpha,t,t') = \sum_{\nu=0}^{\infty}(-i)^{\nu+1}\int_{-\infty}^{\infty} dt_1\cdots dt_\nu\, {}_0\langle 0|\hat{T}\left(\hat{H}_1(t_1)\cdots\hat{H}_1(t_\nu)b_\alpha(t)b^\dagger_\alpha(t')\right)|0\rangle^{\rm c}_0 \ , \tag{1.95}$$

where the index c indicates that only the connected (and unlabeled) diagrams have to be considered.

Before closing the general discussion about Feynman diagrams, let us mention the possible definition of non-diagonal Green functions [B6]. These correspond in the graphical notation to lines with more than one arrow and are defined via the time ordered expectation value of two creation operators or two annihilation operators. In the context of quantum magnets this formulation is for example useful to avoid the Bogoliubov transformation [194–197] for

the interaction terms. Later we will also use the diagrammatic technique for Hermitian fields whose propagators are represented by lines without arrows, see Figs. 2.4 and 4.6. To not confuse the reader at this point we will not give any examples but suggest to read introductions to diagrammatic techniques applied to the φ^4-theory [B31] as needed to understand calculations in the following chapters.

1.5.4 Dyson equation and self-energy

The Green function in frequency space,

$$G(\alpha,\omega) = \int_{-\infty}^{\infty} dt'\, G(\alpha,t')\, e^{i\omega t'} \;, \tag{1.96}$$

for systems with time translation symmetry contains all informations about the single-particle excitations of the physical system. We can calculate related thermodynamic quantities once $G(\alpha,\omega)$ is known. In many cases it unfortunately has singularities and poles, so that an expansion like Eq. (1.95) in powers of the interaction is not valid for all frequencies. To overcome this complication one introduces the irreducible self-energy $\Sigma(\alpha,\omega)$ which connects the free Green function $G_0(\alpha,\omega)$ to the full Green-function via the Dyson equation,

$$G(\alpha,\omega) = \frac{1}{[G_0(\alpha,\omega)]^{-1} - \Sigma(\alpha,\omega)} \;. \tag{1.97}$$

The self-energy that includes the effects of interactions is then calculated using approximation schemes. The full propagator describes the dressed quasiparticles that have a corrected energy dispersion and eventually a finite lifetime which is given by the inverse of the imaginary part of the self-energy. Mathematically the Dyson equation is a reordering of the terms in perturbation theory. For a more detailed discussion and explicit calculations the reader is again referred to literature on many-particle physics [B1, B19, B22, B23].

1.5.5 Finite temperature formalism

The quantum theory of many-particle physics at finite temperature was first introduced by Matsubara [139]. The basic difference between the formalism at zero temperature and that at finite temperature is the use of an imaginary time τ. By help of a Wick rotation, where basically the identity $t = -i\tau$ is substituted, one sees that the quantum mechanical time-evolution operator is identical to the statistical operator which serves to calculate thermodynamic averages. As a consequence, the quantities are defined on the time interval $[0,\beta]$ where $\beta = T^{-1}$ is the inverse temperature of the system under investigation. Without derivation we will just cite some important formulas: Apart from the formal replacement $t \to -i\tau$, the Green functions are continued periodically on

the imaginary time which requires the use of Fourier transformations at finite intervals. For example the Green functions transform as follows,

$$G(\alpha,\tau) = \frac{1}{\beta}\sum_n G(\alpha, i\omega_n)e^{i\omega_n\tau} \ , \tag{1.98}$$

and the corresponding inverse transformation is

$$G(\alpha, i\omega_n) = \int_0^\beta d\tau G(\alpha,\tau)e^{-i\omega_n\tau} \ , \tag{1.99}$$

where the Matsubara frequencies for bosons are given by

$$\omega_n = \frac{2\pi n}{\beta} \ . \tag{1.100}$$

With the modifications described above most of the formulas for $T = 0$ keep their validity also in the finite temperature formalism. For an extended introduction and proofs of the statements above the reader should consult textbooks on statistical many-body theory [B1, B6, B12, B17].

Chapter 2

Quantum antiferromagnet in a magnetic field

2.1 Motivation

For obtaining low-temperature properties of ordered quantum magnets there are two popular field-theoretical techniques, namely the expansion in inverse powers of the spin quantum number ($1/S$ expansion) and an effective low-energy field theory, the non-linear sigma model (NLSM). Although many studies have already recovered physical observables using these methods, it still lacks a precise connection between the approaches, nor is a technique known that combines their advantages. Before coming to details of the calculation, let us briefly summarize these techniques for ordered quantum magnets.

In the $1/S$ expansion the spin-S Hamiltonian is mapped onto an interacting boson model by help of the Holstein-Primakoff (HP) [96], or the Dyson-Maleyev [54, 135] transformation. The next steps are then to use many-body techniques where the parameter $1/S$ is considered to be small. Indeed, this is only strictly justified for large quantum spin S. Apart from the grand success at early applications to quantum antiferromagnets (QAFMs) starting 50 years ago [151], calculations beyond the leading order in $1/S$ become cumbersome [85]. Reasons are the large number of interaction vertices which are additionally singular at certain regions of the Brillouin zone [85, 86, 114]. Since physical quantities have to be finite if the total spin is conserved [134], an inherent challenge of this approach is to combine the singularities properly so that they cancel at the end. Hence, this approach might not be the preferred way to calculate fluctuation corrections to the magnon spectrum.

On the other hand, the NLSM in the case of the QAFM is an effective continuum theory for the staggered spin fluctuations. Instead of singular interaction vertices like in the $1/S$ expansion, the vertices describing interactions between the relevant degrees of freedom, the transverse spin fluctuations, are

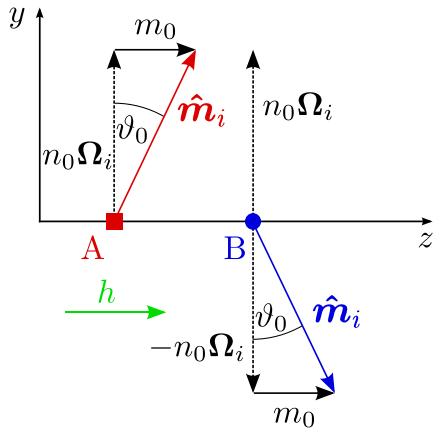

Figure 2.1: *Spin configuration $\langle \boldsymbol{S}_i \rangle = S\hat{\boldsymbol{m}}_i$ in the classical ground state of a two-sublattice antiferromagnet subject to a uniform magnetic field $\boldsymbol{h} = h\boldsymbol{e}_z$ in the z-direction. The hypercubic lattice can be divided into two sublattices, labeled A and B, such that the nearest neighbors of a given site all belong to the other sublattice, compare section 1.4.3. The solid square denotes a site of the A-sublattice and a solid circle denotes a site of the B-sublattice. Here ϑ_0 is the classical canting angle between the direction of the staggered magnetization $\boldsymbol{\Omega}_i$ and the local spin direction $\hat{\boldsymbol{m}}_i$.*

finite in momentum space. The NLSM has been quite successful to recover low-temperature properties of the possible phases in quantum magnets [25] (compare section 1.4.6), but it needs a regularization by an ultraviolet cutoff. Thus, numerical values of observables cannot be obtained.

We therefore reexamine fluctuation corrections to the magnon spectrum in the framework of a hybrid approach combining both the $1/S$ expansion and the NLSM. Using Hermitian field operators one can benefit from the advantages of both methods. This work focuses on methodical improvements on the calculation of the properties of the QAFM, but the results can still be useful for comparison with experimental data. Hence, in appendix A.1 we point out some experimental techniques to measure observables calculated within this work and suggest possible materials where the model system is realized. The work presented in this chapter has been done in collaboration with Francesca Sauli, Nils Hasselmann and Peter Kopietz, and has been published in Ref. [P2].

2.2 Introduction

In order to reconsider the fluctuation corrections to the magnon spectrum of a spin-S Heisenberg antiferromagnet in a uniform magnetic field $\boldsymbol{h}$, we calculate the self-energy at zero temperature up to leading order in $1/S$. Assuming a

finite staggered magnetization [137], we start from the Heisenberg Hamiltonian,

$$\hat{H} = \frac{1}{2}\sum_{ij} J_{ij}\boldsymbol{S}_i \cdot \boldsymbol{S}_j - \boldsymbol{h}\cdot\sum_i \boldsymbol{S}_i \,, \tag{2.1}$$

which is a simplification of the Hamiltonian in Eq. (1.47). The spins are located on a D-dimensional hypercubic lattice with lattice spacing a, total volume $V = a^D N$ and N sites. The antiferromagnetic interaction is mediated by the exchange integrals J_{ij} connecting nearest-neighbor sites $\boldsymbol{R}_i$ and $\boldsymbol{R}_j$.

2.2.1 General properties

As long as the absolute value $|\boldsymbol{h}|$ of the magnetic field is smaller than a critical value h_c, the spin configuration of the classical ground state is canted [234]. It possesses a staggered magnetization $\boldsymbol{M}_s$ perpendicular to the magnetic field $\boldsymbol{h}$ and a uniform magnetization in the direction of $\boldsymbol{h}$. The Hamiltonian Eq. (2.1) has been studied in detail before [233], where it was found that the magnetic field induces a gap in one magnon mode, while the dispersion of the magnons polarized perpendicular to $\boldsymbol{h}$ remains gapless.

The effective Hamiltonian obtained by the HP transformation contains terms cubic in the bosonic operators due to the canting of the spins. Since the cubic vertices are proportional to $S^{-1/2}$ (compare Eq. (1.60)) the cubic terms have to be treated in second order perturbation theory to obtain the complete $1/S$ correction to physical observables. In a previous investigation Zhitomirsky and Chernyshev [233] have shown that for intermediate magnetic fields in the range $h_* = 2/\sqrt{7}h_c < |\boldsymbol{h}| < h_c$ the damping of the magnons is quite large. Due to spontaneous two-magnon decays the magnons are not well-defined quasiparticles in large parts of the Brillouin zone.

In a similar model system of an anisotropic QAFM, Syromyatnikov and Maleyev found an anisotropy-induced gap that is quite large in dimensions $D \leq 3$. In conclusion they suggested that meaningful results could only be obtained if the $1/S$ expansion is resumed to all orders, which is not possible in practice [198].

2.3 Hybrid approach: Combining the advantages of the $1/S$ expansion with those of the NLSM

2.3.1 Holstein-Primakoff boson Hamiltonian

To set up the $1/S$ expansion we follow the steps described in section 1.4: For the expansion around the classical ground state characterized by the

directions $\hat{\boldsymbol{m}}_i = \langle \boldsymbol{S}_i \rangle / |\langle \boldsymbol{S}_i \rangle|$ of the local magnetic moments we choose a local coordinate system [175]. Defining the local right-handed triad $\{\boldsymbol{e}_i^{(1)}, \boldsymbol{e}_i^{(2)}, \hat{\boldsymbol{m}}_i\}$ of orthonormal vectors and a corresponding spherical basis, we are able use the HP transformation to express the spin operators $\boldsymbol{S}_i$ of our model system Eq. (2.1) in terms of canonical boson operators b_i and $b_i^\dagger$. Our bosonic many-body Hamiltonian,

$$\hat{H} = E_0^{\mathrm{cl}} + \hat{H}_2^{\parallel} + \hat{H}_4^{\parallel} + \hat{H}^{\perp} + \hat{H}^{\parallel\perp} \,, \tag{2.2}$$

has then the form discussed in section 1.4.2, except that there is no anisotropy ($\boldsymbol{D}_{ij} = 0$), compare Eqs. (1.55a–1.55e). The part $\hat{H}^{\parallel\perp}$ of this Hamiltonian describes the coupling between transverse and longitudinal spin fluctuations generated by the uniform magnetic field. Expanding the square roots in the HP transformations, Eqs. (1.21b) and (1.21c), the perpendicular part $\hat{H}^{\perp}$ of the Hamiltonian contains even powers of boson operators, while the part $\hat{H}^{\parallel\perp}$ becomes an infinite series of terms involving odd powers of boson operators,

$$\hat{H}^{\perp} = \hat{H}_2^{\perp} + \hat{H}_4^{\perp} + \mathcal{O}(S^{-1}) \,, \tag{2.3a}$$

$$\hat{H}^{\parallel\perp} = \hat{H}_1 + \hat{H}_3 + \mathcal{O}(S^{-1/2}) \,. \tag{2.3b}$$

Guided by the knowledge that in an antiferromagnet on a hypercubic lattice the sublattice magnetization is suppressed but not destroyed by fluctuations [137], we make the assumption that the true spin configuration resembles the classical one. For a finite magnetic field we expect a canted state shown in Fig. 2.1 with a renormalized canting angle ϑ. We then define for a magnetic field $\boldsymbol{h} = h\boldsymbol{e}_z$,

$$\langle \boldsymbol{S}_i \rangle = |\langle \boldsymbol{S}_i \rangle| \hat{\boldsymbol{m}}_i \,, \quad \hat{\boldsymbol{m}}_i = \zeta_i n \boldsymbol{e}_z + m \boldsymbol{e}_x \,. \tag{2.4}$$

The true canting angle is related to n and m via $n = \cos\vartheta$ and $m = \sin\vartheta$. The factor ζ_i takes into account spin flipping in the Néel state, as $\zeta_i = +1$ on one sublattice (which we call the A sublattice) and $\zeta_j = -1$ on the other sublattice (the B sublattice). Without loss of generality we complete the local triad by

$$\boldsymbol{e}_i^{(1)} = \boldsymbol{e}_y \,, \qquad \boldsymbol{e}_i^{(2)} = -\zeta_i n \boldsymbol{e}_z + m \boldsymbol{e}_y \,. \tag{2.5}$$

Defining

$$\alpha = n^2 - m^2 = 1 - 2m^2 = \cos(2\vartheta) \,, \tag{2.6a}$$

$$\lambda = 2nm = \sin(2\vartheta) \,, \tag{2.6b}$$

we can rewrite the relevant scalar products in this basis for nearest-neighbor sites i and j as

$$\hat{\boldsymbol{m}}_i \cdot \hat{\boldsymbol{m}}_j = m^2 - n^2 = -\alpha \,, \tag{2.7a}$$

$$\boldsymbol{e}_i^{+} \cdot \boldsymbol{e}_j^{+} = \boldsymbol{e}_i^{-} \cdot \boldsymbol{e}_j^{-} = 2n^2 \,, \tag{2.7b}$$

$$\boldsymbol{e}_i^{+} \cdot \boldsymbol{e}_j^{-} = \boldsymbol{e}_i^{-} \cdot \boldsymbol{e}_j^{+} = 2m^2 \,, \tag{2.7c}$$

$$\boldsymbol{e}_i^{+} \cdot \hat{\boldsymbol{m}}_j = -\boldsymbol{e}_i^{-} \cdot \hat{\boldsymbol{m}}_j = -2inm\zeta_i = -i\lambda\zeta_i \,, \tag{2.7d}$$

$$\boldsymbol{h} \cdot \hat{\boldsymbol{m}}_i = hm \,, \tag{2.7e}$$

and obtain for the exchange constants in Eqs. (1.56a) and (1.56b),

$$J_{ij}^{\parallel} = -\alpha J_{ij} \ , \tag{2.8a}$$
$$J_{ij}^{++} = J_{ij}^{--} = n^2 J_{ij} \ , \tag{2.8b}$$
$$J_{ij}^{+-} = J_{ij}^{-+} = m^2 J_{ij} \ . \tag{2.8c}$$

Thus, the classical energy Eq. (1.55a) is given by

$$E_0^{\mathrm{cl}} = -NDJS^2\alpha - NShm \ , \tag{2.9}$$

and from Eq. (1.55b) we obtain

$$\hat{H}_2^{\parallel} = \frac{Z_h}{2} h_c \sum_i n_i \ , \tag{2.10}$$

where we defined a renormalization factor

$$Z_h = 1 + \frac{2m\delta h}{h_c} \ . \tag{2.11}$$

The critical field of the QAFM is given by

$$h_c = 4DJS \ , \tag{2.12}$$

and we have introduced the difference

$$\delta h = h - h_c m \ . \tag{2.13}$$

In the classical limit $S \to \infty$, the exchange field $h_c m$ exactly cancels the external field, i.e. in this case $\delta h = 0$. Thus, for finite S the difference δh is nonzero. Later, in section 2.4, we will see that δh is of the order mh_c/S. The longitudinal part $\hat{H}_4^{\perp}$ and the leading two terms of the transverse part can be read off from Eqs. (1.62a) and (1.62b) with the help of Eqs. (2.8a–2.8c). Finally the essential part $\hat{H}^{\parallel\perp}$ of our effective Hamiltonian describing the coupling between transverse and longitudinal fluctuations can be written as

$$\hat{H}^{\parallel\perp} = \lambda \sum_{ij} J_{ij} \zeta_i S_i^{(2)} n_j + n\delta h \sum_i \zeta_i S_i^{(2)} \ , \tag{2.14}$$

where we have decomposed the ladder operator in the local coordinate systems,

$$S_i^{\pm} = S_i^{(1)} \pm i S_i^{(2)} \quad \Leftrightarrow \quad \begin{array}{l} S_i^{(1)} = \boldsymbol{e}_i^{(1)} \cdot \boldsymbol{S}_i = \frac{1}{2}(S_i^{+} + S_i^{-}) \\ S_i^{(2)} = \boldsymbol{e}_i^{(2)} \cdot \boldsymbol{S}_i = \frac{1}{2i}(S_i^{+} - S_i^{-}) \ . \end{array} \tag{2.15}$$

The alternating factor ζ_i in Eq. (2.14) indicates that this term describes umklapp scattering across the boundary of the antiferromagnetic Brillouin zone.

For a strict calculation of the leading order $1/S$ corrections it is sufficient to retain only terms up to three boson operators in the expansion of Eq. (2.3b). With the choice of the basis vectors, Eq. (2.5), these can be written as

$$\hat{H}_1 = n\delta h \frac{\sqrt{2S}}{2i} \sum_i \zeta_i (b_i - b_i^\dagger) \ , \tag{2.16}$$

$$\hat{H}_3 = \lambda \frac{\sqrt{2S}}{2i} \sum_{ij} J_{ij} \zeta_i (b_i - b_i^\dagger) n_j \ . \tag{2.17}$$

To conclude the discussion about bosonization, let us emphasize that the Dyson-Maleyev transformation [54, 135] will not result in different expressions for $\hat{H}_1$, $\hat{H}_2$, $\hat{H}_3$ and $\hat{H}_4^{\parallel}$. Although it leads to a non-Hermitian transverse part $\hat{H}_4^{\perp}$, one does not expect any different results since the main quantities calculated in this chapter are essentially determined by $\hat{H}_3$. Thus, the results will not depend on whether we use the HP or the Dyson-Maleyev formalism.

2.3.2 Linear spin-wave theory

To obtain the magnon spectrum within linear spin-wave theory we follow the instructions in section 1.4: Keeping only the terms quadratic in the boson operators, Eq. (1.70), a transformation to momentum space is done using two different operators anticipated with the sublattices. Different from Eq. (1.69) we now define for sites $\boldsymbol{R}_i$ belonging to the A sublattice,

$$b_i = \sqrt{\frac{2}{N}} \sum_{\boldsymbol{k}} e^{i\boldsymbol{k}\cdot\boldsymbol{R}_i} a_{\boldsymbol{k}} \ , \tag{2.18a}$$

and for sites belonging to the B sublattice,

$$b_j = \sqrt{\frac{2}{N}} \sum_{\boldsymbol{k}} e^{i\boldsymbol{k}\cdot\boldsymbol{R}_j} b_{\boldsymbol{k}} \ , \tag{2.18b}$$

where the wave-vector sums are over the reduced (antiferromagnetic) Brillouin zone, shown in Fig. 1.4. Introducing the structure factor

$$\gamma_{\boldsymbol{k}} = \frac{\tilde{J}_{\boldsymbol{k}}}{\tilde{J}_0} = \frac{1}{D} \sum_{i=1}^{D} \cos(k_i a) \ , \tag{2.19}$$

where

$$\tilde{J}_{\boldsymbol{k}} = \frac{1}{N} \sum_{ij} e^{-i\boldsymbol{k}\cdot(\boldsymbol{R}_i - \boldsymbol{R}_j)} J_{ij} \tag{2.20}$$

is the Fourier transform of the exchange constants, one can rewrite the quadratic part of Eq. (1.70) as

$$\hat{H}_2 = \tilde{J}_0 S \sum_{\boldsymbol{k}} \Big\{ Z_h \Big[a_{\boldsymbol{k}}^\dagger a_{\boldsymbol{k}} + b_{\boldsymbol{k}}^\dagger b_{\boldsymbol{k}} \Big] + \gamma_{\boldsymbol{k}} \Big[n^2 (b_{-\boldsymbol{k}} a_{\boldsymbol{k}} + a_{\boldsymbol{k}}^\dagger b_{-\boldsymbol{k}}^\dagger) + m^2 (b_{\boldsymbol{k}}^\dagger a_{\boldsymbol{k}} + a_{\boldsymbol{k}}^\dagger b_{\boldsymbol{k}} \Big] \Big\} \ . \tag{2.21}$$

Note that for nearest-neighbor exchange the Fourier transform of the exchange constant at zero momentum is related to the critical field by

$$\tilde{J}_0 S = 2DJS = h_c/2 \,, \tag{2.22}$$

and the structure factor simply reads

$$\gamma_{\boldsymbol{k}} = \sum_{\boldsymbol{\delta}} e^{-i\boldsymbol{k}\cdot\boldsymbol{\delta}} \,, \tag{2.23}$$

where $\boldsymbol{\delta}$ are the vectors connecting nearest-neighbor sites, see Figs. 1.2 and 1.3). Since the Hamiltonian of Eq. (2.21) is slightly more complicated than the one discussed in section 1.3.1, we first introduce the symmetric and antisymmetric combinations

$$c_{\boldsymbol{k}\sigma} = \frac{1}{\sqrt{2}} \left[a_{\boldsymbol{k}} + \sigma b_{\boldsymbol{k}} \right] \,, \quad \sigma = \pm 1 \,, \tag{2.24}$$

and then perform a Bogoliubov transformation,

$$\begin{pmatrix} c_{\boldsymbol{k}\sigma} \\ c^{\dagger}_{-\boldsymbol{k}\sigma} \end{pmatrix} = \begin{pmatrix} u_{\boldsymbol{k}\sigma} & -\sigma v_{\boldsymbol{k}\sigma} \\ -\sigma v_{\boldsymbol{k}\sigma} & u_{\boldsymbol{k}\sigma} \end{pmatrix} \begin{pmatrix} \hat{\Psi}_{\boldsymbol{k}\sigma} \\ \hat{\Psi}^{\dagger}_{-\boldsymbol{k}\sigma} \end{pmatrix} \,, \tag{2.25}$$

to new canonical operators $\hat{\Psi}_{\boldsymbol{k}\sigma}$ that satisfy the commutation relations

$$[\hat{\Psi}_{\boldsymbol{k}\sigma}, \hat{\Psi}^{\dagger}_{\boldsymbol{k}'\sigma'}] = \delta_{\boldsymbol{k},\boldsymbol{k}'}\delta_{\sigma,\sigma'} \,. \tag{2.26}$$

The Bogoliubov coefficients are given by

$$u_{\boldsymbol{k}\sigma} = \sqrt{\frac{Z_h + \sigma m^2 \gamma_{\boldsymbol{k}} + \epsilon_{\boldsymbol{k}\sigma}}{2\epsilon_{\boldsymbol{k}\sigma}}} \,, \tag{2.27a}$$

$$v_{\boldsymbol{k}\sigma} = \sqrt{\frac{Z_h + \sigma m^2 \gamma_{\boldsymbol{k}} - \epsilon_{\boldsymbol{k}\sigma}}{2\epsilon_{\boldsymbol{k}\sigma}}} \,, \tag{2.27b}$$

where

$$\epsilon_{\boldsymbol{k}\sigma} = \sqrt{(Z_h + \sigma m^2 \gamma_{\boldsymbol{k}})^2 - (n^2\gamma_{\boldsymbol{k}})^2} = \sqrt{Z_h + \sigma\gamma_{\boldsymbol{k}}}\sqrt{Z_h - \sigma\alpha\gamma_{\boldsymbol{k}}} \tag{2.28}$$

is a dimensionless magnon dispersion. The relations of Eqs. (1.32a) and (1.32b) now read

$$u^2_{\boldsymbol{k}\sigma} + v^2_{\boldsymbol{k}\sigma} = \frac{Z_h + \sigma m^2 \gamma_{\boldsymbol{k}}}{\epsilon_{\boldsymbol{k}\sigma}} \,, \tag{2.29}$$

$$2u_{\boldsymbol{k}\sigma}v_{\boldsymbol{k}\sigma} = \frac{n^2\gamma_{\boldsymbol{k}}}{\epsilon_{\boldsymbol{k}\sigma}} \,. \tag{2.30}$$

Neglecting $1/S$ corrections to linear spin-wave theory we get $\delta h = 0$ and hence $Z_h = 1$. In terms of the magnon operators $\hat{\Psi}_{\boldsymbol{k}\sigma}$ the quadratic spin-wave Hamiltonian is diagonal,

$$\hat{H}_2 = \sum_{\boldsymbol{k}\sigma} E_{\boldsymbol{k}\sigma} \left[\hat{\Psi}^{\dagger}_{\boldsymbol{k}\sigma}\hat{\Psi}_{\boldsymbol{k}\sigma} + \frac{1}{2} \right] + E^{(1)}_{0\|} \,, \tag{2.31}$$

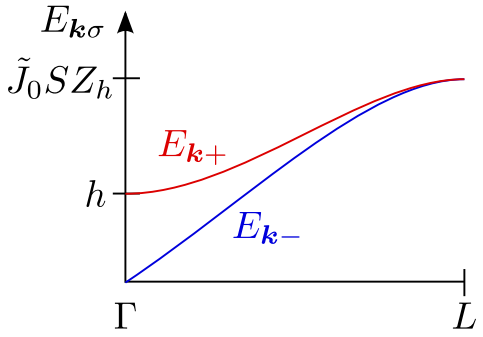

Figure 2.2: *Sketch of the dispersions of the magnon modes in the QAFM given in Eq. (2.32) along a line of high symmetry in the Brillouin zone. The dispersion $E_{\boldsymbol{k}+}$ is gapped, while $E_{\boldsymbol{k}-}$ remains gapless due to the $U(1)$ symmetry in the original Hamiltonian. The endpoints of the plot are points of high symmetry in the Brillouin zone, see Fig. 1.4.*

where

$$E_{\boldsymbol{k}\sigma} = \tilde{J}_0 S \epsilon_{\boldsymbol{k}\sigma} \tag{2.32}$$

are the dispersions of the two magnon branches. The total $1/S$ correction to the ground-state energy,

$$E_0^{(1)} = E_{0\parallel}^{(1)} + E_{0\perp}^{(1)} = -NDJS^2 \frac{C_1(h)}{S} \,, \tag{2.33}$$

where

$$C_1(h) = \frac{1}{N} \sum_{\boldsymbol{k}\sigma} (Z_h - \epsilon_{\boldsymbol{k}\sigma}) \,, \tag{2.34}$$

adds up from the $1/S$ correction to the ground-state energy due to longitudinal fluctuations,

$$E_{0\parallel}^{(1)} = -\frac{N}{2} Z_h \tilde{J}_0 S = -NDJS^2 \frac{Z_h}{S} \,, \tag{2.35}$$

and the zero point energy of the transverse spin waves,

$$E_{0\perp}^{(1)} = \frac{1}{2} \sum_{\boldsymbol{k}\sigma} E_{\boldsymbol{k}\sigma} \,. \tag{2.36}$$

The expressions of the dispersions to linear order in $\delta h = h - h_c m$ and to quadratic order in the momentum $\boldsymbol{k}$ are given by

$$E_{\boldsymbol{k}+}^2 = m h_c h + c_+^2 \boldsymbol{k}^2 \,, \tag{2.37a}$$
$$E_{\boldsymbol{k}-}^2 = n^2 m h_c \delta h + c_-^2 \boldsymbol{k}^2 \,. \tag{2.37b}$$

A sketch of the magnon dispersions within linear spin-wave theory is presented in Fig. 2.2, while a plot of the dispersion including interaction corrections can

be found in Ref. [233]. Defining the leading large-S result for the spin-wave velocity at zero field ($h = 0$),

$$c_0 = 2\sqrt{D}JSa \ , \tag{2.38}$$

compare Eq. (1.73b), an expansion of the spin-wave velocities for small m is given by

$$c_+^2 = c_0^2(1 - 3m^2) \ , \tag{2.39a}$$
$$c_-^2 = c_0^2(n^2 + 2m^3\delta h/h_c) \ . \tag{2.39b}$$

For a consistent leading order $1/S$ calculation at the level of linear spin-wave theory, we may approximate the canting angle by its classical value ϑ_0 which is fixed by the condition $\delta h = 0$, or equivalently

$$m = \sin\vartheta_0 = h/h_c \ . \tag{2.40}$$

One dispersion is then gapped,

$$E_{\boldsymbol{k}+} = h + \mathcal{O}(\boldsymbol{k}^2) \ , \tag{2.41a}$$

and the other is gapless,

$$E_{\boldsymbol{k}-} = c_- \, |\boldsymbol{k}| + \mathcal{O}(|\boldsymbol{k}|^3) \ , \tag{2.41b}$$

with spin-wave velocity

$$c_- = c_0 n = c_0 \sqrt{1 - \frac{h^2}{h_c^2}} \ . \tag{2.42}$$

Finally, let us stress that the quantities given above are analytical functions of the square of the magnetic field h^2 as long as $h \leq h_c$.

2.3.3 Hermitian field operators

Setting up interacting spin-wave theory, terms containing higher powers in the original HP bosons b_i are retained and replaced by the magnon operators $\hat{\Psi}_{\boldsymbol{k}\sigma}$. For the terms corresponding to Eqs. (1.62b, 1.55c, 2.16, 2.17) this yields rather lengthy expressions involving momentum-dependent vertices. However, in order to figure out the effects arising from the transverse staggered spin fluctuations, it is better to separate different kinds of degrees of freedom. The Hermitian field-operator approach discussed in section 1.3.2 is a good method to do this job. Guided by the procedure of solving the quantum mechanical harmonic oscillator, we express the magnon operators $\hat{\Psi}_{\boldsymbol{k}\sigma}$ in terms of two Hermitian field operators $\hat{X}_{\boldsymbol{k}\sigma}$ and $\hat{P}_{\boldsymbol{k}\sigma}$ as follows [3, 86, 87, 182],

$$\hat{\Psi}_{\boldsymbol{k}\sigma} = p_\sigma \left[\sqrt{\frac{\nu_{\boldsymbol{k}\sigma}}{2}} \hat{X}_{\boldsymbol{k}\sigma} + \frac{i}{\sqrt{2\nu_{\boldsymbol{k}\sigma}}} \hat{P}_{\boldsymbol{k}\sigma} \right] . \tag{2.43}$$

The arbitrary phase factors are chosen as $p_+ = -i$ and $p_- = 1$ for later convenience. We define the dimensionless factors $\nu_{\boldsymbol{k}\sigma}$ by

$$\nu_{\boldsymbol{k}\sigma} = \frac{E_{\boldsymbol{k}\sigma}}{\Delta_{\boldsymbol{k}\sigma}} , \tag{2.44}$$

where

$$\Delta_{\boldsymbol{k}\sigma} = 2\tilde{J}_0 S z_{\boldsymbol{k}\sigma} = h_c z_{\boldsymbol{k}\sigma} , \tag{2.45}$$

and

$$z_{\boldsymbol{k}\sigma} = \frac{(u_{\boldsymbol{k}\sigma} + v_{\boldsymbol{k}\sigma})^2 \epsilon_{\boldsymbol{k}\sigma}}{2} = \frac{Z_h + (n^2 + \sigma m^2)\gamma_{\boldsymbol{k}}}{2} . \tag{2.46}$$

The normalization in Eq. (2.43) differs from the normalization in Eqs. (1.43a) and (1.43b), but also guarantees that the transformation is canonical so that

$$[\hat{X}_{\boldsymbol{k}\sigma}, \hat{P}_{\boldsymbol{k}'\sigma'}] = i\delta_{\boldsymbol{k},-\boldsymbol{k}'}\delta_{\sigma,\sigma'} . \tag{2.47}$$

The quadratic part of the spin-wave Hamiltonian is then given by

$$\hat{H}_2 = \frac{1}{2}\sum_{\boldsymbol{k}\sigma} \Delta_{\boldsymbol{k}\sigma}\left[\hat{P}_{-\boldsymbol{k}\sigma}\hat{P}_{\boldsymbol{k}\sigma} + \nu_{\boldsymbol{k}\sigma}^2 \hat{X}_{-\boldsymbol{k}\sigma}\hat{X}_{\boldsymbol{k}\sigma}\right] + E_{0\|}^{(1)} . \tag{2.48}$$

In order to exhibit the relation with the NLSM we have to transform to the fields $\hat{\Pi}_{\boldsymbol{k}\sigma}$ and $\hat{\Phi}_{\boldsymbol{k}\sigma}$ in the continuum limit via

$$\hat{\Psi}_{\boldsymbol{k}\sigma} = p_\sigma \sqrt{\frac{\chi_0}{2VE_{\boldsymbol{k}\sigma}}}\left[E_{\boldsymbol{k}\sigma}\hat{\Pi}_{\boldsymbol{k}\sigma} + i\chi_0^{-1}\hat{\Phi}_{\boldsymbol{k}\sigma}\right] . \tag{2.49}$$

The fields now fulfill the commutation relation

$$[\hat{\Pi}_{\boldsymbol{k}\sigma}, \hat{\Phi}_{\boldsymbol{k}'\sigma'}] = iV\delta_{\boldsymbol{k},-\boldsymbol{k}'}\delta_{\sigma,\sigma'} . \tag{2.50}$$

Note that the variables $\hat{\Phi}_{\boldsymbol{k}\sigma}$ and $\hat{\Pi}_{\boldsymbol{k}\sigma}$ are swapped compared to the definition in section 1.3.2 to match the notation of the fields in the NLSM. In the formula above we have introduced the large S-limit of the uniform transverse susceptibility [86],

$$\chi_0 = (2\tilde{J}_0 a^D)^{-1} . \tag{2.51}$$

The lattice normalization Eq. (2.43) is related to the continuum normalization of Eq. (2.49) by

$$\hat{\Pi}_{\boldsymbol{k}\sigma} = a^D\sqrt{\frac{N}{Sz_{\boldsymbol{k}\sigma}}}\hat{X}_{\boldsymbol{k}\sigma} , \tag{2.52a}$$

$$\hat{\Phi}_{\boldsymbol{k}\sigma} = \sqrt{NSz_{\boldsymbol{k}\sigma}}\hat{P}_{\boldsymbol{k}\sigma} . \tag{2.52b}$$

Writing down the spin-wave Hamiltonian Eq. (2.31) in continuum normalization,

$$\hat{H}_2 = \frac{1}{2V}\sum_{\boldsymbol{k}\sigma}\left[\chi_0^{-1}\hat{\Phi}_{-\boldsymbol{k}\sigma}\hat{\Phi}_{\boldsymbol{k}\sigma} + \chi_0 E_{\boldsymbol{k}\sigma}^2\hat{\Pi}_{-\boldsymbol{k}\sigma}\hat{\Pi}_{\boldsymbol{k}\sigma}\right] + E_{0\|}^{(1)} , \tag{2.53}$$

the correspondence of the field $\hat{\Pi}_{\boldsymbol{k}\sigma}$ to the continuum field representing transverse staggered spin fluctuations in the NLSM is obvious [25].

Since we want to calculate the correction to the magnon spectrum including the regime at short wavelengths, we shall work with the lattice normalization from now on. For later reference we discuss the leading order $1/S$ expansions of the energies introduced above: In this case we have $Z_h = 1$ and thus

$$z_{\boldsymbol{k}+} = (1+\gamma_{\boldsymbol{k}})/2 \;, \tag{2.54a}$$
$$z_{\boldsymbol{k}-} = (1+\alpha\gamma_{\boldsymbol{k}})/2 \;, \tag{2.54b}$$

where $\alpha = n^2 - m^2$. In particular, for $\boldsymbol{k} \to 0$ the quantities have the limits $z_{\boldsymbol{k}+} \to 1$ and $z_{\boldsymbol{k}-} \to (1+\alpha)/2 = n^2$.

2.3.4 Spin-wave interactions

In order to carry out corrections to the magnon spectrum using the $1/S$ expansion we have to express the interaction part of the Hamiltonian in terms of the operators used, in this case $\hat{X}_{\boldsymbol{k}\sigma}$ and $\hat{P}_{\boldsymbol{k}\sigma}$. To obtain the leading $1/S$ correction to linear spin-wave theory it is sufficient to approximate the Hamiltonian by

$$\hat{H} \approx E_0^{\mathrm{cl}} + \hat{H}_1 + \hat{H}_2 + \hat{H}_3 + \hat{H}_4 \;, \tag{2.55}$$

where

$$\hat{H}_4 = \hat{H}_4^{\parallel} + \hat{H}_4^{\perp} \;, \tag{2.56}$$

and we only include terms up to quartic in the boson operators. To use the phase-space path integral formulation it is necessary to symmetrize all expressions in the Hamiltonian whenever powers of non-commuting operators occur [78, 219, B23, B34]. Transforming Eq. (2.16) to Fourier space the linear part of the Hamiltonian is proportional to the operator $\hat{P}_{0-}$,

$$\hat{H}_1 = n\delta h\sqrt{SN}\hat{P}_{0-} \;. \tag{2.57}$$

With the help of the symmetrized products in Eq. (1.82) the cubic part can be written as

$$\begin{aligned}
\hat{H}_3 = &-\sqrt{\frac{N}{2}}\frac{h_c\lambda}{\sqrt{8S}}\hat{P}_{0-} \\
&+ \sqrt{\frac{2}{N}}\sum_{\boldsymbol{k}_1\boldsymbol{k}_2\boldsymbol{k}_3}\delta_{\boldsymbol{k}_1+\boldsymbol{k}_2+\boldsymbol{k}_3,0}\Bigg[\frac{1}{2!}\Gamma^{PXX}_{---}(\boldsymbol{k}_1;\boldsymbol{k}_2,\boldsymbol{k}_3)\Big\{\hat{P}_{\boldsymbol{k}_1-}\hat{X}_{\boldsymbol{k}_2-}\hat{X}_{\boldsymbol{k}_3-}\Big\} \\
&+ \frac{1}{2!}\Gamma^{PXX}_{-++}(\boldsymbol{k}_1;\boldsymbol{k}_2,\boldsymbol{k}_3)\hat{P}_{\boldsymbol{k}_1-}\hat{X}_{\boldsymbol{k}_2+}\hat{X}_{\boldsymbol{k}_3+} + \Gamma^{PXX}_{++-}(\boldsymbol{k}_1;\boldsymbol{k}_2;\boldsymbol{k}_3)\Big\{\hat{P}_{\boldsymbol{k}_1+}\hat{X}_{\boldsymbol{k}_2+}\Big\}\hat{X}_{\boldsymbol{k}_3-} \\
&+ \frac{1}{2!}\Gamma^{PPP}_{-++}(\boldsymbol{k}_1;\boldsymbol{k}_2,\boldsymbol{k}_3)\hat{P}_{\boldsymbol{k}_1-}\hat{P}_{\boldsymbol{k}_2+}\hat{P}_{\boldsymbol{k}_3+} + \frac{1}{3!}\Gamma^{PPP}_{---}(\boldsymbol{k}_1,\boldsymbol{k}_2,\boldsymbol{k}_3)\hat{P}_{\boldsymbol{k}_1-}\hat{P}_{\boldsymbol{k}_2-}\hat{P}_{\boldsymbol{k}_3-}\Bigg] \;,
\end{aligned} \tag{2.58}$$

where the vertices are

$$\Gamma^{PXX}_{---}(\boldsymbol{k}_1;\boldsymbol{k}_2,\boldsymbol{k}_3) = \frac{h_c\lambda}{\sqrt{8S}}\gamma_{\boldsymbol{k}_1} \;, \tag{2.59a}$$

$$\Gamma^{PXX}_{-++}(\boldsymbol{k}_1;\boldsymbol{k}_2,\boldsymbol{k}_3) = \frac{h_c\lambda}{\sqrt{8S}}\left[\gamma_{\boldsymbol{k}_1} - \gamma_{\boldsymbol{k}_2} - \gamma_{\boldsymbol{k}_3}\right] \;, \tag{2.59b}$$

$$\Gamma^{PXX}_{++-}(\boldsymbol{k}_1;\boldsymbol{k}_2;\boldsymbol{k}_3) = \frac{h_c\lambda}{\sqrt{8S}}\gamma_{\boldsymbol{k}_2} \;, \tag{2.59c}$$

$$\Gamma^{PPP}_{-++}(\boldsymbol{k}_1;\boldsymbol{k}_2,\boldsymbol{k}_3) = \frac{h_c\lambda}{\sqrt{8S}}\gamma_{\boldsymbol{k}_1} \;, \tag{2.59d}$$

$$\Gamma^{PPP}_{---}(\boldsymbol{k}_1,\boldsymbol{k}_2,\boldsymbol{k}_3) = \frac{h_c\lambda}{\sqrt{8S}}\left[\gamma_{\boldsymbol{k}_1} + \gamma_{\boldsymbol{k}_2} + \gamma_{\boldsymbol{k}_3}\right] \;. \tag{2.59e}$$

For clarity, we write down the symmetrized products in Eq. (2.58),

$$\left\{\hat{P}_1\hat{X}_2\right\} = \frac{1}{2}\left[\hat{P}_1,\hat{X}_2\right]_+ \;, \tag{2.60}$$

$$\begin{aligned}\left\{\hat{P}_1\hat{X}_2\hat{X}_3\right\} &= \frac{1}{3}(\hat{P}_1\hat{X}_2\hat{X}_3 + \hat{X}_2\hat{X}_3\hat{P}_1) + \frac{1}{6}(\hat{X}_2\hat{P}_1\hat{X}_3 + \hat{X}_3\hat{P}_1\hat{X}_2) \\ &= \frac{1}{2}\left[\hat{P}_1,\hat{X}_2\hat{X}_3\right]_+ \;,\end{aligned} \tag{2.61}$$

using the anti-commutator $[\hat{A}_1,\hat{A}_2]_+ = \hat{A}_1\hat{A}_2 + \hat{A}_2\hat{A}_1$ and the abbreviation for the momentum labels, i.e. $\hat{P}_{\boldsymbol{k}_1} \to \hat{P}_1$. Finally we write down the quartic part Eq. (2.56) in real space

$$\begin{aligned}\hat{H}_4 = &-\frac{n^2}{2}\sum_{ij}J_{ij}\Big[n_in_j + \frac{1}{4}\Big(n_ib_ib_j + b_in_jb_j + b_i^\dagger b_j^\dagger n_j + b_i^\dagger n_ib_j^\dagger\Big)\Big] \\ &+ \frac{m^2}{2}\sum_{ij}J_{ij}\Big[n_in_j - \frac{1}{4}\Big(n_ib_ib_j^\dagger + b_ib_j^\dagger n_j + b_i^\dagger n_ib_j + b_i^\dagger n_jb_j\Big)\Big] \;,\end{aligned} \tag{2.62}$$

and transform it to momentum space. With the transformation of Eq. (2.43) it is rewritten in terms of Hermitian operators $\hat{X}_{\boldsymbol{k}\sigma}$ and $\hat{P}_{\boldsymbol{k}\sigma}$,

$$\hat{H}_4 = E^{(2)}_{0\|} + \delta\hat{H}'_2 + \hat{H}'_4 \;. \tag{2.63}$$

Due to the symmetrization of $\hat{H}'_4$ which is given in the Appendix A.2 we get a $1/S^2$ correction to the classical ground-state energy,

$$E^{(2)}_{0\|} = -\frac{NDJS^2\alpha}{(2S)^2} \;, \tag{2.64}$$

and a $1/S$ correction to the quadratic part,

$$\delta\hat{H}'_2 = \frac{1}{2}\sum_{\boldsymbol{k}\sigma}\Big[\Gamma^P_\sigma(\boldsymbol{k})\hat{P}_{-\boldsymbol{k}\sigma}\hat{P}_{\boldsymbol{k}\sigma} + \Gamma^X_\sigma(\boldsymbol{k})\hat{X}_{-\boldsymbol{k}\sigma}\hat{X}_{\boldsymbol{k}\sigma}\Big] \;, \tag{2.65}$$

where the vertices are given by

$$\Gamma^P_\sigma(\boldsymbol{k}) = \frac{h_c}{4S}\alpha(1+\sigma\gamma_{\boldsymbol{k}}) \;, \tag{2.66a}$$

$$\Gamma^X_\sigma(\boldsymbol{k}) = \frac{h_c}{4S}(\alpha-\sigma\gamma_{\boldsymbol{k}}) \;. \tag{2.66b}$$

Let us once more emphasize that the corresponding interaction vertices of $\hat{H}'_4$ are nonsingular functions of the external momenta and analytic functions of h^2, similar to all quantities arising from linear spin-wave theory, compare section 2.3.2.

2.4 Effective action for the staggered spin fluctuations

In a previous work by Hasselmann and Kopietz [86] the connection between the magnon quasiparticle operators of the $1/S$ expansion and the continuum fields $\hat{\Pi}_{\boldsymbol{k}\sigma}$ describing transverse fluctuations of the staggered magnetization in the NLSM has been discussed. However, a calculation using these Hermitian fields has not yet been performed. This will be done in the following discussion: We will derive the effective action for the staggered spin fluctuations of the Hamiltonian Eq. (2.1) carrying out sub-leading $1/S$ corrections and short wavelength fluctuations in the entire Brillouin zone. The procedure will be the following: The operators $\hat{P}_\sigma$ correspond to transverse fluctuations of the total spin. At weak magnetic fields these ferromagnetic fluctuations are suppressed. In contrast to that, the staggered (antiferromagnetic) fluctuations will directly be connected to the antiferromagnetic magnons. To calculate the self-energy corrections of those quasiparticles we can therefore integrate out the degrees of freedom associated with the generalized momenta $\hat{P}_\sigma$.

2.4.1 Imaginary time phase-space path integral formulation

An appropriate formulation for integrating out the ferromagnetic fluctuations is the imaginary-time phase-space path integral. As a generalization of the one-dimensional quantum mechanical system discussed in section 1.5.1, the partition function is defined as

$$\mathcal{Z} = \int \mathcal{D}[P_\sigma, X_\sigma]\, e^{-S[P_\sigma, X_\sigma]} \;, \tag{2.67}$$

where the Euclidean action corresponding to our spin-wave Hamiltonian is of the form

$$S[P_\sigma, X_\sigma] = \sum_{l=0}^{\infty} S_l[P_\sigma, X_\sigma] \;. \tag{2.68}$$

Recall that the terms $S_l[P_\sigma, X_\sigma]$ containing l powers of the fields can be obtained directly form the parts of the Hamiltonian $\hat{H}_l$ containing l powers of field operators, once the terms $\hat{H}_l$ have been symmetrized with respect to non-commuting operators [78, B34]. In the next step the operators are replaced by their eigenvalues. The quantum fields $P_{\boldsymbol{k}\sigma}(\tau)$ and $X_{\boldsymbol{k}\sigma}(\tau)$ depend on imaginary time. To get rid of the derivative of the measure term $iP_\sigma \partial X_\sigma/\partial\tau$ in the Gaussian action we expand the quantum fields in frequency space,

$$P_{\boldsymbol{k}\sigma}(\tau) = \sum_\omega e^{-i\omega\tau} P_{K\sigma} \ , \tag{2.69a}$$

$$X_{\boldsymbol{k}\sigma}(\tau) = \sum_\omega e^{-i\omega\tau} X_{K\sigma} \ . \tag{2.69b}$$

On the right-hand side we combined the momenta $\boldsymbol{k}$ and the bosonic Matsubara frequencies $i\omega$ to a composite label $K = (\boldsymbol{k}, i\omega)$. The next step is now to obtain the Gaussian propagators. As in linear spin-wave theory we truncate the expansion Eq. (2.68) at the term $l = 2$, yielding the following contributions to the action $S[P_\sigma, X_\sigma]$,

$$S_0 = \beta[E_0^{\mathrm{cl}} + E_{0\|}^{(1)}] \ , \tag{2.70a}$$

$$S_1[P_-] = \beta n \delta h \sqrt{SN} P_{0-} \ , \tag{2.70b}$$

$$S_2[P_\sigma, X_\sigma] = \frac{\beta}{2} \sum_{K,\sigma} \Big[\Delta_{\boldsymbol{k}\sigma} \Big(P_{-K\sigma} P_{K\sigma} + \nu_{\boldsymbol{k}\sigma}^2 X_{-K\sigma} X_{K\sigma} \Big) - \omega \Big(P_{-K\sigma} X_{K\sigma} - X_{-K\sigma} P_{K\sigma} \Big) \Big] \ . \tag{2.70c}$$

As in the pure spin-wave approach the canting angle is determined from the condition that the functional average of the field $P_{\boldsymbol{k}=0-}$ vanishes,

$$\langle P_{0-} \rangle = 0 \ . \tag{2.71}$$

This equation then defines the correction $\delta h = h - h_c m = h - h_c \sin\vartheta$ which can be transformed to the sine of the renormalized canting angle,

$$\sin\vartheta = m = (h - \delta h)/h_c \ . \tag{2.72}$$

This condition simplifies to the classical result Eq. (2.40) within Gaussian approximation, and hence also $S_1[P_-] = 0$ in this case. The Gaussian propagators can then easily be read off from the result of the Gaussian integrals. An inversion of the matrix propagator yields

$$\langle X_{K\sigma} X_{K'\sigma'} \rangle_0 = \delta_{K,-K'} \delta_{\sigma\sigma'} (\beta\Delta_{\boldsymbol{k}\sigma})^{-1} \frac{\Delta_{\boldsymbol{k}\sigma}^2}{E_{\boldsymbol{k}\sigma}^2 + \omega^2} \ , \tag{2.73a}$$

$$\langle P_{K\sigma} P_{K'\sigma'} \rangle_0 = \delta_{K,-K'} \delta_{\sigma\sigma'} (\beta\Delta_{\boldsymbol{k}\sigma})^{-1} \frac{E_{\boldsymbol{k}\sigma}^2}{E_{\boldsymbol{k}\sigma}^2 + \omega^2} \ , \tag{2.73b}$$

$$\langle X_{K\sigma} P_{K'\sigma'} \rangle_0 = \delta_{K,-K'} \delta_{\sigma\sigma'} (\beta\Delta_{\boldsymbol{k}\sigma})^{-1} \frac{\Delta_{\boldsymbol{k}\sigma}\omega}{E_{\boldsymbol{k}\sigma}^2 + \omega^2} \ . \tag{2.73c}$$

Here the symbol $\langle \ldots \rangle_0$ denotes the functional averaging with the Gaussian action $S_2[P_\sigma, X_\sigma]$. Note the identity $\langle X_{K\sigma} P_{K'\sigma'} \rangle_0 = -\langle P_{K'\sigma'} X_{K\sigma} \rangle_0$ that leads to the expectation value of the symmetric operator $\langle \{\hat{X}_{\boldsymbol{k}\sigma} \hat{P}_{\boldsymbol{k}\sigma}\} \rangle_0 = 0$. Observing the asymptotic behavior $\propto 1/\omega$ of the Gaussian propagator Eq. (2.73c) for large frequencies, it is necessary to regularize formally divergent Matsubara sums introducing a convergence factor $\cos(\omega 0^+)$ which is an even function of ω,

$$\langle \{\hat{X}_{\boldsymbol{k}\sigma} \hat{P}_{\boldsymbol{k}\sigma}\} \rangle_0 = \frac{1}{\beta} \sum_\omega \frac{\omega \cos(\omega 0^+)}{E_{\boldsymbol{k}\sigma}^2 + \omega^2} = 0 \; . \tag{2.74}$$

We integrate over the generalized momenta to define the effective action $S_{\text{eff}}[X_\sigma]$ for the staggered fluctuations via

$$e^{-S_{\text{eff}}[X_\sigma]} = \int \mathcal{D}[P_\sigma] \, e^{-S[P_\sigma, X_\sigma]} \; . \tag{2.75}$$

Already at this point, the solution of the Gaussian integral,

$$e^{-S_{\text{eff}}[X_\sigma]} \approx e^{-S_0} \int \mathcal{D}[P_\sigma] \, e^{-S_2[P_\sigma, X_\sigma]} \; , \tag{2.76}$$

yields the effective action for the fields X_σ to leading order in $1/S$. Adding the quadratic complement we use the shifted Gaussian integral Eq. (1.83) and its multidimensional generalization, see Eq. (1.84), to carry out the integration. Absorbing constant terms in the definition of the path integral [B23] the effective action reads $S_{\text{eff}}[X_\sigma] = S_0 + S_{\text{eff}}^{(0)}[X_\sigma]$ where the fluctuating part is given by

$$S_{\text{eff}}^{(0)}[X_\sigma] = \frac{\beta}{2} \sum_{K\sigma} \frac{E_{\boldsymbol{k}\sigma}^2 + \omega^2}{\Delta_{\boldsymbol{k}\sigma}} X_{-K\sigma} X_{K\sigma} \; . \tag{2.77}$$

Considering the expansions Eqs. (2.37a) and (2.37b) one observes that this action has the same form as the Gaussian part of the action in the NLSM, compare section 1.4.6.

2.4.2 $1/S$ corrections to the effective action

As in spin-wave theory we obtain the higher $1/S$ corrections to the effective action $S_{\text{eff}}[X_\sigma]$ by including the spin-wave interactions perturbatively. Rewriting Eq. (2.75) as

$$S_{\text{eff}}[X_\sigma] = S_0 + S_{\text{eff}}^{(0)}[X_\sigma] + S_{\text{eff}}^{\text{int}}[X_\sigma] \; , \tag{2.78}$$

and taking into account that it is possible to factorize and reorganize the integrations in the functional integral we get

$$e^{-S_{\text{eff}}[X_\sigma]} = e^{-S_0} e^{-S_{\text{eff}}^{(0)}[X_\sigma]} \left\langle e^{-S_{\text{int}}[P_\sigma, X_\sigma]} \right\rangle_P \; . \tag{2.79}$$

This finally defines the interaction part $S_{\text{eff}}^{\text{int}}[X_\sigma]$ as the functional average,

$$\begin{aligned} S_{\text{eff}}^{\text{int}}[X_\sigma] &= -\ln \left\langle e^{-S_{\text{int}}[P_\sigma, X_\sigma]} \right\rangle_P \\ &\equiv -\ln \left[\frac{\int \mathcal{D}[P_\sigma] \, e^{-S_2[P_\sigma, X_\sigma]} e^{-S_{\text{int}}[P_\sigma, X_\sigma]}}{\int \mathcal{D}[P_\sigma] \, e^{-S_2[P_\sigma, X_\sigma]}} \right] \; , \end{aligned} \tag{2.80}$$

where in the integrand the Gaussian part of the action is separated from the interaction part,

$$S_{\rm int}[P_\sigma, X_\sigma] = S_1[P_-] + \sum_{l=3}^{\infty} S_l[P_\sigma, X_\sigma] \; . \tag{2.81}$$

Now, performing the calculation, it is necessary to sort out the terms regarding their powers in $1/S$: The leading correction arises from the first-order correction due to $S_4[P_\sigma, X_\sigma]$, and the second order corrections due to the sum of $S_1[P_-]$ and $S_3[P_\sigma, X_\sigma]$. In the Hamiltonian formulation the first term corresponds to $\hat{H}_4$ defined in Eqs. (2.63, 2.64, 2.65, A.2), while the second term has its counterpart in $\hat{H}' \approx \hat{H}_1 + \hat{H}_3$ defined in Eqs. (2.57) and (2.58).

We now write down the condition $\langle P_{0-} \rangle = 0$ for the canting angle and expand in powers of $1/S$. Recalling the definition of the Gaussian average, this can be written as

$$\left\langle P_{0-} e^{-S_{\rm int}[P_\sigma, X_\sigma]} \right\rangle_0 = 0 \; , \tag{2.82}$$

where we expand

$$e^{-S_{\rm int}[P_\sigma, X_\sigma]} \approx 1 - S_{\rm int}[P_\sigma, X_\sigma] + \frac{1}{2} S_{\rm int}[P_\sigma, X_\sigma]^2 + \dots \; , \tag{2.83}$$

and only consider the terms to relative order $1/S$,

$$S_{\rm int}[P_\sigma, X_\sigma] \approx S_1[P_{0-}] + S_3[P_\sigma, X_\sigma] \; , \tag{2.84a}$$

$$S_{\rm int}[P_\sigma, X_\sigma]^2 \approx \Big(S_1[P_{0-}] + S_3[P_\sigma, X_\sigma] \Big)^2 \approx S_1[P_{0-}]^2 \; . \tag{2.84b}$$

Since only integrals with an even number of the fields P_{0-} contribute, the condition for the canting angle simplifies to

$$\left\langle P_{0-} \Big(S_1[P_{0-}] + S_3[P_\sigma, X_\sigma] \Big) \right\rangle_0 = 0 \; . \tag{2.85}$$

Now we see that to order $1/S$ the difference $\delta h = h - h_c m$ and hence $S_1[P_-]$ are finite. Carrying out the Gaussian averages using the propagators Eqs. (2.73a–2.73c) and the special values of the vertices,

$$\Gamma^{PXX}_{---}(0; -K, K) = \frac{h_c \lambda}{\sqrt{8S}} \; , \tag{2.86a}$$

$$\Gamma^{PXX}_{-++}(0; -K, K) = \frac{h_c \lambda}{\sqrt{8S}} (1 - 2\gamma_{\boldsymbol{k}}) \; , \tag{2.86b}$$

$$\Gamma^{PPP}_{---}(0, -K, K) = \frac{h_c \lambda}{\sqrt{8S}} (1 + 2\gamma_{\boldsymbol{k}}) \; , \tag{2.86c}$$

one can combine the difference to

$$\delta h = m[1 - C_2(h)] \frac{h_c}{2S} \; , \tag{2.87}$$

which contains corrections to first order in $1/S$ in the numerical constant

$$\begin{aligned} C_2(h) &= \frac{1}{N}\sum_{\boldsymbol{k}\sigma}\left[u_{\boldsymbol{k}\sigma}^2 + v_{\boldsymbol{k}\sigma}^2 - \sigma\gamma_{\boldsymbol{k}}(u_{\boldsymbol{k}\sigma}+\sigma v_{\boldsymbol{k}\sigma})^2\right] \\ &= \frac{1}{N}\sum_{\boldsymbol{k}\sigma}\frac{1-\gamma_{\boldsymbol{k}}^2-\sigma n^2\gamma_{\boldsymbol{k}}}{\epsilon_{\boldsymbol{k}\sigma}}\ . \end{aligned} \tag{2.88}$$

This result, Eq. (2.87), yields the same $1/S$ corrections to the canting angle and the uniform magnetization m as in Ref. [234]. For the following let us point out that $S_1[P_-]$ is of the order $S^{-1/2}$ and has to be taken together with $S_3[P_\sigma, X_\sigma]$ in second order perturbation theory to sum up all corrections of relative order $1/S$. Taking into account the correction to the canting angle by help of the condition Eq. (2.87) we obtain for the total contribution of order $S^{-1/2}$ to our action $S'[P_\sigma, X_\sigma]$ corresponding to $\hat{H}'$ in Eq. (2.3b),

$$\begin{aligned} S'[P_\sigma, X_\sigma] &\approx S_1[P_-] + S_3[P_\sigma, X_\sigma] \\ &= -\beta\sqrt{\frac{N}{2}}\frac{h_c\lambda}{\sqrt{8S}}C_2(h)P_{0-} \\ &+ \beta\sqrt{\frac{2}{N}}\sum_{K_1K_2K_3}\delta_{K_1+K_2+K_3,0}\Bigg[\frac{1}{2!}\Gamma^{PXX}_{---}(\boldsymbol{k}_1;\boldsymbol{k}_2,\boldsymbol{k}_3)P_{K_1-}X_{K_2-}X_{K_3-} \\ &+ \frac{1}{2!}\Gamma^{PXX}_{-++}(\boldsymbol{k}_1;\boldsymbol{k}_2,\boldsymbol{k}_3)P_{K_1-}X_{K_2+}X_{K_3+} + \Gamma^{PXX}_{++-}(\boldsymbol{k}_1;\boldsymbol{k}_2;\boldsymbol{k}_3)P_{K_1+}X_{K_2+}X_{K_3-} \\ &+ \frac{1}{2!}\Gamma^{PPP}_{-++}(\boldsymbol{k}_1;\boldsymbol{k}_2,\boldsymbol{k}_3)P_{K_1-}P_{K_2+}P_{K_3+} + \frac{1}{3!}\Gamma^{PPP}_{---}(\boldsymbol{k}_1,\boldsymbol{k}_2,\boldsymbol{k}_3)P_{K_1-}P_{K_2-}P_{K_3-}\Bigg]\ . \end{aligned} \tag{2.89}$$

Using again the expansion Eq. (2.83), but now with the action including the renormalization of the canting angle, we collect all terms to the effective action

$$S_{\text{eff}}^{\text{int}}[X_\sigma] = S_{\text{eff}}^{(1/2)}[X_\sigma] + S_{\text{eff}}^{(1)}[X_\sigma] + \dots\ , \tag{2.90}$$

where the superscript indicates the power of $1/S$. Explicitly we have

$$S_{\text{eff}}^{(1/2)}[X_\sigma] = \langle S'[P_\sigma, X_\sigma]\rangle_P\ , \tag{2.91a}$$

$$S_{\text{eff}}^{(1)}[X_\sigma] = \langle S_4[P_\sigma, X_\sigma]\rangle_P - \frac{1}{2}\Big\langle\Big(S'[P_\sigma, X_\sigma] - \langle S'[P_\sigma, X_\sigma]\rangle_P\Big)^2\Big\rangle_P\ . \tag{2.91b}$$

The Gaussian averages of the field $P_{\boldsymbol{k}\sigma}$ for fixed $X_{\boldsymbol{k}\sigma}$ in Eqs. (2.91a) and (2.91b) are given by

$$\begin{aligned} \langle P_{K\sigma}\rangle_P &= \frac{\int\mathcal{D}[P_\sigma]\, e^{-S_2[P_\sigma,X_\sigma]}P_{K\sigma}}{\int\mathcal{D}[P_\sigma]\, e^{-S_2[P_\sigma,X_\sigma]}} \\ &= \frac{e^{-S_{\text{eff}}^{(0)}[X_\sigma]}\frac{\omega}{\Delta_{\boldsymbol{k}\sigma}}X_{K\sigma}}{e^{-S_{\text{eff}}^{(0)}[X_\sigma]}} = \frac{\omega}{\Delta_{\boldsymbol{k}\sigma}}X_{K\sigma}\ . \end{aligned} \tag{2.92}$$

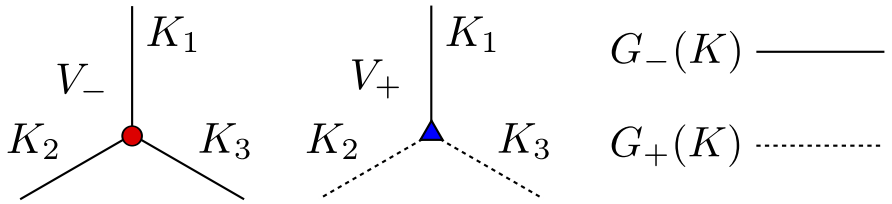

Figure 2.3: *Graphical representation of the interaction vertices $V_+(K_1, K_2, K_3)$ and $V_-(K_1, K_2, K_3)$ defined in Eqs. (2.95a) and (2.95b) (left). Solid lines represent propagators $G_-(K)$ of the gapless field X_-, while dashed lines correspond to those of the gapped field X_+ (right). Note that the propagators of the Hermitian fields are not directed, i.e. do not have any arrows. The shape of the symbols reflects the symmetry of the vertices with respect to the permutation of the labels.*

This gives rise to the $1/\sqrt{S}$ correction

$$S_{\text{eff}}^{(1/2)}[X_\sigma] = \beta\sqrt{\frac{2}{N}} \sum_{K_1K_2K_3} \delta_{K_1+K_2+K_3,0} \Big[\frac{1}{3!}\Gamma^{(3)}_{---}(K_1, K_2, K_3) X_{K_1-} X_{K_2-} X_{K_3-} + \frac{1}{2!}\Gamma^{(3)}_{-++}(K_1; K_2, K_3) X_{K_1-} X_{K_2+} X_{K_3+} \Big] , \tag{2.93}$$

with the fully symmetrized vertices

$$\Gamma^{(3)}_{---}(K_1, K_2, K_3) = \frac{h_c\lambda}{\sqrt{8S}} \Big[\frac{\gamma_{\boldsymbol{k}_1}\omega_1}{\Delta_{\boldsymbol{k}_1-}} + \frac{\gamma_{\boldsymbol{k}_2}\omega_2}{\Delta_{\boldsymbol{k}_2-}} + \frac{\gamma_{\boldsymbol{k}_3}\omega_3}{\Delta_{\boldsymbol{k}_3-}} + \frac{(\gamma_{\boldsymbol{k}_1} + \gamma_{\boldsymbol{k}_2} + \gamma_{\boldsymbol{k}_2})\omega_1\omega_2\omega_3}{\Delta_{\boldsymbol{k}_1-}\Delta_{\boldsymbol{k}_2-}\Delta_{\boldsymbol{k}_3-}} \Big] , \tag{2.94a}$$

$$\Gamma^{(3)}_{-++}(K_1; K_2, K_3) = \frac{h_c\lambda}{\sqrt{8S}} \Big[(\gamma_{\boldsymbol{k}_1} - \gamma_{\boldsymbol{k}_2} - \gamma_{\boldsymbol{k}_3}) \frac{\omega_1}{\Delta_{\boldsymbol{k}_1-}} + \frac{\gamma_{\boldsymbol{k}_2}\omega_3}{\Delta_{\boldsymbol{k}_3+}} + \frac{\gamma_{\boldsymbol{k}_3}\omega_2}{\Delta_{\boldsymbol{k}_2+}} + \frac{\gamma_{\boldsymbol{k}_1}\omega_1\omega_2\omega_3}{\Delta_{\boldsymbol{k}_1-}\Delta_{\boldsymbol{k}_2+}\Delta_{\boldsymbol{k}_3+}} \Big] . \tag{2.94b}$$

For the calculation of the self-energy in the upcoming section, only the frequency-dependent terms will be crucial to give rise to nonanalytic contributions. Due to energy conservation restrictions in the on-resonance calculation later on, one can omit all terms cubic in the frequencies which come from the terms cubic in the fields $P_{K\sigma}$ in Eq. (2.89). Below we will therefore use a simplified action obtained by the replacement

$$\Gamma^{(3)}_{---}(K_1, K_2, K_3) \to V_-(K_1, K_2, K_3) \equiv \frac{h_c\lambda}{\sqrt{8S}} \Big[\frac{\gamma_{\boldsymbol{k}_1}\omega_1}{\Delta_{\boldsymbol{k}_1-}} + \frac{\gamma_{\boldsymbol{k}_2}\omega_2}{\Delta_{\boldsymbol{k}_2-}} + \frac{\gamma_{\boldsymbol{k}_3}\omega_3}{\Delta_{\boldsymbol{k}_3-}} \Big] , \tag{2.95a}$$

$$\Gamma^{(3)}_{-++}(K_1; K_2, K_3) \to V_+(K_1, K_2, K_3) \equiv \frac{h_c\lambda}{\sqrt{8S}} \Big[(\gamma_{\boldsymbol{k}_1} - \gamma_{\boldsymbol{k}_2} - \gamma_{\boldsymbol{k}_3}) \frac{\omega_1}{\Delta_{\boldsymbol{k}_1-}} + \frac{\gamma_{\boldsymbol{k}_2}\omega_3}{\Delta_{\boldsymbol{k}_3+}} + \frac{\gamma_{\boldsymbol{k}_3}\omega_2}{\Delta_{\boldsymbol{k}_2+}} \Big] . \tag{2.95b}$$

For later reference we also introduce the graphical representation of the interaction vertices and the propagators shown in Fig. 2.3.

2.4.3 Comparison to NLSM

Taking the NLSM from section 1.4.6 and substituting $\partial_\tau \to \partial_\tau - i\boldsymbol{h}\times$ for obtaining the corresponding model for finite magnetic field, one gets the Euclidean action in the presence of a uniform magnetic field, Eq. (1.76), which still only depends on two parameters, the spin stiffness ρ_s and the (renormalized) spin-wave velocity c. From Eqs. (2.39a) and (2.39b) it is clear that the spin-wave velocities for the modes of our magnet differ. As pointed out in the work by Hasselmann *et al.* [87] the spin-wave mode polarized parallel to the magnetic field involves a different spin-wave velocity than the mode polarized perpendicular to the magnetic field. Subsequently, we will actually calculate the $1/S$ corrections to the spin-wave velocity $c_-(h)$ of the gapless magnon and show that the magnetic field dependence is nonanalytic in h^2. To compare our spin-wave approach with the NLSM we parametrize the magnetization as $\boldsymbol{M} = \chi\boldsymbol{h}$ with $\chi = \rho_s/c^2$. Expanding the term of the covariant derivative as

$$(\partial_\tau\boldsymbol{\Omega} - i\boldsymbol{h}\times\boldsymbol{\Omega})^2 = (\partial_\tau\boldsymbol{\Omega})^2 - 2i\boldsymbol{h}\cdot(\boldsymbol{\Omega}\times\partial_\tau\boldsymbol{\Omega}) + (\boldsymbol{\Omega}\cdot\boldsymbol{h})^2 - \boldsymbol{\Omega}^2\boldsymbol{h}^2 \;, \tag{2.96}$$

and using $|\boldsymbol{\Omega}| = 1$ we rewrite the Euclidean action Eq. (1.76) as

$$\begin{aligned} S_{\mathrm{NLSM}}[\boldsymbol{\Omega}] = \frac{\rho_s}{2}\int_0^\beta d\tau \int d^D r \left[\sum_{\mu=1}^{D}(\partial_\mu\boldsymbol{\Omega})^2 + c^{-2}(\partial_\tau\boldsymbol{\Omega})^2\right] \\ - \beta V\frac{\chi}{2}h^2 + \frac{\chi}{2}\int_0^\beta d\tau\int d^D r(\boldsymbol{h}\cdot\boldsymbol{\Omega})^2 \\ - i\int_0^\beta d\tau\int d^D r\,\boldsymbol{M}\cdot(\boldsymbol{\Omega}\times\partial_\tau\boldsymbol{\Omega}) \;. \end{aligned} \tag{2.97}$$

Choosing now the coordinate system such that the staggered magnetization points in direction $\boldsymbol{e}_y$ and considering the direction of the magnetic field $\boldsymbol{h} = h\boldsymbol{e}_z$ (compare also Fig. 2.1) we set $\boldsymbol{\Omega} = \sqrt{1-\boldsymbol{\Pi}^2}\boldsymbol{e}_y + \boldsymbol{\Pi}$, i.e.

$$\boldsymbol{\Omega} = \begin{pmatrix} \Omega_x \\ \Omega_y \\ \Omega_z \end{pmatrix} = \begin{pmatrix} \Pi_- \\ \sqrt{1-\boldsymbol{\Pi}^2} \\ \Pi_+ \end{pmatrix} \;, \tag{2.98}$$

where the transverse fluctuations are parametrized as

$$\boldsymbol{\Pi} = \Pi_+\boldsymbol{e}_z + \Pi_-\boldsymbol{e}_x \;. \tag{2.99}$$

This automatically fulfills the normalization condition of the field $|\boldsymbol{\Omega}| = 1$. For small fluctuations we expand Eq. (2.97) in powers of the transverse fluctuations $\boldsymbol{\Pi}$,

$$\Omega_y = \sqrt{1-(\Pi_+^2+\Pi_-^2)} \approx 1 - \frac{1}{2}(\Pi_+^2+\Pi_-^2) \;, \tag{2.100}$$

to obtain an approximation for the effective action in momentum frequency space,

$$S_{\mathrm{NLSM}}[\mathbf{\Omega}] \approx -\beta V \frac{\chi}{2} h^2 + \frac{\chi}{2} \int_K \sum_\sigma \left(\omega^2 + c^2 \boldsymbol{k}^2 + m_\sigma^2\right) \Pi_{-K\sigma} \Pi_{K\sigma} + \chi h \int_{K,K'} \omega \, \Pi_{K'+} \Pi_{-K-K'+} \Pi_{K-} + O(\Pi_{K\sigma}^4) \; , \tag{2.101}$$

where we have defined the two masses as $m_-^2 = 0$ and $m_+^2 = h^2$. For a comparison one still has to expand the vertices Eqs. (2.94a) and (2.94b) since the NLSM is only valid to leading order in the derivatives. Using the expansions Eqs. (2.54a) and (2.54b) we set $\Delta_{\boldsymbol{k}\sigma} \approx h_c$ and obtain to leading order in frequencies and momenta

$$\Gamma^{(3)}_{---}(K_1, K_2, K_3) \approx \frac{\lambda}{\sqrt{8S}} [\omega_1 + \omega_2 + \omega_3] = 0 \; , \tag{2.102a}$$

$$\Gamma^{(3)}_{-++}(K_1; K_2, K_3) \approx \frac{\lambda}{\sqrt{8S}} [-\omega_1 + \omega_2 + \omega_3] = -2 \frac{\lambda}{\sqrt{8S}} \omega_1 \; . \tag{2.102b}$$

In the last equal sign of the equations above we have used the energy conservation $\omega_1 + \omega_2 + \omega_3 = 0$ at the vertices. Taking also into account the prefactors that connect the representation in lattice normalization and continuum normalization, Eqs. (2.52a) and (2.52b), one sees that the continuum limit of the lattice action $S_{\mathrm{eff}}^{(1/2)}[X_\sigma]$ in Eq. (2.93) reduces to the cubic term in the expansion of the NLSM, Eq. (2.101).

2.5 Perturbation theory

2.5.1 Dyson equation and frequency-dependent part of the self-energy

In order to calculate the correction to the magnon spectrum of the gapless mode to order $1/S$ we consider the effective action derived in the last section and work with a model which only contains the degrees of freedom of the staggered (antiferromagnetic) spin fluctuations $X_{\boldsymbol{k}\sigma}$. From the Gaussian action, Eq. (2.77), we read off the noninteracting propagators of this field with the help of the Gaussian integral Eq. (1.84),

$$G_{0,\sigma}(K) \equiv \beta \langle X_{K\sigma} X_{-K\sigma} \rangle_0 = \frac{\Delta_{\boldsymbol{k}\sigma}}{E_{\boldsymbol{k}\sigma}^2 + \omega^2} \; . \tag{2.103}$$

The full propagators can now be expressed in terms of the self-energies $\Sigma_\sigma(K)$ as

$$G_\sigma^{-1}(K) = G_{0,\sigma}^{-1}(K) + \Sigma_\sigma(K) \; . \tag{2.104}$$

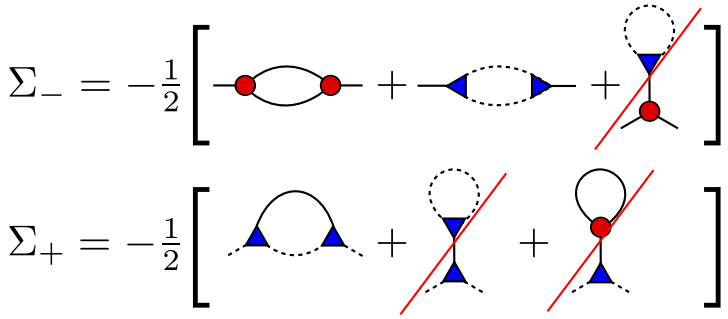

Figure 2.4: *Feynman diagrams of the self-energy corrections to second order in the three-legged vertices, see Eqs. (2.106a) and (2.106b). The slashed tadpole diagrams give frequency-independent contributions of order $1/S$ which are analytic functions of the magnetic field. Since in this work we are only interested in the frequency-dependent part of the self-energy, we shall omit these tadpole diagrams.*

Following the procedure of the $1/S$ expansion, the self-energy can be written as

$$\Sigma'_{-}(K) = \frac{1}{\beta N}\Big[\sum_{K'}\sum_{\sigma} G_{0,\sigma}(K')G_{0,\sigma}(K'+K)V_{\sigma}^{2}(K,K',-K-K') - G_{0,-}(0)V_{-}(K,K,0)\sum_{K'} G_{+}(K')V_{+}(0,K',K')\Big] , \tag{2.105a}$$

$$\Sigma'_{+}(K) = \frac{1}{\beta N}\Big[\sum_{K'} G_{0,-}(K')G_{0,+}(K'+K)V_{+}^{2}(K',K,-K-K') - G_{0,-}(0)V_{+}(0,K,K)\sum_{K'}\sum_{\sigma} G_{0,\sigma}(K')V_{\sigma}(0,K',K')\Big] . \tag{2.105b}$$

Focusing on the frequency-dependent contribution we may replace $\Sigma'_{\sigma}(K) \to \Sigma_{\sigma}(K)$, see also Fig. 2.4. Using the symmetry $V_{\sigma}(-K,-K',K+K') = -V_{\sigma}(K,K',-K-K')$ the self-energy of the gapless magnon can be simplified to

$$\Sigma_{-}(K) = \frac{1}{\beta N}\sum_{K'}\sum_{\sigma} G_{0,\sigma}(K')G_{0,\sigma}(K'+K)V_{\sigma}^{2}(K,K',-K-K') , \tag{2.106a}$$

whereas the self-energy of the gapped magnon mode reads

$$\Sigma_{+}(K) = \frac{1}{\beta N}\sum_{K'} G_{0,-}(K')G_{0,+}(K'+K)V_{+}^{2}(K',K,-K-K') . \tag{2.106b}$$

Note that there is an asymmetry regarding the contributing terms, since we have only one vertex which mixes the gapped and the gapless fields. All terms of the self-energy can be read off from the Feynman diagrams in Fig. 2.4.

Next, we carry out the frequency integrations analytically by use of the relevant integrals,

$$I^{(n)}(E_1,E_2,\omega)=\int_{-\infty}^{\infty}\frac{dx}{2\pi}\frac{x^n}{[x^2+E_1^2][(x+\omega)^2+E_2^2]} =\frac{i^n}{2}\left[\frac{E_1^{n-1}}{E_2^2-(E_1-i\omega)^2}+\frac{(E_2+i\omega)^n}{E_2[E_1^2-(E_2+i\omega)^2]}\right], \tag{2.107}$$

for $n=0,1,2$. Explicitly, we need the integrals

$$I^{(0)}=\frac{E_1+E_2}{2E_1E_2[(E_1+E_2)^2+\omega^2]}, \tag{2.108a}$$

$$I^{(1)}=-\frac{\omega}{2E_2[(E_1+E_2)^2+\omega^2]}, \tag{2.108b}$$

$$I^{(2)}=\frac{E_2(E_1+E_2)+\omega^2}{2E_2[(E_1+E_2)^2+\omega^2]}, \tag{2.108c}$$

which can be calculated using complex integration and the Residue theorem. For simplification of the integrals we use the identity

$$\sum_{\boldsymbol{q}}f(\boldsymbol{q})\gamma_{\boldsymbol{k}+\boldsymbol{q}}=\gamma_{\boldsymbol{k}}\sum_{\boldsymbol{q}}f(\boldsymbol{q})\gamma_{\boldsymbol{q}}, \tag{2.109}$$

which holds if the total integrand only contains even powers of q_i, where $\boldsymbol{q}=(q_1,\ldots,q_D)$. For the QAFM on a hypercubic lattice we have $\gamma_{\boldsymbol{k}}=\gamma_{-\boldsymbol{k}}$, see Eq. (2.19); thus the condition reduces to $f(\boldsymbol{q})=f(-\boldsymbol{q})$. The result of the self-energies then reads

$$\begin{aligned}\Sigma_-(K)=\frac{h_c^2\lambda^2}{16S}\frac{2}{N}\sum_{\boldsymbol{q}}\Big\{&z_{\boldsymbol{q}+}z_{\boldsymbol{k}-\boldsymbol{q}+}\Big[M_0^2(\boldsymbol{k},\boldsymbol{q})I_{++}^{(0)}(i\omega,\boldsymbol{k},\boldsymbol{q})\\&+2M_0(\boldsymbol{k},\boldsymbol{q})M_+(\boldsymbol{k},\boldsymbol{q})I_{++}^{(1)}(i\omega,\boldsymbol{k},\boldsymbol{q})+M_+^2(\boldsymbol{k},\boldsymbol{q})I_{++}^{(2)}(i\omega,\boldsymbol{k},\boldsymbol{q})\Big]\\&+z_{\boldsymbol{q}-}z_{\boldsymbol{k}-\boldsymbol{q}-}\Big[M_-^2(\boldsymbol{k},\boldsymbol{q})I_{--}^{(0)}(i\omega,\boldsymbol{k},\boldsymbol{q})\\&+2M_-(\boldsymbol{k},\boldsymbol{q})M_-(\boldsymbol{q},\boldsymbol{k})I_{--}^{(1)}(i\omega,\boldsymbol{k},\boldsymbol{q})+M_-^2(\boldsymbol{q},\boldsymbol{k})I_{--}^{(2)}(i\omega,\boldsymbol{k},\boldsymbol{q})\Big]\Big\},\end{aligned} \tag{2.110a}$$

$$\begin{aligned}\Sigma_+(K)=\frac{h_c^2\lambda^2}{16S}\frac{2}{N}\sum_{\boldsymbol{q}}&z_{\boldsymbol{q}-}z_{\boldsymbol{k}-\boldsymbol{q}+}\Big[M_+^2(\boldsymbol{q},\boldsymbol{k})I_{-+}^{(0)}(i\omega,\boldsymbol{k},\boldsymbol{q})\\&+2M_+(\boldsymbol{q},\boldsymbol{k})M_0(\boldsymbol{q},\boldsymbol{k})I_{-+}^{(1)}(i\omega,\boldsymbol{k},\boldsymbol{q})+M_0^2(\boldsymbol{q},\boldsymbol{k})I_{-+}^{(2)}(i\omega,\boldsymbol{k},\boldsymbol{q})\Big],\end{aligned} \tag{2.110b}$$

where we have introduced the abbreviation

$$I_{\sigma\sigma'}^{(n)}(i\omega,\boldsymbol{k},\boldsymbol{q})=\omega^{2-n}I^{(n)}(E_{\boldsymbol{q}\sigma},E_{\boldsymbol{k}-\boldsymbol{q}\sigma'},\omega), \tag{2.111}$$

and the functions

$$M_0(\boldsymbol{k},\boldsymbol{q}) = \frac{\gamma_{\boldsymbol{q}}}{z_{\boldsymbol{k}-\boldsymbol{q}+}} - \frac{\gamma_{\boldsymbol{k}} - \gamma_{\boldsymbol{q}} - \gamma_{\boldsymbol{k}-\boldsymbol{q}}}{z_{\boldsymbol{k}-}} \,, \tag{2.112a}$$

$$M_+(\boldsymbol{k},\boldsymbol{q}) = \frac{\gamma_{\boldsymbol{q}}}{z_{\boldsymbol{k}-\boldsymbol{q}+}} - \frac{\gamma_{\boldsymbol{k}-\boldsymbol{q}}}{z_{\boldsymbol{q}+}} \,, \tag{2.112b}$$

$$M_-(\boldsymbol{k},\boldsymbol{q}) = \frac{\gamma_{\boldsymbol{k}}}{z_{\boldsymbol{k}-}} - \frac{\gamma_{\boldsymbol{k}-\boldsymbol{q}}}{z_{\boldsymbol{k}-\boldsymbol{q}-}} \,. \tag{2.112c}$$

For later reference for the calculation below we write down the special cases

$$M_0(0,\boldsymbol{q}) = \frac{\gamma_{\boldsymbol{q}}}{z_{\boldsymbol{q}+}} + \frac{2\gamma_{\boldsymbol{q}} - 1}{z_{0-}} \,, \tag{2.113a}$$

$$M_+(0,\boldsymbol{q}) = 0 \,, \tag{2.113b}$$

$$M_-(0,\boldsymbol{q}) = \frac{1}{z_{0-}} - \frac{\gamma_{\boldsymbol{q}}}{z_{\boldsymbol{q}-}} \,, \tag{2.113c}$$

$$M_0(\boldsymbol{k},0) = \frac{1}{z_{\boldsymbol{k}+}} + \frac{1}{z_{\boldsymbol{k}-}} \,, \tag{2.113d}$$

$$M_+(\boldsymbol{k},0) = \frac{1}{z_{\boldsymbol{k}+}} - \frac{\gamma_{\boldsymbol{k}}}{z_{0+}} \,, \tag{2.113e}$$

$$M_-(\boldsymbol{k},0) = 0 \,, \tag{2.113f}$$

and the expansion

$$M_-(\boldsymbol{k},\boldsymbol{q}) = \frac{a^2}{4Dn^4}\left[\boldsymbol{q}^2 - 2\boldsymbol{k}\cdot\boldsymbol{q}\right] + \mathcal{O}(k^4, q^4, k^2q^2) \,, \tag{2.114}$$

if both momenta $\boldsymbol{k}$ and $\boldsymbol{q}$ are small.

2.5.2 Renormalization of the gapless magnon

Effects of the magnetic field, arising from a renormalization of the spin-wave velocity, should be most visible in the spectrum of the gapless magnon. We therefore deduce the spin-wave velocity, the quasiparticle residue and the magnon damping for this mode.

Spin-wave velocity

Below, we show that in dimensions $D \leq 3$ already the leading $1/S$ correction to the spin-wave velocity $\tilde{c}_-(h)$ of the gapless magnon is nonanalytic in h^2. To arrive at this result, we expand the self-energy, Eq. (2.110a), for small frequencies ω and small momenta $|\boldsymbol{k}|$,

$$\Sigma_-(\boldsymbol{k}, i\omega) = f_0\omega^2 + f_1\omega_{\boldsymbol{k}}^2 + f_2\omega^4 + f_3\omega^2\omega_{\boldsymbol{k}}^2 + f_4\omega_{\boldsymbol{k}}^4 + O(\omega^6) \,. \tag{2.115}$$

Since we expect a gapless magnon also within corrections to all orders $1/S$ due to the Goldstone theorem, it is justified to assume that ω and $\omega_{\boldsymbol{k}} = c_-|\boldsymbol{k}|$

have the same order of magnitude. At this point we substitute the spin-wave velocity within linear spin-wave theory $c_- = c_0 n$. For the calculation of the renormalized spin-wave velocity it is sufficient to retain only the first two terms in Eq. (2.115), i.e. neglecting terms of order ω^4 in the equation above. Using the free propagator, Eq. (2.103), and the Dyson equation we obtain for the infrared behavior of the propagator,

$$G_-(\boldsymbol{k}, i\omega) = \frac{Z_- h_c n^2}{\omega^2 + \tilde{c}_-^2 \boldsymbol{k}^2} \,, \tag{2.116}$$

where we have introduced the quasiparticle residue Z_- (also called wave-function renormalization factor). With the help of the dimensionless constants,

$$F_0 = h_c n^2 f_0 \,, \tag{2.117a}$$
$$F_1 = h_c n^2 f_1 \,, \tag{2.117b}$$

the wave-function renormalization factor can be written as

$$Z_- = \frac{1}{1+F_0} = 1 - F_0 + \mathcal{O}\Big(\frac{1}{S^2}\Big) \,, \tag{2.118}$$

and the renormalized spin-wave velocity obeys

$$\frac{\tilde{c}_-^2}{c_-^2} = \frac{1+F_1}{1+F_0} = 1 + F_1 - F_0 + \mathcal{O}\Big(\frac{1}{S^2}\Big) \,. \tag{2.119}$$

Note that in both formulas we expand formally in $1/S$ as $F_0 = \mathcal{O}(1/S)$ and $F_1 = \mathcal{O}(1/S)$. The constants f_0 and f_1 will now be calculated by expanding the perturbative self-energy in powers of frequencies and momenta. First we set $\boldsymbol{k} = 0$ in Eq. (2.115) to expand $\Sigma_-(0,\omega)$ in powers of ω^2. Using Eq. (2.110a) and Eqs. (2.113a–2.113f) we get for the self-energy

$$\begin{aligned}\Sigma_-(0, i\omega) &= \frac{h_c^2 \lambda^2}{16S} \frac{2}{N} \sum_{\boldsymbol{q}} \Big\{ z_{\boldsymbol{q}+}^2 M_0^2(0,\boldsymbol{q}) I_{++}^{(0)}(i\omega, 0, \boldsymbol{q}) + z_{\boldsymbol{q}-}^2 M_-^2(0,\boldsymbol{q}) I_{--}^{(0)}(i\omega, 0, \boldsymbol{q}) \Big\} \\ &= \omega^2 \frac{h_c^2 \lambda^2}{16S} \frac{2}{N} \sum_{\boldsymbol{q}} \left\{ \frac{\Big[\gamma_{\boldsymbol{q}} + \frac{1+\gamma_{\boldsymbol{q}}}{2n^2}(2\gamma_{\boldsymbol{q}} - 1)\Big]^2}{E_{\boldsymbol{q}+}[(2E_{\boldsymbol{q}+})^2 + \omega^2]} + \frac{\Big[\frac{z_{\boldsymbol{q}-}}{z_{0-}} - \gamma_{\boldsymbol{q}}\Big]^2}{E_{\boldsymbol{q}-}[(2E_{\boldsymbol{q}-})^2 + \omega^2]} \right\} ,\end{aligned} \tag{2.120}$$

and the coefficients

$$f_0 = \frac{n^2 h^2}{16S} \frac{2}{N} \sum_{\boldsymbol{q}} \left\{ \frac{\Big[\gamma_{\boldsymbol{q}} + \frac{1+\gamma_{\boldsymbol{q}}}{2n^2}(2\gamma_{\boldsymbol{q}} - 1)\Big]^2}{E_{\boldsymbol{q}+}^3} + \frac{\Big[\frac{z_{\boldsymbol{q}-}}{z_{0-}} - \gamma_{\boldsymbol{q}}\Big]^2}{E_{\boldsymbol{q}-}^3} \right\} , \tag{2.121a}$$

$$f_2 = -\frac{n^2 h^2}{16S} \frac{2}{N} \sum_{\boldsymbol{q}} \left\{ \frac{\Big[\gamma_{\boldsymbol{q}} + \frac{1+\gamma_{\boldsymbol{q}}}{2n^2}(2\gamma_{\boldsymbol{q}} - 1)\Big]^2}{4E_{\boldsymbol{q}+}^5} + \frac{\Big[\frac{z_{\boldsymbol{q}-}}{z_{0-}} - \gamma_{\boldsymbol{q}}\Big]^2}{4E_{\boldsymbol{q}-}^5} \right\} , \tag{2.121b}$$

where we have substituted $h_c^2\lambda^2 = 4n^2h^2$. To estimate the integrals in the equations above one can use the fact that $z_{\boldsymbol{q}-}/z_{0-} - \gamma_{\boldsymbol{q}} = \mathcal{O}(q^2)$ for small q. Thus, the integrals are dominated by the first term involving the gapped mode $E_{\boldsymbol{q}+}$ in the regime of small magnetic field $h \ll h_c$. At this point we see that the QAFM is rather characterized by two spin-wave velocities with different values than only one. For an analytical approximation we may restrict the momentum integrals in Eqs. (2.121a) and (2.121b) by an ultraviolet cutoff at the inverse of the length scale

$$\xi = \frac{c_0}{h} \, . \tag{2.122}$$

Then, in dimensions $D \leq 3$ the contribution from wave vectors at small momenta $|\boldsymbol{q}|\xi \lesssim 1$ induces contributions to the magnon self-energy which are nonanalytic in h^2. Accounting for large length ξ compared to the lattice spacing a in the regime of small magnetic field, we may expand the integrand in Eqs. (2.121a) and (2.121b) in powers of $\boldsymbol{q}$.

The coefficient f_1 in front of the $\boldsymbol{k}^2$ correction to the self-energy is for small fields h proportional to h^2 so that for $h \ll h_c$ we only have to consider the term f_0 to compute the leading magnetic-field dependence of the spin-wave velocity $\tilde{c}_-$ associated with the gapless magnon, i.e.

$$\frac{\tilde{c}_-^2}{c_-^2} \approx 1 - F_0 \, . \tag{2.123}$$

Focusing on $h \ll h_c$ we work out the nonanalytic terms in h^2. We may set $n = 1 + \mathcal{O}(h^2) \approx 1$ to calculate the dominant contribution to the integral in Eq. (2.121a) in the thermodynamic limit,

$$f_0 \approx \frac{h^2 a^D}{2S} \int \frac{d^D q}{(2\pi)^D} \frac{1}{E_{\boldsymbol{q}+}^3} \, . \tag{2.124}$$

Next, we carry out the integration by consistently neglecting all terms which are analytic in h^2: We may drop the magnetic field dependence of the noninteracting spin-wave velocities

$$c_\pm = c_0 + \mathcal{O}(h^2) \approx c_0 = 2\sqrt{D} JSa \, , \tag{2.125}$$

and approximate the dispersions by

$$E_{\boldsymbol{q}-} \approx c_0 |\boldsymbol{q}| \, , \tag{2.126a}$$

$$E_{\boldsymbol{q}+} \approx \sqrt{h^2 + c_0^2 \boldsymbol{q}^2} \, . \tag{2.126b}$$

Using now the critical field $h_c = 2\sqrt{D} c_0/a$, the dimensionless coefficient in $1 < D \leq 3$ in Eq. (2.124) simplifies to

$$F_0 = h_c n^2 f_0 = \alpha_D \frac{m^{D-1}}{S} \, , \tag{2.127}$$

where $m = h/h_c = ha/(2\sqrt{D}c_0)$ is the dimensionless magnetic field defined in Eq. (2.72). The constant α_D is given by the integral

$$\alpha_D = 2^{D-1} D^{D/2} K_D \int_0^{1/m} dy \frac{y^{D-1}}{[1+y^2]^{3/2}} \,, \tag{2.128}$$

where we have introduced the surface area of the D-dimensional unit sphere divided by $(2\pi)^D$,

$$K_D = \frac{2^{1-D}}{\pi^{D/2}\Gamma(D/2)} \,. \tag{2.129}$$

To calculate the integral in Eq. (2.128) we may take the limit $1/m \to \infty$ and obtain

$$\alpha_D = \left(\frac{D}{\pi}\right)^{D/2} \frac{\Gamma(\frac{3-D}{2})}{\sqrt{\pi}} \,, \tag{2.130}$$

while for $D = 3$ the integral depends for small m logarithmically on the upper limit,

$$\alpha_3 \sim \alpha_3' \ln(1/m) \,, \quad \alpha_3' = \frac{6\sqrt{3}}{\pi^2} \,. \tag{2.131}$$

Using Eq. (2.123) together with the result of Eqs. (2.130) and (2.131), $\alpha_2 = 2/\pi$ in particular, the final result for the spin-wave velocity simplifies to

$$\frac{\tilde{c}_-^2}{c_0^2} \approx \begin{cases} 1 - \dfrac{2}{\pi S}\dfrac{|\boldsymbol{h}|}{h_c} \,, & D = 2 \\ 1 - \dfrac{6\sqrt{3}}{\pi^2 S}\dfrac{\boldsymbol{h}^2}{h_c^2} \ln\left(\dfrac{h_c}{|\boldsymbol{h}|}\right) \,, & D = 3 \end{cases} \tag{2.132}$$

Recall, that in this formula all contributions which are analytic in h^2 and all $1/S$ corrections that are independent from the magnetic field have been dropped. To understand the simplification of this result one has to keep in mind that the magnetic field dependence of the velocity c_- within linear spin-wave theory is analytic in $h^2 = h_c^2 m^2$, compare Eq. (2.42). Explicitly the linear spin-wave result has the expansion

$$c_- \approx c_0 \Big(1 - \frac{m^2}{2}\Big) \,, \tag{2.133}$$

which means that the corrections to the spin-wave velocity $\tilde{c}_-$ at small fields are dominated by the spin-wave interactions.

As a side remark, let us point out that the formula Eq. (2.132) has been checked numerically by use of the expressions for the magnon self-energy given in a work by Zhitomirsky and Chernyshev [233]. Details of this calculation are given in section 2.6.1.

2.5.3 Quasiparticle residue

Knowing that the magnetic field dependence of the spin-wave velocity of the gapless magnon is dominated by effects from the spin-wave interactions, we expect also nonanalytic behavior in the higher coefficients of the expansion of the self-energy Eq. (2.115). To observe this, we consider the renormalized magnon Green function of the gapless magnon for small m,

$$G_-(\boldsymbol{k}, i\omega) = Z_-(i\omega)\frac{h_c n^2}{\omega^2 + \tilde{c}_-^2 \boldsymbol{k}^2} \,, \tag{2.134}$$

which is parametrized by the frequency-dependent wave-function renormalization factor $Z_-(i\omega)$ and the renormalized spin-wave velocity $\tilde{c}_-$ given in Eq. (2.132). To calculate $Z_-(i\omega)$ we have to work out the coefficients f_2, f_3 and f_4 in Eq. (2.115). Let us first consider the coefficient f_2 related to the ω^4 term in the expansion of the self-energy $\Sigma_-(0, i\omega)$ for small frequencies. Again, the integral defining f_2 in Eq. (2.121b) is dominated by wave vectors $|\boldsymbol{q}|\xi \lesssim 1$. Hence, we approximate

$$f_2 \approx -\frac{h^2 a^D}{8S} \int \frac{d^D q}{(2\pi)^D} \frac{1}{E_{\boldsymbol{q}+}^5} \,, \tag{2.135}$$

and evaluate the integral to leading order for small $m \ll 1$. If we introduce the dimensionless coefficient,

$$F_2 \equiv \frac{c_0^2 h_c f_2}{a^2} \,, \tag{2.136}$$

we get for $D < 3$

$$F_2 \approx -\frac{\beta_D}{S}\left[m^{D-3} + \mathcal{O}(m^{D-1})\right] \,, \tag{2.137}$$

with the numerical coefficient

$$\begin{aligned} \beta_D &= \frac{(2\sqrt{D})^{D-2}}{8} K_D \int_0^\infty dx \frac{x^{D-1}}{[1+x^2]^{5/2}} \\ &= \frac{(2\sqrt{D})^{D-2}}{8} K_D \frac{2}{3\sqrt{\pi}} \Gamma\Big(\frac{5-D}{2}\Big)\Gamma\Big(\frac{D}{2}\Big) \,. \end{aligned} \tag{2.138}$$

In particular, in two dimensions $\beta_2 = 1/(48\pi)$. Next, we show that the singular contribution to the coefficient f_3 has the same value as the singular part of f_2. In order to extract the dominant contributions, it is sufficient to approximate the magnon self-energy by

$$\Sigma_-(\boldsymbol{k}, i\omega) \approx \frac{2h^2 a^D}{S} \int \frac{d^D q}{(2\pi)^D} I_{++}^{(0)}(i\omega, \boldsymbol{k}, \boldsymbol{q}) \,. \tag{2.139}$$

Expanding now the integrand to second order in $\boldsymbol{k}$ and comparing coefficients with Eq. (2.115), we obtain

$$f_3 \approx -\frac{h^2 a^D}{8S} \int \frac{d^D q}{(2\pi)^D} \frac{1}{E_{\boldsymbol{q}+}^5} \left[3 - \frac{10}{D}\frac{c_0^2 \boldsymbol{q}^2}{E_{\boldsymbol{q}+}^2}\right] \,. \tag{2.140}$$

Carrying out the integration analytically both coefficients are equal to leading order in the dimensionless magnetic field m,

$$f_3 = f_2 + \mathcal{O}(m^{D-1}) \,. \tag{2.141}$$

To finalize the discussion of the coefficients, an analysis of the integrand in Eq. (2.110a) shows that the coefficient f_4 is of order $a^2 m^{D-1}/S$ and can be neglected whenever it appears in conjunction with f_2 and f_3. Writing down the self-energy $\Sigma_-(\boldsymbol{k}, \omega + i0^+)$ off resonance, the magnetic-field dependence appearing in the coefficients f_2 and f_3 does not cancel. Retaining only the singular contributions, i.e. approximating $f_2 \approx f_3$ our expansion simplifies to

$$\Sigma_-(\boldsymbol{k}, \omega + i0^+) \approx -f_0\omega^2 + f_2\omega^2(\omega^2 - \tilde{c}_-^2 \boldsymbol{k}^2) \,. \tag{2.142}$$

Comparing with the parametrization of the Green function, Eq. (2.134), this leads to

$$Z_-(i\omega) = \frac{1}{1 + F_0 + h_c n^2 f_2 \omega^2} \approx 1 - F_0 - \frac{a^2 F_2}{c_0^2}\,\omega^2 \,, \tag{2.143}$$

and after analytical continuation to real frequencies, i.e. replacing $i\omega \to \omega + i0^+$, we obtain for the renormalized residue of the magnon peak at small m,

$$\begin{aligned} Z_{\boldsymbol{k}-} \equiv Z_-(i\omega \to \tilde{c}_-|\boldsymbol{k}|) &= 1 - F_0 + F_2 \boldsymbol{k}^2 a^2 \\ &= 1 - F_0 - \beta_D \frac{\boldsymbol{k}^2 a^2}{S m^{3-D}} \,. \end{aligned} \tag{2.144}$$

Inserting the length scale ξ defined in Eq. (2.122) by use of $m = h/h_c = ha/(2\sqrt{D}c_0) = a/(2\sqrt{D}\xi)$ we may also write

$$\begin{aligned} Z_{\boldsymbol{k}-} &= 1 - F_0 - \frac{\tilde{\beta}_D}{S}\left(\frac{\xi}{a}\right)^{3-D} \boldsymbol{k}^2 a^2 \\ &= 1 - \frac{1}{S}\left(\frac{a}{\xi}\right)^{D-1} \left[\tilde{\alpha}_D - \tilde{\beta}_D \boldsymbol{k}^2 \xi^2\right] \,, \end{aligned} \tag{2.145}$$

where we have abbreviated $\tilde{\alpha}_D = \alpha_D (2\sqrt{D})^{1-D}$ and $\tilde{\beta}_D = \beta_D (2\sqrt{D})^{3-D}$. For $D = 2$ the leading momentum dependence is proportional to $\boldsymbol{k}^2 \xi a = \boldsymbol{k}^2 c_0 a/h$. Higher powers in the wave vector $\boldsymbol{k}$ become important for $|\boldsymbol{k}|\xi \gtrsim 1$, so that the expansion Eq. (2.145) is only valid in the regime $|\boldsymbol{k}| \lesssim \xi^{-1} \ll a^{-1}$, where the leading $1/S$ corrections are small compared to unity. We thus conclude that the result Eq. (2.145) is a suitable expansion of the wave-function renormalization factor in the regime of small magnetic fields.

2.5.4 Magnon damping

Before actually calculating the magnon damping we have to take a closer look at the magnon dispersions and at the corrections due to the self-energy. In

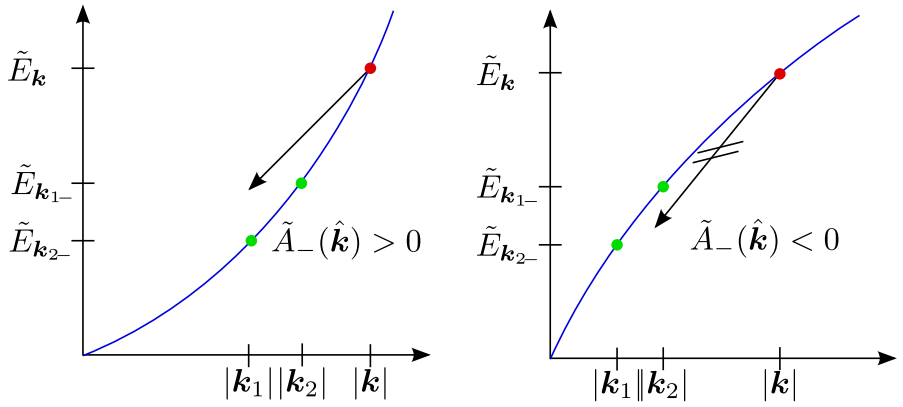

Figure 2.5: *Illustration of the decay condition due to energy-momentum conservation Eq. (2.148): If the coefficient $A_-(\hat{\boldsymbol{k}})$ is larger than zero, decays at certain regions near the center of the Brillouin zone are possible (left), while for negative $A_-(\hat{\boldsymbol{k}})$ no spontaneous decay due to the cubic interaction term is possible (right). Note that for simplicity only a projection of the momenta on a plane is shown in the graphs.*

order to work out the behavior of the magnons we consider the renormalized magnon energies $\tilde{E}_{\boldsymbol{k}\sigma}$. Looking at Eqs. (2.77) and (2.104) they can be defined as

$$\tilde{E}^2_{\boldsymbol{k}\sigma} = E^2_{\boldsymbol{k}\sigma} + \Delta_{\boldsymbol{k}\sigma}\mathrm{Re}\Sigma_\sigma(\boldsymbol{k}, \tilde{E}_{\boldsymbol{k}\sigma} + i0^+) \; . \tag{2.146}$$

An expansion for small wave vectors defines two coefficients $\tilde{A}_\pm(\hat{\boldsymbol{k}})$ via

$$\tilde{E}^2_{\boldsymbol{k}-} = \tilde{c}^2_- \boldsymbol{k}^2 \left[1 + \tilde{A}_-(\hat{\boldsymbol{k}})\boldsymbol{k}^2 + O(\boldsymbol{k}^4)\right] \; , \tag{2.147a}$$

$$\tilde{E}^2_{\boldsymbol{k}+} = h^2 + \tilde{c}^2_+ \boldsymbol{k}^2 \left[1 + \tilde{A}_+(\hat{\boldsymbol{k}})\boldsymbol{k}^2 + O(\boldsymbol{k}^4)\right] \; . \tag{2.147b}$$

In general, there are two possible types of quasiparticle decays: the first is a scattering with other quasiparticles to another state. In the QAFM this process is mediated by terms containing four or more bosonic operators and is suppressed at low temperatures as the density of bosons is low. In contrast, the spontaneous decay in two or more quasiparticles with the boundary condition of energy-momentum conservation is always possible. Now we consider only the process of a decay to two other quasiparticles as it is of the lowest order in $1/S$. From a simple analysis of energy-momentum conservation it is well known [B18], that only if the coefficient $\tilde{A}_-$ is positive, a gapless magnon with momentum $\boldsymbol{k}$ can spontaneously decay in two magnons with momenta $\boldsymbol{q}$ and $\boldsymbol{k} - \boldsymbol{q}$. A sketch of possible magnon decays is presented in Fig. 2.5 where the graphical solution of the equation

$$\tilde{E}_{\boldsymbol{k}} = \tilde{E}_{\boldsymbol{k}-\boldsymbol{q}} + \tilde{E}_{\boldsymbol{q}} \tag{2.148}$$

is illustrated. Starting from the dispersion within linear spin-wave theory we expand the square of Eq. (2.32) in D dimensions

$$E_{\boldsymbol{k}-}^2 = c_-^2 \boldsymbol{k}^2 \left[1 + A_-(\hat{\boldsymbol{k}})\boldsymbol{k}^2 + O(\boldsymbol{k}^4)\right], \tag{2.149a}$$

$$E_{\boldsymbol{k}+}^2 = h^2 + c_+^2 \boldsymbol{k}^2 \left[1 + A_+(\hat{\boldsymbol{k}})\boldsymbol{k}^2 + O(\boldsymbol{k}^4)\right], \tag{2.149b}$$

with the coefficients

$$A_-(\hat{\boldsymbol{k}}) = -\frac{a^2}{4}\left[\frac{1-2m^2}{D(1-m^2)} + \frac{1}{3}\sum_\mu \hat{k}_\mu^4\right], \tag{2.150a}$$

$$A_+(\hat{\boldsymbol{k}}) = -\frac{a^2}{4}\left[\frac{1-2m^2}{D(1-3m^2)} + \frac{1}{3}\sum_\mu \hat{k}_\mu^4\right]. \tag{2.150b}$$

Obviously, for small magnetic field $m \ll 1$ the coefficient $A_-(\hat{\boldsymbol{k}})$ is negative for all directions of $\hat{\boldsymbol{k}}$, so that to this order in spin-wave theory, the gapless magnon cannot spontaneously decay at long wavelengths. If m increases the coefficient $A_-(\hat{\boldsymbol{k}})$ decreases and eventually vanishes at a critical field $m_*(\hat{\boldsymbol{k}})$ which still depends on the direction. Observing that the sum $\sum_\mu \hat{k}_\mu^4$ is smallest for the diagonal $\hat{k}_x = \ldots = \hat{k}_D = 1/\sqrt{D}$ one can show that the associated minimum,

$$m_* = h_*/h_c = 2/\sqrt{7} \approx 0.76\,, \tag{2.151}$$

is independent of the dimension. For the special case $D = 2$ this result has been calculated previously by Zhitomirsky and Chernyshev [233]. They examined the whole magnon spectrum containing leading $1/S$ corrections in the regime $h_* < h < h_c$ numerically. But they apparently did not analyze the leading $1/S$ correction in the limit of small magnetic fields $m \ll 1$. The expansion coefficient $\tilde{A}_-(\hat{\boldsymbol{k}})$ can now be parametrized by

$$\tilde{A}_-(\hat{\boldsymbol{k}}) = A_-(\hat{\boldsymbol{k}}) + \delta A_- \tag{2.152}$$

where $A_-(\hat{\boldsymbol{k}})$ is the result of linear spin-wave theory and the $1/S$ correction is given by

$$\delta A_- = c_0^2 h_c \left[f_2 - f_3 + f_4\right]. \tag{2.153}$$

Recalling the divergence of the coefficients f_2 and f_3, Eqs. (2.137) and (2.141), it is obvious that in the combination $f_2 - f_3$ the divergent contribution proportional to m^{D-3} cancels out for small magnetic fields, so that the leading magnetic field dependence of $\tilde{A}_-$ is proportional to $m^{D-1} \propto |\boldsymbol{h}|^{D-1}$. This is small compared to the value of $A_-(\hat{\boldsymbol{k}})$ in linear spin-wave theory, but nonanalytic in h^2. Therefore it will hardly change the value of the minimal critical field m_* in Eq. (2.151) but is dominant at small fields. From Eq. (2.110b) we can also show that the coefficient f_4 is of order $a^2 m^{D-1}/S$ and will not change the qualitative behavior of δA_-.

The damping rate $\gamma_{\boldsymbol{k}\sigma}$ of the quasiparticles in the Bogoliubov basis is generally defined using the correlation function in time,

$$iG_t(\boldsymbol{k}\sigma) = \left\langle \hat{\Psi}_{\boldsymbol{k}\sigma}(t)\hat{\Psi}^\dagger_{\boldsymbol{k}\sigma}(0)\right\rangle = Z_\sigma e^{i\tilde{E}_{\boldsymbol{k}\sigma}t}e^{-\gamma_{\boldsymbol{k}\sigma}t} \ , \tag{2.154}$$

where we also introduced the wave-function renormalization factor Z_σ. Inserting the transformation Eq. (2.43) to the Hermitian field operators one can calculate this correlator which is a sum of the correlators for the Hermitian field operators Eqs. (2.73a–2.73c). Considering the corrections to the dispersion $\tilde{E}_{\boldsymbol{k}\sigma}$ in Eq. (2.146) given by the magnon self-energies $\Sigma_\sigma(K)$, Eqs. (2.110a) and (2.110b), and comparing the expressions with Eq. (2.154), one can obtain the magnon damping from

$$\gamma_{\boldsymbol{k}\sigma} = -\frac{\Delta_{\boldsymbol{k}\sigma}}{2\tilde{E}_{\boldsymbol{k}\sigma}}\mathrm{Im}\,\Sigma_\sigma(\boldsymbol{k}, \tilde{E}_{\boldsymbol{k}\sigma} + i0^+) \ . \tag{2.155}$$

Zhitomirsky and Chernyshev [233] have shown that for the QAFM in two dimensions it is necessary to take into account the imaginary part of the magnon self-energy when evaluating the integrals in Eq. (2.110a). But if we are not too close to the critical field h_*, the result for the magnon damping is nonsingular even if we ignore the damping of intermediate magnons in this equation. Therefore a simplified calculation where only the renormalization of the real part of the magnon dispersion is taken into account should also give a correct estimate for the magnon damping at small fields $m \ll 1$. To simplify the calculation of the damping $\gamma_{\boldsymbol{k}-}$ for wave vectors $|\boldsymbol{k}| \ll h/c_0 = \xi^{-1}$, it is possible to retain in Eq. (2.110a) only the terms involving the functions $I^{(n)}_{--}(\omega+i0^+, \boldsymbol{k}, \boldsymbol{q})$, as the imaginary part of the other functions $I^{(n)}_{++}(\omega+i0^+, \boldsymbol{k}, \boldsymbol{q})$ vanishes for $\omega < 2h$. Using the expansion Eq. (2.114) and the identity

$$\lim_{\eta\to 0}\mathrm{Im}\frac{\eta}{x^2+\eta^2} = \pi\ \delta(x) \ , \tag{2.156}$$

we obtain for positive frequencies

$$\begin{aligned}\mathrm{Im}\Big[&M^2_-(\boldsymbol{k},\boldsymbol{q})I^{(0)}_{--}(\omega+i0^+,\boldsymbol{k},\boldsymbol{q}) + 2M_-(\boldsymbol{k},\boldsymbol{q})M_-(\boldsymbol{q},\boldsymbol{k})I^{(1)}_{--}(\omega+i0^+,\boldsymbol{k},\boldsymbol{q}) \\ &+M^2_-(\boldsymbol{q},\boldsymbol{k})I^{(2)}_{--}(\omega+i0^+,\boldsymbol{k},\boldsymbol{q})\Big] \\ &= -\frac{\pi}{4}\left(\frac{a^2}{4Dn^4}\right)^2 W(\boldsymbol{k},\boldsymbol{q})\delta(\omega - \tilde{E}_{\boldsymbol{k}-\boldsymbol{q}-} - \tilde{E}_{\boldsymbol{q}-}) \ ,\end{aligned} \tag{2.157}$$

where

$$\begin{aligned}W(\boldsymbol{k},\boldsymbol{q}) = &\frac{q}{|\boldsymbol{k}-\boldsymbol{q}|}(k^2-q^2)^2 + \frac{|\boldsymbol{k}-\boldsymbol{q}|}{q}(q^2-2\boldsymbol{k}\cdot\boldsymbol{q})^2 \\ &- 2(k^2-q^2)(q^2-2\boldsymbol{k}\cdot\boldsymbol{q}) \ .\end{aligned} \tag{2.158}$$

To emphasize the advantage of our approach compared to the NLSM, the damping of the gapless magnon cannot be obtained in the framework of the

NLSM, because the relevant vertex $\Gamma_{---}(K_1, K_2, K_3)$ involving three gapless fields is set equal to zero, see Eq. (2.102a). This is correct to leading order in the derivatives, but will result in neglecting the dominant contribution corresponding to Eq. (2.157). To estimate the magnon damping we now set $\omega = \tilde{E}_{\boldsymbol{k}-}$ and approximate the renormalized magnon dispersion by

$$\tilde{E}_{\boldsymbol{k}-} \approx c_-|\boldsymbol{k}|\Big(1 + \frac{1}{2}\bar{A}_-\boldsymbol{k}^2\Big) , \tag{2.159}$$

where we have replaced the direction-dependent coefficient $\tilde{A}_-(\hat{\boldsymbol{k}})$ defined in Eq. (2.147a) by some angular average $\bar{A}_-$. The damping at long wavelengths reads

$$\gamma_{\boldsymbol{k}-} = \frac{\pi\sqrt{D}}{8(4D)^2}\frac{h^2 a^{D+3}}{S}\int \frac{d^D q}{(2\pi)^D}\frac{W(\boldsymbol{k},\boldsymbol{q})}{k}\,\delta(\tilde{E}_{\boldsymbol{k}-} - \tilde{E}_{\boldsymbol{k}-\boldsymbol{q}-} - \tilde{E}_{\boldsymbol{q}-}) . \tag{2.160}$$

As discussed above, the energy conservation Eq. (2.148) can only be satisfied for $\bar{A}_- > 0$, and if the $1/S$ corrections δA_- to the cubic coefficient in the dispersion are small. Therefore we restrict ourselves to the calculation of the damping without actually calculating the magnetic field dependence of the coefficient $\bar{A}_- > 0$ in the regime $h_* < |\boldsymbol{h}| < h_c$ below the saturation field. Expecting $\bar{A}_-/a^2$ to be a number of the order of unity from dimensional analysis, we can conclude from Eq. (2.148) that the allowed vectors $\boldsymbol{q}$ are almost parallel to the direction of $\boldsymbol{k}$ and satisfy $q \leq k$, see Fig. 2.5. Then the angle ϑ between $\boldsymbol{k}$ and $\boldsymbol{q}$ is $\vartheta \approx \sqrt{6\bar{A}_-}(k-q)$ and we may approximate for $\bar{A}_- k^2 \ll 1$

$$\delta(\tilde{E}_{\boldsymbol{k}-} - \tilde{E}_{\boldsymbol{k}-\boldsymbol{q}-} - \tilde{E}_{\boldsymbol{q}-}) \approx \frac{\delta(\vartheta - \sqrt{3\bar{A}_-}\,(k-q))}{\sqrt{3\bar{A}_-}\,c_- kq} , \tag{2.161}$$

and

$$\begin{aligned} |\boldsymbol{k}-\boldsymbol{q}| &\approx k - q + \frac{kq}{k-q}(1-\cos\vartheta) \\ &\approx (k-q)\Big(1 + \frac{3}{2}\bar{A}_-\, kq\Big) \end{aligned} \tag{2.162}$$

to reduce the integrations to one radial and one angular integration. Keeping in mind $\bar{A}_- kq \ll 1$, we obtain from Eq. (2.158),

$$\frac{W(\boldsymbol{k},\boldsymbol{q})}{k} \approx 9kq(k-q) , \tag{2.163}$$

and the integrations in Eq. (2.160) become elementary with the result

$$\frac{\gamma_{\boldsymbol{k}-}}{E_{\boldsymbol{k}-}} = \frac{\gamma_D}{S}\left(\frac{h}{h_c}\right)^2\left(\sqrt{3\bar{A}_-}\right)^{D-3} a^{D+1}|\boldsymbol{k}|^{2D-2} , \tag{2.164}$$

where

$$\begin{aligned}\gamma_D &= \frac{9}{64\sqrt{D}} K_{D-1} \int_0^1 dx [x(1-x)]^{D-1} \\ &= \frac{9}{64\sqrt{D}} K_{D-1} 2^{1-2D} \frac{\sqrt{\pi}\Gamma(D)}{\Gamma(D+\frac{1}{2})} \,. \end{aligned} \tag{2.165}$$

The result Eq. (2.164) is only valid in the regime $|\boldsymbol{k}| \lesssim h/c_0 \ll a^{-1}$ at zero temperature. In two dimensions we get $\gamma_2 = 3/(128\sqrt{2}\pi)$ and the damping reads

$$\gamma_{\boldsymbol{k}-} = \frac{\gamma_2}{S} \left(\frac{h}{h_c}\right)^2 \frac{\tilde{c}_- |\boldsymbol{k}|^3 a^3}{\sqrt{3\bar{A}_-}} \propto |\boldsymbol{k}|^3 \,. \tag{2.166}$$

2.6 Comparison to other studies

2.6.1 Numerical confirmation of the renormalization of the spin-wave velocity

One of the main results of this chapter, the renormalization of the spin-wave velocity due to a uniform magnetic field Eq. (2.132), is also accessible in the framework of the conventional spin-wave approach. Zhitomirsky and Chernyshev [233] calculated the field-dependent spin-wave dispersion by a numerical analysis of the magnon self-energies. As they did not focus on the behavior in the low field regime, we will present the main formulas and a study of the spin-wave velocity from Ref. [P2] to confirm our linear behavior in two dimensions.

Translated to our notation, the on-shell renormalized magnon energy $\tilde{E}_{\boldsymbol{k}\sigma}$ can be written as

$$\tilde{E}_{\boldsymbol{k}\sigma} = E_{\boldsymbol{k}\sigma} + \mathrm{Re}\ \Sigma_\sigma^{1/S}(\boldsymbol{k}, E_{\boldsymbol{k}\sigma} + i0^+) \,, \tag{2.167}$$

where the self-energy has the form

$$\Sigma_\sigma^{1/S}(\boldsymbol{k}, i\omega) = \Sigma_{1\sigma}^{1/S}(\boldsymbol{k}, i\omega) + \Sigma_{2\sigma}^{1/S}(\boldsymbol{k}, i\omega) + \Sigma_{3\sigma}^{1/S}(\boldsymbol{k}) + \Sigma_{4\sigma}^{1/S}(\boldsymbol{k}) \,. \tag{2.168}$$

The frequency-dependent contributions to the self-energy are given by[1]

$$\Sigma_{1\sigma}^{1/S}(\boldsymbol{k}, i\omega) = \frac{h_c^2\lambda^2}{16S}\frac{2}{N} \sum_{\boldsymbol{q}\sigma'=\pm} \frac{\Phi_1^2(\boldsymbol{k}\sigma, \boldsymbol{q}\sigma', \boldsymbol{k}-\boldsymbol{q}\overline{\sigma\sigma'})}{i\omega - E_{\boldsymbol{q}\sigma'} - E_{\boldsymbol{k}-\boldsymbol{q}\overline{\sigma\sigma'}}} \,, \tag{2.169a}$$

$$\Sigma_{2\sigma}^{1/S}(\boldsymbol{k}, i\omega) = -\frac{h_c^2\lambda^2}{16S}\frac{2}{N} \sum_{\boldsymbol{q}\sigma'=\pm} \frac{\Phi_2^2(\boldsymbol{k}\sigma, \boldsymbol{q}\sigma', \boldsymbol{k}+\boldsymbol{q}\overline{\sigma\sigma'})}{i\omega + E_{\boldsymbol{q}\sigma'} + E_{\boldsymbol{k}+\boldsymbol{q}\overline{\sigma\sigma'}}} \,. \tag{2.169b}$$

[1] Note that there is a misprint in [P2]: In the equations defining the self-energies, the bar labels indicating terms from interactions with the other mode $\bar{\sigma}'$ are missing. The correct expressions can be found in the document arXiv:0804.1704v2.

$\Sigma^{1/S}_{1\sigma}(\boldsymbol{k}, i\omega) =$ 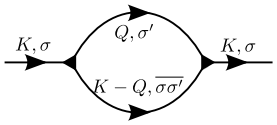

$\Sigma^{1/S}_{2\sigma}(\boldsymbol{k}, i\omega) =$ 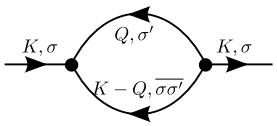

$\Sigma^{1/S}_{3\sigma}(\boldsymbol{k}) =$ 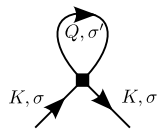

Figure 2.6: *Graphical representation of the self-energy contributions to Eq. (2.168): The first two diagrams are corrections in second order perturbation theory due to $\hat{H}_3$, while the third diagram is a frequency-independent contribution arising from $\hat{H}_4$. Note that the external legs are only included to better separate the different vertices which can be read off from the formulas in Refs. [233, 234].*

Note that second-order perturbation theory due to the cubic terms in the Hamiltonian gives rise to these terms, and that $\overline{\sigma} = -\sigma$ denotes a sign change such that $\overline{\sigma\sigma'} = -\sigma\sigma'$. The functions Φ_1 and Φ_2 involving three powers of the Bogoliubov coefficients Eqs. (2.27a) and (2.27b) are defined as

$$\begin{aligned}\Phi_1(\boldsymbol{k}_1\sigma_1, \boldsymbol{k}_2\sigma_2, \boldsymbol{k}_3\sigma_3) = {}& \sigma_1\gamma_{\mathbf{1}}(u_{\mathbf{1}\sigma_1} + \sigma_1 v_{\mathbf{1}\sigma_1})(\sigma_3 u_{\mathbf{2}\sigma_2} v_{\mathbf{3}\sigma_3} + \sigma_2 u_{\mathbf{3}\sigma_3} v_{\mathbf{2}\sigma_2}) \\ & + \sigma_2\gamma_{\mathbf{2}}(u_{\mathbf{2}\sigma_2} + \sigma_2 v_{\mathbf{2}\sigma_2})(u_{\mathbf{1}\sigma_1} u_{\mathbf{3}\sigma_3} + \sigma_3\sigma_1 v_{\mathbf{3}\sigma_3} v_{\mathbf{1}\sigma_1}) \\ & + \sigma_3\gamma_{\mathbf{3}}(u_{\mathbf{3}\sigma_3} + \sigma_3 v_{\mathbf{3}\sigma_3})(u_{\mathbf{2}\sigma_2} u_{\mathbf{1}\sigma_1} + \sigma_1\sigma_2 v_{\mathbf{1}\sigma_1} v_{\mathbf{2}\sigma_2}) \,,\end{aligned} \tag{2.170a}$$

$$\begin{aligned}\Phi_2(\boldsymbol{k}_1\sigma_1, \boldsymbol{k}_2\sigma_2, \boldsymbol{k}_3\sigma_3) = {}& \sigma_1\gamma_{\mathbf{1}}(u_{\mathbf{1}\sigma_1} + \sigma_1 v_{\mathbf{1}\sigma_1})(\sigma_2 u_{\mathbf{3}\sigma_3} v_{\mathbf{2}\sigma_2} + \sigma_3 u_{\mathbf{2}\sigma_2} v_{\mathbf{3}\sigma_3}) \\ & + \sigma_2\gamma_{\mathbf{2}}(u_{\mathbf{2}\sigma_2} + \sigma_2 v_{\mathbf{2}\sigma_2})(\sigma_1 u_{\mathbf{3}\sigma_3} v_{\mathbf{1}\sigma_1} + \sigma_3 u_{\mathbf{1}\sigma_1} v_{\mathbf{3}\sigma_3}) \\ & + \sigma_3\gamma_{\mathbf{3}}(u_{\mathbf{3}\sigma_3} + \sigma_3 v_{\mathbf{3}\sigma_3})(\sigma_1 u_{\mathbf{2}\sigma_2} v_{\mathbf{1}\sigma_1} + \sigma_2 u_{\mathbf{1}\sigma_1} v_{\mathbf{2}\sigma_2}) \,.\end{aligned} \tag{2.170b}$$

Finally one has also to add the frequency-independent $1/S$ contributions to the self-energy coming from the Hartree-Fock approximation of $\hat{H}_4$ and the corrections to the canting angle [234],

$$\begin{aligned}\Sigma^{1/S}_{3\sigma}(\boldsymbol{k}) = {}& \frac{h_c}{2S}(u^2_{\boldsymbol{k}\sigma} + v^2_{\boldsymbol{k}\sigma})\Big[-\kappa_1\alpha + \kappa_2 n^2 - \kappa_3 m^2 \\ & \qquad + \sigma\gamma_{\boldsymbol{k}}(-\kappa_3\alpha + \kappa_4 n^2/2 - \kappa_1 m^2)\Big] \\ & - \frac{h_c}{2S}\sigma u_{\boldsymbol{k}\sigma} v_{\boldsymbol{k}\sigma}\Big[\kappa_2 m^2 - \kappa_3 n^2 + 2\sigma\gamma_{\boldsymbol{k}}(\kappa_2\alpha - \kappa_1 n^2 + \kappa_4 m^2/2)\Big] \,,\end{aligned} \tag{2.171a}$$

$$\Sigma^{1/S}_{4\sigma}(\boldsymbol{k}) = \frac{h_c}{S} m^2(\kappa_2 - \kappa_1 + \kappa_3)\Big[(u^2_{\boldsymbol{k}\sigma} + v^2_{\boldsymbol{k}\sigma})(1 - \sigma\gamma_{\boldsymbol{k}}) - 2\gamma_{\boldsymbol{k}} u_{\boldsymbol{k}\sigma} v_{\boldsymbol{k}\sigma}\Big] \,, \tag{2.171b}$$

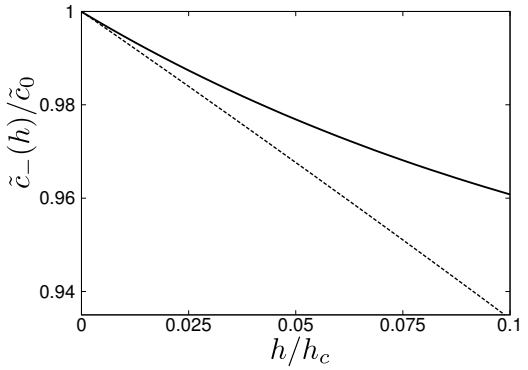

Figure 2.7: *Evolution of the spin-wave velocity of the gapless magnon as a function of the external magnetic field for $S = 1/2$. The full line shows the spin-wave velocity obtained numerically from Eq. (2.167) normalized by the zero-field value $\tilde{c}_0 \approx 1.16 c_0$ for $S = 1/2$ [151]. The dashed line shows the prediction of Eq. (2.132). Good agreement is obtained in the limit of vanishing fields which confirms that the leading field dependence is described by Eq. (2.132), taken from [P2].*

with the mean-field averages

$$\kappa_1 = \frac{2}{N} \sum_{\boldsymbol{k}\sigma} v_{\boldsymbol{k}\sigma}^2 \,, \tag{2.172a}$$

$$\kappa_2 = \frac{2}{N} \sum_{\boldsymbol{k}\sigma} v_{\boldsymbol{k}\sigma} u_{\boldsymbol{k}\sigma} \gamma_{\boldsymbol{k}} \,, \tag{2.172b}$$

$$\kappa_3 = \frac{2}{N} \sum_{\boldsymbol{k}\sigma} \sigma v_{\boldsymbol{k}\sigma}^2 \gamma_{\boldsymbol{k}} \,, \tag{2.172c}$$

$$\kappa_4 = \frac{2}{N} \sum_{\boldsymbol{k}\sigma} \sigma v_{\boldsymbol{k}\sigma} u_{\boldsymbol{k}\sigma} \,. \tag{2.172d}$$

The latter self-energies come from the Hartree-Fock approximation of the quartic interaction, compare Fig. 2.6. While the self-energy Eq. (2.168) can be easily evaluated numerically, it is not convenient for analytical treatments since the Bogoliubov coefficients give rise to nonanalytic terms. This is why the small field behavior has not yet been extracted from it. To do so it is easier to use the equivalent expression Eq. (2.110a) in the Hermitian field parametrization to investigate the dispersion in the long-wavelength regime.

To calculate numerical data for the spin-wave velocity, one has to perform a two-dimensional integration and an analytical continuation to real frequencies ($i\omega \to \omega + i0^+$). After carrying out a numerical derivative with respect to the momentum $\boldsymbol{k}$ in the center of the Brillouin zone we finally get the spin-wave velocity. In Fig. 2.7 we compare the numerical result for the spin-wave velocity $\tilde{c}_-(h)$ of the gapless mode at small fields with the prediction of Eq. (2.132). At very small fields both approaches give the same result, while for larger fields

deviations coming from corrections in second and higher orders in $\boldsymbol{h}$ become more important. These have been consistently neglected within our work. Note also that the zero-field corrections have been divided out using the renormalized zero-field value $\tilde{c}_0 \approx 1.16 c_0$ for $S = 1/2$ from a work by Oguchi [151].

2.6.2 Damping of antiferromagnetic magnons

Both, the real part of the self-energies and the imaginary part can be measured via neutron scattering experiments. Because of the power of this experimental technique a broad class of magnetic materials can be investigated. Among them are also insulating antiferromagnets, see Appendix A.1.

From a theoretical point of view, our result for the damping contains informations on two quantities: The magnetic field dependence of the damping is special for the antiferromagnetic magnons. The second feature, the dependence on the momentum arises from the volume of the scattering surface and is a general property of interacting Bose gases [34, 53, 184–186]. The $|\boldsymbol{k}|^3$-dependence of the magnon damping Eq. (2.166) has been obtained previously by Zhitomirsky and Chernyshev [233], and the general case $1 < D \leq 3$ was recalculated later [28]. Results from exact diagonalization of finite spin systems can be compared to our work [120]. In a recent work by Mourigal *et al.* [146] corrections to the spin-wave dispersion and the damping of the magnons were calculated for general magnetic fields up to the critical field. These perturbative corrections in a $1/S$ expansion have been obtained using a modified Dyson equation in the Bogoliubov basis, where only the magnon decay rate is calculated self-consistently. Apart from the calculation of the dynamical structure factor using the fluctuation-dissipation theorem, the authors also reconsidered the calculation of the damping near the magnetic ordering vector. This is equivalent to the damping rate $\gamma_{\boldsymbol{k}-}$ of the gapless magnon mode. Introducing the cubic coefficient $\alpha = \bar{A}_- c_-/2$ in the expansion of the quasiparticle dispersion $\tilde{E}_{\boldsymbol{k}-} = \tilde{c}_-|\boldsymbol{k}| + \alpha|\boldsymbol{k}|^3$, one can write the damping rate in the two-dimensional case as[2]

$$\Gamma_{\boldsymbol{k}-} = \frac{3J}{64\pi}\left(\frac{h}{h_c}\right)^2 \sqrt{\frac{c_-}{6\alpha}}|\boldsymbol{k}|^3 a^3 \,. \tag{2.173}$$

2.6.3 Nonanalyticities and the hydrodynamic relation

From calculations of the magnetization curves of the two-dimensional QAFM [233] it is known that the magnetization behaves for small magnetic fields as

$$M(h) = \chi_0 h + \frac{2}{\pi}\frac{h^2}{h_c^2} \,, \tag{2.174}$$

[2] There is still a disagreement in the prefactor between the result of Mourigal *et al.* [146] and the present work. However, the result for the damping Eq. (2.166), and also the reformulation Eq. (2.173) is not that powerful, since it behaves unphysically for $\alpha \to 0$. A more sophisticated improvement would be a self-consistent calculation [85, 146].

which yields a correction to the magnetic susceptibility that is nonanalytic in h^2,

$$\chi = \frac{\partial M}{\partial h} = \chi_0 \Big(1 + \frac{4}{\pi S} \frac{h}{h_c} \Big) \, . \tag{2.175}$$

Note that this result can also be obtained from the energy density $\varepsilon(h)$ of the ground state [66],

$$\varepsilon(h) \approx \begin{cases} \varepsilon_0 - \frac{1}{2}\chi_0 h^2 - \frac{|h|^3}{12\pi c_0^2} \, , & D = 2 \\ \varepsilon_0 - \frac{1}{2}\chi_0 h^2 - \frac{h^4}{32\pi^2 c_0^3} \ln\Big(\frac{c_0}{\lambda_0 h}\Big) \, , & D = 3 \end{cases} \tag{2.176}$$

where in three dimensions the length scale $\lambda_0 = (\rho\chi_0)^{-1/2}$ has been introduced. By taking derivatives, the same linear correction Eq. (2.175) emerges, whereas in three dimensions one obtains terms analytic in h^2 and a logarithmic correction,

$$\chi = -\frac{\partial^2 \varepsilon}{\partial h^2} = \chi_0 \Big\{ 1 + \frac{\sqrt{3}3}{2\pi S} \Big(\frac{h}{h_c} \Big)^2 \Big[\frac{7}{4} + 3 \ln\Big(\frac{h\lambda_0}{c_0} \Big) \Big] \Big\} \, . \tag{2.177}$$

Since the nonanalytic corrections to the susceptibility are similar to those of the spin-wave velocity, Eq. (2.132), the physical origin seems likely to be the same, namely the strong correlations of the staggered spin fluctuations in the QAFM. The hydrodynamic relation

$$c^2 = \frac{\rho}{\chi} \, , \tag{2.178}$$

connects the spin-wave velocity to the ratio of the spin stiffness and susceptibility. The spin stiffness, obtained from a spin-wave calculation using its definition via a twist in the boundary conditions [166] has been calculated with the result

$$\rho = \rho^0 \Big(1 + \frac{2}{\pi S} |h| \Big) \, , \tag{2.179}$$

where ρ^0 is the spin stiffness at zero field [84, 97]. Together with the corrections to the susceptibility χ and the spin-wave velocity the validity of the relation Eq. (2.178) has been checked analytically in the case of a two-dimensional QAFM at small magnetic fields [27]. A numerical calculation in the same work for fields $0 \leq h \leq h_c$ also confirms the hydrodynamic relation.

2.7 Summary and conclusions

The main results of the last chapter can be summarized in one statement: The leading $1/S$ correction to the self-energy of the gapless magnon in a QAFM subject to a weak magnetic field is a nonanalytic function of $\boldsymbol{h}^2$ in dimensions $D \leq 3$.

To come in contact with physical observables we explicitly calculated the magnetic-field dependence of the spin-wave velocity Eq. (2.132) and the damping rate Eq. (2.164) of the gapless magnon. Also the momentum-dependent quasiparticle residue Eq. (2.145) of this magnon is a key quantity in many-body physics. It is quite surprising that for a QAFM in a uniform magnetic field at zero temperature, the dimension $D = 3$ is a critical dimension. For $D \leq 3$ fluctuations lead to nonanalytic terms in the magnon spectrum. Certainly, the gapless magnon can be identified with the degrees of freedom of an interacting Bose gas in the condensed phase [P1]. It is well known that the Bogoliubov mean-field theory breaks down in dimensions $D \leq 3$ [23, 53, 156, 185, 187, 218].

To conclude and give an outlook to upcoming investigations let us stress that our hybrid approach between $1/S$ expansion and NLSM is a convenient parametrization of the spin-wave expansion which separates the ferromagnetic and antiferromagnetic fluctuations. Although the quantities that were calculated in the context of the QAFM can also be obtained within the conventional parametrization of the $1/S$ expansion, our hybrid approach eases the identification of relevant terms of the frequency-dependent contributions to the magnon self-energies, that give rise to the dominant magnetic-field dependent corrections to the magnon spectrum. In future investigations it would be interesting to consider more complicated model systems where the conventional spin-wave approach does not give reasonable results. In the case of the anisotropic, frustrated QAFM a lower symmetry of the Hamiltonian, namely the lack of inversion symmetry in real space causes unphysical divergencies. In chapter 4 we will again use our Hermitian operator approach to sort out these divergencies in the spin-wave expansion and calculate the renormalization of phonons due to the spin-phonon interaction.

Chapter 3

Microscopic spin-wave theory for yttrium-iron garnet films

3.1 Motivation

In this chapter we will extend the Heisenberg model Eq. (1.2) by taking the dipole-dipole interactions into account, and will analyze the spin-wave spectrum in thin films of the ferromagnetic insulator yttrium-iron garnet (YIG). This work is originally motivated by a recent series of experiments where strong correlations of highly occupied magnon states in thin films of the compound YIG were discovered [47–51, 57]. Spin-waves were injected by parametric pumping and the magnon density $\langle n_{\boldsymbol{k}} \rangle$ was optically observed with momentum resolution. Demokritov and co-workers then suggested to interpret the strong enhancement of the magnon density at the bottom of the spectrum as a Bose-Einstein condensation at room temperature [50, 189]. For a proper analysis of the experimental results, peculiar features of the spin waves, which are the relevant quasiparticles, are important: Firstly, the energy dispersion $E_{\boldsymbol{k}}$ of the lowest magnon band in YIG films exhibits a local minimum at a finite wave vector $\boldsymbol{k}_{\min}$. This feature occurs due to a subtle interplay between finite-size effects, short-range exchange interactions and the presence of long-range dipole-dipole interactions. The existence of such a minimum in the dispersion has been predicted by Kalinikos and Slavin [103, 188, B44] using a phenomenological approach based on the Landau-Lifshitz equation. Unfortunately, this phenomenological theory does not provide a microscopic understanding of correlation effects which might be important to explain some aspects of the behavior of the magnon gas. Moreover to describe the condensation phenomena of a non-equilibrium magnon gas one also needs an understanding of the interaction processes and the time-dependent terms in the Hamiltonian. A pumped magnon gas is an important source for possible data processing with spin-waves. Recent technical advances have demonstrated that computing based on spin waves [108] can be realized: Thin films of YIG are good candidates for spintronic devices [102, 171, 176]. The first idea to

use the spin for transporting signals emerged when spin polarized currents were injected and detected in metals [101]. The use of spin polarized currents in conductors suffers from high scattering rates and is therefore restricted to small distances. Spin currents alone are also realized in traveling spin-wave packets, and the low damping rates in YIG [26] allow transport at macroscopic distances. Recently, the conversion and recovery of spin currents using Pt films on YIG samples has been shown [102]. By the help of the spin-Hall effect, electrical signals have been converted to spin-waves which provides a useful spintronic device. A new efficient magnon detection using the inverse spin-Hall effect in combination with spin pumping makes the observation of spin-waves in a wider range of wave vectors possible. This method delivers new insights in the physics of magnons with sub-micron wavelengths to further miniaturize the magnon-based spintronic devices [171].

In this work we will mainly concentrate on building up a spin-wave theory within the framework of the $1/S$ expansion for ordered spin systems to provide a starting point for further investigations on magnons in thin-film ferromagnets. The bosonization of an effective microscopic Heisenberg model and the classification of the interaction processes in powers of the small parameter $1/S$ will set up a theory describing the magnons as elementary excitations in thin films of YIG. Parts of this chapter were published in Refs. [P3, P6]. The theoretical part was done in collaboration with Francesca Sauli, who set up the numerical approach (section 3.4.1), Lorenz Bartosch and Peter Kopietz, while the comparison of the theoretical results with the experimental data was done together with Christian Sandweg and Alexander Serga. Further research, which is not presented in this thesis, also uses our framework to calculate corrections to the magnon spectrum due to interactions [172] or investigate condensation phenomena for quasiparticles with finite momentum [P7].

From a more theoretical point of view this work can also be motivated by the proximity of our model to the model of a dipolar ferromagnet in two and three dimensions, where no finite-size effects are considered [21, 79, 194–197]: The anisotropic and long-range dipole-dipole interactions violate the assumptions of the Mermin-Wagner theorem [141] and therefore finally stabilize the magnetic ordering in two dimensions at finite temperature. Moreover the magnon spectrum is greatly renormalized and exhibits an excitation gap in two and three dimensional dipolar magnets. Although this particular behavior of the magnon spectrum is probably not observable in YIG[1], the models are related and can be studied using similar approaches.

[1] A. A. Serga, private communication.

3.2 Introduction

In previous investigations, several authors have used the $1/S$ expansion to obtain the spin-wave spectra in ultrathin ferromagnetic films with exchange and dipole-dipole interactions [46, 60, 61, 99, 164] or investigated thermodynamic properties [59, 227]. Also interaction effects as corrections to the energy dispersion and the damping of spin waves have been calculated [43, 44]. To extend this approach to realistic models for experimentally relevant YIG films, it is required to evaluate numerically rather large dipolar sums [12]. To finally obtain the dispersion of the magnon modes for films that have a thickness of a few microns, corresponding to a few thousand lattice spacings, Ewald summation techniques [10, 63, 172, B40] are advantageous to carry out the summations that result from the discrete Fourier transformation. To get a physical insight in the results of the numerical implementation, one also needs some analytical approximations that are at least valid in some physically important ranges. We will therefore compare the results of two different analytical approximations to those of a numerical approach.

Effective model for YIG films

To begin our discussion, we motivate our effective model for the experimentally relevant samples. The compound YIG with stoichiometric formula $Y_3Fe_2(FeO_4)_3$ has been known for a long time [74, 75] and has been subject to a great quantity of experimental and theoretical research [26, 117, 181, B10, B14, B42]. One evident advantage of YIG is that it can be grown in very pure crystals, and subsequently has a very narrow ferromagnetic resonance line, indicating a low spin-wave damping. Concerning the magnetic properties, YIG is a ferrimagnet at accessible magnetic fields [B43] and has a rather complicated crystal structure, for details see Appendix B.1. On the energy scales relevant to experiments [31, 47–51, 57, 149, 169, 170, 177, 180, P6] only the lowest ferromagnetic magnon band is important. The magnetic properties can therefore be described in terms of an effective spin-S quantum Heisenberg ferromagnet on a cubic lattice with lattice spacing [75]

$$a = 12.376\,\text{Å}\,. \tag{3.1}$$

We now add to the ferromagnetic Heisenberg model the dipole-dipole interactions, introduced in Eq. (1.8), so that the effective Hamiltonian for YIG is

$$\begin{aligned}\hat{H} = &-\frac{1}{2}\sum_{ij} J_{ij}\boldsymbol{S}_i\cdot\boldsymbol{S}_j - \mu\boldsymbol{H}_e\cdot\sum_i \boldsymbol{S}_i \\ &-\frac{1}{2}\sum_{ij,i\neq j}\frac{\mu^2}{|\boldsymbol{R}_{ij}|^3}\left[3(\boldsymbol{S}_i\cdot\hat{\boldsymbol{R}}_{ij})(\boldsymbol{S}_j\cdot\hat{\boldsymbol{R}}_{ij}) - \boldsymbol{S}_i\cdot\boldsymbol{S}_j\right].\end{aligned} \tag{3.2}$$

Anticipating a rapid decay of the exchange energies (compare section 1.1.1) we restrict ourselves to nearest-neighbor exchange couplings, setting $J_{ij} = J > 0$

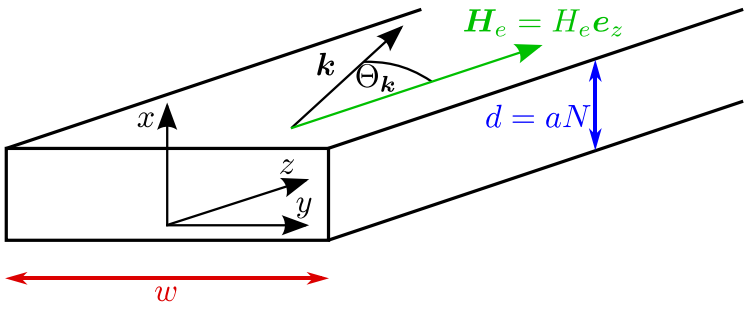

Figure 3.1: *Orientation of our coordinate system for an infinitely long stripe of width w and thickness d. The external magnetic field $\boldsymbol{H}_e = H_e\boldsymbol{e}_z$ is assumed to be parallel to the long axis (z-axis) of the stripe.*

if $\boldsymbol{R}_i$ and $\boldsymbol{R}_j$ are nearest neighbors, and $J_{ij} = 0$ otherwise. We do not consider anisotropies that might be present especially at the surface of the film or at the connection to the substrate. In order to finally calculate the spectrum and compare to experiments, one has to collect the relevant parameters of our effective model: The material YIG is characterized by its saturation magnetization [203]

$$4\pi M_S = 1750\,\mathrm{G}\ , \tag{3.3}$$

and the exchange stiffness ρ_{ex} at low magnon densities [B10],

$$\frac{\rho_{\mathrm{ex}}}{\mu} = \frac{JSa^2}{\mu} \approx 5.17 \times 10^{-13}\ \mathrm{Oe\,m^2}\ . \tag{3.4}$$

Setting the effective g-factor equal to two [203] so that $\mu = 2\mu_B$, we calculate the effective spin from Eqs. (3.3) and (3.4) with the result

$$S = \frac{M_S a^3}{\mu} \approx 14.2\ . \tag{3.5}$$

The exchange coupling is then given by [208]

$$J = 1.29\,\mathrm{K}\ . \tag{3.6}$$

Introducing the dipolar tensor $D_{ij}^{\alpha\beta} = D^{\alpha\beta}(\boldsymbol{R}_i - \boldsymbol{R}_j)$,

$$\begin{aligned} D_{ij}^{\alpha\beta} &= (1-\delta_{ij})\frac{\mu^2}{|\boldsymbol{R}_{ij}|^3}\left[3\hat{R}_{ij}^{\alpha}\hat{R}_{ij}^{\beta} - \delta^{\alpha\beta}\right] \\ &= (1-\delta_{ij})\mu^2\frac{\partial^2}{\partial R_{ij}^{\alpha}\partial R_{ij}^{\beta}}\frac{1}{|\boldsymbol{R}_{ij}|}\ , \end{aligned} \tag{3.7}$$

the effective Hamiltonian Eq. (3.2) can be written in the compact form

$$\hat{H} = -\frac{1}{2}\sum_{ij}\sum_{\alpha\beta}\left[J_{ij}\delta^{\alpha\beta} + D_{ij}^{\alpha\beta}\right]S_i^{\alpha}S_j^{\beta} - h\sum_i S_i^z\ . \tag{3.8}$$

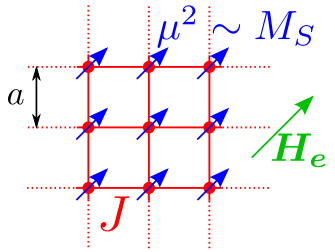

Figure 3.2: *Our basic model consists of a spin-S Heisenberg ferromagnet on a cubic lattice of lattice spacing a with exchange coupling J, dipole-dipole interactions that are characterized by the saturation magnetization M_S, and a magnetic field $\boldsymbol{H}_e$.*

We have chosen our coordinate system such that the z-axis points into the direction defined by the magnetic field $\boldsymbol{H}_e$ which is connected to the Zeemann energy h by

$$h = \mu |\boldsymbol{H}_e| \; . \tag{3.9}$$

In summary, we start from a microscopic Hamiltonian Eq. (3.8) which contains the set of parameters a, S, J, h that are related to experimentally measurable quantities, see Fig. 3.2.

3.3 Spin-wave approach

In order to continue, we restrict ourselves to the description of an infinitely long stripe of width w and thickness $d = Na$, i.e. a thin film of N layers. Following the steps described in section 1.4 to set up spin-wave theory, we start with the discussion of the classical ground state. For the stripe geometry, where the magnetic field is parallel to the stripe, we have a saturated ferromagnet. Noting that the effective spin $S \approx 14.2$ is quite large, the expansion in powers of $1/S$ is justified and can be truncated at low orders. Inserting the Holstein-Primakoff (HP) or Dyson-Maleyev transformation [96, B2, B21] (see also page 15 ff.) we expand the Hamiltonian in fluctuations around the classical ground state. In terms of these bosonic fluctuations the Hamiltonian in real space can be written as

$$\hat{H} = E_0^{\rm cl} + \sum_{n=2}^{\infty} \hat{H}_n \; . \tag{3.10}$$

It is well known [190, B21] that the HP and Dyson-Maleyev transformations give different results for $\hat{H}_n$ with $n \geq 4$, but the expressions for $\hat{H}_2$ and $\hat{H}_3$ are identical in both transformations, so that these differences do not play any role for our discussion. The first term in the expansion above, the classical ground-state energy is

$$E_0^{\rm cl} = -\frac{S^2}{2} \sum_{ij} \left[J_{ij} + D_{ij}^{zz} + \frac{2J_{ij} - D_{ij}^{zz}}{2S} \right] , \tag{3.11}$$

and the quadratic part of the Hamiltonian reads

$$\hat{H}_2 = \sum_{ij} \left[A_{ij} b_i^\dagger b_j + \frac{B_{ij}}{2} \left(b_i b_j + b_i^\dagger b_j^\dagger \right) \right] , \tag{3.12}$$

where $b_i^\dagger$ and b_i are creation and annihilation operators of bosons and the coefficients are given by

$$A_{ij} = \delta_{ij} h + S(\delta_{ij} \sum_n J_{in} - J_{ij}) + S \left[\delta_{ij} \sum_n D_{in}^{zz} - \frac{D_{ij}^{xx} + D_{ij}^{yy}}{2} \right] , \tag{3.13a}$$

$$B_{ij} = -\frac{S}{2} \left[D_{ij}^{xx} - 2iD_{ij}^{xy} - D_{ij}^{yy} \right] . \tag{3.13b}$$

As the terms of the Hamiltonian are of a defined order in $1/S$, i.e. $\hat{H}_n \propto S^{2-\frac{n}{2}}$ (see Eq. (1.60)), and the effective spin S is large, one should get accurate results even if we only keep the first two terms,

$$\hat{H} \approx E_0^{\mathrm{cl}} + \hat{H}_2 . \tag{3.14}$$

Contrarily to the models for spin-wave calculations in bulk magnets[2], our system, describing a stripe of thickness d and width w, is obviously not translationally invariant. Thus, we cannot use a full Fourier transform to diagonalize this Hamiltonian. Because in the experimentally studied samples the width w of the stripe is three orders of magnitude larger than the thickness d, we assume w to be practically infinite. Thus, we consider for $w \to \infty$ a slab which has discrete translational invariance in the y- and z-directions. To partially diagonalize $\hat{H}_2$ in Eq. (3.12) we perform a partial Fourier transformation in the yz-plane. Defining $\boldsymbol{r}_i = (y_i, z_i)$, so that $\boldsymbol{R}_i = (x_i, \boldsymbol{r}_i)$ and introducing the two-dimensional wave vector $\boldsymbol{k} = (k_y, k_z)$ in the yz-plane, we expand

$$b_i = \frac{1}{\sqrt{N_y N_z}} \sum_{\boldsymbol{k}} e^{i\boldsymbol{k}\cdot\boldsymbol{r}_i} b_{\boldsymbol{k}}(x_i) , \tag{3.15}$$

where N_y and N_z is the number of lattice sites in the y- and z-direction. Substituting this in Eq. (3.12) we rewrite the Hamiltonian under consideration as

$$\begin{aligned} \hat{H}_2 = \sum_{\boldsymbol{k}} \sum_{x_i, x_j} \Big[& A_{\boldsymbol{k}}(x_{ij}) b_{\boldsymbol{k}}^\dagger(x_i) b_{\boldsymbol{k}}(x_j) + \frac{B_{\boldsymbol{k}}(x_{ij})}{2} b_{\boldsymbol{k}}(x_i) b_{-\boldsymbol{k}}(x_j) \\ & + \frac{B_{\boldsymbol{k}}^*(x_{ij})}{2} b_{\boldsymbol{k}}^\dagger(x_i) b_{-\boldsymbol{k}}^\dagger(x_j) \Big] . \end{aligned} \tag{3.16}$$

We define the matrix describing the isotropic exchange interaction by

$$J_{\boldsymbol{k}}(x_{ij}) = J \Big\{ \delta_{ij} \big[6 - \delta_{j1} - \delta_{jN} - 2[\cos(k_y a) + \cos(k_z a)] \big] - \delta_{ij+1} - \delta_{ij-1} \Big\} , \tag{3.17}$$

[2]Details on spin-wave calculations for bulk dipolar ferromagnets including magnon-magnon interactions can be found in Refs. [B2, B45, B35].

and the partial Fourier transform of the dipolar tensor by

$$D_{\boldsymbol{k}}^{\alpha\beta}(x_{ij}) = \sum_{\boldsymbol{r}_{ij}} e^{-i\boldsymbol{k}\cdot\boldsymbol{r}_{ij}} D_{ij}^{\alpha\beta} \tag{3.18}$$

to write down the amplitude factors [43, 44],

$$\begin{aligned} A_{\boldsymbol{k}}(x_{ij}) &= \sum_{\boldsymbol{r}} e^{-i\boldsymbol{k}\cdot\boldsymbol{r}} A(x_i - x_j, \boldsymbol{r}) \\ &= SJ_{\boldsymbol{k}}(x_{ij}) + \delta_{ij}\Big[h + S\sum_n D_0^{zz}(x_{in})\Big] - \frac{S}{2}\Big[D_{\boldsymbol{k}}^{xx}(x_{ij}) + D_{\boldsymbol{k}}^{yy}(x_{ij})\Big] , \end{aligned} \tag{3.19a}$$

$$\begin{aligned} B_{\boldsymbol{k}}(x_{ij}) &= \sum_{\boldsymbol{r}} e^{-i\boldsymbol{k}\cdot\boldsymbol{r}} B(x_i - x_j, \boldsymbol{r}) \\ &= -\frac{S}{2}\Big[D_{\boldsymbol{k}}^{xx}(x_{ij}) - 2iD_{\boldsymbol{k}}^{xy}(x_{ij}) - D_{\boldsymbol{k}}^{yy}(x_{ij})\Big] . \end{aligned} \tag{3.19b}$$

3.4 Spin-wave spectra of YIG films in linear spin-wave theory

3.4.1 Numerical approach

For a film with N layers in the x-direction there are N allowed magnon energies $E_{n\boldsymbol{k}}$, $n = 0, \ldots, N-1$, for a fixed two-dimensional wave vector $\boldsymbol{k}$. These energies are given by the positive zeros of the secular determinant

$$\det \begin{pmatrix} E_{\boldsymbol{k}} - \mathbf{A}_{\boldsymbol{k}} & -\mathbf{B}_{\boldsymbol{k}} \\ -\mathbf{B}_{\boldsymbol{k}}^* & -E_{\boldsymbol{k}} - \mathbf{A}_{\boldsymbol{k}} \end{pmatrix} = 0 , \tag{3.20}$$

where the $N \times N$-matrices $\mathbf{A}_{\boldsymbol{k}}$ and $\mathbf{B}_{\boldsymbol{k}}$ are defined by

$$[\mathbf{A}_{\boldsymbol{k}}]_{ij} = A_{\boldsymbol{k}}(x_{ij}) , \tag{3.21a}$$

$$[\mathbf{B}_{\boldsymbol{k}}]_{ij} = B_{\boldsymbol{k}}(x_{ij}) . \tag{3.21b}$$

Note that the indices $1 \leq i, j \leq N$ now label the lattice sites or layers in the x-direction. The condition Eq. (3.20) follows simply from the fact that the magnon energies can be identified with the poles of the magnon propagators of the Gaussian field theory defined by the quadratic Hamiltonian Eq. (3.16). Reducing the model to one single layer, i.e. $N = 1$, our secular determinant correctly reduces to the result from the diagonalization of this Hamiltonian via a Bogoliubov transformation, compare section 1.3.1.

In order to obtain all magnon energies of the thin-film ferromagnet, we first have to calculate the dipolar matrices that contribute to the amplitude factors

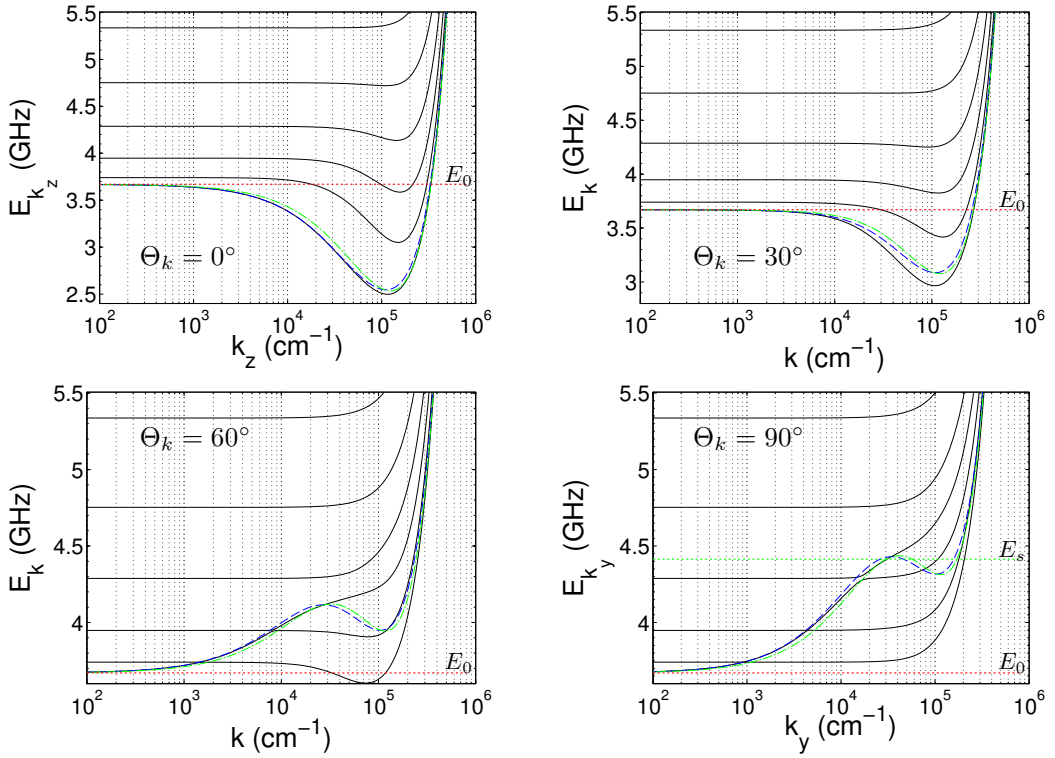

Figure 3.3: *Spin-wave dispersion of a YIG film with thickness* $d = 400a \approx 0.495\,\mu$m *in a magnetic field of* 700 Oe *for wave vectors in the plane of the film and for different propagation angles* $\Theta_{\boldsymbol{k}} = 0°, 30°, 60°, 90°$ *relative to the magnetic field (from top left to bottom right). The black solid curves represent the results from the numerical approach for the lowest modes. The other curves are calculated from Eq. (3.41) using the full form factor* $f_{\boldsymbol{k}}$ *defined in Eq. (3.36) (dashed) and Eq. (3.52) (dash dotted). The thick dotted line labeled* E_0 *marks the energy of the ferromagnetic resonance given by Eq. (3.24); the thick dotted line labeled* E_s *is the energy* $E_s = h + \Delta/2$ *of the classical surface mode for* $\Theta_{\boldsymbol{k}} = 90°$ *at large wave vectors, see Eqs. (3.25) and (3.26), taken from [P3].*

Eqs. (3.19a) and (3.19b). This leads to the calculation of the following dipolar sums for fixed difference x_{ij},

$$D^{\alpha\beta}_{\boldsymbol{k}}(x_{ij}) = -\mu^2 \sum_{y_{ij},z_{ij}}{}' e^{-i(k_y y_{ij} + k_z z_{ij})} \left[\frac{\delta^{\alpha\beta}}{(x_{ij}^2 + y_{ij}^2 + z_{ij}^2)^{3/2}} - \frac{3 r_{ij}^{\alpha} r_{ij}^{\beta}}{(x_{ij}^2 + y_{ij}^2 + z_{ij}^2)^{5/2}} \right], \tag{3.22}$$

where $\sum'$ takes the Kronecker delta in the definition of the dipolar tensor, Eq. (3.7), into account, i.e. excludes the term $y_{ij} = z_{ij} = 0$ when $x_{ij} = 0$. These sums are slowly converging, and previously used summation techniques [43, 99] are not very efficient whenever the momentum $\boldsymbol{k}$ is small. We therefore use the Ewald summation technique to calculate the localized contribution of the sum in real space and the oscillating tails in reciprocal space. This method

also provides a control variable that shifts weights from the sums in real space to the sums in reciprocal space [10, 18, 46, 72, 79]. Details of the calculation can be found in Refs. [172, P3]. In the second step we numerically calculate the roots of Eq. (3.20) resulting in a positive and an identical negative set of the eigenenergies. Without further considerations this calculation can be done up to a film thickness of $d \approx 7\,\mu$m which covers experimentally relevant samples [31, 47–51, 57, 149, 169, 177, 180, P6]. Since the direct calculation of the roots is numerically expensive, we map this problem to the problem of the calculation of the eigenvalues of the $2N \times 2N$ matrix [150, 168],

$$\mathbf{F}_{\boldsymbol{k}} = \begin{pmatrix} \mathbf{A}_{\boldsymbol{k}} & \mathbf{B}_{\boldsymbol{k}} \\ \mathbf{B}^{*}_{-\boldsymbol{k}} & -\mathbf{A}^{T}_{-\boldsymbol{k}} \end{pmatrix} . \tag{3.23}$$

Using the ratio $\mu/h \approx 2.803 \times 10^{-3}\,\mathrm{GHz/Oe}$ [110] we plot all results in units of frequency which is most convenient for experiments utilizing microwave resonators and antennas operating at radio frequencies to pump magnetic excitations. To illustrate our results we present magnon dispersions for different angles $\Theta_{\boldsymbol{k}}$, between the momentum $\boldsymbol{k}$ of the spin-waves and the magnetic field, compare Fig. 3.1. In Fig. 3.3 the black solid lines represent the energies of the lowest modes for a film with thickness $d = 400a$. Independently from the thickness d, the dispersion of the lowest mode approaches for $\boldsymbol{k} \to 0$ the classical ferromagnetic resonance energy

$$E_0 = \sqrt{h(h+\Delta)}\,, \tag{3.24}$$

indicated by a red dotted line in the plots. Here we have introduced the characteristic magnon energy,

$$\Delta = 4\pi\mu M_S\,, \tag{3.25}$$

due to dipolar interactions. Note that the ferromagnetic resonance is a spectroscopic technique to probe spin waves and magnetization in ferromagnetic compounds. In the picture of classical electrodynamics, the observed absorption of microwave radiation arises from the precessional motion of the magnetization in an external magnetic field. Solving the classical equations of motion for the macroscopic magnetization, which is subject to a torque from the magnetic field, Kittel's equation can be obtained. In the case of a thin film it reduces to Eq. (3.24) [110, B2] and has been verified experimentally for tangentially magnetized thin films of metallic or nonmetallic materials [B10].

Studying the effects of the finite thickness, one recognizes that the spacing between different magnon modes decreases with increasing film thickness. The magnon spectrum for a film with thickness $d = 4040a = 5\,\mu$m, shown in Fig. 3.4, already forms a quasi-continuum for energies close to the ferromagnetic resonance. In the regime $dk \ll 1$ it is easy to see that the nth mode deviates from the first mode by an energy $\Delta E_n = \rho_{\mathrm{ex}}\pi^2 n^2/d^2$. If one associates a

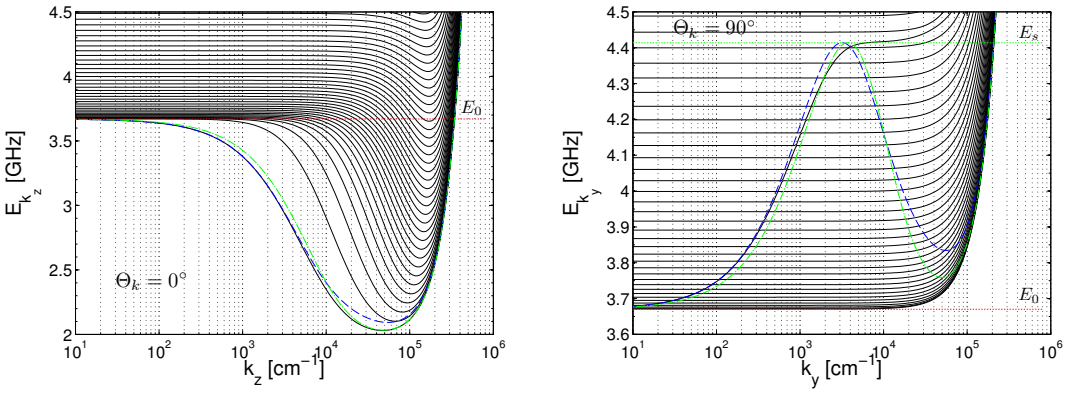

Figure 3.4: *Spin-wave dispersion of a YIG film with thickness* $d = 4040a = 5\ \mu$m *for wave vectors parallel to the external field* $H_e = 700$ Oe *for* $\Theta_{\boldsymbol{k}} = 0°$ *(left) and for* $\Theta_{\boldsymbol{k}} = 90°$ *(right).*

perpendicular momentum $k_n = (n+1)\pi/d$ with the nth mode, this reflects the well known behavior of ferromagnetic spin waves, and indicates the crossover from the quasi two-dimensional case discussed here to the dispersion of three-dimensional spin waves.

Note that the dispersion of the magnon modes has been obtained previously in the framework of the Landau-Lifshitz equation in a semiclassical approach [103, 188, B44]. The basic idea of this method of calculating magnon spectra goes back to solving Walker's wave equation [216]. Without explaining the details of this calculation, we mention that the resulting solutions can be categorized in two types: The first type are the volume waves. Their amplitude inside the ferromagnet is represented by trigonometric functions of the coordinate in the direction perpendicular to the surface. For the second type, the surface waves, this dependence is represented by hyperbolic functions such that these waves propagate on the surface of the ferromagnet [B10].

In a typical experimental setup that optically detects the spin waves using Brillouin light scattering spectroscopy (BLS) [50, P6, B47] the lowest mode is mainly observed due to restrictions in the installation upon collecting the scattered light. For details on this experimental technique consult the description in the Appendix B.2 [P6]. Fig. 3.5 illustrates the dispersion of the lowest mode that exhibits the well known [103] minimum for a momentum $\boldsymbol{k}_{\min}$ parallel to the external magnetic field ($\Theta_{\boldsymbol{k}} = 0$), where large magnon densities have been detected [50, 51]. Fig. 3.6 brings out the dependence of the position of the minimum as a function of the film thickness for different magnetic fields. It turns out that the minimum, which is only present in the quasi two-dimensional case, is less pronounced for ultrathin films. As a function of the propagation angle $\Theta_{\boldsymbol{k}}$ the minimum becomes more shallow if the angle increases and completely disappears for $\Theta_{\boldsymbol{k}} = 90°$. Figs. 3.3 and 3.4 show that for angles $\Theta_{\boldsymbol{k}} > 45°$ the

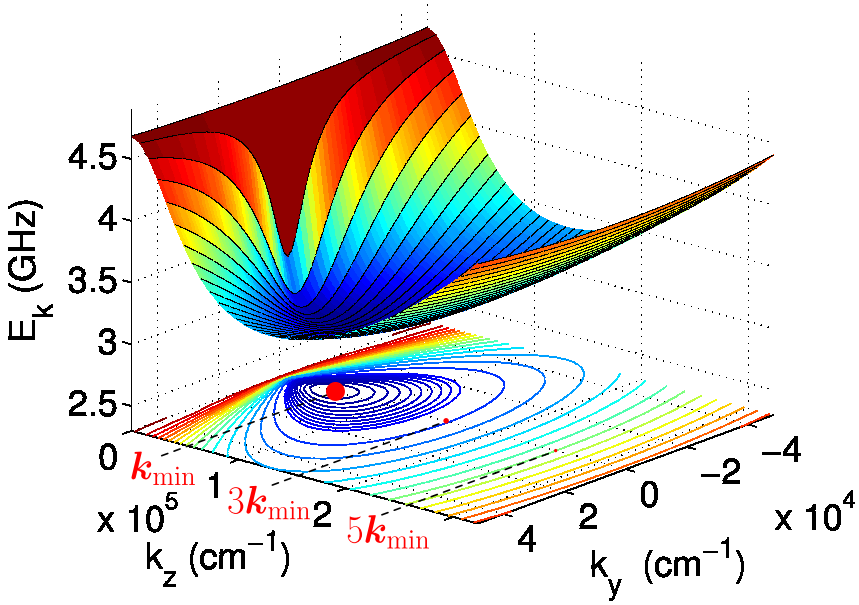

Figure 3.5: *Spin-wave dispersion of the lowest mode of a YIG film with* $H_e = 1000$ Oe *and* $d = 5.1$ μm *obtained from the numerical solution of Eq. (3.20). Starting from the minimal energy* $E_{\min}$ *contour lines with the spacing* 20 MHz *are shown to illustrate the rather flat minimum, whereas for larger energies the distance between contour lines is* 100 MHz. *Knowing the properties of the spectrum calculated within our microscopic approach and the interaction processes from the spin-wave expansion in our analytical approximation, a Bose condensate at finite momentum* $\boldsymbol{k}_{\min}$ *was investigated. Once there is a condensate at* $\boldsymbol{k}_{\min}$*, condensates at all odd multiples of this momentum* $3\boldsymbol{k}_{\min}, 5\boldsymbol{k}_{\min}, \ldots$ *also emerge. The red dots symbolize the position in momentum space where condensates are expected. Their areas reflect the magnitude of the coefficient of the corresponding Fourier component of the condensate wave function at strong pumping [P7].*

lowest modes shift upwards and tend to hybridize with higher modes if the momentum becomes larger. Since there are no additional symmetries present, the energy levels never cross. However, the splitting is rather small and for a quantitative discussion with regard to the experimental relevant samples one should also consider anisotropies [155, B44]. Nevertheless, the magnon modes with finite group velocities $\boldsymbol{v}_g(\boldsymbol{k}) = \boldsymbol{\nabla}_{\boldsymbol{k}} E_{\boldsymbol{k}}$ form the quasi-continuous surface mode. From the data it is obvious that no further hybridizations occur as soon as the mode energies reach the energy

$$E_s = h + \Delta/2 \tag{3.26}$$

of the classical surface mode. The general case of this equation has been obtained from a classical approach for magnetostatic waves [62].

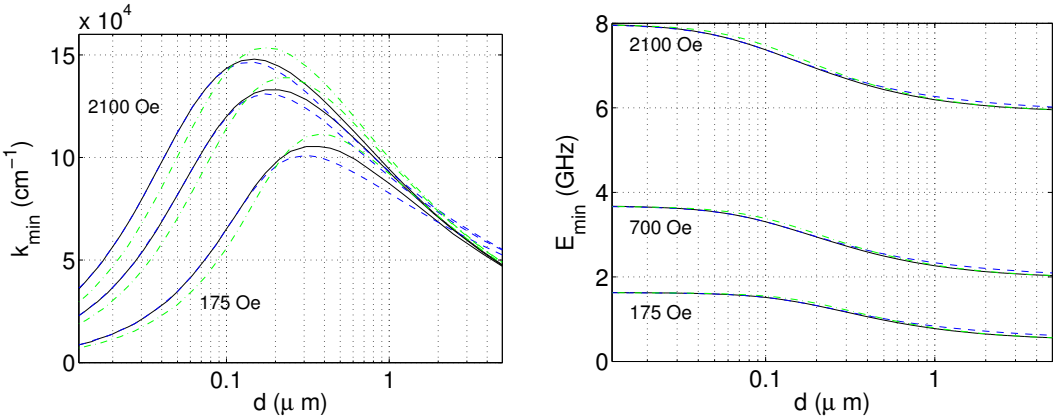

Figure 3.6: *Momentum $k_{\min}$ (left) and energy $E_{\min}$ (right) of the minimum in the dispersion of the lowest magnon mode for $\Theta_{\boldsymbol{k}} = 0$ as a function of film thickness for different magnetic fields. From top to bottom $H_e = 2100, 700, 175$ Oe. The black solid lines are the values obtained from the numerical approach, while the other plots are calculated within the uniform mode approximation (blue, dashed) and the lowest eigenmode approximation (green, dash dotted), as explained in section 3.4.2 and 3.4.3.*

3.4.2 Uniform mode approximation

In order to calculate the dispersion of the lowest magnon band it is convenient to reduce the Hamiltonian, Eq. (3.16), to an effective in-plane Hamiltonian using various approximations. In the simplest approach we ignore the fact that the system is not translationally invariant in the x-direction. Approximating the corresponding eigenfunctions by plane waves we can obtain the lowest magnon band by replacing the operators $b_{\boldsymbol{k}}(x_i)$ as follows,

$$b_{\boldsymbol{k}}(x_i) \approx \frac{1}{N} \sum_j b_{\boldsymbol{k}}(x_j) \equiv \frac{1}{\sqrt{N}} b_{\boldsymbol{k}} \; . \tag{3.27}$$

The relevant effective Hamiltonian in this approximation is then

$$\hat{H}_2^{\text{eff}} = \sum_{\boldsymbol{k}} \left[A_{\boldsymbol{k}} b_{\boldsymbol{k}}^\dagger b_{\boldsymbol{k}} + \frac{B_{\boldsymbol{k}}}{2} b_{\boldsymbol{k}} b_{-\boldsymbol{k}} + \frac{B_{\boldsymbol{k}}^*}{2} b_{\boldsymbol{k}}^\dagger b_{-\boldsymbol{k}}^\dagger \right] \; , \tag{3.28}$$

with coefficients

$$A_{\boldsymbol{k}} = \frac{1}{N} \sum_{ij} A_{\boldsymbol{k}}(x_{ij}) \; , \tag{3.29a}$$

$$B_{\boldsymbol{k}} = \frac{1}{N} \sum_{ij} B_{\boldsymbol{k}}(x_{ij}) \; , \tag{3.29b}$$

that are just the averaged amplitude factors Eqs. (3.19a) and (3.19b). In order to proceed, we parametrize the in-plane wave vector in terms of its magnitude

and the angle $\Theta_{\boldsymbol{k}}$ as

$$\boldsymbol{k} = |\boldsymbol{k}| \left(\cos\Theta_{\boldsymbol{k}}\, \boldsymbol{e}_z + \sin\Theta_{\boldsymbol{k}}\, \boldsymbol{e}_y\right) \ . \tag{3.30}$$

Next, we use the representation of the dipolar tensor as derivative, Eq. (3.7), and the integral

$$\int_{-\infty}^{\infty} dz\, e^{-ikz} \frac{z^2 - x^2}{(x^2+z^2)^2} = -\pi\, |k|\, e^{-|k||x|} \tag{3.31}$$

to carry out the integrations over the two infinite directions and obtain for $x_{ij} \neq 0$,

$$D_{\boldsymbol{k}}^{xx}(x_{ij}) = D_{\boldsymbol{k}}(x_{ij}) \ , \tag{3.32a}$$
$$D_{\boldsymbol{k}}^{yy}(x_{ij}) = -\sin^2\Theta_{\boldsymbol{k}}\ D_{\boldsymbol{k}}(x_{ij}) \ , \tag{3.32b}$$
$$D_{\boldsymbol{k}}^{zz}(x_{ij}) = -\cos^2\Theta_{\boldsymbol{k}}\ D_{\boldsymbol{k}}(x_{ij}) \ , \tag{3.32c}$$
$$D_{\boldsymbol{k}}^{xy}(x_{ij}) = \sin\Theta_{\boldsymbol{k}}\ D_{\boldsymbol{k}}(x_{ij}) \Big[\frac{|\boldsymbol{k}|}{x_{ij}} + \frac{\mathrm{sign}(x_{ij})}{x_{ij}^2}\Big] \ , \tag{3.32d}$$

where

$$D_{\boldsymbol{k}}(x_{ij}) = \frac{2\pi\mu^2}{a^2} |\boldsymbol{k}| e^{-|\boldsymbol{k}||x_{ij}|} \ . \tag{3.33}$$

In the derivation of the dipolar tensor Eqs. (3.32a–3.32d) by the integration in the continuum limit, it is necessary to assume $x_{ij} \neq 0$. If we also replace the sum $\sum_{x_i}$ by the integral $a^{-1}\int_{-d/2}^{d/2} dx$ we have to worry about the factor $(1-\delta_{ij})$ that formally removes one term from the sum Eq. (3.22). To properly include this feature in the integral we remove a sphere of infinitesimal radius around $x_{ij} = y_{ij} = z_{ij} = 0$ from the integrations[3]. Taking into account the integral

$$\int_a^b dx\, f(|x|) = F(|a|) - \mathrm{sign}(ab) F(|b|) - 2\int_a^b dx\, \delta(x) F(x) \tag{3.34}$$

with $a < b$ for a continuous and integrable function $f(x)$ and its antiderivative $F(x)$ we find that the dipole matrix elements

$$D_{\boldsymbol{k}}^{xx} = \frac{4\pi\mu^2}{a^3}\Big[\frac{1}{3} - f_{\boldsymbol{k}}\Big] \ , \tag{3.35a}$$
$$D_{\boldsymbol{k}}^{yy} = \frac{4\pi\mu^2}{a^3}\Big[\frac{1}{3} + \sin^2\Theta_{\boldsymbol{k}}\,(f_{\boldsymbol{k}} - 1)\Big] \ , \tag{3.35b}$$
$$D_{\boldsymbol{k}}^{zz} = \frac{4\pi\mu^2}{a^3}\Big[\frac{1}{3} + \cos^2\Theta_{\boldsymbol{k}}\,(f_{\boldsymbol{k}} - 1)\Big] \ , \tag{3.35c}$$

and $D_{\boldsymbol{k}}^{xy} = 0$ can now be written as function of the angle $\Theta_{\boldsymbol{k}}$ and the form factor [208]

[3]Thanks to Lorenz Bartosch who called the attention to this crucial step and finally calculated the results cited below.

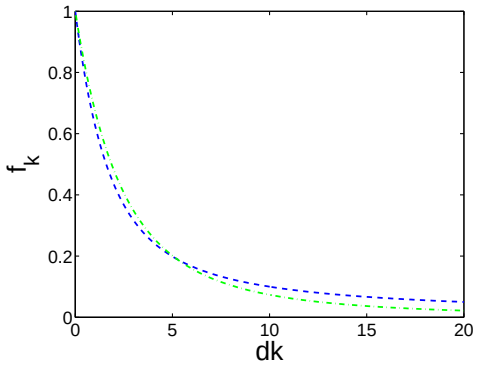

Figure 3.7: *Plot of the form factors Eq. (3.36) for the uniform mode approximation (blue, dashed) and Eq. (3.52) for the lowest eigenmode approximation (green, dash dotted). For the samples used in the experiments the minimum of the lowest mode is at* $dk \gtrsim 5$ *where the lowest eigenmode approximation is more accurate.*

$$f_{\boldsymbol{k}} = \frac{1 - e^{-|\boldsymbol{k}|d}}{|\boldsymbol{k}|d} = 1 - \frac{|\boldsymbol{k}|d}{2} + \mathcal{O}(\boldsymbol{k}^2 d^2) \; . \tag{3.36}$$

Eqs. (3.35a–3.35c) directly imply the constraint

$$D^{xx}_{\boldsymbol{k}} + D^{yy}_{\boldsymbol{k}} + D^{zz}_{\boldsymbol{k}} = 0 \; , \tag{3.37}$$

which is also obvious from the definition Eq. (3.7) of the dipolar tensor and agrees with the corresponding matrix elements obtained from the numerical approach. The coefficients $A_{\boldsymbol{k}}$ and $B_{\boldsymbol{k}}$ in the effective in-plane Hamiltonian are now given by

$$A_{\boldsymbol{k}} = h + JS\Big[4 - 2\cos(k_y a) - 2\cos(k_z a)\Big] - \frac{S}{2}\Big(D^{xx}_{\boldsymbol{k}} + D^{yy}_{\boldsymbol{k}}\Big) + \frac{\Delta}{3} \; , \tag{3.38a}$$

$$B_{\boldsymbol{k}} = -\frac{S}{2}\Big(D^{xx}_{\boldsymbol{k}} - D^{yy}_{\boldsymbol{k}}\Big) \; , \tag{3.38b}$$

which makes it possible to diagonalize it via a Bogoliubov transformation Eq. (1.29) [B2, B21], resulting in the spectrum

$$E_{\boldsymbol{k}} = \sqrt{A^2_{\boldsymbol{k}} - |B_{\boldsymbol{k}}|^2} = \sqrt{(A_{\boldsymbol{k}} - |B_{\boldsymbol{k}}|)(A_{\boldsymbol{k}} + |B_{\boldsymbol{k}}|)} \; . \tag{3.39}$$

Since in experiments on thin films mainly magnon modes at long wavelengths are under investigation, it is advantageous to expand the terms involving the exchange interaction for small $\boldsymbol{k}$,

$$JS\Big[4 - 2\cos(k_y a) - 2\cos(k_z a)\Big] \approx JSa^2\boldsymbol{k}^2 = \rho_{\mathrm{ex}}\boldsymbol{k}^2 \; . \tag{3.40}$$

We can then simplify the dispersion to

$$E_{\boldsymbol{k}} = \sqrt{[h + \rho_{\mathrm{ex}}\boldsymbol{k}^2 + \Delta(1 - f_{\boldsymbol{k}})\sin^2\Theta_{\boldsymbol{k}}][h + \rho_{\mathrm{ex}}\boldsymbol{k}^2 + \Delta f_{\boldsymbol{k}}]} \; . \tag{3.41}$$

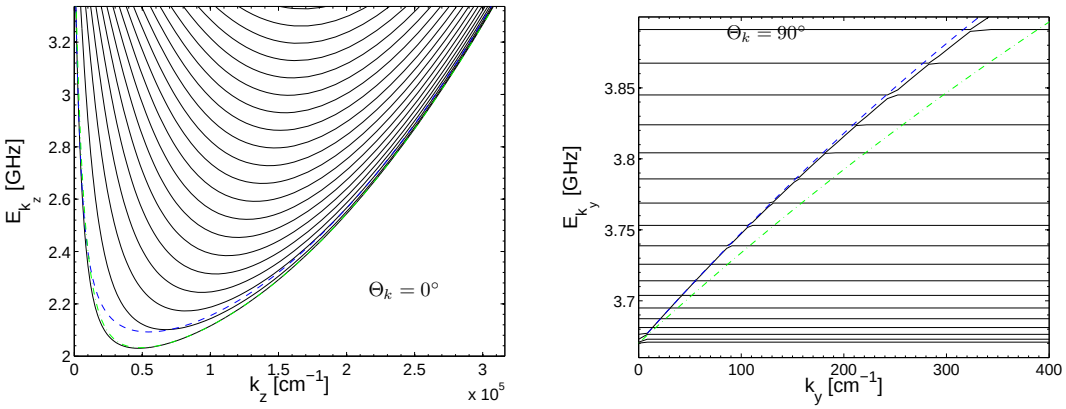

Figure 3.8: *Enlarged details of Fig. 3.4 on a linear momentum scale: spin-wave dispersion of a YIG film with thickness* $d = 4040a = 5$ *μm for wave vectors parallel to the external magnetic field* $H_e = 700$ Oe *(*$\Theta_{\boldsymbol{k}} = 0°$*, left) and for wave vectors perpendicular to the magnetic field (*$\Theta_{\boldsymbol{k}} = 90°$*, right). The solid lines are exact numerical results obtained from the solution of Eq. (3.20). The dashed line is our approximate expression Eq. (3.41) for the lowest magnon band, using the uniform mode approximation Eq. (3.36) for the form factor. The dash dotted line is the lowest magnon band with form factor (3.52) calculated in the lowest eigenmode approximation, taken from [P3].*

The results of the spectrum in this approximation are included in Figs. 3.3, 3.4, 3.6 and 3.8 to show that they are in good qualitative agreement with the numerical result for the lowest mode as long as $\Theta_{\boldsymbol{k}} \lesssim 45°$. Eq. (3.41), that can also be obtained in the phenomenological approach [103], has been used to discuss the role of magnon-magnon interactions for condensation phenomena in YIG [208]. Rezende [164, 165] rederived it recently to discuss dynamical properties of the magnon gas in YIG. Finally, it has to be mentioned that the results of the uniform approximation clearly deviate from the numerical result at intermediate wave vectors in the interval $5 \lesssim |\boldsymbol{k}|d \lesssim 50$, compare Fig. 3.4. A more quantitative comparison is presented in Fig. 3.9 and reveals that for samples used in experiments [31, 47–51, 57, 149, 169, 177, 180, P6] the minimum of the dispersion is in this range. Thus, better analytical approximations are needed to describe the magnon dispersion more accurately in the vicinity of the minimum.

3.4.3 Lowest eigenmode approximation

The effective in-plane Hamiltonian derived above is obtained using an expansion of the operators $b_{\boldsymbol{k}}(x_i)$ in terms of plain waves. This is in fact not the only possible system of functions that is suitable for an expansion. To approximate the dispersion of the lowest magnon mode more systematically, we consider the functions $\psi_{n\boldsymbol{k}}(x_i)$ that form (for fixed $\boldsymbol{k}$) a complete set of orthogonal functions

with respect to the x-direction, i.e.

$$\sum_{x_i} \psi^*_{n\boldsymbol{k}}(x_i)\psi_{m\boldsymbol{k}}(x_i) = \delta_{nm} \ , \tag{3.42a}$$

$$\sum_{n} \psi_{n\boldsymbol{k}}(x_i)\psi^*_{n\boldsymbol{k}}(x_j) = \delta_{ij} \ . \tag{3.42b}$$

We now may expand the operators $b_{\boldsymbol{k}}(x_i)$ in this basis

$$b_{\boldsymbol{k}}(x_i) = \sum_{n} \psi_{n\boldsymbol{k}}(x_i) b_{n\boldsymbol{k}} \ , \tag{3.43}$$

where the expansion coefficients are given by

$$b_{n\boldsymbol{k}} = \sum_{x_i} \psi^*_{n\boldsymbol{k}}(x_i) b_{\boldsymbol{k}}(x_i) \ . \tag{3.44}$$

For the simplest approximation we only keep the first term in the expansion Eq. (3.43),

$$b_{\boldsymbol{k}}(x_i) \approx \psi_{0\boldsymbol{k}}(x_i) b_{0\boldsymbol{k}} \ . \tag{3.45}$$

If we choose $\psi_{0\boldsymbol{k}}(x_i) = 1/\sqrt{N}$ which is the $n = 0$ term in the expansion in plane waves and identify the operator $b_{\boldsymbol{k}} \equiv b_{0\boldsymbol{k}}$, Eq. (3.27) of the uniform mode approximation is recovered. However, a truncated expansion in plane waves seems not to be a good approximation for our magnet of finite thickness. To improve on the approximation we either have to retain more terms, or expand in terms of the eigenfunctions of the exchange matrix given in Eq. (3.17),

$$\sum_{x_j} J_{\boldsymbol{k}}(x_{ij}) \psi_{n\boldsymbol{k}}(x_j) = \lambda_{n\boldsymbol{k}} \psi_{n\boldsymbol{k}}(x_i) \ . \tag{3.46}$$

These eigenfunctions are standing waves with nodes at $x = \pm d/2$, i.e.

$$\psi_{n\boldsymbol{k}}(x_i) = \sqrt{\frac{2}{N}} \sin\Big[k_n(x_i + d/2)\Big] \ , \tag{3.47}$$

with eigenvalues

$$\lambda_{n\boldsymbol{k}} = 2J\Big[3 - \cos(k_y a) - \cos(k_z a) - \cos(k_n a)\Big] \ . \tag{3.48}$$

$k_n = (n+1)\pi/d$ can be referred to as the perpendicular momentum of the associated exchange magnon mode where $n = 0, 1, \ldots, N-1$. Our approximation that retains the first term then reduces to

$$b_{\boldsymbol{k}}(x_i) \approx \sqrt{\frac{2}{N}} \cos(k_0 x_i) b_{\boldsymbol{k}} \ , \tag{3.49}$$

where $k_0 = \pi/d$, and the coefficient is given by

$$b_{\boldsymbol{k}} = \sum_{x_i} \sqrt{\frac{2}{N}} \cos(k_0 x_i) b_{\boldsymbol{k}}(x_i) \ . \tag{3.50}$$

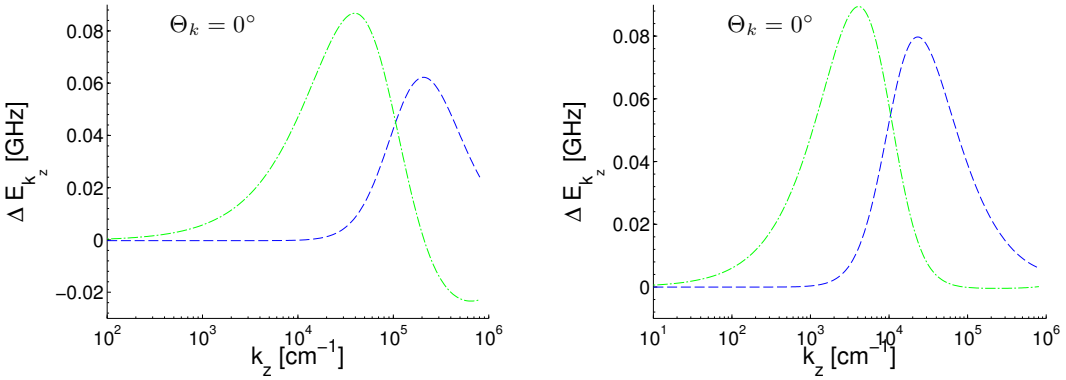

Figure 3.9: *Accuracy of our two analytical approximations for the lowest magnon mode for a YIG film with $N = 400$ layers (left) and $N = 4040$ layers (right). Dashed line (blue): difference between the numerical result and the uniform mode approximation; dash dotted line (green): difference between the numerical result and the lowest eigenmode approximation, taken from [P3].*

Substituting this approximation, Eq. (3.49), in the quadratic Hamiltonian Eq. (3.16) we obtain an effective Hamiltonian for the lowest mode Eq. (3.28), but the diagonal and off-diagonal coefficients in the Hamiltonian are now given by

$$A_{\boldsymbol{k}} = \frac{2}{N} \sum_{ij} \cos(k_0 x_i) \cos(k_0 x_j) A_{\boldsymbol{k}}(x_{ij}) \;, \tag{3.51a}$$

$$B_{\boldsymbol{k}} = \frac{2}{N} \sum_{ij} \cos(k_0 x_i) \cos(k_0 x_j) B_{\boldsymbol{k}}(x_{ij}) \;. \tag{3.51b}$$

Following the same steps as described in the previous section, we carry out the integrations of the Fourier transform of the dipolar tensor. The dispersion Eq. (3.41) now contains a different form factor

$$\begin{aligned} f_{\boldsymbol{k}} &= 1 - |\boldsymbol{k}d| \frac{|\boldsymbol{k}d|^3 + |\boldsymbol{k}d|\pi^2 + 2\pi^2(1 + e^{-|\boldsymbol{k}d|})}{(\boldsymbol{k}^2 d^2 + \pi^2)^2} \\ &= 1 - \frac{4}{\pi^2}|\boldsymbol{k}|d + \mathcal{O}(\boldsymbol{k}^2 d^2) \;. \end{aligned} \tag{3.52}$$

3.4.4 Comparison of the results

First of all, our analytical approach is at this point only suitable for the calculation of the dispersion of the lowest magnon mode, that is of particular interest in experiments using the BLS technique to observe magnon densities in YIG films. In Fig. 3.3 we compare the results for the magnon dispersions in ultrathin films while in Figs. 3.4 and 3.8 a comparison for films with a larger thickness $d = 5$ μm is made. Both analytical approaches give reasonable approximations for the so-called backward volume waves with $\Theta_{\boldsymbol{k}} = 0°$. The

surface mode for $\Theta_{\boldsymbol{k}} = 90°$ is only well described as long as the wave vectors are small. A reason for this restriction is probably that both sets of eigenfunctions which we used for our approximation are not suitable in this case[4]. Note that the results of the two analytical approximations only deviate in the different form factors Eqs. (3.36) and (3.52). A direct comparison of these functions, shown in Fig. 3.7, suggests that also the dispersions should be nearly identical. However, the dispersion in the eigenmode approximation has a smaller slope at $\boldsymbol{k} = 0$ since the coefficient in the Taylor series of the form factor Eq. (3.36) is also smaller. In Fig. 3.9 the difference between the numerical result and the analytical approximations is shown and suggests that the uniform approximation gives better results in the vicinity of $\boldsymbol{k} = 0$, while a closer look at Fig. 3.8 shows that the eigenmode approximation is more accurate to describe the dispersion near the minimum. In fact, the analytical result lies nearly on top of the numerical data. We therefore believe that the lowest eigenmode approximation is more suitable for a quantitative description if one is interested in physical effects related to the dispersion minimum at $\boldsymbol{k}_{\min}$.

3.5 Application to real system and comparison to experimental data

Since the real system of YIG is quite complicated one has to be careful in comparing the results of our calculation to data from experimental investigations. A lot of details like for example anisotropies, influences of the substrate material used to produce the films or thermal effects were not taken into account [124, 147]. However, on performing experiments with YIG films the external magnetic field h is usually fixed as one of the external parameters. Moreover YIG is an excellent material to inject and manipulate magnons in a controlled way [170], and possible technical applications are under development [107, 117, 121, 181, 214, B11]. Non thermal magnons result in high boson densities which change the macroscopic magnetization by a notable fraction. Noting that the effective spin is directly proportional to the total magnetization Eq. (3.5), and the relevant exchange stiffness ρ_{ex} is related to the total spin Eq. (3.4), we may combine these relations to

$$\frac{\rho_{\text{ex}}}{\mu} = \frac{J M_S a^5}{\mu^2} \,. \tag{3.53}$$

Fixing now the exchange coupling $J = 1.29\,\text{K}$ the only free parameter is the magnetization M_S. A measurement of the ferromagnetic resonance, which is the gap of our dispersion Eq. (3.24), fixes the magnetization for a given magnetic field h. Significant changes of the magnetization can be observed on change of temperature or on change of the densities of the non-thermal magnons. The latter effect is directly visible in experiments where the density of these magnons can be controlled by the variation of the power of the external

[4] A. Slavin, private communication.

microwave pumping [169]. Using the BLS technique in conjunction with a wave-vector resolving method [P6], the dispersion of the lowest magnon can be deduced. Although the ferromagnetic resonance is quite narrow in YIG, the error of the measured gap E_0 using BLS can be large, since the dispersion as a function of the momentum is quite steep for waves propagating parallel to the magnetic field (compare the left plot for $\Theta_k = 0°$ in Fig. 3.8). On the other hand for magnons propagating perpendicular to the magnetic field ($\Theta_k = 90°$, see Fig. 3.8, right) contributions of surface waves are visible. In a comparison to experimental data it is better to fit the whole spectrum, obtained from the maxima of the BLS signal at fixed pumping frequency, to fix the magnetization. In Fig. 3.10 we compare the result of the measurements to our prediction from the numerical method for magnon modes with $\Theta_{\boldsymbol{k}} = 90°$. In this series of experiments the magnetization is reduced by the injected magnons. As a consequence, the ferromagnetic resonance Eq. (3.24) reduces and the magnons soften according to Eq. (3.53). Although the total magnon densities,

$$n = \frac{1}{N} \sum_{\boldsymbol{k}} \langle n_{\boldsymbol{k}} \rangle \ , \tag{3.54}$$

are quite large, we believe that our approach is still valid. Eq. (3.5) shows that the total spin reduces to $S \approx 13.6$ in the case of the strongest pumping power of 10 W. Still in this case our approach based on linear spin-wave theory gives reasonable results for the spectrum, as shown in Fig. 3.10.

3.6 Summary and conclusions

In this chapter we have presented a discussion of the spin-wave spectra of experimentally relevant samples of thin films of the magnetic insulator YIG. The microscopic model, an effective spin-S Heisenberg Hamiltonian with exchange and dipole-dipole interactions on a cubic lattice, has been justified to be a good starting point to explore the physics of the magnetic excitations in this compound. Using a truncated HP transformation we have obtained an effective quadratic boson Hamiltonian. The corresponding eigenenergies can be identified with the magnon energies and have been calculated using a numerical method and two analytical approximations. The accuracy of the latter was then estimated by a comparison of the results: While the uniform mode approximation (where the transverse spatial variation of the eigenmodes is ignored) gives more reasonable results for the dispersion in the vicinity of $\boldsymbol{k} = 0$, the lowest eigenmode approximation is more suitable to describe the dispersion near its minimum. Subsequently, we compared the calculated dispersions to recent measurements using optical observation of magnon densities. Taking effects of high magnon densities into account as well, a change of the effective spin stiffness is observed in the experimental investigations [169].

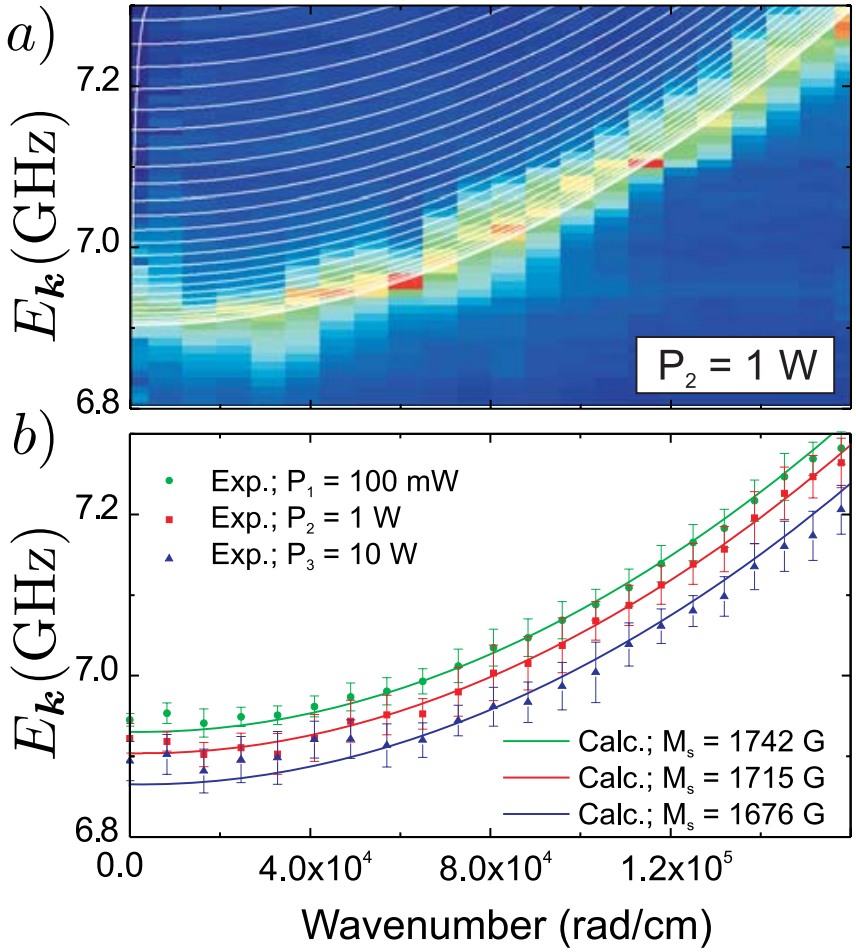

Figure 3.10: *Measured magnon spectrum for magnons propagating perpendicular to the magnetic field h ($\Theta_{\boldsymbol{k}} = 90°$). (a) Color-coded BLS-intensity map for a pumping power of $P_2 = 1$W in combination with the theoretical calculations of the relevant modes of the magnon spectrum. (b) Fit of the spectrum calculated using the numerical approach defined by Eq. (3.20) to experimental data (points) obtained from the maxima of the BLS intensity for different pumping powers of $P_1 = 0.1$W (green circles), $P_2 = 1$W (red squares) and $P_3 = 10$W (blue dots). Data and figures provided by Christian Sandweg [169].*

Although the spectra can also be obtained using a phenomenological approach based on the Landau-Lifshitz equation [103, B44], our method provides a scheme to systematically take into account interaction effects. A derivation of the momentum-dependent interaction vertices opens the possibility to calculate the intrinsic magnon damping [172]. Starting from the effective in-plane Hamiltonian in the lowest eigenmode approximation, that is more accurate in the experimentally relevant regime close to $\boldsymbol{k}_{\mathrm{min}}$, one can study condensation phenomena. In a static approach using the Gross-Pitaevskii equation it has been shown that a condensation at finite momenta $\boldsymbol{k}_{\mathrm{min}}$ invokes a cascade of condensates at odd multiple integers of the wave vector $\boldsymbol{k}_{\mathrm{min}}$ [P7],

see Fig. 3.5. Dynamical models to describe non-equilibrium behavior of the pumped magnon gas also need an understanding of the microscopic processes. As a first step to gain insights in the non-equilibrium dynamics of magnons, a simplified toy model that contains some features of the magnon gas under the influence of external pumping fields was considered in Ref. [P5]. The physics of parametric resonance and condensation of magnons can be explored within this model using time-dependent Hartree-Fock theory. However, this perturbative approach is not sufficient to describe the regime of strong interactions. One possible approach to overcome this is the generalization of the functional renormalization group [B13] to non-equilibrium systems. A new cutoff scheme seems to be appropriate to calculate non-equilibrium dynamics of magnons in YIG [111]. A long-term goal is of course to extend the microscopic model in order to close the gap between the theoretical description and experimental observations. For example, the nature of the phase transition to the magnon condensate in presence of interactions and external pumping could be studied. In order to achieve this it is necessary to use the free spectrum and the interaction processes obtained from the spin-wave approach in conjunction with a functional integral formulation of the Keldysh technique [111, B13, B28].

Apart from the experimental realization, the dipolar ferromagnet is interesting from a theoretical point of view: A similar model system, a ferromagnet in one dimension with long-range dipole-dipole interactions shows an interesting feature: The dipole energy stabilizes the order parallel to the chain [65] so that a perpendicular magnetic field induces a competing Zeeman energy. The system is quantum critical if the external magnetic field is adjusted to a certain value where both energy contributions are equal. Close to this region the nature of the physical excitations changes drastically; fluctuations on all length scales become important. Although good approaches for the ordered system like spin-wave theory fail to explore physical properties in the vicinity of such a quantum critical point [167], the methods can still help to understand this peculiar behavior of quantum systems. Evidences for a quantum critical point of the Ising universality class have been reported for dipolar ferromagnets [15, 22, 127]. Indications of quantum criticality are visible in many physical observables, and will be investigated in the next chapter within a frustrated antiferromagnet. We will again use the spin-wave theory for ordered magnets to calculate magnon spectra and consider the coupling to lattice vibrations (spin-phonon interactions).

Chapter 4

Elastic constants and ultrasonic attenuation in frustrated quantum antiferromagnets

4.1 Motivation

Frustrated antiferromagnets were already considered as interesting theoretical models a long time ago [1, 64] because they show interesting phases due to strong quantum correlations. Low-dimensional spin systems came into focus of solid-state physics in the last decades because it was possible to realize these spin systems in new materials or explore known compounds within a larger range of external parameters. A large amount of theoretical and experimental work was dedicated to quantum magnets on frustrated lattices [B4, B16] where enhanced quantum fluctuations and competing interactions stabilize disordered ground states in certain parameter regimes. The nature of the disordered and ordered magnetic phases and the transitions between them invoked by a non-thermal control parameter have been studied extensively. In the magnetic insulator Cs_2CuCl_4 such a frustrated magnet is realized. The material has been known for a long time [7, 36, 94, 148], but the magnetic nature has only been investigated recently. The compound shows a rather complex phase diagram where phase transitions can be controlled by the external magnetic field as a control parameter. Since the magnetic exchange couplings are quite small, they are of the order of 1 meV, the magnetic structure was not explored until Coldea *et al.* [35] pointed out that it is a realization of a triangular antiferromagnet. Using neutron scattering data the full model Hamiltonian including couplings was deduced. The effective g-factor had been measured earlier using electron paramagnetic resonance [6]. Investigations on the phase diagram showed that for a special direction of the magnetic field a ferromagnetic phase is connected to an ordered cone state by a quantum critical point. The properties in the vicinity of this quantum critical point could also be explained by the concept of Bose-Einstein condensation of magnons [162]. For a review

on critical properties of frustrated Heisenberg magnets, see Ref. [106].

The experimental investigations on Cs_2CuCl_4 stimulated theoretical studies to obtain an understanding of the observations on this compound. Starting from a microscopic model there are two complementary approaches: In the first approach the spin system is considered as an ensemble of weakly coupled spin chains which is justified by the fact that the Heisenberg model is spatially anisotropic with two competing exchange interactions [112, 113, 192, 193]. To calculate the properties of the model within this approach one can use bosonization techniques in conjunction with a mean-field approximation for interactions between the spin chains. The elementary spin excitations of the spin chains, the spinons, are related to the elementary excitations in the frustrated magnet and are believed to form a spin liquid phase [8, 32, 33, 91, 98, 112, 113, 158, 192, 193, 217, 229]. The spin-lattice coupling has been considered recently for spin liquids [235]. While the spinon picture can describe the spin-liquid phase, it is not straightforward to connect the spinons to the magnetic excitations in the ordered phase. In this regime it is more appropriate to use the spin-wave expansion from the ordered classical ground state [45, 67, 116, 211–213]. The spin-wave approach assumes the total spin S to be large, but also for $S = 1/2$ as in our case the results of calculations on similar Heisenberg-models are promising [14, 28, 129–131, 140, 152, 153, 205, 221]. Focusing on the cone state, Veillette *et al.* [213] calculated the dynamical structure factor of Cs_2CuCl_4 including the leading $1/S$ corrections to linear spin-wave theory. Since in the frustrated spin system quantum fluctuations are quite strong [129, 130] (but do not necessarily destroy long-range ordering [228]), it is not surprising that the spin-wave interactions can not fully describe all features of the experimental data.

4.2 Introduction

In this work we will use the spin-wave picture to obtain theoretical results for the magnetic field dependence of the elastic constants and the ultrasonic attenuation rate in the compound Cs_2CuCl_4. Restricting ourselves to low temperatures and weak magnetic fields where a magnetic ordered state is stable, we consider the magnetic excitations that weakly couple to the lattice vibrations at long wavelengths. By this mechanism, the energy and the damping of the phonons depend on the magnetic field so that these observables deliver insights in the magnetic properties. Indeed, one expects strong effects in the vicinity of the magnetic phase transition. This is actually used to explore the phase diagram [30, 90, 92, 128, 199, 200, 223, 232]. From a theoretical point of view the elastic constants have been obtained previously using phenomenological approaches starting from thermodynamic potentials [B15] or relaxation rates to determine the ultrasonic attenuation rate [199, 201]. To calculate the elastic constants and the attenuation rate we will provide a complementary

approach using a microscopic calculation starting from the relevant Heisenberg Hamiltonian

$$\hat{H}_{\text{spin}}^{\text{pho}} = \frac{1}{2}\sum_{ij}\left[J_{ij}\boldsymbol{S}_i\cdot\boldsymbol{S}_j + \boldsymbol{D}_{ij}\cdot(\boldsymbol{S}_i\times\boldsymbol{S}_j)\right] - \sum_i \boldsymbol{h}\cdot\boldsymbol{S}_i \ . \tag{4.1}$$

This was already discussed in section 1.4. We will use the spin-wave expansion for the ordered state and add the magneto-elastic coupling [5, 109, 125, B15]. The work presented in this chapter has been published recently in Ref. [P8] and was done in collaboration with Peter Kopietz, Pham Tanh Cong, Bernd Wolf, and Michael Lang.

4.3 Spin-phonon interactions

In order to model the magneto-elastic properties, we start from the following spin-phonon Hamiltonian,

$$\hat{H} = \hat{H}_{\text{spin}}^{\text{pho}} + \hat{H}^{\text{pho}} \ , \tag{4.2}$$

with the spin-phonon part Eq. (4.1) cited above and the quadratic phonon part,

$$\hat{H}^{\text{pho}} = \sum_{\boldsymbol{k}\lambda}\omega_{\boldsymbol{k}\lambda}\left(a_{\boldsymbol{k}\lambda}^{\dagger}a_{\boldsymbol{k}\lambda} + \frac{1}{2}\right) \ , \tag{4.3}$$

that adds the degrees of freedom of acoustic phonons with polarization λ. These can be derived from the harmonic approximation of the lattice potentials and the calculation of the eigenmodes respecting the symmetries of the space group of the crystal. The approximate dispersions for small momenta are then linear in the momenta [B30]

$$\omega_{\boldsymbol{k}\lambda} = c_\lambda(\hat{\boldsymbol{k}})|\boldsymbol{k}| \ , \tag{4.4}$$

with the phonon velocities $c_\lambda(\hat{\boldsymbol{k}})$. The indices i and j in Eq. (4.1) label the actual positions $\boldsymbol{r}_i$ and $\boldsymbol{r}_j$ of the spins for a given configuration of lattice distortions $\{\hat{\boldsymbol{X}}_i\}$. The positions $\{\boldsymbol{R}_i\}$ of the corresponding Bravais lattice relate the two former quantities via

$$\boldsymbol{r}_i = \boldsymbol{R}_i + \hat{\boldsymbol{X}}_i \ . \tag{4.5}$$

Describing lattice vibrations, we quantize the lattice distortions $\hat{\boldsymbol{X}}_{\boldsymbol{k}}$ in momentum space by

$$\hat{\boldsymbol{X}}_i = \frac{1}{\sqrt{N}}\sum_{\boldsymbol{k}} e^{i\boldsymbol{k}\cdot\boldsymbol{R}_i}\hat{\boldsymbol{X}}_{\boldsymbol{k}} \ , \tag{4.6a}$$

$$\hat{\boldsymbol{X}}_{\boldsymbol{k}} = \sum_\lambda \hat{X}_{\boldsymbol{k}\lambda}\boldsymbol{e}_{\boldsymbol{k}\lambda} \ , \tag{4.6b}$$

where the lattice distortions are expanded as

$$\hat{X}_{\boldsymbol{k}\lambda} = \frac{1}{\sqrt{2M\omega_{\boldsymbol{k}\lambda}}}(a_{\boldsymbol{k}\lambda} + a^{\dagger}_{-\boldsymbol{k}\lambda}) \; . \tag{4.7}$$

Since the operators $a_{\boldsymbol{k}\lambda}$ and $a^{\dagger}_{\boldsymbol{k}\lambda}$ are bosonic operators of the phononic degrees of freedom, we can define the conjugate momentum operators[1]

$$\hat{P}_{\boldsymbol{k}\lambda} = \frac{1}{i}\sqrt{\frac{M\omega_{\boldsymbol{k}\lambda}}{2}}(a_{\boldsymbol{k}\lambda} - a^{\dagger}_{-\boldsymbol{k}\lambda}) \; . \tag{4.8}$$

In the spirit of a Hermitian parametrization we also write the pure phonon Hamiltonian as a sum of the kinetic and potential energy,

$$\hat{H}^{\mathrm{pho}} = \sum_{\boldsymbol{k}\lambda}\left[\frac{\hat{P}_{-\boldsymbol{k}\lambda}\hat{P}_{\boldsymbol{k}\lambda}}{2M} + \frac{M}{2}\omega^2_{\boldsymbol{k}\lambda}\hat{X}_{-\boldsymbol{k}\lambda}\hat{X}_{\boldsymbol{k}\lambda}\right] \; . \tag{4.9}$$

Assuming the positions $\boldsymbol{r}_i$ of the spins deviate only slightly from their equilibrium values $\boldsymbol{R}_i$ we may expand the exchange couplings J_{ij} and the Dzyaloshinsky-Moriya (DM) vectors $\boldsymbol{D}_{ij}$ in powers of the difference vectors $\hat{\boldsymbol{X}}_{ij} = \hat{\boldsymbol{X}}_i - \hat{\boldsymbol{X}}_j$ [24],

$$J_{ij} = J(\boldsymbol{R}_{ij}) + (\hat{\boldsymbol{X}}_{ij}\cdot\nabla_{\boldsymbol{r}})\; J(\boldsymbol{r})|_{\boldsymbol{r}=\boldsymbol{R}_{ij}} + \frac{1}{2}(\hat{\boldsymbol{X}}_{ij}\cdot\nabla_{\boldsymbol{r}})^2\; J(\boldsymbol{r})|_{\boldsymbol{r}=\boldsymbol{R}_{ij}} + \dots \; , \tag{4.10a}$$

$$\boldsymbol{D}_{ij} = \boldsymbol{D}(\boldsymbol{R}_{ij}) + (\hat{\boldsymbol{X}}_{ij}\cdot\nabla_{\boldsymbol{r}})\; \boldsymbol{D}(\boldsymbol{r})|_{\boldsymbol{r}=\boldsymbol{R}_{ij}} + \frac{1}{2}(\hat{\boldsymbol{X}}_{ij}\cdot\nabla_{\boldsymbol{r}})^2\; \boldsymbol{D}(\boldsymbol{r})|_{\boldsymbol{r}=\boldsymbol{R}_{ij}} + \dots \; . \tag{4.10b}$$

This expansion contains the values of the couplings at the equilibrium positions, i.e. as a function of the Bravais lattice vectors $\boldsymbol{R}_{ij} = \boldsymbol{R}_i - \boldsymbol{R}_j$ and their spatial derivatives. Observing that each power of the derivative will introduce one power of phonon operators according to Eq. (4.7), we now substitute the expansion Eqs. (4.10a) and (4.10b) to represent the spin-phonon Hamiltonian as

$$\hat{H}^{\mathrm{pho}}_{\mathrm{spin}} = \hat{H}_{\mathrm{spin}} + \hat{H}^{\mathrm{1pho}}_{\mathrm{spin}} + \hat{H}^{\mathrm{2pho}}_{\mathrm{spin}} + \dots \; . \tag{4.11}$$

Note that the pure spin part $\hat{H}_{\mathrm{spin}}$ is formally identical to our starting model Eq. (4.1) where the spins are located exactly at the sites $\boldsymbol{R}_i$ of the Bravais lattice and that the additional terms describe the spin-phonon interactions with one and more powers of the phonon operators. In principle this expansion is an infinite series, but will be truncated after the term containing 2 phonon operators, which is a good approximation for low temperatures where the lattice distortions are expected to be small [132].

[1] At this point the reader should not confuse the conjugate momentum operator of the phonons with the operator of the Hermitian fields used in chapter 2. In order to match the notation of Refs. [P2, P8] the same symbol is used.

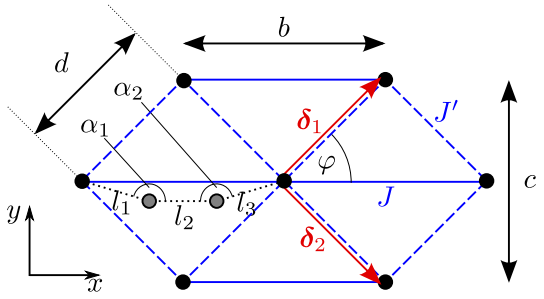

Figure 4.1: *Triangular lattice with lattice parameters b and c: The magnetic ions are located at the edges of the triangles (black dots) and are mainly coupled via the coupling J (solid lines) in the x-direction and J′ along the diagonals (dashed lines) with bond lengths b and d. The gray dots indicate the position of chlorine atoms mediating the exchange interaction in the compound Cs_2CuCl_4 which depends in a simple model on the three distances l_1, l_2, l_3 and the two bonding angles α_1 and α_2. For our purpose we lump these dependences into a simple dependence on the bond length. In the same manner the dependence of the coupling J′ on the angle φ is also neglected.*

4.4 Spin-wave expansion

For the setup of the spin-wave expansion we first consider a Heisenberg magnet on a two-dimensional distorted triangular lattice characterized by the lattice parameters b and c as shown in Fig. 4.1. This model includes the spatially anisotropic nearest-neighbor exchange,

$$J_{ij} = J(\boldsymbol{R}_i - \boldsymbol{R}_j) = \begin{cases} J & \text{if } \boldsymbol{R}_i - \boldsymbol{R}_j = \pm(\boldsymbol{\delta}_1 + \boldsymbol{\delta}_2) \ , \\ J' & \text{if } \boldsymbol{R}_i - \boldsymbol{R}_j = \pm\boldsymbol{\delta}_1 \text{ or } \pm\boldsymbol{\delta}_2 \ , \end{cases} \tag{4.12}$$

where the basis vectors are given by

$$\boldsymbol{\delta}_1 = \frac{b}{2}\boldsymbol{e}_x + \frac{c}{2}\boldsymbol{e}_y \ , \tag{4.13a}$$

$$\boldsymbol{\delta}_2 = \frac{b}{2}\boldsymbol{e}_x - \frac{c}{2}\boldsymbol{e}_y \ , \tag{4.13b}$$

so that $\boldsymbol{\delta}_1 + \boldsymbol{\delta}_2 = b\boldsymbol{e}_x$, see Fig. 4.1. The DM vectors $\boldsymbol{D}_{ij}$ are assumed to point out of the plane and connect sites in the directions $\pm\boldsymbol{\delta}_1$ and $\pm\boldsymbol{\delta}_2$,

$$\boldsymbol{D}_{ij} = D_{ij}\boldsymbol{e}_z = D(\boldsymbol{R}_i - \boldsymbol{R}_j)\boldsymbol{e}_z \ , \tag{4.14}$$

with $D_{ij} = -D_{ji}$ given by

$$D_{ij} = D(\boldsymbol{R}_i - \boldsymbol{R}_j) = \pm D \ , \tag{4.15}$$

if $\boldsymbol{R}_i - \boldsymbol{R}_j = \pm\boldsymbol{\delta}_1$ or $\pm\boldsymbol{\delta}_2$. This model is believed to describe the magnetic properties of the compound Cs_2CuCl_4 quite accurately [35–38], and the couplings

Parameter	value
J	0.374 (5) meV
J'	0.128 (5) meV
J''	0.017 (2) meV
D	0.020 (2) meV

Table 4.1: *Values of the in-plane exchange interactions J and J', the inter-plane interaction J'', and the Dzyaloshinsky-Moriya interaction D in Cs_2CuCl_4 that are used within this work [37, 212].*

have been obtained from high-field measurements, see Table 4.1. Additional couplings as exchange interactions between spins on neighboring planes, next nearest-neighbor interactions [68–70], or other allowed anisotropies [193] have been discussed in the literature. For simplicity we will not consider this extensions of the model in the following. We introduce the magnetic field perpendicular to the plane of the lattice $\boldsymbol{h} = h\boldsymbol{e}_z$ to obtain a model that is still symmetric under rotations around the z-axis.

4.4.1 General procedure

To set up the spin-wave expansion we follow the steps described in section 1.4: For $J' < 2J$ the classical ground state of our model is a spiral in the plane that is tilted toward the direction of the magnetic field. We now parametrize the local magnetization of this cone state in terms of the opening angle ϑ and the wave vector $\boldsymbol{Q}$ of the spiral and choose the orthogonal triad of unit vectors $\{\boldsymbol{e}_i^{(1)}, \boldsymbol{e}_i^{(2)}, \hat{\boldsymbol{m}}_i\}$ according to Eq. (1.67) as

$$\boldsymbol{e}_i^{(1)} = \sin(\boldsymbol{Q}\cdot\boldsymbol{R}_i)\boldsymbol{e}_x - \cos(\boldsymbol{Q}\cdot\boldsymbol{R}_i)\boldsymbol{e}_y \,, \tag{4.16a}$$

$$\boldsymbol{e}_i^{(2)} = s_\vartheta[\cos(\boldsymbol{Q}\cdot\boldsymbol{R}_i)\boldsymbol{e}_x + \sin(\boldsymbol{Q}\cdot\boldsymbol{R}_i)\boldsymbol{e}_y] - c_\vartheta\,\boldsymbol{e}_z \,, \tag{4.16b}$$

$$\hat{\boldsymbol{m}}_i = c_\vartheta[\cos(\boldsymbol{Q}\cdot\boldsymbol{R}_i)\boldsymbol{e}_x + \sin(\boldsymbol{Q}\cdot\boldsymbol{R}_i)\boldsymbol{e}_y] + s_\vartheta\,\boldsymbol{e}_z \,. \tag{4.16c}$$

Note that we have introduced the abbreviations

$$s_\vartheta = \sin\vartheta \,, \quad c_\vartheta = \cos\vartheta \,, \tag{4.17}$$

and that the transverse basis vectors $\boldsymbol{e}_i^{(1)}$ and $\boldsymbol{e}_i^{(2)}$ are defined up to a local $U(1)$ gauge transformation [175] which corresponds to the remaining symmetry of our Hamiltonian. Following the general procedure to bosonize the spin Hamiltonian we introduce the spherical basis vectors $\boldsymbol{e}_i^{\pm}$ defined in Eq. (1.51) and use the Holstein-Primakoff transformation with the result given in Eq. (1.54). For our specific model, the relevant scalar products in Eqs. (1.56a) and (1.56b) can be

evaluated,

$$\hat{\boldsymbol{m}}_i \cdot \hat{\boldsymbol{m}}_j = c_\vartheta^2 \cos\varphi_{ij} + s_\vartheta^2 \,, \tag{4.18a}$$
$$\boldsymbol{e}_i^+ \cdot \boldsymbol{e}_j^+ = \boldsymbol{e}_i^- \cdot \boldsymbol{e}_j^- = -c_\vartheta^2(1-\cos\varphi_{ij}) \,, \tag{4.18b}$$
$$\boldsymbol{e}_i^\pm \cdot \boldsymbol{e}_j^\mp = c_\vartheta^2 + (1+s_\vartheta^2)\cos\varphi_{ij} \mp 2is_\vartheta \sin\varphi_{ij} \,, \tag{4.18c}$$
$$\boldsymbol{e}_i^\pm \cdot \hat{\boldsymbol{m}}_j = c_\vartheta \left[\sin\varphi_{ij} \mp is_\vartheta(1-\cos\varphi_{ij})\right] \,, \tag{4.18d}$$
$$\boldsymbol{e}_i^\pm \cdot [\boldsymbol{e}_z \times \hat{\boldsymbol{m}}_j] = c_\vartheta \left[-\cos\varphi_{ij} \pm is_\vartheta \sin\varphi_{ij}\right] \,, \tag{4.18e}$$
$$\boldsymbol{e}_z \cdot (\hat{\boldsymbol{m}}_i \times \hat{\boldsymbol{m}}_j) = -c_\vartheta^2 \sin\varphi_{ij} \,, \tag{4.18f}$$
$$\boldsymbol{e}_z \cdot (\boldsymbol{e}_i^p \times \boldsymbol{e}_j^{p'}) = -(1-pp's_\vartheta^2)\sin\varphi_{ij} - i(p-p')s_\vartheta \cos\varphi_{ij} \,, \tag{4.18g}$$

where we have defined the angles $\varphi_i = \boldsymbol{Q}\cdot\boldsymbol{R}_i$ and their differences $\varphi_{ij} = \varphi_i - \varphi_j = \boldsymbol{Q}\cdot(\boldsymbol{R}_i - \boldsymbol{R}_j)$. Thus, the effective exchange couplings between longitudinal and transverse spin fluctuations are given by

$$J_{ij}^{\parallel} = J_{ij}[s_\vartheta^2 + c_\vartheta^2\cos\varphi_{ij}] - D_{ij}c_\vartheta^2 \sin\varphi_{ij} \,, \tag{4.19a}$$
$$\begin{aligned} J_{ij}^{+-} = (J_{ij}^{-+})^* &= J_{ij}[c_\vartheta^2 + (1+s_\vartheta^2)\cos\varphi_{ij} - 2is_\vartheta\sin\varphi_{ij}] \\ &\quad - D_{ij}[(1+s_\vartheta^2)\sin\varphi_{ij} + 2is_\vartheta\cos\varphi_{ij}] \,, \end{aligned} \tag{4.19b}$$
$$J_{ij}^{++} = J_{ij}^{--} = -c_\vartheta^2\left[J_{ij}(1-\cos\varphi_{ij}) + D_{ij}\sin\varphi_{ij}\right] \,. \tag{4.19c}$$

For later reference and to simplify the calculation we introduce the Fourier transforms of the exchange and DM couplings

$$J_{\boldsymbol{k}} = \sum_{\boldsymbol{R}} e^{-i\boldsymbol{k}\cdot\boldsymbol{R}} J(\boldsymbol{R}) = 2J\cos(k_x b) + 4J'\cos(k_x b/2)\cos(k_y c/2) \,, \tag{4.20a}$$
$$D_{\boldsymbol{k}} = \sum_{\boldsymbol{R}} e^{-i\boldsymbol{k}\cdot\boldsymbol{R}} D(\boldsymbol{R}) = -4iD\sin(k_x b/2)\cos(k_y c/2) \,. \tag{4.20b}$$

These have the symmetries $J_{\boldsymbol{k}} = J_{-\boldsymbol{k}}$ and $D_{\boldsymbol{k}} = -D_{-\boldsymbol{k}} = (D_{-\boldsymbol{k}})^*$, so that the combination

$$J_{\boldsymbol{k}}^D = J_{\boldsymbol{k}} - iD_{\boldsymbol{k}} \tag{4.21}$$

is real but has no definite symmetry. The Fourier transforms of the effective couplings Eqs. (4.19a–4.19c) can then be written as

$$J_{\boldsymbol{k}}^{\parallel} = s_\vartheta^2 J_{\boldsymbol{k}} + c_\vartheta^2 \frac{J_{\boldsymbol{Q}+\boldsymbol{k}}^D + J_{\boldsymbol{Q}-\boldsymbol{k}}^D}{2} \,, \tag{4.22a}$$
$$J_{\boldsymbol{k}}^{+-} = J_{-\boldsymbol{k}}^{-+} = c_\vartheta^2 J_{\boldsymbol{k}} + (1+s_\vartheta^2)\frac{J_{\boldsymbol{Q}+\boldsymbol{k}}^D + J_{\boldsymbol{Q}-\boldsymbol{k}}^D}{2} + s_\vartheta\left[J_{\boldsymbol{Q}+\boldsymbol{k}}^D - J_{\boldsymbol{Q}-\boldsymbol{k}}^D\right] \,, \tag{4.22b}$$
$$J_{\boldsymbol{k}}^{++} = J_{\boldsymbol{k}}^{--} = -c_\vartheta^2\left[J_{\boldsymbol{k}} - \frac{J_{\boldsymbol{Q}+\boldsymbol{k}}^D + J_{\boldsymbol{Q}-\boldsymbol{k}}^D}{2}\right] \,. \tag{4.22c}$$

4.4.2 Classical ground state

To fix the parameters ϑ and $\boldsymbol{Q}$ that specify the classical ground state we read off the corresponding classical energy from Eq. (1.55a) with the result

$$\begin{aligned} E_0^{\mathrm{cl}} &= N\frac{S^2}{2}J^{\parallel}_{\boldsymbol{k}=0} - NShs_\vartheta \\ &= N\frac{S^2}{2}\left[s_\vartheta^2 J_{\boldsymbol{k}=0} + c_\vartheta^2 J^D_{\boldsymbol{Q}}\right] - NShs_\vartheta \ . \end{aligned} \tag{4.23}$$

Minimizing this with respect to ϑ and the wave vector $\boldsymbol{Q}$ of the spiral yields

$$NSc_\vartheta\left[Ss_\vartheta\left(J_0^D - J^D_{\boldsymbol{Q}}\right) - h\right] = 0 \ , \tag{4.24a}$$

$$\boldsymbol{\nabla}_{\boldsymbol{Q}} J^D_{\boldsymbol{Q}} = \boldsymbol{\nabla}_{\boldsymbol{k}}\big(J_{\boldsymbol{k}} - iD_{\boldsymbol{k}}\big)_{\boldsymbol{k}=\boldsymbol{Q}} = 0 \ . \tag{4.24b}$$

Introducing the critical magnetic field,

$$h_c = S(J_0^D - J^D_{\boldsymbol{Q}}) = S(J_0 - J_{\boldsymbol{Q}} + iD_{\boldsymbol{Q}}) \ , \tag{4.25}$$

and abbreviating the dimensionless nonzero component of the spiral wave vector $\boldsymbol{Q} = Q_x\boldsymbol{e}_x$ as $x = Q_x b$ these equations reduce to [213]

$$s_\vartheta \equiv \sin\vartheta = h/h_c \ , \tag{4.26a}$$

$$\cos\left(\frac{x}{2}\right) = -\frac{J'}{2J} - \frac{D}{2J}\cot\left(\frac{x}{2}\right) \ , \tag{4.26b}$$

where we have ruled out the ferromagnetic ordering because it maximizes the energy. The second equation that determines $\boldsymbol{Q}$ has been obtained using the above expressions for $J_{\boldsymbol{k}}$ and $D_{\boldsymbol{k}}$ and is a transcendental equation for x and independent of the magnetic field. For $D = 0$ the solution of this equation is just $x = 2\arccos(-J'/2J)$ [212] and reduces to the ordering vector of the 120° ground state of an isotropic triangular lattice antiferromagnet ($J' = J$) [28]. The visualization of the ground state using the parameters of Table 4.1 in Fig. 4.2 only deviates slightly from the visualization without DM anisotropy, see Fig. 1.5.

4.4.3 Linear spin-wave theory

To obtain the magnon spectrum to leading order in the $1/S$ expansion, we simply retain the first term of the expansion in Eqs. (1.23a) and (1.23b), $S_i^+ \approx \sqrt{2S}b_i$ and $S_i^- \approx \sqrt{2S}b_i^\dagger$, and add up the longitudinal part Eq. (1.55b) and the transverse part Eq. (1.62a) to the quadratic Hamiltonian Eq. (1.70). The next steps are the Fourier transformation using Eq. (1.69) to obtain the Hamiltonian in momentum space,

$$\hat{H}_{2\mathrm{mag}} = \sum_{\boldsymbol{k}}\left[A_{\boldsymbol{k}} b^\dagger_{\boldsymbol{k}} b_{\boldsymbol{k}} + \frac{B_{\boldsymbol{k}}}{2}\left(b^\dagger_{\boldsymbol{k}} b^\dagger_{-\boldsymbol{k}} + b_{-\boldsymbol{k}} b_{\boldsymbol{k}}\right)\right] , \tag{4.27}$$

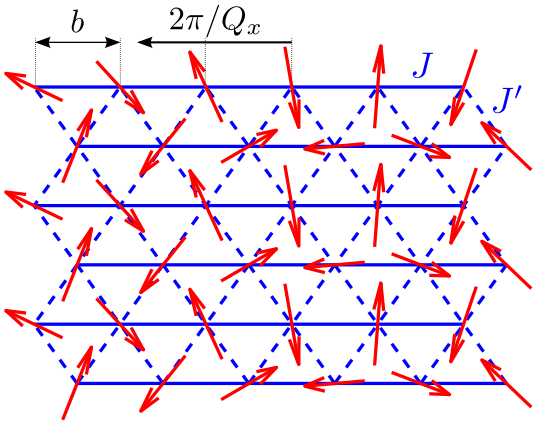

Figure 4.2: *Projection of the graph of the "cone state", which is the classical ground state of the anisotropic triangular lattice antiferromagnet for $J' < 2J$ and a magnetic field perpendicular to the lattice plane. Note that the wave vector $\boldsymbol{Q}$ of the spiral has the length indicated in the figure and points to the x-direction.*

where the real-valued coefficients are given by

$$A_{\boldsymbol{k}}^{+} = -B_{\boldsymbol{k}} - S\left[J_{\boldsymbol{Q}}^{D} - \frac{J_{\boldsymbol{Q}+\boldsymbol{k}}^{D} + J_{\boldsymbol{Q}-\boldsymbol{k}}^{D}}{2}\right] , \tag{4.28a}$$

$$A_{\boldsymbol{k}}^{-} = S s_{\vartheta} \frac{J_{\boldsymbol{Q}+\boldsymbol{k}}^{D} - J_{\boldsymbol{Q}-\boldsymbol{k}}^{D}}{2} , \tag{4.28b}$$

$$B_{\boldsymbol{k}} = -\frac{S}{2} c_{\vartheta}^{2} \left[J_{\boldsymbol{k}} - \frac{J_{\boldsymbol{Q}+\boldsymbol{k}}^{D} + J_{\boldsymbol{Q}-\boldsymbol{k}}^{D}}{2}\right] . \tag{4.28c}$$

Note that the coefficient $A_{\boldsymbol{k}} = A_{\boldsymbol{k}}^{+} + A_{\boldsymbol{k}}^{-}$ has a symmetric and antisymmetric contribution, $A_{-\boldsymbol{k}}^{\pm} = \pm A_{\boldsymbol{k}}^{\pm}$, while $B_{\boldsymbol{k}} = B_{-\boldsymbol{k}} < 0$. As a consequence of the $U(1)$ symmetry of the spin Hamiltonian Eq. (4.1) the absolute values of the two coefficients are equal for $\boldsymbol{k} \to 0$,

$$B_0 = -\frac{S}{2} c_{\vartheta}^{2} \left[J_0 - J_{\boldsymbol{Q}}^{D}\right] = -\frac{c_{\vartheta}^{2}}{2} h_c , \tag{4.29a}$$

$$A_0 = \frac{c_{\vartheta}^{2}}{2} h_c , \tag{4.29b}$$

resulting in a gapless magnon dispersion in accordance to the Goldstone theorem [76, 77]. We also observe that the linear coefficient in the Taylor expansion of $A_{\boldsymbol{k}}^{-}$ vanishes due to Eq. (4.21),

$$A_{\boldsymbol{k}}^{-} = \mathcal{O}(\boldsymbol{k}^3) . \tag{4.30}$$

Using a canonical Bogoliubov transformation, see section 1.3.1, we diagonalize our quadratic Hamiltonian. In terms of the magnon quasiparticle operators $\beta_{\boldsymbol{k}}^{\dagger}$

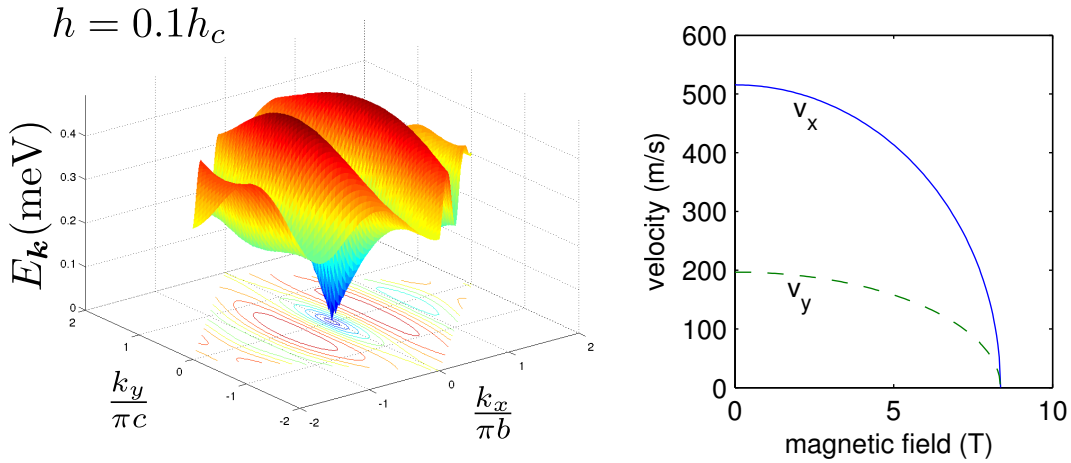

Figure 4.3: *Graph of the magnon dispersion $E_{\boldsymbol{k}}$ of the anisotropic triangular lattice antiferromagnet for $J'/J = 0.34$ and $h = 0.1h_c$, see Eq. (4.32). Due to the residual $U(1)$ symmetry, the magnons remain gapless at $\boldsymbol{k} = 0$ (left). Plot of the magnon velocities in linear spin-wave theory using the values in Table 4.1 in the two principal directions of the lattice as a function of the magnetic field. Note that the numerical values of the velocities are far below the velocities of the phonons in Cs_2CuCl_4 (right) [148].*

and $\beta_{\boldsymbol{k}}$ it is given by

$$\hat{H}_2 = \sum_{\boldsymbol{k}} \left[E_{\boldsymbol{k}} \beta^\dagger_{\boldsymbol{k}} \beta_{\boldsymbol{k}} + \frac{\epsilon_{\boldsymbol{k}} - A^+_{\boldsymbol{k}}}{2} \right] , \tag{4.31}$$

with the magnon dispersion [212]

$$E_{\boldsymbol{k}} = \sqrt{(A^+_{\boldsymbol{k}})^2 - B^2_{\boldsymbol{k}}} + A^-_{\boldsymbol{k}} , \tag{4.32}$$

which does not have any definite symmetry with respect to $\boldsymbol{k} \to -\boldsymbol{k}$ as soon as the DM anisotropy is nonzero. However, this lack of symmetry is not directly visible in the graph of the magnon dispersion $E_{\boldsymbol{k}}$ that is presented in Fig. 4.3. Looking at the energy dispersion and the expansion Eq. (4.30) we may neglect $A^-_{\boldsymbol{k}}$ for small $\boldsymbol{k}$ and obtain the leading limit of the magnon dispersion

$$E_{\boldsymbol{k}} = \sqrt{v_x^2 k_x^2 + v_y^2 k_y^2} + \mathcal{O}(\boldsymbol{k}^3) = v(\hat{\boldsymbol{k}})|\boldsymbol{k}| + \mathcal{O}(\boldsymbol{k}^3) , \tag{4.33}$$

with magnon velocity

$$v(\hat{\boldsymbol{k}}) = \sqrt{v_x^2 \hat{k}_x^2 + v_y^2 \hat{k}_y^2} \tag{4.34}$$

depending on the direction $\hat{\boldsymbol{k}} = \boldsymbol{k}/|\boldsymbol{k}|$ of the momentum.

4.4.4 Interactions between magnons

There are various interaction terms arising from the transverse Hamiltonian $\hat{H}^\perp$, the longitudinal part $\hat{H}^\parallel_4$, and the term $\hat{H}^{\parallel\perp}$ that contain more than

two boson operators. These will renormalize the properties of the magnon quasiparticles. In the spirit of the $1/S$ expansion, the corresponding interaction vertices are small compared to the free magnon dispersion $E_{\boldsymbol{k}}$ and can be treated perturbatively if S is considered to be large. However, the interactions play an important role in the calculation of the ultrasonic attenuation rate. The lowest-order contribution containing three magnon operators arises from the mixing term and cannot be ignored. Using the expansion in Eqs. (1.23a) and (1.23b) this term can be written in real space as

$$\hat{H}_{3\mathrm{mag}} = -c_\vartheta \frac{\sqrt{2S}}{2i} \sum_{ij} \left[K_{ij} b_i^\dagger b_j^\dagger b_j - K_{ij}^* b_j^\dagger b_j b_i \right] , \tag{4.35}$$

with amplitudes

$$K_{ij} = s_\vartheta \left[J_{ij}(1 - \cos\varphi_{ij}) + D_{ij} \sin\varphi_{ij} \right] + i \left[J_{ij} \sin\varphi_{ij} + D_{ij} \cos\varphi_{ij} \right] . \tag{4.36}$$

In momentum space this term reads

$$\begin{aligned} \hat{H}_{3\mathrm{mag}} = \frac{1}{\sqrt{N}} \sum_{\boldsymbol{k}_1 \boldsymbol{k}_2 \boldsymbol{k}_3} \delta_{\boldsymbol{k}_1+\boldsymbol{k}_2+\boldsymbol{k}_3,0} \Big[& \frac{1}{2!} \Gamma_3^{b^\dagger b^\dagger b}(\boldsymbol{k}_1, \boldsymbol{k}_2; \boldsymbol{k}_3) b_{-\boldsymbol{k}_1}^\dagger b_{-\boldsymbol{k}_2}^\dagger b_{\boldsymbol{k}_3} \\ & + \frac{1}{2!} \Gamma_3^{b^\dagger b b}(\boldsymbol{k}_1; \boldsymbol{k}_2, \boldsymbol{k}_3) b_{-\boldsymbol{k}_1}^\dagger b_{\boldsymbol{k}_2} b_{\boldsymbol{k}_3} \Big] , \end{aligned} \tag{4.37}$$

where the purely imaginary vertices are given by

$$\Gamma_3^{b^\dagger b^\dagger b}(\boldsymbol{k}_1, \boldsymbol{k}_2; \boldsymbol{k}_3) = -c_\vartheta \frac{\sqrt{2S}}{2i} \left[K_{-\boldsymbol{k}_1} + K_{-\boldsymbol{k}_2} \right] , \tag{4.38a}$$

$$\Gamma_3^{b^\dagger b b}(\boldsymbol{k}_1; \boldsymbol{k}_2, \boldsymbol{k}_3) = c_\vartheta \frac{\sqrt{2S}}{2i} \left[K_{\boldsymbol{k}_2} + K_{\boldsymbol{k}_3} \right] , \tag{4.38b}$$

and have the symmetry

$$\Gamma_3^{b^\dagger b^\dagger b}(\boldsymbol{k}_1, \boldsymbol{k}_2; \boldsymbol{k}_3) = -\Gamma_3^{b^\dagger b b}(-\boldsymbol{k}_3, -\boldsymbol{k}_2; -\boldsymbol{k}_1) . \tag{4.39}$$

From the Fourier transform

$$K_{\boldsymbol{k}} = s_\vartheta \left[J_{\boldsymbol{k}} - \frac{J_{\boldsymbol{Q}+\boldsymbol{k}}^D + J_{\boldsymbol{Q}-\boldsymbol{k}}^D}{2} \right] - \frac{J_{\boldsymbol{Q}+\boldsymbol{k}}^D - J_{\boldsymbol{Q}-\boldsymbol{k}}^D}{2} , \tag{4.40}$$

of the function K_{ij} and its value at vanishing momentum,

$$K_0 = s_\vartheta (J_0 - J_{\boldsymbol{Q}}^D) = s_\vartheta \frac{h_c}{S} , \tag{4.41}$$

we can deduce the expansion

$$\Gamma_3^{b^\dagger b^\dagger b}(\boldsymbol{k}_1, \boldsymbol{k}_2; \boldsymbol{k}_3) = -c_\vartheta s_\vartheta \frac{\sqrt{2S}}{i} \frac{h_c}{S} + \mathcal{O}(\boldsymbol{k}^2) \tag{4.42}$$

of the vertices. Note that a finite magnetic field $0 \leq h \leq h_c$ leads to a constant contribution of the three-magnon interaction at zero momentum which strongly influences the properties of the lattice vibrations.

4.5 Magnon-phonon interactions

If we substitute the expansions Eqs. (4.10a) and (4.10b) for the exchange couplings and the DM anisotropy into the spin-phonon Hamiltonian, Eq. (4.1), the expansion Eq. (4.11) in powers of the phonon operators is generated. To be more specific, we will discuss the individual terms in the following sections. The coupling terms containing n phonons can be written as

$$\hat{H}_{\text{spin}}^{n\text{pho}} = \frac{1}{2}\sum_{ij} U_{ij}^{(n)} \boldsymbol{S}_i \cdot \boldsymbol{S}_j \ , \tag{4.43}$$

where $U_{ij}^{(n)} = U_{ji}^{(n)}$ is symmetric because the scalar product of the spin operators is also symmetric with respect to $i \leftrightarrow j$. Since the DM anisotropy is rather small compared to the exchange couplings, we may neglect the dependence of the DM couplings $\boldsymbol{D}_{ij}$ on the phonon coordinates in the rest of this work, even though interesting features might appear due to the dependence of the DM couplings [179]. Thus, the amplitudes in the interaction terms for $n = 1$ and $n = 2$ only depend on the gradients of the exchange couplings via

$$U_{ij}^{(1)} = (\hat{\boldsymbol{X}}_{ij} \cdot \nabla_{\boldsymbol{r}})\ J(\boldsymbol{r})|_{\boldsymbol{r}=\boldsymbol{R}_{ij}} \equiv \hat{\boldsymbol{X}}_{ij} \cdot \boldsymbol{J}_{ij}^{(1)} \ , \tag{4.44a}$$

$$U_{ij}^{(2)} = \frac{1}{2}(\hat{\boldsymbol{X}}_{ij} \cdot \nabla_{\boldsymbol{r}})^2\ J(\boldsymbol{r})|_{\boldsymbol{r}=\boldsymbol{R}_{ij}} \equiv \frac{1}{2}\hat{\boldsymbol{X}}_{ij}^T \mathbf{J}_{ij}^{(2)} \hat{\boldsymbol{X}}_{ij} \ , \tag{4.44b}$$

where we have defined the vector

$$\boldsymbol{J}_{ij}^{(1)} \equiv \boldsymbol{J}^{(1)}(\boldsymbol{R}_{ij}) = \nabla_{\boldsymbol{r}}\ J(\boldsymbol{r})|_{\boldsymbol{r}=\boldsymbol{R}_{ij}} \ , \tag{4.45}$$

and the second derivative tensor

$$\left[\mathbf{J}_{ij}^{(2)}\right]_{\alpha\beta} \equiv \left[\mathbf{J}^{(2)}(\boldsymbol{R}_{ij})\right]_{\alpha\beta} = \left.\frac{J(\boldsymbol{r})}{\partial r_\alpha \partial r_\beta}\right|_{\boldsymbol{r}=\boldsymbol{R}_{ij}} \ . \tag{4.46}$$

To complete the definitions, we write down the Fourier transforms of the functions defined in Eqs. (4.44a) and (4.44b),

$$U_{\boldsymbol{k},\boldsymbol{k}'}^{(1)} = \frac{1}{N}\sum_{ij} e^{-i\boldsymbol{k}\cdot\boldsymbol{R}_i - i\boldsymbol{k}'\cdot\boldsymbol{R}_j} U_{ij}^{(1)} = -\frac{1}{\sqrt{N}}\hat{\boldsymbol{X}}_{\boldsymbol{k}+\boldsymbol{k}'} \cdot (\boldsymbol{J}_{\boldsymbol{k}}^{(1)} + \boldsymbol{J}_{\boldsymbol{k}'}^{(1)}) \ , \tag{4.47a}$$

$$\begin{aligned} U_{\boldsymbol{k},\boldsymbol{k}'}^{(2)} &= \frac{1}{N}\sum_{ij} e^{-i\boldsymbol{k}\cdot\boldsymbol{R}_i - i\boldsymbol{k}'\cdot\boldsymbol{R}_j} U_{ij}^{(2)} \\ &= \frac{1}{2N}\sum_{\boldsymbol{q}} \hat{\boldsymbol{X}}_{\boldsymbol{q}}^\dagger (\mathbf{J}_{\boldsymbol{k}}^{(2)} - \mathbf{J}_{\boldsymbol{k}+\boldsymbol{q}}^{(2)} + \mathbf{J}_{\boldsymbol{k}'}^{(2)} - \mathbf{J}_{\boldsymbol{k}'+\boldsymbol{q}}^{(2)}) \hat{\boldsymbol{X}}_{\boldsymbol{q}+\boldsymbol{k}+\boldsymbol{k}'} \ , \end{aligned} \tag{4.47b}$$

where

$$\boldsymbol{J}_{\boldsymbol{k}}^{(n)} = \sum_{\boldsymbol{R}} e^{-i\boldsymbol{k}\cdot\boldsymbol{R}} \boldsymbol{J}^{(n)}(\boldsymbol{R}) \ . \tag{4.48}$$

From its definition, one sees that the Fourier transform $\boldsymbol{J}_{\boldsymbol{k}}^{(1)}$ of the gradient has the symmetries

$$\boldsymbol{J}_{-\boldsymbol{k}}^{(1)} = -\boldsymbol{J}_{\boldsymbol{k}}^{(1)} = (\boldsymbol{J}_{\boldsymbol{k}}^{(1)})^* \,, \tag{4.49}$$

implying that $\boldsymbol{J}_{\boldsymbol{k}}^{(1)}$ is purely imaginary and moreover vanishes at zero momentum, i.e. $\boldsymbol{J}_0^{(1)} = 0$. The second derivative tensor is symmetric,

$$\mathbf{J}_{-\boldsymbol{k}}^{(2)} = \mathbf{J}_{\boldsymbol{k}}^{(2)} \,. \tag{4.50}$$

Since we did not include the inter-layer coupling J'' in our spin model, we are restricted to describe the spin-phonon interactions for phonons in the plane. In principle this reduces the theoretically accessible phonon modes, but fortunately it is technically easier to measure acoustical longitudinal phonon modes[2] representing lattice distortions in the plane. In the case of Cs_2CuCl_4, where two rather strong antiferromagnetic couplings are present (see Fig. 4.1), lattice deformations in the x-y plane give rise to a change of the couplings J and J'. In principle one should consider the changes of these couplings with respect to motions of the spins in the two possible directions, which leads to four independent parameters. Usually the exchange couplings originate from an electronic exchange path where orbitals of neighboring atoms overlap. For Cs_2CuCl_4 the exchange is mediated by the chlorine atoms in between the copper atoms, as shown in Fig. 4.1. In a rough approximation where only few atoms are considered, the exchange couplings do not change to first order when one of the copper atoms moves up or down. Therefore one can neglect the variation of J with respect to movements in the y-direction; it will vary strongly if the atom moves in x-direction. By a similar argument one can also neglect the dependence of the coupling $J'(\boldsymbol{r}) = J'(r, \varphi)$ on the polar angle φ setting

$$\frac{\partial J'}{\partial x} = \cos\varphi_0 \frac{\partial J'}{\partial r} \,, \quad \frac{\partial J'}{\partial y} = \sin\varphi_0 \frac{\partial J'}{\partial r} \,, \tag{4.51}$$

where $\sin\varphi_0 = c/(2d)$ with bond length $d = (b^2 + c^2)^{1/2}/2$, and where $\partial J'/\partial r$ is the derivative of the coupling J' with respect to the distance between the spins. For the vector $\boldsymbol{J}_{\boldsymbol{k}}^{(1)}$ we obtain within these assumptions the explicit expression

$$\begin{aligned} \boldsymbol{J}_{\boldsymbol{k}}^{(1)} = & -2i \frac{\partial J}{\partial x} \boldsymbol{e}_x \sin(k_x b) \\ & -4i \frac{\partial J'}{\partial r} \Big[\boldsymbol{e}_x \cos\varphi_0 \sin(k_x b/2) \cos(k_y c/2) + \boldsymbol{e}_y \sin\varphi_0 \cos(k_x b/2) \sin(k_y c/2) \Big] \,, \end{aligned} \tag{4.52}$$

[2] B. Wolf, private communication.

while the tensor $\mathbf{J}_{\boldsymbol{k}}^{(2)}$ has the relevant elements

$$\left[\mathbf{J}_{\boldsymbol{k}}^{(2)}\right]_{11} = 2\cos(k_x b)\frac{\partial^2 J}{\partial x^2} + 4\cos^2\varphi_0\cos(k_x b/2)\cos(k_y c/2)\frac{\partial^2 J'}{\partial r^2}\ , \tag{4.53a}$$

$$\left[\mathbf{J}_{\boldsymbol{k}}^{(2)}\right]_{21} = \left[\mathbf{J}_{\boldsymbol{k}}^{(2)}\right]_{12} = 4\cos\varphi_0\sin\varphi_0\sin(k_x b/2)\sin(k_y c/2)\frac{\partial^2 J'}{\partial r^2}\ , \tag{4.53b}$$

$$\left[\mathbf{J}_{\boldsymbol{k}}^{(2)}\right]_{22} = 4\sin^2\varphi_0\cos(k_x b/2)\cos(k_y c/2)\frac{\partial^2 J'}{\partial r^2}\ . \tag{4.53c}$$

Due to the $U(1)$ symmetry of the Hamiltonian, the quantities $\boldsymbol{J}_{\boldsymbol{k}}^{(1)}$ and $\mathbf{J}_{\boldsymbol{k}}^{(2)}$ are only fixed up to a phase that depends on the choice of the coordinate system Eq. (1.50) [174].

Concerning the signs of the derivatives, the geometry shown in Fig. 4.1 suggests that the couplings J_{ij} will become stronger if the bond length is enlarged [B9]. This behavior is quite unusual, but it originates from the fact that the bond angles between the chlorine atoms increase which usually results in a stronger coupling.[3] Later we will see that only the squares of the derivatives enter in the final result for the change in the elastic constants and the ultrasonic attenuation rate, so that we cannot directly determine the sign of the change of the coupling strengths from the experimental measurements of these quantities.

To acquire the double expansion of the spin-phonon Hamiltonian in powers of phonon and magnon operators we use the expansion of the spin operators in Eq. (4.43). Since the amplitudes of the lattice vibrations are usually considered to be small, we only retain terms up to two phonon operators [132, 133, B15]. Inserting the expansion (1.23a) and (1.23b) we also generate phonon dependent terms that do not include any magnon operators. But looking at the lowest-order term $\hat{H}_0^{1\mathrm{pho}}$ more closely we see that

$$\hat{H}_{0\mathrm{mag}}^{1\mathrm{pho}} = \frac{S^2}{2}\left[s_\vartheta^2 U_{0,0}^{(1)} + \frac{c_\vartheta^2}{2}\left(U_{-\boldsymbol{Q},\boldsymbol{Q}}^{(1)} + U_{\boldsymbol{Q},-\boldsymbol{Q}}^{(1)}\right)\right] \tag{4.54}$$

vanishes because of the property $\boldsymbol{J}_{\boldsymbol{k}=0}^{(1)} = 0$ of the Fourier transform, which implies $U_{0,0}^{(1)} = U_{-\boldsymbol{Q},\boldsymbol{Q}}^{(1)} = 0$ and thus $H_{0\mathrm{mag}}^{1\mathrm{pho}} = 0$.

4.5.1 One-phonon one-magnon hybridization

The lowest-order term which has an effect on physical observables is the part $\hat{H}_{1\mathrm{mag}}^{1\mathrm{pho}}$ of our spin-phonon Hamiltonian. It contains one power of phonon and magnon operators and can be written in real space as

$$\hat{H}_{1\mathrm{mag}}^{1\mathrm{pho}} = \frac{(2S)^{3/2}}{4}\sum_{ij} U_{ij}^{(1)}\left[b_i^\dagger(\boldsymbol{e}_i^+\cdot\hat{\boldsymbol{m}}_j) + b_i(\boldsymbol{e}_i^-\cdot\hat{\boldsymbol{m}}_j)\right]\ , \tag{4.55}$$

[3] K. Foyevtsova, private communication.

where the scalar products can be read off from Eq. (4.18d). The Fourier transformation to momentum space results in

$$\hat{H}^{\mathrm{1pho}}_{\mathrm{1mag}} = \sum_{\boldsymbol{k}} \boldsymbol{\Gamma}^{Xb}_{\boldsymbol{k}} \cdot \left(\hat{\boldsymbol{X}}_{-\boldsymbol{k}} b_{\boldsymbol{k}} + \hat{\boldsymbol{X}}_{\boldsymbol{k}} b^{\dagger}_{\boldsymbol{k}} \right) , \tag{4.56}$$

with the hybridization vertex function

$$\boldsymbol{\Gamma}^{Xb}_{\boldsymbol{k}} = \frac{i}{4} (2S)^{3/2} c_{\vartheta} \left[\boldsymbol{J}^{(1+)}_{\boldsymbol{k},\boldsymbol{Q}} + s_{\vartheta} \boldsymbol{J}^{(1-)}_{\boldsymbol{k},\boldsymbol{Q}} \right] , \tag{4.57}$$

that includes symmetric and antisymmetric combinations,

$$\boldsymbol{J}^{(1+)}_{\boldsymbol{k},\boldsymbol{Q}} = \boldsymbol{J}^{(1)}_{\boldsymbol{Q}} - \frac{\boldsymbol{J}^{(1)}_{\boldsymbol{k}+\boldsymbol{Q}} - \boldsymbol{J}^{(1)}_{\boldsymbol{k}-\boldsymbol{Q}}}{2} , \tag{4.58a}$$

$$\boldsymbol{J}^{(1-)}_{\boldsymbol{k},\boldsymbol{Q}} = \boldsymbol{J}^{(1)}_{\boldsymbol{k}} - \frac{\boldsymbol{J}^{(1)}_{\boldsymbol{k}+\boldsymbol{Q}} + \boldsymbol{J}^{(1)}_{\boldsymbol{k}-\boldsymbol{Q}}}{2} . \tag{4.58b}$$

These functions have the symmetries

$$\boldsymbol{J}^{(1\pm)}_{-\boldsymbol{k},\boldsymbol{Q}} = \pm \boldsymbol{J}^{(1\pm)}_{\boldsymbol{k},\boldsymbol{Q}} , \tag{4.59}$$

so that the vertex function $\boldsymbol{\Gamma}^{Xb}_{\boldsymbol{k}}$ does not have any definite symmetry under $\boldsymbol{k} \to -\boldsymbol{k}$, except for the cases $s_{\vartheta} = 0$ (no canting of the spins without magnetic field) or $c_{\vartheta} = 0$ (saturated ferromagnet in strong field). To avoid this technical complication due to the lack of symmetry, we use the Hermitian parametrization Eqs. (1.43a) and (1.43b) that is discussed in section 1.3.2 to obtain

$$\hat{H}^{\mathrm{1pho}}_{\mathrm{1mag}} = \frac{1}{2} \sum_{\boldsymbol{k}} \Big\{ \boldsymbol{\Gamma}^{X\Phi}_{\boldsymbol{k}} \cdot (\hat{\boldsymbol{X}}_{-\boldsymbol{k}} \hat{\Phi}_{\boldsymbol{k}} + \hat{\boldsymbol{X}}_{\boldsymbol{k}} \hat{\Phi}_{-\boldsymbol{k}}) + \boldsymbol{\Gamma}^{X\Pi}_{\boldsymbol{k}} \cdot (\hat{\boldsymbol{X}}_{-\boldsymbol{k}} \hat{\Pi}_{\boldsymbol{k}} - \hat{\boldsymbol{X}}_{\boldsymbol{k}} \hat{\Pi}_{-\boldsymbol{k}}) \Big\} . \tag{4.60}$$

The resulting vertices are now linear combinations of the vertices in the magnon basis,

$$\boldsymbol{\Gamma}^{X\Phi}_{\boldsymbol{k}} = \sqrt{\frac{\Delta_{\boldsymbol{k}}}{2}} \left[\boldsymbol{\Gamma}^{Xb}_{\boldsymbol{k}} + \boldsymbol{\Gamma}^{Xb}_{-\boldsymbol{k}} \right] = \boldsymbol{\Gamma}^{X\Phi}_{-\boldsymbol{k}} , \tag{4.61a}$$

$$\boldsymbol{\Gamma}^{X\Pi}_{\boldsymbol{k}} = \frac{i}{\sqrt{2\Delta_{\boldsymbol{k}}}} \left[\boldsymbol{\Gamma}^{Xb}_{\boldsymbol{k}} - \boldsymbol{\Gamma}^{Xb}_{-\boldsymbol{k}} \right] = -\boldsymbol{\Gamma}^{X\Pi}_{-\boldsymbol{k}} , \tag{4.61b}$$

and have definite symmetries under $\boldsymbol{k} \to -\boldsymbol{k}$. Considering the magnon-phonon hybridization Eq. (4.60) together with the Gaussian contributions for the magnons, Eq. (1.46), and the phonons, Eq. (4.9), we can calculate the effect of hybridization on the magnetoelastic modes. The corresponding energies will be shifted such that they repel each other because there is no symmetry that would allow any level crossing. Observing that the coupling vertex $\boldsymbol{\Gamma}^{Xb}_{\boldsymbol{k}}$ vanishes linearly in $\boldsymbol{k}$ for $\boldsymbol{k} \to 0$, it is obvious that the magnon-like mode will remain gapless. Moreover, the acoustic phonons will not acquire any gap as expected from the Goldstone theorem [76, 77]. Apart from the symmetries, the Hermitian parametrization separates strong and weak interactions in the long-wavelength limit, because the vertex $\boldsymbol{\Gamma}^{X\Phi}_{\boldsymbol{k}} = \mathcal{O}(\boldsymbol{k}^2)$, while $\boldsymbol{\Gamma}^{X\Pi}_{\boldsymbol{k}}$ only vanishes linearly as soon as the external magnetic field is nonzero.

4.5.2 One-phonon two-magnon interaction

To continue our discussion of the mixed expansion, we write down the part of the Hamiltonian involving one phonon and two magnon operators,

$$\hat{H}^{\text{1pho}}_{\text{2mag}} = \frac{S}{2}\sum_{ij} U^{(1)}_{ij}\Big\{-\hat{\boldsymbol{m}}_i\cdot\hat{\boldsymbol{m}}_j(n_i+n_j) + \frac{1}{2}\Big[(\boldsymbol{e}^+_i\cdot\boldsymbol{e}^-_j)b^\dagger_i b_j + (\boldsymbol{e}^-_i\cdot\boldsymbol{e}^+_j)b_i b^\dagger_j + (\boldsymbol{e}^+_i\cdot\boldsymbol{e}^+_j)b^\dagger_i b^\dagger_j + (\boldsymbol{e}^-_i\cdot\boldsymbol{e}^-_j)b_i b_j\Big]\Big\}\,. \tag{4.62}$$

Using the scalar products Eqs. (4.18a–4.18c) of the basis vectors and the definitions Eqs. (4.6a) and (1.69) of the Fourier transforms we can rewrite this as

$$\hat{H}^{\text{1pho}}_{\text{2mag}} = \frac{1}{\sqrt{N}}\sum_{\boldsymbol{k}\boldsymbol{k}'}\Big[\boldsymbol{\Gamma}^{b^\dagger b}_{\boldsymbol{k},\boldsymbol{k}'}\cdot\hat{\boldsymbol{X}}_{\boldsymbol{k}-\boldsymbol{k}'}b^\dagger_{\boldsymbol{k}}b_{\boldsymbol{k}'} + \frac{1}{2!}\left(\boldsymbol{\Gamma}^{b^\dagger b^\dagger}_{\boldsymbol{k},\boldsymbol{k}'}\cdot\hat{\boldsymbol{X}}_{\boldsymbol{k}+\boldsymbol{k}'}b^\dagger_{\boldsymbol{k}}b^\dagger_{\boldsymbol{k}'} + \boldsymbol{\Gamma}^{bb}_{\boldsymbol{k},\boldsymbol{k}'}\cdot\hat{\boldsymbol{X}}_{-\boldsymbol{k}-\boldsymbol{k}'}b_{\boldsymbol{k}}b_{\boldsymbol{k}'}\right)\Big]\,, \tag{4.63}$$

where the vertex functions are given by

$$\boldsymbol{\Gamma}^{b^\dagger b}_{\boldsymbol{k},\boldsymbol{k}'} = \frac{S}{2}\Big\{(2s^2_\vartheta - c^2_\vartheta)(\boldsymbol{J}^{(1-)}_{\boldsymbol{k},\boldsymbol{Q}} - \boldsymbol{J}^{(1-)}_{\boldsymbol{k}',\boldsymbol{Q}}) + 2\left[\boldsymbol{J}^{(1)}_{\boldsymbol{k}-\boldsymbol{k}'} - \boldsymbol{J}^{(1)}_{\boldsymbol{k}} + \boldsymbol{J}^{(1)}_{\boldsymbol{k}'}\right] - 2c^2_\vartheta\left[\boldsymbol{J}^{(1-)}_{\boldsymbol{k}-\boldsymbol{k}',\boldsymbol{Q}} - \boldsymbol{J}^{(1-)}_{\boldsymbol{k},\boldsymbol{Q}} + \boldsymbol{J}^{(1-)}_{\boldsymbol{k}',\boldsymbol{Q}}\right] + 2s_\vartheta(\boldsymbol{J}^{(1+)}_{\boldsymbol{k},\boldsymbol{Q}} - \boldsymbol{J}^{(1+)}_{\boldsymbol{k}',\boldsymbol{Q}})\Big\}\,, \tag{4.64a}$$

$$\boldsymbol{\Gamma}^{b^\dagger b^\dagger}_{\boldsymbol{k},\boldsymbol{k}'} = -\boldsymbol{\Gamma}^{bb}_{\boldsymbol{k},\boldsymbol{k}'} = \frac{S}{2}c^2_\vartheta\left[\boldsymbol{J}^{(1-)}_{\boldsymbol{k},\boldsymbol{Q}} + \boldsymbol{J}^{(1-)}_{\boldsymbol{k}',\boldsymbol{Q}}\right]\,. \tag{4.64b}$$

Recalling the symmetries of $\boldsymbol{J}^{(1\pm)}_{-\boldsymbol{k},\boldsymbol{Q}}$ it is easy to see that the normal vertex $\boldsymbol{\Gamma}^{b^\dagger b}_{\boldsymbol{k},\boldsymbol{k}'}$ is antisymmetric, while the anomalous vertices $\boldsymbol{\Gamma}^{b^\dagger b^\dagger}_{\boldsymbol{k},\boldsymbol{k}'}$ and $\boldsymbol{\Gamma}^{bb}_{\boldsymbol{k},\boldsymbol{k}'}$ are symmetric under $\boldsymbol{k}\leftrightarrow\boldsymbol{k}'$. Since the Fourier transforms $\boldsymbol{J}^{(1)}_{\boldsymbol{k}}$ are purely imaginary, this is also the case for the vertex functions $\boldsymbol{\Gamma}^{b^\dagger b}_{\boldsymbol{k},\boldsymbol{k}'}$, $\boldsymbol{\Gamma}^{b^\dagger b^\dagger}_{\boldsymbol{k},\boldsymbol{k}'}$ and $\boldsymbol{\Gamma}^{bb}_{\boldsymbol{k},\boldsymbol{k}'}$ above, and we directly write down the following relations:

$$\boldsymbol{\Gamma}^{b^\dagger b}_{\boldsymbol{k},\boldsymbol{k}'} = -\boldsymbol{\Gamma}^{b^\dagger b}_{\boldsymbol{k}',\boldsymbol{k}} = (\boldsymbol{\Gamma}^{b^\dagger b}_{\boldsymbol{k}',\boldsymbol{k}})^*\,, \tag{4.65a}$$

$$\boldsymbol{\Gamma}^{b^\dagger b^\dagger}_{\boldsymbol{k},\boldsymbol{k}'} = \boldsymbol{\Gamma}^{b^\dagger b^\dagger}_{\boldsymbol{k}',\boldsymbol{k}} = -\boldsymbol{\Gamma}^{bb}_{\boldsymbol{k}',\boldsymbol{k}} = (\boldsymbol{\Gamma}^{bb}_{\boldsymbol{k}',\boldsymbol{k}})^*\,, \tag{4.65b}$$

$$\boldsymbol{\Gamma}^{bb}_{\boldsymbol{k},\boldsymbol{k}'} = \boldsymbol{\Gamma}^{bb}_{\boldsymbol{k}',\boldsymbol{k}} = -\boldsymbol{\Gamma}^{b^\dagger b^\dagger}_{\boldsymbol{k}',\boldsymbol{k}} = (\boldsymbol{\Gamma}^{b^\dagger b^\dagger}_{\boldsymbol{k}',\boldsymbol{k}})^*\,. \tag{4.65c}$$

For later reference we will need the leading behavior of the vertices at small $\boldsymbol{k}$ and $\boldsymbol{k}'$,

$$\boldsymbol{\Gamma}^{b^\dagger b}_{\boldsymbol{k},\boldsymbol{k}'} = \frac{S}{2}\Big\{(2s^2_\vartheta - c^2_\vartheta)\big[(\boldsymbol{k}-\boldsymbol{k}')\cdot\nabla_{\boldsymbol{Q}}\big]\big[\boldsymbol{J}^{(1)}_{\boldsymbol{Q}}\big|_{\boldsymbol{Q}=0} - \boldsymbol{J}^{(1)}_{\boldsymbol{Q}}\big] - s_\vartheta\big[(\boldsymbol{k}\cdot\nabla_{\boldsymbol{Q}})^2 - (\boldsymbol{k}'\cdot\nabla_{\boldsymbol{Q}})^2\big]\boldsymbol{J}^{(1)}_{\boldsymbol{Q}}\Big\} + \mathcal{O}(\boldsymbol{k}^3)\,, \tag{4.66a}$$

$$\boldsymbol{\Gamma}^{b^\dagger b^\dagger}_{\boldsymbol{k},\boldsymbol{k}'} = \frac{S}{2}c^2_\vartheta\big[(\boldsymbol{k}+\boldsymbol{k}')\cdot\nabla_{\boldsymbol{Q}}\big]\big[\boldsymbol{J}^{(1)}_{\boldsymbol{Q}}\big|_{\boldsymbol{Q}=0} - \boldsymbol{J}^{(1)}_{\boldsymbol{Q}}\big] + \mathcal{O}(\boldsymbol{k}^3)\,. \tag{4.66b}$$

From a formal point of view the term $\hat{H}^{\mathrm{1pho}}_{\mathrm{2mag}}$ in Eq. (4.63) is the only part of the Hamiltonian containing one phonon and one magnon operator $b_{\boldsymbol{k}}$. However, considering the proper magnon quasiparticle operators, it turns out that these are a linear combination of the original phonon type operators and the magnon type operators due to the magnon-phonon hybridization Eq. (4.56). To avoid the full diagonalization of the quadratic magnon-phonon Hamiltonian $\hat{H}_{\mathrm{2mag}} + \hat{H}^{\mathrm{pho}} + \hat{H}^{\mathrm{1pho}}_{\mathrm{1mag}}$ (which is not straightforward because of the finite DM anisotropy), we use the properties of our theory in the Hermitian parametrization (see section 1.3.2) to take this effect into account in a consistent way to first order in $1/S$. At long wavelengths the diagonalization will result in a shift of the canonical momentum $\hat{\Pi}_{\boldsymbol{k}}$ to the true canonical momentum $\tilde{\Pi}_{\boldsymbol{k}}$ such that the coupling between the phonon coordinate $\hat{\boldsymbol{X}}_{\boldsymbol{k}}$ and the Hermitian field $\tilde{\Pi}_{\boldsymbol{k}}$ vanishes. In order to achieve this condition, we define a shift transformation from the original Holstein-Primakoff operators $b_{\boldsymbol{k}}$ to the proper magnon operators $\tilde{b}_{\boldsymbol{k}}$ via

$$b_{\boldsymbol{k}} = \tilde{b}_{\boldsymbol{k}} + \boldsymbol{\lambda}_{\boldsymbol{k}} \cdot \hat{\boldsymbol{X}}_{\boldsymbol{k}} \,. \tag{4.67}$$

The true Hermitian operators $\tilde{\Phi}_{\boldsymbol{k}}$ and $\tilde{\Pi}_{\boldsymbol{k}}$ are related to the magnon operators $\tilde{b}_{\boldsymbol{k}}$ by the parametrization in Eqs. (1.43a) and (1.43b) where all operators carry a tilde. Inserting the shift transformation and the Hermitian parametrization, the formerly pure magnon Hamiltonian Eq. (4.27) transforms to

$$\begin{aligned}\hat{H}_{\mathrm{2mag}} = \frac{1}{2}\sum_{\boldsymbol{k}} \Big\{ \tilde{\Pi}_{-\boldsymbol{k}}\tilde{\Pi}_{\boldsymbol{k}} + \epsilon^2_{\boldsymbol{k}}\tilde{\Phi}_{-\boldsymbol{k}}\tilde{\Phi}_{\boldsymbol{k}} + iA^-_{\boldsymbol{k}}(\tilde{\Phi}_{-\boldsymbol{k}}\tilde{\Pi}_{\boldsymbol{k}} - \tilde{\Phi}_{\boldsymbol{k}}\tilde{\Pi}_{-\boldsymbol{k}}) - A^+_{\boldsymbol{k}} \Big\} \\ -i\sum_{\boldsymbol{k}} \sqrt{\frac{\Delta_{\boldsymbol{k}}}{2}} \left(\boldsymbol{\lambda}_{-\boldsymbol{k}} \cdot \hat{\boldsymbol{X}}_{-\boldsymbol{k}}\, \tilde{\Pi}_{\boldsymbol{k}} + \boldsymbol{\lambda}_{\boldsymbol{k}} \cdot \hat{\boldsymbol{X}}_{\boldsymbol{k}}\, \tilde{\Pi}_{-\boldsymbol{k}} \right) \\ -2\sum_{\boldsymbol{k}} \Delta_{\boldsymbol{k}}\, \boldsymbol{\lambda}_{\boldsymbol{k}} \cdot \hat{\boldsymbol{X}}_{\boldsymbol{k}}\, \boldsymbol{\lambda}_{-\boldsymbol{k}} \cdot \hat{\boldsymbol{X}}_{-\boldsymbol{k}}\end{aligned} \tag{4.68}$$

while the one-phonon one-magnon hybridization can be written as

$$\begin{aligned}\hat{H}^{\mathrm{1pho}}_{\mathrm{1mag}} = \frac{1}{2}\sum_{\boldsymbol{k}} \Big\{ \boldsymbol{\Gamma}^{X\Phi}_{\boldsymbol{k}} \cdot (\hat{\boldsymbol{X}}_{-\boldsymbol{k}}\tilde{\Phi}_{\boldsymbol{k}} + \hat{\boldsymbol{X}}_{\boldsymbol{k}}\tilde{\Phi}_{-\boldsymbol{k}}) + \boldsymbol{\Gamma}^{X\Pi}_{\boldsymbol{k}} \cdot (\hat{\boldsymbol{X}}_{-\boldsymbol{k}}\tilde{\Pi}_{\boldsymbol{k}} - \hat{\boldsymbol{X}}_{\boldsymbol{k}}\tilde{\Pi}_{-\boldsymbol{k}}) \Big\} \\ -i\sum_{\boldsymbol{k}} \sqrt{2\Delta_{\boldsymbol{k}}}\, \boldsymbol{\Gamma}^{X\Phi}_{\boldsymbol{k}} \cdot \hat{\boldsymbol{X}}_{-\boldsymbol{k}}\, \boldsymbol{\lambda}_{\boldsymbol{k}} \cdot \hat{\boldsymbol{X}}_{\boldsymbol{k}} \,.\end{aligned} \tag{4.69}$$

We choose the shift amplitude proportional to the antisymmetric vertex $\boldsymbol{\Gamma}^{X\Pi}_{\boldsymbol{k}}$ which mediates strong magnon-phonon hybridization,

$$\boldsymbol{\lambda}_{\boldsymbol{k}} = \frac{i}{\sqrt{2\Delta_{\boldsymbol{k}}}} \boldsymbol{\Gamma}^{X\Pi}_{\boldsymbol{k}} \,. \tag{4.70}$$

The last terms in Eqs. (4.68) and (4.69) cancel and the coupling between the true canonical momentum $\tilde{\Pi}_{\boldsymbol{k}}$ and the phonon coordinate $\hat{\boldsymbol{X}}_{\boldsymbol{k}}$ vanishes at the same time. As discussed in section 4.5.1, the interaction mediated by the vertex $\boldsymbol{\Gamma}^{X\Phi}_{\boldsymbol{k}}$ is weak and does not produce any unphysical divergencies.

We now have to insert this transformation into the part $\hat{H}_{3\mathrm{mag}}$, Eq. (4.37). In this manner the pure magnon Hamiltonian involving three powers of the Holstein-Primakoff operators generates additional terms describing magnon-phonon interactions. Some of these terms give rise to an additional one-phonon two-magnon interaction that is proportional to the same power of the total spin S as $\hat{H}^{1\mathrm{pho}}_{2\mathrm{mag}}$. In the spirit of the $1/S$ expansion these terms have to be taken into account on equal footing with Eq. (4.62). We can accomplish this by a redefinition of the vertices in Eq. (4.63) to the following vertices,

$$\tilde{\boldsymbol{\Gamma}}^{b^\dagger b}_{\boldsymbol{k},\boldsymbol{k}'} = \boldsymbol{\Gamma}^{b^\dagger b}_{\boldsymbol{k},\boldsymbol{k}'} + \delta\boldsymbol{\Gamma}^{b^\dagger b}_{\boldsymbol{k},\boldsymbol{k}'} \;, \tag{4.71a}$$

$$\tilde{\boldsymbol{\Gamma}}^{b^\dagger b^\dagger}_{\boldsymbol{k},\boldsymbol{k}'} = \boldsymbol{\Gamma}^{b^\dagger b^\dagger}_{\boldsymbol{k},\boldsymbol{k}'} + \delta\boldsymbol{\Gamma}^{b^\dagger b^\dagger}_{\boldsymbol{k},\boldsymbol{k}'} \;, \tag{4.71b}$$

$$\tilde{\boldsymbol{\Gamma}}^{bb}_{\boldsymbol{k},\boldsymbol{k}'} = \boldsymbol{\Gamma}^{bb}_{\boldsymbol{k},\boldsymbol{k}'} + \delta\boldsymbol{\Gamma}^{bb}_{\boldsymbol{k},\boldsymbol{k}'} \;, \tag{4.71c}$$

where the correction terms are products of the three-magnon vertices and the shift amplitudes,

$$\delta\boldsymbol{\Gamma}^{b^\dagger b}_{\boldsymbol{k},\boldsymbol{k}'} = \Gamma_3^{b^\dagger b^\dagger b}(\boldsymbol{k}-\boldsymbol{k}',-\boldsymbol{k};\boldsymbol{k}')\boldsymbol{\lambda}_{\boldsymbol{k}'-\boldsymbol{k}} + \Gamma_3^{b^\dagger bb}(-\boldsymbol{k};\boldsymbol{k}',\boldsymbol{k}-\boldsymbol{k}')\boldsymbol{\lambda}_{\boldsymbol{k}-\boldsymbol{k}'} \;, \tag{4.72a}$$

$$\delta\boldsymbol{\Gamma}^{b^\dagger b^\dagger}_{\boldsymbol{k},\boldsymbol{k}'} = \Gamma_3^{b^\dagger b^\dagger b}(-\boldsymbol{k},-\boldsymbol{k}';\boldsymbol{k}+\boldsymbol{k}')\boldsymbol{\lambda}_{\boldsymbol{k}+\boldsymbol{k}'} \;, \tag{4.72b}$$

$$\delta\boldsymbol{\Gamma}^{bb}_{\boldsymbol{k},\boldsymbol{k}'} = \Gamma_3^{b^\dagger bb}(-\boldsymbol{k}-\boldsymbol{k}';\boldsymbol{k},\boldsymbol{k}')\boldsymbol{\lambda}_{\boldsymbol{k}+\boldsymbol{k}'} \;. \tag{4.72c}$$

Denoting all renormalized quantities by an extra tilde, the effective one-phonon two-magnon Hamiltonian now reads

$$\begin{aligned}\tilde{H}^{1\mathrm{pho}}_{2\mathrm{mag}} = \frac{1}{\sqrt{N}}\sum_{\boldsymbol{k}\boldsymbol{k}'}\Bigg[&\tilde{\boldsymbol{\Gamma}}^{b^\dagger b}_{\boldsymbol{k},\boldsymbol{k}'}\cdot\hat{\boldsymbol{X}}_{\boldsymbol{k}-\boldsymbol{k}'}\tilde{b}^\dagger_{\boldsymbol{k}}\tilde{b}_{\boldsymbol{k}'} \\ &+\frac{1}{2!}\left(\tilde{\boldsymbol{\Gamma}}^{b^\dagger b^\dagger}_{\boldsymbol{k},\boldsymbol{k}'}\cdot\hat{\boldsymbol{X}}_{\boldsymbol{k}+\boldsymbol{k}'}\tilde{b}^\dagger_{\boldsymbol{k}}\tilde{b}^\dagger_{\boldsymbol{k}'}+\tilde{\boldsymbol{\Gamma}}^{bb}_{\boldsymbol{k},\boldsymbol{k}'}\cdot\hat{\boldsymbol{X}}_{-\boldsymbol{k}-\boldsymbol{k}'}\tilde{b}_{\boldsymbol{k}}\tilde{b}_{\boldsymbol{k}'}\right)\Bigg] .\end{aligned} \tag{4.73}$$

Using now the approximation for the three-magnon vertex Eq. (4.42) together with its symmetries Eq. (4.39) we expand the shifts at long wavelengths,

$$\delta\boldsymbol{\Gamma}^{b^\dagger b}_{\boldsymbol{k},\boldsymbol{k}'} = -2Ss^2_\vartheta\Big[(\boldsymbol{k}-\boldsymbol{k}')\cdot\nabla_{\boldsymbol{Q}}\Big]\Big[\boldsymbol{J}^{(1)}_{\boldsymbol{Q}}\Big|_{\boldsymbol{Q}=0}-\boldsymbol{J}^{(1)}_{\boldsymbol{Q}}\Big]+\mathcal{O}(\boldsymbol{k}^3) \;, \tag{4.74a}$$

$$\delta\boldsymbol{\Gamma}^{b^\dagger b^\dagger}_{\boldsymbol{k},\boldsymbol{k}'} = Ss^2_\vartheta\Big[(\boldsymbol{k}+\boldsymbol{k}')\cdot\nabla_{\boldsymbol{Q}}\Big]\Big[\boldsymbol{J}^{(1)}_{\boldsymbol{Q}}\Big|_{\boldsymbol{Q}=0}-\boldsymbol{J}^{(1)}_{\boldsymbol{Q}}\Big]+\mathcal{O}(\boldsymbol{k}^3) \;. \tag{4.74b}$$

Combining this with Eqs. (4.66a) and (4.66b) we write down the expansion of the proper one-phonon two-magnon vertices,

$$\begin{aligned}\tilde{\boldsymbol{\Gamma}}^{b^\dagger b}_{\boldsymbol{k},\boldsymbol{k}'} = -\frac{S}{2}\Bigg\{&(2s^2_\vartheta+c^2_\vartheta)\Big[(\boldsymbol{k}-\boldsymbol{k}')\cdot\nabla_{\boldsymbol{Q}}\Big]\Big[\boldsymbol{J}^{(1)}_{\boldsymbol{Q}}\Big|_{\boldsymbol{Q}=0}-\boldsymbol{J}^{(1)}_{\boldsymbol{Q}}\Big] \\ &+s_\vartheta\Big[(\boldsymbol{k}\cdot\nabla_{\boldsymbol{Q}})^2-(\boldsymbol{k}'\cdot\nabla_{\boldsymbol{Q}})^2\Big]\boldsymbol{J}^{(1)}_{\boldsymbol{Q}}\Bigg\}+\mathcal{O}(\boldsymbol{k}^3) \;,\end{aligned} \tag{4.75a}$$

$$\tilde{\boldsymbol{\Gamma}}^{b^\dagger b^\dagger}_{\boldsymbol{k},\boldsymbol{k}'} = \frac{S}{2}(2s^2_\vartheta+c^2_\vartheta)\Big[(\boldsymbol{k}+\boldsymbol{k}')\cdot\nabla_{\boldsymbol{Q}}\Big]\Big[\boldsymbol{J}^{(1)}_{\boldsymbol{Q}}\Big|_{\boldsymbol{Q}=0}-\boldsymbol{J}^{(1)}_{\boldsymbol{Q}}\Big]+\mathcal{O}(\boldsymbol{k}^3) \;. \tag{4.75b}$$

The first terms on the right-hand side of these expressions that are linear in the momenta only differ by a minus sign and will cancel out in the calculation of the ultrasonic attenuation rate. But before we can start our calculation, it is useful to express the effective one-phonon two-magnon Hamiltonian in terms of the Bogoliubov magnon operators $\beta_{\boldsymbol{k}}$ and $\beta^\dagger_{\boldsymbol{k}}$ defined in Eq. (1.29),

$$\tilde{H}^{\text{1pho}}_{\text{2mag}} = \frac{1}{\sqrt{N}} \sum_{\boldsymbol{k}\boldsymbol{k}'} \Bigg[\tilde{\boldsymbol{\Gamma}}^{\beta^\dagger\beta}_{\boldsymbol{k},\boldsymbol{k}'} \cdot \hat{\boldsymbol{X}}_{\boldsymbol{k}-\boldsymbol{k}'} \beta^\dagger_{\boldsymbol{k}} \beta_{\boldsymbol{k}'} + \frac{1}{2!} \left(\tilde{\boldsymbol{\Gamma}}^{\beta^\dagger\beta^\dagger}_{\boldsymbol{k},\boldsymbol{k}'} \cdot \hat{\boldsymbol{X}}_{\boldsymbol{k}+\boldsymbol{k}'} \beta^\dagger_{\boldsymbol{k}} \beta^\dagger_{\boldsymbol{k}'} + \tilde{\boldsymbol{\Gamma}}^{\beta\beta}_{\boldsymbol{k},\boldsymbol{k}'} \cdot \hat{\boldsymbol{X}}_{-\boldsymbol{k}-\boldsymbol{k}'} \beta_{\boldsymbol{k}} \beta_{\boldsymbol{k}'} \right) \Bigg] . \tag{4.76}$$

The vertices are just products of the Bogoliubov coefficients and the vertices in the Holstein-Primakoff basis,

$$\tilde{\boldsymbol{\Gamma}}^{\beta^\dagger\beta}_{\boldsymbol{k},\boldsymbol{k}'} = u_{\boldsymbol{k}} u_{\boldsymbol{k}'} \tilde{\boldsymbol{\Gamma}}^{b^\dagger b}_{\boldsymbol{k},\boldsymbol{k}'} - v_{\boldsymbol{k}} v_{\boldsymbol{k}'} \tilde{\boldsymbol{\Gamma}}^{b^\dagger b}_{-\boldsymbol{k},-\boldsymbol{k}'} - u_{\boldsymbol{k}} v_{\boldsymbol{k}'} \tilde{\boldsymbol{\Gamma}}^{b^\dagger b^\dagger}_{\boldsymbol{k},-\boldsymbol{k}'} - v_{\boldsymbol{k}} u_{\boldsymbol{k}'} \tilde{\boldsymbol{\Gamma}}^{bb}_{-\boldsymbol{k},\boldsymbol{k}'} , \tag{4.77a}$$

$$\tilde{\boldsymbol{\Gamma}}^{\beta^\dagger\beta^\dagger}_{\boldsymbol{k},\boldsymbol{k}'} = u_{\boldsymbol{k}} u_{\boldsymbol{k}'} \tilde{\boldsymbol{\Gamma}}^{b^\dagger b^\dagger}_{\boldsymbol{k},\boldsymbol{k}'} + v_{\boldsymbol{k}} v_{\boldsymbol{k}'} \tilde{\boldsymbol{\Gamma}}^{bb}_{-\boldsymbol{k},-\boldsymbol{k}'} - u_{\boldsymbol{k}} v_{\boldsymbol{k}'} \tilde{\boldsymbol{\Gamma}}^{b^\dagger b}_{\boldsymbol{k},-\boldsymbol{k}'} + v_{\boldsymbol{k}} u_{\boldsymbol{k}'} \tilde{\boldsymbol{\Gamma}}^{b^\dagger b}_{-\boldsymbol{k},\boldsymbol{k}'} , \tag{4.77b}$$

$$\tilde{\boldsymbol{\Gamma}}^{\beta\beta}_{\boldsymbol{k},\boldsymbol{k}'} = u_{\boldsymbol{k}} u_{\boldsymbol{k}'} \tilde{\boldsymbol{\Gamma}}^{bb}_{\boldsymbol{k},\boldsymbol{k}'} + v_{\boldsymbol{k}} v_{\boldsymbol{k}'} \tilde{\boldsymbol{\Gamma}}^{b^\dagger b^\dagger}_{-\boldsymbol{k},-\boldsymbol{k}'} + u_{\boldsymbol{k}} v_{\boldsymbol{k}'} \tilde{\boldsymbol{\Gamma}}^{b^\dagger b}_{\boldsymbol{k},-\boldsymbol{k}'} - v_{\boldsymbol{k}} u_{\boldsymbol{k}'} \tilde{\boldsymbol{\Gamma}}^{b^\dagger b}_{-\boldsymbol{k},\boldsymbol{k}'} . \tag{4.77c}$$

For later reference we use the approximations,

$$u_{\boldsymbol{k}} u_{\boldsymbol{k}'} - v_{\boldsymbol{k}} v_{\boldsymbol{k}'} \approx \frac{\epsilon_{\boldsymbol{k}} + \epsilon_{\boldsymbol{k}'}}{2\sqrt{\epsilon_{\boldsymbol{k}} \epsilon_{\boldsymbol{k}'}}} , \tag{4.78a}$$

$$v_{\boldsymbol{k}} u_{\boldsymbol{k}'} - u_{\boldsymbol{k}} v_{\boldsymbol{k}'} \approx \frac{\epsilon_{\boldsymbol{k}} - \epsilon_{\boldsymbol{k}'}}{2\sqrt{\epsilon_{\boldsymbol{k}} \epsilon_{\boldsymbol{k}'}}} , \tag{4.78b}$$

and write down the long-wavelength limit of the anomalous vertex,

$$\tilde{\boldsymbol{\Gamma}}^{\beta^\dagger\beta^\dagger}_{\boldsymbol{k},\boldsymbol{k}'} = \frac{S}{2} \Bigg\{ \left(\frac{2 s_\vartheta^2}{c_\vartheta^2} + 1 \right) \sqrt{\frac{\epsilon_{\boldsymbol{k}} \epsilon_{\boldsymbol{k}'}}{h_c^2}} \left[(\boldsymbol{k} + \boldsymbol{k}') \cdot \nabla_{\boldsymbol{Q}} \right] \left[\boldsymbol{J}^{(1)}_{\boldsymbol{Q}} \big|_{\boldsymbol{Q}=0} - \boldsymbol{J}^{(1)}_{\boldsymbol{Q}} \right] + \frac{s_\vartheta}{2} \frac{\epsilon_{\boldsymbol{k}} - \epsilon_{\boldsymbol{k}'}}{\sqrt{\epsilon_{\boldsymbol{k}} \epsilon_{\boldsymbol{k}'}}} \left[(\boldsymbol{k} \cdot \nabla_{\boldsymbol{Q}})^2 - (\boldsymbol{k}' \cdot \nabla_{\boldsymbol{Q}})^2 \right] \boldsymbol{J}^{(1)}_{\boldsymbol{Q}} \Bigg\} + \mathcal{O}(\boldsymbol{k}^3) , \tag{4.79}$$

that will determine the ultrasonic attenuation rate at zero temperature as calculated in section 4.6.2.

4.5.3 Two-phonon shift

The two-phonon part of the spin-phonon Hamiltonian,

$$\hat{H}^{\text{2pho}}_{\text{spin}} = \frac{1}{2} \sum_{ij} U^{(2)}_{ij} \boldsymbol{S}_i \cdot \boldsymbol{S}_j , \tag{4.80}$$

(compare Eq. (4.43)) gives rise to interactions between 2 phonons and $n = 0, 1, 2, 3 \ldots$ magnons if one expands the spin operators in powers of magnon operators using the Holstein-Primakoff transformation. The first term in the

$1/S$ expansion is a shift of the phonon Hamiltonian with a form similar to the vanishing term Eq. (4.54),

$$\hat{H}^{\text{2pho}}_{\text{0mag}} = \frac{S^2}{2}\left[s^2_\vartheta U^{(2)}_{0,0} + \frac{c^2_\vartheta}{2}\left(U^{(2)}_{-\boldsymbol{Q},\boldsymbol{Q}} + U^{(2)}_{\boldsymbol{Q},-\boldsymbol{Q}}\right)\right] . \tag{4.81}$$

This term yields a contribution to the magnetic field dependence of the elastic constants. It describes the motion of phonons in the classical spin background. Recalling the definition of the second derivative Eq. (4.47b) together with its symmetry Eq. (4.50) we see that this term is diagonal in the phonon modes and can be written as

$$\hat{H}^{\text{2pho}}_{\text{0mag}} = \frac{M}{2}\sum_{\boldsymbol{k}\lambda}\Sigma^{\text{pho}}_0(\boldsymbol{k},\lambda)\hat{X}_{-\boldsymbol{k}\lambda}\hat{X}_{\boldsymbol{k}\lambda} , \tag{4.82}$$

with the additional energy

$$\Sigma^{\text{pho}}_0(\boldsymbol{k},\lambda) = \frac{S^2}{M}\boldsymbol{e}^\dagger_{\boldsymbol{k}\lambda}\left[s^2_\vartheta\left(\mathbf{J}^{(2)}_0 - \mathbf{J}^{(2)}_{\boldsymbol{k}}\right) + c^2_\vartheta\mathbf{J}^{(2+)}_{\boldsymbol{Q},\boldsymbol{k}}\right]\boldsymbol{e}_{\boldsymbol{k}\lambda} , \tag{4.83}$$

that is the diagonal part of the second order spin-phonon interaction. At this point we have introduced symmetric and antisymmetric combinations of the second derivative tensor of the exchange couplings $\mathbf{J}^{(2)}_{\boldsymbol{k}}$,

$$\mathbf{J}^{(2-)}_{\boldsymbol{k},\boldsymbol{Q}} = \frac{\mathbf{J}^{(2)}_{\boldsymbol{k}+\boldsymbol{Q}} - \mathbf{J}^{(2)}_{\boldsymbol{k}-\boldsymbol{Q}}}{2} , \tag{4.84a}$$

$$\mathbf{J}^{(2+)}_{\boldsymbol{k},\boldsymbol{Q}} = \mathbf{J}^{(2)}_{\boldsymbol{k}} - \frac{\mathbf{J}^{(2)}_{\boldsymbol{k}+\boldsymbol{Q}} + \mathbf{J}^{(2)}_{\boldsymbol{k}-\boldsymbol{Q}}}{2} , \tag{4.84b}$$

that have the symmetries

$$\mathbf{J}^{(2\pm)}_{\boldsymbol{k}} = \pm\mathbf{J}^{(2\pm)}_{-\boldsymbol{k}} . \tag{4.85}$$

4.5.4 Two-phonon one-magnon interaction

Finally we will also consider the two-phonon one-magnon interaction although its quantitative contribution to the phonon damping is small if we calculate it for the compound Cs_2CuCl_4. In momentum space we write this interaction term as

$$\hat{H}^{\text{2pho}}_{\text{1mag}} = \frac{1}{2!\sqrt{N}}\sum_{\boldsymbol{k},\boldsymbol{k}'}\sum_{\lambda\lambda'}\left[\Gamma^{XXb^\dagger}_{\boldsymbol{k}\lambda,\boldsymbol{k}'\lambda'}\hat{X}_{\boldsymbol{k}\lambda}\hat{X}_{\boldsymbol{k}'\lambda'}b^\dagger_{\boldsymbol{k}+\boldsymbol{k}'} + \Gamma^{XXb}_{\boldsymbol{k}\lambda,\boldsymbol{k}'\lambda'}\hat{X}_{-\boldsymbol{k}\lambda}\hat{X}_{-\boldsymbol{k}'\lambda'}b_{\boldsymbol{k}+\boldsymbol{k}'}\right] , \tag{4.86}$$

where the vertices are given by

$$\Gamma^{XXb^\dagger}_{\boldsymbol{k}\lambda,\boldsymbol{k}'\lambda'} = \boldsymbol{e}^\dagger_{\boldsymbol{k}\lambda}\boldsymbol{\Gamma}^{XXb^\dagger}_{\boldsymbol{k}\boldsymbol{k}'}\boldsymbol{e}_{\boldsymbol{k}'\lambda'} , \tag{4.87a}$$

$$\Gamma^{XXb}_{\boldsymbol{k}\lambda,\boldsymbol{k}'\lambda'} = \boldsymbol{e}^\dagger_{\boldsymbol{k}\lambda}\boldsymbol{\Gamma}^{XXb}_{\boldsymbol{k}\boldsymbol{k}'}\boldsymbol{e}_{\boldsymbol{k}'\lambda'} . \tag{4.87b}$$

The matrices $\mathbf{\Gamma}^{XXb}_{\boldsymbol{k}}$ and $\mathbf{\Gamma}^{XXb}_{\boldsymbol{k}\boldsymbol{k}'}$ in the direction labels are defined via the expansion coefficients of the exchange interaction,

$$\begin{aligned}\mathbf{\Gamma}^{XXb^\dagger}_{\boldsymbol{k}\boldsymbol{k}'} &= \frac{i}{4}(2S)^{3/2}c_\vartheta\Big[\mathbf{J}^{(2-)}_{\boldsymbol{k}+\boldsymbol{k}',\boldsymbol{Q}} - \mathbf{J}^{(2-)}_{\boldsymbol{k},\boldsymbol{Q}} - \mathbf{J}^{(2-)}_{\boldsymbol{k}',\boldsymbol{Q}} \\ &\qquad - s_\vartheta\Big(\mathbf{J}^{(2+)}_{\boldsymbol{k}+\boldsymbol{k}',\boldsymbol{Q}} - \mathbf{J}^{(2+)}_{\boldsymbol{k},\boldsymbol{Q}} - \mathbf{J}^{(2+)}_{\boldsymbol{k}',\boldsymbol{Q}} + \mathbf{J}^{(2+)}_{0,\boldsymbol{Q}}\Big)\Big] \\ &= -\mathbf{\Gamma}^{XXb}_{\boldsymbol{k}\boldsymbol{k}'}\,, \end{aligned} \tag{4.88}$$

where we just inserted Eq. (4.47b). Therefore the vertices $\mathbf{\Gamma}^{XXb^\dagger}_{\boldsymbol{k}\boldsymbol{k}'}$ and $\mathbf{\Gamma}^{XXb}_{\boldsymbol{k}\boldsymbol{k}'}$ vanish quadratically in the external momenta $\boldsymbol{k}$ and $\boldsymbol{k}'$ in the long-wavelength limit. To complete our definitions for the two-phonon one-magnon interaction we write down the Hamiltonian in the Bogoliubov basis,

$$\hat{H}^{\text{2pho}}_{\text{1mag}} = \frac{1}{2!\sqrt{N}}\sum_{\boldsymbol{k},\boldsymbol{k}'}\sum_{\lambda\lambda'}\Big[\Gamma^{XX\beta^\dagger}_{\boldsymbol{k}\lambda,\boldsymbol{k}'\lambda'}\hat{X}_{\boldsymbol{k}\lambda}\hat{X}_{\boldsymbol{k}'\lambda'}\beta^\dagger_{\boldsymbol{k}+\boldsymbol{k}'} + \Gamma^{XX\beta}_{\boldsymbol{k}\lambda,\boldsymbol{k}'\lambda'}\hat{X}_{-\boldsymbol{k}\lambda}\hat{X}_{-\boldsymbol{k}'\lambda'}\beta_{\boldsymbol{k}+\boldsymbol{k}'}\Big]\,, \tag{4.89}$$

with the following vertices in matrix notation:

$$\mathbf{\Gamma}^{XX\beta^\dagger}_{\boldsymbol{k}\boldsymbol{k}'} = u_{\boldsymbol{k}+\boldsymbol{k}'}\mathbf{\Gamma}^{XXb^\dagger}_{\boldsymbol{k}\boldsymbol{k}'} - v_{\boldsymbol{k}+\boldsymbol{k}'}\mathbf{\Gamma}^{XXb}_{-\boldsymbol{k},-\boldsymbol{k}'}\,, \tag{4.90a}$$

$$\mathbf{\Gamma}^{XX\beta}_{\boldsymbol{k}\boldsymbol{k}'} = u_{\boldsymbol{k}+\boldsymbol{k}'}\mathbf{\Gamma}^{XXb}_{\boldsymbol{k}\boldsymbol{k}'} - v_{\boldsymbol{k}+\boldsymbol{k}'}\mathbf{\Gamma}^{XXb^\dagger}_{-\boldsymbol{k},-\boldsymbol{k}'}\,. \tag{4.90b}$$

Physically this interaction gives rise to two effects: The renormalization of the canting angle and thus the magnons in presence of phonons [109, 133, 206], and a renormalization of the phonons that will be considered in detail later. For later reference we expand the interaction vertex in powers of the external momenta

$$\begin{aligned}\mathbf{\Gamma}^{XX\beta}_{\boldsymbol{k},-\boldsymbol{k}'} \approx -\frac{i}{4}(2S)^{3/2}\Bigg\{& s_\vartheta\sqrt{\frac{\epsilon_{\boldsymbol{k}-\boldsymbol{k}'}}{h_c}}(\boldsymbol{k}\cdot\nabla_{\boldsymbol{Q}})(\boldsymbol{k}'\cdot\nabla_{\boldsymbol{Q}})\left[\mathbf{J}^{(2)}_{\boldsymbol{Q}}\big|_{\boldsymbol{Q}=0} - \mathbf{J}^{(2)}_{\boldsymbol{Q}}\right] \\ &- \frac{c^2_\vartheta}{2}\sqrt{\frac{h_c}{\epsilon_{\boldsymbol{k}-\boldsymbol{k}'}}}[(\boldsymbol{k}-\boldsymbol{k}')\cdot\nabla_{\boldsymbol{Q}}](\boldsymbol{k}\cdot\nabla_{\boldsymbol{Q}})(\boldsymbol{k}'\cdot\nabla_{\boldsymbol{Q}})\mathbf{J}^{(2)}_{\boldsymbol{Q}}\Bigg\}\,. \end{aligned} \tag{4.91}$$

4.5.5 Formulation in terms of a Lagrangian path integral

At this point it is advantageous to introduce the path-integral formulation of our mixed magnon-phonon theory. The partition function is then given as a functional integral over the complex boson fields β_K and the real phonon fields $P_{K\lambda}$ and $X_{K\lambda}$,

$$\mathcal{Z} = \int \mathcal{D}[\boldsymbol{P},\boldsymbol{X},\beta,\bar{\beta}]e^{-S'[\boldsymbol{P},\boldsymbol{X},\beta,\bar{\beta}]}\,, \tag{4.92}$$

where $S[\boldsymbol{P},\boldsymbol{X},\beta,\bar{\beta},]$ is the Euclidean action obtained from our Hamiltonian in the basis of the Bogoliubov quasiparticle operators. Note that the Fourier

components of the operators are defined via

$$A_{\boldsymbol{k}}(\tau) = \sum_{\omega} e^{-i\omega\tau} A_K \ , \qquad\qquad A = P_\lambda, X_\lambda, \beta \ , \tag{4.93}$$

and $K = (i\omega, \boldsymbol{k})$ is a collective label containing the bosonic Matsubara frequency $i\omega$ and the wave vector $\boldsymbol{k}$. Since the magnons only couple to the phonons via the combination $\boldsymbol{X}_{\boldsymbol{k}} = \sum_\lambda X_{\boldsymbol{k}\lambda} \boldsymbol{e}_{\boldsymbol{k}\lambda}$ we can integrate over the canonical phonon momenta $P_{K\lambda}$ with a result similar to that discussed in section 2.4.1. At this point the integration can be done exactly and the result will be the analogue of the path-integral formulation using an effective Lagrangian [B34]. In this case the partition function simplifies to

$$\mathcal{Z} = \int \mathcal{D}[\boldsymbol{X}, \beta, \bar{\beta}] e^{-S[\boldsymbol{X}, \beta, \bar{\beta}]} \ , \tag{4.94}$$

where the effective action reads

$$\begin{aligned} S[\boldsymbol{X}, \bar{\beta}, \beta] = S^{\text{2pho}}[\boldsymbol{X}] + S_{\text{2mag}}[\bar{\beta}, \beta] + S^{\text{1pho}}_{\text{1mag}}[\boldsymbol{X}, \bar{\beta}, \beta] \\ + S^{\text{1pho}}_{\text{2mag}}[\boldsymbol{X}, \bar{\beta}, \beta] + S_{\text{3mag}}[\bar{\beta}, \beta] + \dots \ . \end{aligned} \tag{4.95}$$

The first two terms describe non-interacting phonons and magnons,

$$S^{\text{2pho}}[\boldsymbol{X}] = \frac{1}{2T} \sum_{K\lambda} M(\omega^2 + \omega^2_{\boldsymbol{k}\lambda} + \Sigma^{\text{pho}}_0(\boldsymbol{k}, \lambda) X_{-K\lambda} X_{K\lambda} \ , \tag{4.96}$$

$$S_{\text{2mag}}[\bar{\beta}, \beta] = -\frac{1}{T} \sum_K (i\omega - E_{\boldsymbol{k}}) \bar{\beta}_K \beta_K \ , \tag{4.97}$$

where T is the temperature. The action describing the magnon-phonon hybridization Eq. (4.56) in the Bogoliubov basis defined in Eq. (1.29) is given by

$$S^{\text{1pho}}_{\text{1mag}}[\boldsymbol{X}, \bar{\beta}, \beta] = \frac{1}{T} \sum_{K\lambda} \boldsymbol{\Gamma}^{X\beta}_{\boldsymbol{k}} \cdot \left(\boldsymbol{X}_{-K} \beta_K + \boldsymbol{X}_K \bar{\beta}_K \right) \ , \tag{4.98}$$

where the vertices combine to

$$\boldsymbol{\Gamma}^{X\beta}_{\boldsymbol{k}} = u_{\boldsymbol{k}} \boldsymbol{\Gamma}^{Xb}_{\boldsymbol{k}} - v_{\boldsymbol{k}} \boldsymbol{\Gamma}^{Xb}_{-\boldsymbol{k}} \ . \tag{4.99}$$

Note that the contributions to the effective action with more than two powers of fluctuating fields can be read off from the corresponding parts of the Hamiltonian. Parameterizing the true Green functions of the phonons and magnons using the Dyson equation Eq. (1.96),

$$G^{\text{pho}}(K, \lambda) = \frac{M}{T} \langle X_{-K\lambda} X_{K\lambda} \rangle = \frac{1}{\omega^2 + \omega^2_{\boldsymbol{k}\lambda} + \Sigma^{\text{pho}}(K, \lambda)} \ , \tag{4.100a}$$

$$G_{\text{mag}}(K) = -\frac{1}{T} \langle \bar{\psi}_K \psi_K \rangle = \frac{1}{i\omega - E_{\boldsymbol{k}} - \Sigma_{\text{mag}}(K)} \ , \tag{4.100b}$$

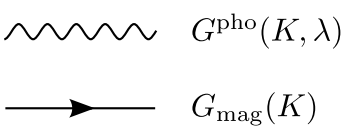

Figure 4.4: *Graphical representation of the propagators $G^{\mathrm{pho}}(K,\lambda)$ of the phonons (wiggly lines) and the magnon Green functions $G_{\mathrm{mag}}(K)$ (directed lines).*

we have introduced the self-energies $\Sigma^{\mathrm{pho}}(K,\lambda)$ and $\Sigma_{\mathrm{mag}}(K)$ associated with the phonons and magnons, and where $\langle \ldots \rangle$ denotes the functional average,

$$\langle \ldots \rangle = \frac{1}{\mathcal{Z}} \int \mathcal{D}[\boldsymbol{X}, \beta, \bar{\beta},] \ldots e^{-S[\boldsymbol{X},\beta,\bar{\beta},]} \; . \tag{4.101}$$

For simplicity we do not consider the off-diagonal structure of the self-energy of the phonons with respect to the modes λ.

4.6 Phonon self-energy due to magnon-phonon interactions

4.6.1 Magnetic field dependence of the elastic constants

The elastic constants are directly related to the velocities of the acoustic phonons that can be determined experimentally with high accuracy. Although the spin-phonon coupling is expected to be small, its influence on the phonon properties is visible as a change of the elastic constants that depends on the magnetic field. The leading $1/S$ contribution to this shift is already contained in the quadratic magnon-phonon Hamiltonian $\hat{H}_{2\mathrm{mag}} + \hat{H}^{\mathrm{pho}} + \hat{H}^{1\mathrm{pho}}_{1\mathrm{mag}} + \hat{H}^{2\mathrm{pho}}_{0\mathrm{mag}}$. The part $\Sigma^{\mathrm{pho}}_0(\boldsymbol{k},\lambda)$ of the phonon self-energy given in Eq. (4.83) renormalizes the phonon frequencies according to the substitution $\omega^2_{\boldsymbol{k}\lambda} \to \omega^2_{\boldsymbol{k}\lambda} + \Sigma^{\mathrm{pho}}_0(\boldsymbol{k},\lambda)$. Thus, the coupling to the classical spin background gives rise to the following relative shift of the phonon velocities:

$$\frac{(\Delta c_\lambda)_0}{c_\lambda} = \sqrt{1 - \lim_{|\boldsymbol{k}|\to 0} \frac{\Sigma^{\mathrm{pho}}_0(\boldsymbol{k},\lambda)}{\omega^2_{\boldsymbol{k}\lambda}}} - 1 \; . \tag{4.102}$$

In principle, one can construct a canonical transformation which diagonalizes the full quadratic Hamiltonian [B27]. But since the magnon dispersion $E_{\boldsymbol{k}}$ is not symmetric with respect to $\boldsymbol{k} \leftrightarrow -\boldsymbol{k}$ it is not possible to construct a block diagonal Hamiltonian via a symmetric and antisymmetric combination of the operators, like we did in section 2.3.2 [81, 220, P2]. To avoid the mathematical problem of constructing a matrix-Bogoliubov transformation, we will obtain the renormalized phonon spectrum in a straightforward manner by integrating over the magnon field in the path-integral formulation, Eq. (4.94). We truncate

the expansion in Eq. (4.95) to leading order in $1/S$ and obtain the effective Euclidean action

$$S_1[\boldsymbol{X}, \bar{\beta}, \beta] = S^{\text{2pho}}[\boldsymbol{X}] + S_{\text{2mag}}[\bar{\beta}, \beta] + S^{\text{1pho}}_{\text{1mag}}[\boldsymbol{X}, \bar{\beta}, \beta] \,, \tag{4.103}$$

which is the sum of Eqs. (4.96–4.98). The Gaussian integral over the complex magnon fields can now be carried out using Eq. (1.84). Defining an effective phonon action $S^{\text{2pho}}_{\text{eff}}[\boldsymbol{X}]$ in Gaussian approximation via

$$e^{-S^{\text{2pho}}_{\text{eff}}[\boldsymbol{X}]} = \int \mathcal{D}[\beta, \bar{\beta}] e^{-S_1[\boldsymbol{X}, \bar{\beta}, \beta]} \,, \tag{4.104}$$

we obtain

$$\begin{aligned} S^{\text{2pho}}_{\text{eff}}[\boldsymbol{X}] = \frac{1}{2T} \sum_{K\lambda\lambda'} \Bigg[& \delta_{\lambda,\lambda'} M(\omega^2 + \omega^2_{\boldsymbol{k}\lambda} + \Sigma^{\text{pho}}_0(\boldsymbol{k}, \lambda) \\ & + \frac{\left(\boldsymbol{\Gamma}^{X\beta}_{\boldsymbol{k}} \cdot \boldsymbol{e}_{\boldsymbol{k}\lambda}\right)^* \left(\boldsymbol{\Gamma}^{X\beta}_{\boldsymbol{k}} \cdot \boldsymbol{e}_{\boldsymbol{k}\lambda'}\right)}{i\omega - E_{\boldsymbol{k}}} \Bigg] X_{-K\lambda} X_{K\lambda'} \,, \end{aligned} \tag{4.105}$$

where also the contribution from the phonon shift Eq. (4.82) has been included. Since the renormalized phonon dispersions $\tilde{\omega}_{\boldsymbol{k}\lambda}$ are given by the pole of the Gaussian propagator, we may safely neglect optical phonons because the denominator $i\omega - E_{\boldsymbol{k}}$ will be large in the long-wavelength limit. For simplicity we furthermore neglect off-diagonal terms $\lambda \neq \lambda'$ that could be considered as further corrections. Thus, we obtain the phonon self-energy

$$\Sigma^{\text{pho}}_1(K, \lambda) = \frac{\left|\boldsymbol{\Gamma}^{X\beta}_{\boldsymbol{k}} \cdot \boldsymbol{e}_{\boldsymbol{k}\lambda}\right|^2}{M(i\omega - E_{\boldsymbol{k}})} \,, \tag{4.106}$$

that parametrizes the effect of the coupling to magnons in our approximation. From the phonon propagator,

$$G^{\text{pho}}(K, \lambda) = \frac{1}{\omega^2 + \omega^2_{\boldsymbol{k}\lambda} + \Sigma^{\text{pho}}_0(\boldsymbol{k}, \lambda) + \Sigma^{\text{pho}}_1(K, \lambda)} \,, \tag{4.107}$$

one can obtain the renormalized phonon dispersion $\tilde{\omega}_{\boldsymbol{k}}$. It is given by the real positive root of the cubic equation

$$\begin{aligned} \tilde{\omega}^2_{\boldsymbol{k}\lambda} &= \omega^2_{\boldsymbol{k}\lambda} + \Sigma^{\text{pho}}_0(\boldsymbol{k}, \lambda) + \Sigma^{\text{pho}}_1(i\omega \to \tilde{\omega}_{\boldsymbol{k}\lambda}, \boldsymbol{k}, \lambda) \\ &= \omega^2_{\boldsymbol{k}\lambda} + \Sigma^{\text{pho}}_0(\boldsymbol{k}, \lambda) + \frac{\left|\boldsymbol{\Gamma}^{X\beta}_{\boldsymbol{k}} \cdot \boldsymbol{e}_{\boldsymbol{k}\lambda}\right|^2}{M(\tilde{\omega}_{\boldsymbol{k}\lambda} - E_{\boldsymbol{k}})} \,. \end{aligned} \tag{4.108}$$

Both self-energy contributions on the right-hand side of Eq. (4.108) have the same order of magnitude in the formal $1/S$ expansion: The classical self-energy $\Sigma^{\text{pho}}_0(\boldsymbol{k}, \lambda)$ in Eq. (4.83) is proportional to S^2. The self-energy $\Sigma^{\text{pho}}_1(K, \lambda)$ exhibits the same power of S because the hybridization vertex $\boldsymbol{\Gamma}^{X\beta}_{\boldsymbol{k}}$ is of order

$S^{3/2}$ and the denominator in Eq. (4.106) contains one power of S from the dispersion $E_{\boldsymbol{k}}$. This cubic equation in $\tilde{\omega}_{\boldsymbol{k}}$ is exactly the same as the equation arising from the diagonalization of the quadratic magnon-phonon Hamiltonian $\hat{H}_{2\mathrm{mag}} + \hat{H}^{\mathrm{pho}} + \hat{H}^{1\mathrm{pho}}_{1\mathrm{mag}} + \hat{H}^{2\mathrm{pho}}_{0\mathrm{mag}}$. Regarding real materials where the critical magnetic fields h_c are experimentally accessible, it is obvious that the magnon velocities are small compared with the phonon velocities, $v(\hat{\boldsymbol{k}})/c_\lambda \ll 1$. This adiabatic limit is also realized in the compound Cs_2CuCl_4, where the phonon velocities are approximately 2800 m/s [148, 209], while the magnon velocities are smaller than 500 m/s, see Fig. 4.3, and therefore $v(\hat{\boldsymbol{k}})/c_\lambda \lesssim 1/6$. Thus, we may approximate the shift in the phonon velocity due to magnon-phonon coupling by

$$\frac{(\Delta c_\lambda)_1}{c_\lambda} = \lim_{|\boldsymbol{k}|\to 0} \frac{\left|\boldsymbol{\Gamma}^{X\beta}_{\boldsymbol{k}} \cdot \boldsymbol{e}_{\boldsymbol{k}\lambda}\right|^2}{2M\omega^3_{\boldsymbol{k}\lambda}} \,. \tag{4.109}$$

Note that within our approximation the shift is always positive which is the result of two facts: The magnon and the phonon bands repel upon hybridization and the magnon energies are smaller than the phonon energies. Eq. (4.109) above demonstrates that the elastic constants increase when the magnon-phonon coupling is considered. To explicitly take the limit on the r.h.s. of this equation we need the value of the vertex $\boldsymbol{\Gamma}^{X\beta}_{\boldsymbol{k}}$ at small momenta. Using its definition Eq. (4.99) together with Eq. (4.99) we obtain to leading order in the momenta,

$$\boldsymbol{\Gamma}^{X\beta}_{\boldsymbol{k}} = \frac{i}{4}(2S)^{3/2}|\boldsymbol{k}|^{3/2}\sqrt{\frac{v(\hat{\boldsymbol{k}})}{h_c}}\boldsymbol{F}^{X\beta}(\hat{\boldsymbol{k}}) \,, \tag{4.110}$$

where the dimensionless vector $\boldsymbol{F}^{X\beta}(\hat{\boldsymbol{k}})$ is given by

$$\boldsymbol{F}^{X\beta}(\hat{\boldsymbol{k}}) = s_\vartheta \boldsymbol{f}^{X\beta}_1(\hat{\boldsymbol{k}}) - c^2_\vartheta \boldsymbol{f}^{X\beta}_2(\hat{\boldsymbol{k}}, \hat{\boldsymbol{k}}) \,. \tag{4.111}$$

Here we have introduced the vector functions

$$\boldsymbol{f}^{X\beta}_1(\hat{\boldsymbol{k}}) = \frac{1}{h_c}(\hat{\boldsymbol{k}} \cdot \nabla_{\boldsymbol{Q}})\left[\boldsymbol{J}^{(1)}_{\boldsymbol{Q}}\Big|_{\boldsymbol{Q}=0} - \boldsymbol{J}^{(1)}_{\boldsymbol{Q}}\right] , \tag{4.112a}$$

$$\boldsymbol{f}^{X\beta}_2(\hat{\boldsymbol{k}}, \hat{\boldsymbol{k}}') = \frac{1}{2v(\hat{\boldsymbol{k}})}(\hat{\boldsymbol{k}} \cdot \nabla_{\boldsymbol{Q}})(\hat{\boldsymbol{k}}' \cdot \nabla_{\boldsymbol{Q}})\boldsymbol{J}^{(1)}_{\boldsymbol{Q}} \,. \tag{4.112b}$$

In order to arrive at this result, we have approximated the symmetric part of the magnon dispersion by $E_{\boldsymbol{k}} \approx v(\hat{\boldsymbol{k}})|\boldsymbol{k}|$ according to Eq. (4.33). Combining Eq. (4.109) and Eq. (4.111) we finally obtain

$$\begin{aligned}\frac{(\Delta c_\lambda)_1}{c_\lambda} &= \frac{S^3}{4}\left(\frac{v(\hat{\boldsymbol{k}})}{c_\lambda}\right)\left(\frac{h_c}{Mc^2_\lambda}\right)\left|\boldsymbol{F}^{X\beta}(\hat{\boldsymbol{k}}) \cdot \boldsymbol{e}_{\boldsymbol{k}\lambda}\right|^2 \\ &= \frac{S^3}{4}\left(\frac{v(\hat{\boldsymbol{k}})}{c_\lambda}\right)\left(\frac{h_c}{Mc^2_\lambda}\right)\left|s_\vartheta \boldsymbol{f}^{X\beta}_1(\hat{\boldsymbol{k}}) \cdot \boldsymbol{e}_{\boldsymbol{k}\lambda} - c^2_\vartheta \boldsymbol{f}^{X\beta}_2(\hat{\boldsymbol{k}}, \hat{\boldsymbol{k}}) \cdot \boldsymbol{e}_{\boldsymbol{k}\lambda}\right|^2 .\end{aligned} \tag{4.113}$$

Formally this is the leading order contribution in the small parameters $v(\hat{\boldsymbol{k}})/c_\lambda$ and $h_c/(Mc_\lambda^2)$. Note that the dependence on the magnetic field in the vertex, Eq. (4.111) is hidden in the canting angle, that we will approximate by its classical value Eq. (4.26a). Which of the two additive terms of the vertex dominates depends on the polarization vector of the considered phonon $\boldsymbol{e}_{\boldsymbol{k}\lambda}$ and the structure of the vector $\boldsymbol{J}_{\boldsymbol{k}}^{(1)}$. Both contributions add up to the total shift of the sound velocity

$$\frac{\Delta c_\lambda}{c_\lambda} = \frac{(\Delta c_\lambda)_0 + (\Delta c_\lambda)_1}{c_\lambda} \,. \tag{4.114}$$

4.6.2 Ultrasonic attenuation

The ultrasonic attenuation rate measured in experiments has several contributions, including contributions from lattice defects and from couplings to other degrees of freedom. However, the magnetic field dependence of the attenuation rate is related to the magnon-phonon coupling. Usually one would obtain the phonon damping in our microscopic approach using Fermi's golden rule. The matrix elements of the relevant interaction vertices are rather complicated. Therefore it is more convenient to apply many-body techniques and calculate the damping rate from the imaginary part of the self-energy. In this approach we start from the effective Euclidean action

$$S_2[\boldsymbol{X},\bar{\beta},\beta] = S^{\mathrm{2pho}}[\boldsymbol{X}]+S_{\mathrm{2mag}}[\bar{\beta},\beta]+\tilde{S}^{\mathrm{1pho}}_{\mathrm{2mag}}[\boldsymbol{X},\bar{\beta},\beta]+S^{\mathrm{2pho}}_{\mathrm{1mag}}[\boldsymbol{X},\bar{\beta},\beta] \,, \tag{4.115}$$

which contains all relevant effects to leading order in $1/S$. Note that the Gaussian parts $S^{\mathrm{2pho}}[\boldsymbol{X}]$ and $S_{\mathrm{2mag}}[\bar{\beta},\beta]$ are given in Eqs. (4.96) and (4.97), while the effective magnon-phonon interaction is given by

$$\begin{aligned}\tilde{S}^{\mathrm{1pho}}_{\mathrm{2mag}}[\boldsymbol{X},\bar{\beta},\beta] = \frac{1}{\sqrt{N}T}\sum_{K,K'}\Bigg[&\tilde{\boldsymbol{\Gamma}}^{\beta^\dagger\beta}_{\boldsymbol{k},\boldsymbol{k}'}\cdot\boldsymbol{X}_{K-K'}\bar{\beta}_K\beta_{K'} \\ &+\frac{1}{2!}\left(\tilde{\boldsymbol{\Gamma}}^{\beta^\dagger\beta^\dagger}_{\boldsymbol{k},\boldsymbol{k}'}\cdot\boldsymbol{X}_{K+K'}\bar{\beta}_K\bar{\beta}_{K'}+\tilde{\boldsymbol{\Gamma}}^{\beta\beta}_{\boldsymbol{k},\boldsymbol{k}'}\cdot\boldsymbol{X}_{-K-K'}\beta_K\beta_{K'}\right)\Bigg] \,,\end{aligned} \tag{4.116}$$

and

$$\begin{aligned}S^{\mathrm{2pho}}_{\mathrm{1mag}}[\boldsymbol{X},\bar{\beta},\beta] = \frac{1}{2!\sqrt{N}T}\sum_{K,K'}\sum_{\lambda\lambda'}\Big[&\Gamma^{XX\beta^\dagger}_{\boldsymbol{k}\lambda,\boldsymbol{k}'\lambda'}X_{K\lambda}X_{K'\lambda'}\beta^\dagger_{K+K'} \\ &+\Gamma^{XX\beta}_{\boldsymbol{k}\lambda,\boldsymbol{k}'\lambda'}X_{-K\lambda}X_{-K'\lambda'}\beta_{K+K'}\Big] \,.\end{aligned} \tag{4.117}$$

The hybridization is taken into account to leading order in $1/S$ by considering the effective interaction corresponding to the effective one-phonon two-magnon Hamiltonian $\tilde{H}^{\mathrm{1pho}}_{\mathrm{2mag}}$ defined in Eq. (4.76). Graphical representations of the terms in the effective action that will be used to illustrate the contributions to

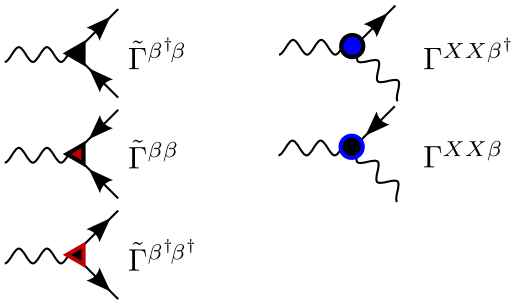

Figure 4.5: *Graphical representation of the interaction vertices for the processes included in the effective action Eq. (4.115). For the one-phonon two-magnon interaction we have three different vertices: The black triangle represents the shifted one-phonon two-magnon vertex defined in Eq. (4.77a) that connects one incoming and one outgoing magnon to a real phonon field. The red triangle with black border connects the phonon field to two incoming magnons, Eq. (4.77b), and the black triangle with red border connects two outgoing magnons to the phonon field Eq. (4.77c) (left). The two-phonon one-magnon interaction has only two vertices that connect one outgoing magnon to two phonon fields (blue circle with black border, Eq. (4.90a)) or one incoming magnon to two phonon fields (black circle with blue border, Eq. (4.90b)). Note that an inversion of the colors of border and body corresponds to a complex conjugation of the vertex functions.*

the phonon self-energy are shown in Fig. 4.5. The full propagators Eqs (4.100a) and (4.100b) are now parametrized by the self-energies $\Sigma^{\text{pho}}(K,\lambda)$ and $\Sigma_{\text{mag}}(K)$, where we again neglected all off-diagonal contributions. To leading order there are two processes that contribute to the phonon damping, see Fig. 4.6. The process (a) involves two magnons in the intermediate state and leads to a strong magnetic field dependence of the ultrasonic attenuation rate for strong magnetic fields $h \lesssim h_c$ where the magnons are expected to fluctuate strongly. The other process (b) has an intermediate state with one magnon and one phonon and contributes less. Note that all other possible processes are of higher order in the $1/S$ expansion and will not be considered at this point.

The ultrasonic attenuation rate $\gamma_{\boldsymbol{k}\lambda}$ of a phonon with energy $\omega_{\boldsymbol{k}\lambda}$ is then obtained from the imaginary part of the self-energy on resonance,

$$\gamma_{\boldsymbol{k}\lambda} = -\frac{\text{Im}\Sigma_2^{\text{pho}}(\omega_{\boldsymbol{k}\lambda} + i0^+, \boldsymbol{k}, \lambda)}{2\omega_{\boldsymbol{k}\lambda}}\,, \tag{4.118}$$

where the additional denominator appears due to the formulation of our theory in terms of Hermitian fields and the use of a Lagrangian for the phononic degrees of freedom.

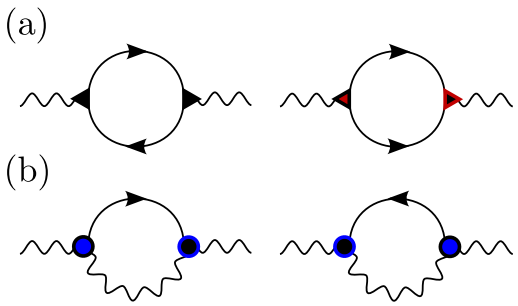

Figure 4.6: *These Feynman diagrams for the phonon self-energy contribute to the ultrasonic attenuation rate to leading order in the large-S expansion. (a) One-phonon two-magnon processes. (b) Two-phonon one-magnon processes. Both processes lead to an attenuation rate proportional to* $\boldsymbol{k}^4$ *at long wavelengths and zero temperature. The processes (a) exhibit a strong dependence on the external magnetic field and dominate if the magnon velocities are small compared to the phonon velocities.*

Processes (a)

The diagrams shown in Fig. 4.6 (a) result in the following contribution to the phonon self-energy:

$$\Sigma_{2\mathrm{a}}^{\mathrm{pho}}(K,\lambda) = -\frac{T}{N}\sum_{K'}\Bigg[\frac{|\tilde{\boldsymbol{\Gamma}}^{\beta^\dagger\beta}_{\boldsymbol{k}',\boldsymbol{k}'-\boldsymbol{k}}\cdot\boldsymbol{e}_{\boldsymbol{k}\lambda}|^2}{2M}G_{\mathrm{mag}}(K')G_{\mathrm{mag}}(K'-K) + \frac{|\tilde{\boldsymbol{\Gamma}}^{\beta^\dagger\beta^\dagger}_{\boldsymbol{k}',\boldsymbol{k}-\boldsymbol{k}'}\cdot\boldsymbol{e}_{\boldsymbol{k}\lambda}|^2}{2M}G_{\mathrm{mag}}(K')G_{\mathrm{mag}}(K-K')\Bigg] + (K\to -K)\,. \tag{4.119}$$

In the spirit of the $1/S$ expansion where only the leading order contributions are kept, we may also neglect the self-energy corrections to the magnon propagators. By help of the expansion into partial fractions,

$$\frac{1}{(x-i\omega)(x+i\omega)} = \frac{1}{2x}\Big(\frac{1}{x-i\omega}+\frac{1}{x+i\omega}\Big)\,, \tag{4.120}$$

we can use

$$T\sum_{i\omega_n}\frac{e^{i\omega_n 0^+}}{i\omega_n - E_{\boldsymbol{k}}} = -n(E_{\boldsymbol{k}})\,, \tag{4.121a}$$

$$T\sum_{i\omega_n}\frac{e^{-i\omega_n 0^+}}{i\omega_n - E_{\boldsymbol{k}}} = -n(E_{\boldsymbol{k}})-1 \tag{4.121b}$$

to solve the frequency sums. The self-energy then simplifies to

$$\Sigma_{2\mathrm{a}}^{\mathrm{pho}}(K,\lambda) = -\frac{1}{N}\sum_{\boldsymbol{k}'}\Bigg[\frac{|\tilde{\boldsymbol{\Gamma}}^{\beta^\dagger\beta}_{\boldsymbol{k}',\boldsymbol{k}'-\boldsymbol{k}}\cdot\boldsymbol{e}_{\boldsymbol{k}\lambda}|^2}{2M}\frac{n(E_{\boldsymbol{k}'})-n(E_{\boldsymbol{k}'-\boldsymbol{k}})}{i\omega - E_{\boldsymbol{k}'}+E_{\boldsymbol{k}'-\boldsymbol{k}}} + \frac{|\tilde{\boldsymbol{\Gamma}}^{\beta^\dagger\beta^\dagger}_{\boldsymbol{k}',\boldsymbol{k}-\boldsymbol{k}'}\cdot\boldsymbol{e}_{\boldsymbol{k}\lambda}|^2}{2M}\frac{n(E_{\boldsymbol{k}'})+n(E_{\boldsymbol{k}-\boldsymbol{k}'})+1}{-i\omega + E_{\boldsymbol{k}'}+E_{\boldsymbol{k}-\boldsymbol{k}'}}\Bigg] + (K\to -K)\,, \tag{4.122}$$

where

$$n(E) = 1/(e^{E/T} - 1) \tag{4.123}$$

is the Bose function that accounts for finite temperatures. Similar to the calculation in section 2.5.4 we have to analytically continue this expression to the real frequency axis to obtain the phonon damping. Thus, we replace $i\omega \to \omega + i\eta$, perform the limit $\eta \to 0$ and take the imaginary part with the result

$$\begin{aligned}\mathrm{Im}\Sigma^{\mathrm{pho}}_{2\mathrm{a}}(\omega + i0^+, \boldsymbol{k}, \lambda) = -[1 - e^{-\omega/T}]\frac{\pi}{N}\sum_{\boldsymbol{k}'}\Bigg[\\ \frac{|\tilde{\boldsymbol{\Gamma}}^{\beta^\dagger\beta}_{\boldsymbol{k}',\boldsymbol{k}'-\boldsymbol{k}} \cdot \boldsymbol{e}_{\boldsymbol{k}\lambda}|^2}{2M}\delta(\omega - E_{\boldsymbol{k}'} + E_{\boldsymbol{k}'-\boldsymbol{k}})[1 + n(E_{\boldsymbol{k}'})]n(E_{\boldsymbol{k}'-\boldsymbol{k}}) \\ + \frac{|\tilde{\boldsymbol{\Gamma}}^{\beta^\dagger\beta^\dagger}_{\boldsymbol{k}',\boldsymbol{k}-\boldsymbol{k}'} \cdot \boldsymbol{e}_{\boldsymbol{k}\lambda}|^2}{2M}\delta(\omega - E_{\boldsymbol{k}'} - E_{\boldsymbol{k}-\boldsymbol{k}'})[1 + n(E_{\boldsymbol{k}'})][1 + n(E_{\boldsymbol{k}-\boldsymbol{k}'})]\Bigg] \\ - (\omega \to -\omega, \boldsymbol{k} \to -\boldsymbol{k}) \,,\end{aligned} \tag{4.124}$$

where we have used the identities

$$\begin{aligned}&\delta(\omega - E_1 + E_2)[n(E_1) - n(E_2)] \\ &= -\delta(\omega - E_1 + E_2)[1 - e^{-\beta\omega}][1 + n(E_1)]n(E_2) \,, &\text{(4.125a)} \\ &\delta(\omega - E_1 - E_2)[n(E_1) + n(E_2) + 1] \\ &= \delta(\omega - E_1 - E_2)[1 - e^{-\beta\omega}][1 + n(E_1)][1 + n(E_2)] \,, &\text{(4.125b)}\end{aligned}$$

which can be verified using the definition Eq. (4.123) of the Bose function. Considering Eq. (4.118) we simplify the result for the attenuation rate in the limit of zero temperature to

$$\gamma^{(\mathrm{a})}_{\boldsymbol{k}\lambda} = \frac{\pi}{2\omega_{\boldsymbol{k}\lambda}}\frac{1}{N}\sum_{\boldsymbol{k}'}\frac{|\tilde{\boldsymbol{\Gamma}}^{\beta^\dagger\beta^\dagger}_{\boldsymbol{k}',\boldsymbol{k}-\boldsymbol{k}'} \cdot \boldsymbol{e}_{\boldsymbol{k}\lambda}|^2}{2M}\delta(\omega_{\boldsymbol{k}\lambda} - E_{\boldsymbol{k}'} - E_{\boldsymbol{k}-\boldsymbol{k}'}) \,, \tag{4.126}$$

because only one term of Eq. (4.125a) contributes when the magnons are much softer than the phonons. In Fig. 4.7 one sees that the first δ-function condition of this equation is not satisfied at any point in the Brillouin zone, while the second term contributes on an ellipse in momentum space. Now we are able to calculate the leading behavior of $\gamma^{(a)}_{\boldsymbol{k}\lambda}$ for small $\boldsymbol{k}$ analytically. In this limit it is sufficient to approximate the magnon dispersion by $E_{\boldsymbol{k}} \approx v(\hat{\boldsymbol{k}})|\boldsymbol{k}|$ according to Eq. (4.33). At this point we introduce rescaled momenta,

$$p_x = \frac{v_x}{v}k_x \,, \quad p_y = \frac{v_y}{v}k_y \,, \quad p'_x = \frac{v_x}{v}k'_x \,, \quad p'_y = \frac{v_y}{v}k'_y \,, \tag{4.127}$$

to eliminate the different magnon velocities in the x- and y-direction. By help of the velocity $v^2 = v_x^2 + v_y^2$ it is possible to rewrite the magnon dispersion at small momenta as

$$E_{\boldsymbol{k}} = v|\boldsymbol{p}| \,, \tag{4.128}$$

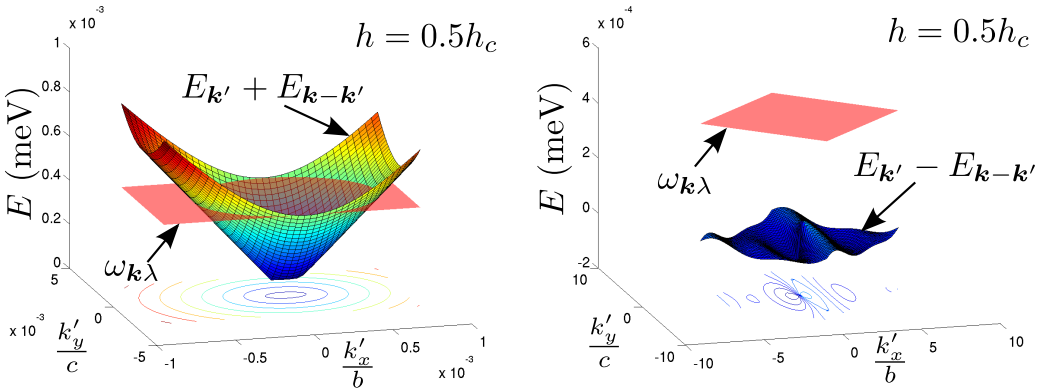

Figure 4.7: *Graphical solution of the equation $\omega_{k\lambda} = E_{k'} + E_{k-k'}$ defining the scattering surface that contributes to the imaginary part of the self-energy Eq. (4.124) (left). The other three terms do not contribute if the magnons are soft, i.e. the gradient of the energy dispersion fulfills $\nabla_k E_k < c_\lambda$ (right). The plots were obtained using the parameters of Cs_2CuCl_4 [37, 209] and for phonons of the c_{22}-mode with frequency $f = 110$ MHz.*

so that the equation for the scattering surface is

$$\omega_{k\lambda} = v|\boldsymbol{p}'| + v|\boldsymbol{p} - \boldsymbol{p}'| \,. \tag{4.129}$$

This defines an ellipse in the $\boldsymbol{p}'$-plane, see Fig. 4.7, with the parametric representation

$$\boldsymbol{p}'(\varphi) = \frac{1}{2}\left[\boldsymbol{p} - \frac{\omega_{k\lambda}}{v}\cos\varphi\,\hat{\boldsymbol{p}} + \frac{\sqrt{\omega_{k\lambda}^2 - \epsilon_k^2}}{v}\sin\varphi\,\hat{\boldsymbol{p}}_\perp\right] \,, \tag{4.130}$$

in spherical coordinates, where we have defined the orthogonal unit vectors

$$\hat{\boldsymbol{p}} = \frac{1}{v|\boldsymbol{p}|}\begin{pmatrix} v_x k_x \\ v_y k_y \end{pmatrix} \,, \tag{4.131}$$

$$\hat{\boldsymbol{p}}_\perp = \frac{1}{v|\boldsymbol{p}|}\begin{pmatrix} -v_y k_y \\ v_x k_x \end{pmatrix} \,. \tag{4.132}$$

We introduce the ratio

$$r_{k\lambda} = \frac{v(\hat{\boldsymbol{k}})}{c_\lambda} \tag{4.133}$$

of the magnon velocities and the phonon velocities to rewrite Eq. (4.130) as

$$\frac{v\boldsymbol{p}'(\varphi)}{\omega_{k\lambda}} = \frac{1}{2}\left[(r_{k\lambda} - \cos\varphi)\,\hat{\boldsymbol{p}} + \sqrt{1 - r_{k\lambda}^2}\sin\varphi\,\hat{\boldsymbol{p}}_\perp\right] . \tag{4.134}$$

Substituting Eq. (4.127) in the integrand of Eq. (4.126) and taking into account identities for the calculus of integrals over δ-functions we use

$$\frac{v|\boldsymbol{p}'(\varphi)|}{\omega_{\boldsymbol{k}\lambda}} = \frac{1}{2}\left[1 - r_{\boldsymbol{k}\lambda}\cos\varphi\right] , \tag{4.135}$$

$$\frac{v}{\omega_{\boldsymbol{k}\lambda}}\left|\frac{d\boldsymbol{p}'(\varphi)}{d\varphi}\right| = \frac{1}{2}\sqrt{1 - r_{\boldsymbol{k}\lambda}^2\cos^2\varphi} , \tag{4.136}$$

to get

$$\begin{aligned}\gamma_{\boldsymbol{k}\lambda}^{(\mathrm{a})} = {} & \frac{\pi S^2}{16}\left(\frac{\boldsymbol{k}^2}{2M}\right)\left(\frac{\boldsymbol{k}^2}{V_{\mathrm{BZ}}}\right)\frac{c_\lambda^2}{v_x v_y} \\ & \times \int_0^{2\pi} d\varphi \frac{\sqrt{1 - r_{\boldsymbol{k}\lambda}^2\cos^2\varphi}}{\left|\nabla_{\boldsymbol{p}'}\left(|\boldsymbol{p}'| + |\boldsymbol{p} - \boldsymbol{p}'|\right)\right|_{\boldsymbol{p}'=\boldsymbol{p}'(\varphi)}} \left|\boldsymbol{F}^{X\beta^\dagger\beta^\dagger}(\hat{\boldsymbol{k}},\varphi)\cdot\boldsymbol{e}_{\boldsymbol{k}\lambda}\right|^2 ,\end{aligned} \tag{4.137}$$

where we have introduced the dimensionless function $\boldsymbol{F}^{X\beta^\dagger\beta^\dagger}(\hat{\boldsymbol{k}},\varphi)$ via the long-wavelength limit given in Eq. (4.79),

$$\tilde{\boldsymbol{\Gamma}}^{\beta^\dagger\beta^\dagger}_{\boldsymbol{k}'(\varphi),\boldsymbol{k}-\boldsymbol{k}'(\varphi)} = \frac{S}{2}c_\lambda \boldsymbol{k}^2 \boldsymbol{F}^{X\beta^\dagger\beta^\dagger}(\hat{\boldsymbol{k}},\varphi) . \tag{4.138}$$

On the scattering surface this is given by

$$\begin{aligned}\boldsymbol{F}^{X\beta^\dagger\beta^\dagger}(\hat{\boldsymbol{k}},\varphi) = {} & \left(\frac{2s_\vartheta^2}{c_\vartheta^2} + 1\right)\sqrt{\frac{v|\boldsymbol{p}'|}{\omega_{\boldsymbol{k}\lambda}}\left(1 - \frac{v|\boldsymbol{p}'|}{\omega_{\boldsymbol{k}\lambda}}\right)}\boldsymbol{f}_1^{X\beta}(\hat{\boldsymbol{k}}) \\ & + s_\vartheta \frac{\frac{2v|\boldsymbol{p}'|}{\omega_{\boldsymbol{k}\lambda}} - 1}{\sqrt{\frac{v|\boldsymbol{p}'|}{\omega_{\boldsymbol{k}\lambda}}\left(1 - \frac{v|\boldsymbol{p}'|}{\omega_{\boldsymbol{k}\lambda}}\right)}}\left[\frac{2\boldsymbol{k}'(\varphi) - \boldsymbol{k}}{2\omega_{\boldsymbol{k}\lambda}}\cdot\nabla_{\boldsymbol{Q}}\right](\hat{\boldsymbol{k}}\cdot\nabla_{\boldsymbol{Q}})\boldsymbol{J}_{\boldsymbol{Q}}^{(1)} \\ = {} & \frac{1}{2\sqrt{1 - r_{\boldsymbol{k}\lambda}^2\cos^2\varphi}}\Bigg\{\left(\frac{2s_\vartheta^2}{c_\vartheta^2} + 1\right)\left(1 - r_{\boldsymbol{k}\lambda}^2\cos^2\varphi\right)\boldsymbol{f}_1^{X\beta}(\hat{\boldsymbol{k}}) \\ & + 4s_\vartheta\frac{v(\hat{\boldsymbol{k}})}{c_\lambda}\left[\cos^2\varphi\,\boldsymbol{f}_2^{X\beta}(\hat{\boldsymbol{k}},\hat{\boldsymbol{k}}) - \sqrt{1 - r_{\boldsymbol{k}\lambda}^2}\cos\varphi\sin\varphi\;\boldsymbol{f}_2^{X\beta}(\hat{\boldsymbol{k}}'_\perp,\hat{\boldsymbol{k}})\right]\Bigg\} .\end{aligned} \tag{4.139}$$

Now we calculate the absolute value of the gradient

$$\left|\nabla_{\boldsymbol{p}'}\left(|\boldsymbol{p}'| + |\boldsymbol{p} - \boldsymbol{p}'|\right)\right|_{\boldsymbol{p}'=\boldsymbol{p}'(\varphi)} = \frac{2\sqrt{1 - r_{\boldsymbol{k}\lambda}^2}}{\sqrt{1 - r_{\boldsymbol{k}\lambda}^2\cos^2\varphi}} , \tag{4.140}$$

and use

$$\frac{2\boldsymbol{k}'(\varphi) - \boldsymbol{k}}{\omega_{\boldsymbol{k}\lambda}} = \frac{1}{v(\hat{\boldsymbol{k}})}\left[-\cos\varphi\,\hat{\boldsymbol{k}} + \sqrt{1 - r_{\boldsymbol{k}\lambda}^2}\sin\varphi\,\hat{\boldsymbol{k}}'_\perp\right] . \tag{4.141}$$

By help of elementary integrals over sine and cosine functions we finally obtain the result

$$\gamma_{\boldsymbol{k}\lambda}^{(\mathrm{a})} = \frac{\pi^2}{64}\left(\frac{\boldsymbol{k}^2}{2M}\right)\left(\frac{S^2 c_\lambda^2 \boldsymbol{k}^2}{V_{\mathrm{BZ}} v_x v_y}\right)\frac{I_\lambda(\hat{\boldsymbol{k}})}{\sqrt{1-r_{\boldsymbol{k}\lambda}^2}}\ . \tag{4.142}$$

The dimensionless function $I_\lambda(\hat{\boldsymbol{k}})$ is given by

$$\begin{aligned} I_\lambda(\hat{\boldsymbol{k}}) = &\left(\frac{2s_\vartheta^2}{c_\vartheta^2}+1\right)^2\left(1-r_{\boldsymbol{k}\lambda}^2+\frac{3}{8}r_{\boldsymbol{k}\lambda}^4\right)\left[\boldsymbol{f}_1^{X\beta}(\hat{\boldsymbol{k}})\cdot\boldsymbol{e}_{\boldsymbol{k}\lambda}\right]^2 \\ &+8s_\vartheta\left(\frac{2s_\vartheta^2}{c_\vartheta^2}+1\right)\left(1-\frac{3}{4}r_{\boldsymbol{k}\lambda}^2\right)\left[\boldsymbol{f}_1^{X\beta}(\hat{\boldsymbol{k}})\cdot\boldsymbol{e}_{\boldsymbol{k}\lambda}\right]\frac{v(\hat{\boldsymbol{k}})}{c_\lambda}\left[\boldsymbol{f}_2^{X\beta}(\hat{\boldsymbol{k}},\hat{\boldsymbol{k}})\cdot\boldsymbol{e}_{\boldsymbol{k}\lambda}\right] \\ &+s_\vartheta^2\frac{v(\hat{\boldsymbol{k}})}{c_\lambda}\left\{3\left[\boldsymbol{f}_2^{X\beta}(\hat{\boldsymbol{k}},\hat{\boldsymbol{k}})\cdot\boldsymbol{e}_{\boldsymbol{k}\lambda}\right]^2+(1-r_{\boldsymbol{k}\lambda}^2)\left[\boldsymbol{f}_2^{X\beta}(\hat{\boldsymbol{k}},\hat{\boldsymbol{k}}_\perp)\cdot\boldsymbol{e}_{\boldsymbol{k}\lambda}\right]^2\right\}\ . \end{aligned} \tag{4.143}$$

For convenience we have introduced the vector $\hat{\boldsymbol{k}}_\perp = -(v_y/v_x)\hat{k}_y\boldsymbol{e}_x+(v_x/v_y)\hat{k}_x\boldsymbol{e}_y$ to write this function in a compact way. A graphical solution of the equation defining the scattering surface using the full dispersion $E_{\boldsymbol{k}}$ is shown in Fig. 4.7. No differences emerging from the approximation in Eq. (4.33) are visible with the naked eye and an examination of the terms shows that it is justified to drop the asymmetry of the dispersion with respect to $\boldsymbol{k}\to-\boldsymbol{k}$ at this point, while this was not possible in the derivation of the magnon-phonon vertices.

Processes (b)

The processes (b) in Fig. 4.6 are of second order in the two-phonon one-magnon vertex and give rise to the phonon self-energy

$$\Sigma_{\mathrm{2b}}^{\mathrm{pho}}(K,\lambda) = \frac{T}{N}\sum_{K'\lambda'}\frac{|\Gamma_{\boldsymbol{k}\lambda,\boldsymbol{k}'\lambda'}^{XX\beta}|^2}{M^2}G^{\mathrm{pho}}(K',\lambda')G_{\mathrm{mag}}(K'+K)+(K\to-K)\ , \tag{4.144}$$

where $\Gamma_{\boldsymbol{k}\lambda,\boldsymbol{k}'\lambda'}^{XX\beta} = \boldsymbol{e}_{\boldsymbol{k}\lambda}^\dagger\boldsymbol{\Gamma}_{\boldsymbol{k}\boldsymbol{k}'}^{XX\beta}\boldsymbol{e}_{\boldsymbol{k}'\lambda'}$ is the projection of the vertex on the phonon branches. Approximating the propagators by their Gaussian values, we can carry out the Matsubara sums to obtain

$$\begin{aligned} \Sigma_{\mathrm{2b}}^{\mathrm{pho}}(K,\lambda) = \frac{1}{N}\sum_{\boldsymbol{k}'\lambda'}\frac{|\Gamma_{\boldsymbol{k}\lambda,-\boldsymbol{k}'\lambda'}^{XX\beta}|^2}{2\omega_{\boldsymbol{k}'\lambda'}M^2}\Bigg[&\frac{n(\omega_{\boldsymbol{k}'\lambda'})-n(E_{\boldsymbol{k}-\boldsymbol{k}'})}{i\omega+\omega_{\boldsymbol{k}'\lambda}-E_{\boldsymbol{k}-\boldsymbol{k}'}} \\ &+\frac{n(\omega_{\boldsymbol{k}'\lambda'})+n(E_{\boldsymbol{k}-\boldsymbol{k}'})+1}{i\omega-\omega_{\boldsymbol{k}'\lambda'}-E_{\boldsymbol{k}-\boldsymbol{k}'}}\Bigg]+(K\to-K)\ . \end{aligned} \tag{4.145}$$

At zero temperature this leads to the following contribution to the ultrasonic attenuation rate:

$$\gamma_{\boldsymbol{k}\lambda}^{(\mathrm{b})} = \frac{\pi}{2\omega_{\boldsymbol{k}\lambda}}\frac{1}{N}\sum_{\boldsymbol{k}'\lambda'}\frac{\left|\Gamma_{\boldsymbol{k}\lambda,-\boldsymbol{k}'\lambda'}^{XX\beta}\right|^2}{2\omega_{\boldsymbol{k}'\lambda'}M^2}\delta(\omega_{\boldsymbol{k}\lambda}-\omega_{\boldsymbol{k}'\lambda'}-E_{\boldsymbol{k}-\boldsymbol{k}'})\ . \tag{4.146}$$

This integral can now be carried out numerically applying a triangular method to take the condition from the δ-function into account [100]. In Fig. 4.11 a comparison of the exact result and the calculation to leading order in $r_{\boldsymbol{k}\lambda}$ is presented. It turns out that the contribution is small compared to that from the dominant processes (a) and that the analytical approximation deviates only slightly from the exact result. To arrive at the analytical result, we use the expansion Eq. (4.91) and the approximation Eq. (4.33) to carry out the integration in Eq. (4.146) for the case of soft magnons. Anticipating that the phonon velocities are much larger than the magnon velocities, we may again parametrize the scattering surface, defined by the equation

$$\omega_{\boldsymbol{k}\lambda} - \omega_{\boldsymbol{k}'\lambda'} - E_{\boldsymbol{k}-\boldsymbol{k}'} = 0 \; . \tag{4.147}$$

It is again an ellipse if we additionally restrict our calculation to leading order in $r_{\boldsymbol{k}\lambda}$. The parametric representation in circular coordinates is now given by

$$\boldsymbol{k}'(\varphi') = |\boldsymbol{k}| \frac{c_\lambda - u(\hat{\boldsymbol{k}}, \varphi')}{c_{\lambda'}} \hat{\boldsymbol{k}}'(\varphi') \; , \tag{4.148}$$

where we have parametrized

$$\hat{\boldsymbol{k}}'(\varphi') = \cos\varphi' \boldsymbol{e}_x + \sin\varphi' \boldsymbol{e}_y \; , \tag{4.149}$$

and introduced the velocity

$$u(\hat{\boldsymbol{k}}, \varphi') = \sqrt{v_x^2(\hat{k}_x - \cos\varphi')^2 + v_y^2(\hat{k}_y - \sin\varphi')^2} \; . \tag{4.150}$$

With similar steps as in the discussion of the processes (a) we can carry out the radial integration, but the angular integration has to be done numerically as one can read off from the result,

$$\begin{aligned} \gamma_{\boldsymbol{k}\lambda}^{(\mathrm{b})} = {} & \frac{\pi S^3}{4} \left(\frac{\boldsymbol{k}^2}{2M}\right) \left(\frac{\boldsymbol{k}^2}{V_{\mathrm{BZ}}}\right) \sum_{\lambda'} \left(\frac{h_c}{M c_{\lambda'}^2}\right) \left(\frac{c_\lambda}{c_{\lambda'}}\right)^2 \\ & \times \int_0^{2\pi} d\varphi' \frac{u(\hat{\boldsymbol{k}}, \varphi')}{c_{\lambda'}} |\boldsymbol{e}_{\boldsymbol{k}\lambda}^\dagger \mathbf{F}^{XX\beta}(\hat{\boldsymbol{k}}, \varphi') \boldsymbol{e}_{\boldsymbol{k}'\lambda'}|^2 \; , \end{aligned} \tag{4.151}$$

where we have introduced the dimensionless matrix element

$$\begin{aligned} \mathbf{F}^{XX\beta}(\hat{\boldsymbol{k}}, \varphi') = {} & \frac{s_\vartheta}{h_c} \left(\hat{\boldsymbol{k}} \cdot \nabla_{\boldsymbol{Q}}\right) \left(\hat{\boldsymbol{k}}'(\varphi') \cdot \nabla_{\boldsymbol{Q}}\right) \left[\mathbf{J}_{\boldsymbol{Q}}^{(2)}\Big|_{\boldsymbol{Q}=0} - \mathbf{J}_{\boldsymbol{Q}}^{(2)}\right] \\ & - \frac{c_\vartheta^2}{2u(\hat{\boldsymbol{k}}, \varphi')} \left\{\left[\hat{\boldsymbol{k}} - \frac{c_\lambda}{c_{\lambda'}} \hat{\boldsymbol{k}}'(\varphi')\right] \cdot \nabla_{\boldsymbol{Q}}\right\} (\hat{\boldsymbol{k}} \cdot \nabla_{\boldsymbol{Q}})(\hat{\boldsymbol{k}}'(\varphi') \cdot \nabla_{\boldsymbol{Q}}) \mathbf{J}_{\boldsymbol{Q}}^{(2)} \; . \end{aligned} \tag{4.152}$$

Summary

Adding the two contributions Eqs. (4.142) and (4.151) to the total attenuation rate

$$\gamma_{\boldsymbol{k}\lambda} = \gamma_{\boldsymbol{k}\lambda}^{(\mathrm{a})} + \gamma_{\boldsymbol{k}\lambda}^{(\mathrm{b})} \; , \tag{4.153}$$

we conclude that in the regime of small wave vectors the damping of the phonons at zero temperature will have a contribution from the spin-phonon interaction that is proportional to $\boldsymbol{k}^4$. In the regime where the magnon velocities are small compared with the phonon velocities, we conclude that the term $\gamma^{(\mathrm{a})}_{\boldsymbol{k}\lambda}$ from the processes (a) is much larger than the contribution $\gamma^{(\mathrm{b})}_{\boldsymbol{k}\lambda}$ from the processes where also an intermediate phonon is participating. Note that our calculations are in general valid for ordered two-dimensional QAFMs that are described by the Hamiltonian Eq. (1.47) with soft magnon modes where the critical magnetic field h_c is also accessible experimentally. Note also that in the case of a finite magnetic field in conjunction with a DM anisotropy it is crucial to take the renormalization of the one-phonon two-magnon vertices due to magnon-phonon hybridization into account. Otherwise one observes that the symmetries of the vertices do not match the expected symmetries and one would incorrectly find from Eq. (4.118) that $\gamma_{\boldsymbol{k}\lambda}$ will approach a non-zero constant for $\boldsymbol{k} \to 0$. This is of course unphysical, because it would imply that phonons are not well defined quasiparticles.

4.7 Comparison to experiments

Data for the frequency shift and the ultrasonic attenuation rate of phonons with a frequency of $f = 110$ MHz has been obtained from measurements on single crystals of Cs_2CuCl_4 for temperatures down to $T \approx 50$ mK and for magnetic fields up to 10 Tesla[4]. In order to calculate predictions for the velocity shift and the attenuation rate we need realistic estimates for the first and second derivatives $\partial J/\partial x$, $\partial J'/\partial r$, $\partial^2 J/\partial x^2$, and $\partial^2 J'/\partial r^2$ of the exchange couplings in Eqs. (4.52) and (4.53a–4.53c). *Ab initio* methods can in principle obtain the spatial dependence of the exchange couplings [231], but we are not aware of quantitative results for the compound Cs_2CuCl_4. We therefore use the rough behavior of the exchange couplings $J(x)$ and $J'(r)$ discussed in section 1.1.1 to model their spatial dependence as

$$J(x) = J(b)e^{-\kappa(x-b)/b} \,, \tag{4.154a}$$

$$J'(r) = J'(d)e^{-\kappa'(r-d)/d} \,, \tag{4.154b}$$

where b and $d = \sqrt{b^2 + c^2}/2$ are the bond lengths at the equilibrium positions, compare Fig. 4.1. The dimensionless quantities κ and κ' are unknown at this point and shall be fixed by a fitting procedure of our theoretical predictions to the experimental data. To start with the shift in the phonon velocities, we have to calculate the classical contribution $(\Delta c_\lambda)_0$ given in Eqs. (4.83) and (4.102). For longitudinal phonons in the x-direction (c_{22}-mode) we get the

[4] P. T. Cong, private communication.

dimensionless ratio

$$\lim_{|\boldsymbol{k}|\to 0}\frac{\Sigma_0^{\mathrm{pho}}(\boldsymbol{k},\lambda)}{\omega_{\boldsymbol{k}\lambda}^2}=-\frac{S^2}{Mc_\lambda^2}\Big[s_\vartheta^2\Big(J\kappa^2+\frac{J'}{2}\kappa'^2\cos^4\varphi_0\Big) +c_\vartheta^2\Big(J\kappa^2\cos(Q_xb)+\frac{J'}{2}\kappa'^2\cos^4\varphi_0\cos(Q_xb/2)\Big)\Big]\ , \quad (4.155a)$$

while for longitudinal phonons in the y-direction (c_{33}-mode) this ratio is given by

$$\lim_{|\boldsymbol{k}|\to 0}\frac{\Sigma_0^{\mathrm{pho}}(\boldsymbol{k},\lambda)}{\omega_{\boldsymbol{k}\lambda}^2}=-\frac{S^2}{2Mc_\lambda^2}J'\kappa'^2\sin^4\varphi_0\Big[s_\vartheta^2+c_\vartheta^2\cos(Q_xb/2)\Big]\ . \quad (4.155b)$$

According to Eqs. (4.154a) and (4.154b) the quantities above depend on the bare couplings $J=J(b)$ and $J'=J'(d)$ given in Table 4.1. Note that the dependence on the magnetic field is contained in the canting angle ϑ and the expression for the c_{33}-mode only depends on the parameter κ' since longitudinal phonons in the y-direction only modulate the bond length of the coupling J'. For the calculation of the contribution due to magnon-phonon hybridization $(\Delta c_\lambda)_1$ to the velocity shift Eq. (4.113) and the dominant term for the attenuation rate given in Eqs. (4.142) and (4.143) we have to evaluate the dimensionless scalar products $\boldsymbol{f}_1^{X\beta}(\hat{\boldsymbol{k}})\cdot\boldsymbol{e}_{\boldsymbol{k}\lambda}$, $\boldsymbol{f}_2^{X\beta}(\hat{\boldsymbol{k}},\hat{\boldsymbol{k}})\cdot\boldsymbol{e}_{\boldsymbol{k}\lambda}$, and $\boldsymbol{f}_2^{X\beta}(\hat{\boldsymbol{k}},\hat{\boldsymbol{k}}_\perp)\cdot\boldsymbol{e}_{\boldsymbol{k}\lambda}$. For the longitudinal phonon modes in the plane we set $\hat{\boldsymbol{k}}=(\hat{k}_x,\hat{k}_y)=\boldsymbol{e}_{\boldsymbol{k}\lambda}$ and obtain the relevant scalar products

$$\boldsymbol{f}_1^{X\beta}(\hat{\boldsymbol{k}})\cdot\hat{\boldsymbol{k}}=-\frac{2i}{h_c}\Big\{\hat{k}_x^2\Big[J\kappa(1-\cos(Q_xb))+2J'\kappa'\cos^2\varphi_0(1-\cos(Q_xb/2))\Big] +\hat{k}_y^2 2J'\kappa'\sin^2\varphi_0(1-\cos(Q_xb/2))\Big\}\ , \quad (4.156a)$$

$$\boldsymbol{f}_2^{X\beta}(\hat{\boldsymbol{k}},\hat{\boldsymbol{k}})\cdot\hat{\boldsymbol{k}}=\frac{i}{v(\hat{\boldsymbol{k}})}\Big\{\hat{k}_x^3b\Big[J\kappa\sin(Q_xb)+J'\kappa'\sin(Q_xb/2)\cos^2\varphi\Big] +3\hat{k}_x\hat{k}_y^2cJ'\kappa'\sin\varphi_0\cos\varphi_0\sin(Q_xb/2)\Big\}\ , \quad (4.156b)$$

$$\boldsymbol{f}_2^{X\beta}(\hat{\boldsymbol{k}},\hat{\boldsymbol{k}}_\perp)\cdot\hat{\boldsymbol{k}}=\frac{i\hat{k}_x}{v(\hat{\boldsymbol{k}})}\Big\{\frac{v_y}{v_x}\hat{k}_y^2b\Big[J\kappa\sin(Q_xb)+J'\kappa'\cos^2\varphi_0\sin(Q_xb/2)\Big] +\Big[\frac{v_y}{v_x}\hat{k}_y^2-\frac{v_x}{v_y}\hat{k}_x(\hat{k}_x+\hat{k}_y)\Big]cJ'\kappa'\sin\varphi_0\cos\varphi_0\sin(Q_xb/2)\Big\}\ , \quad (4.156c)$$

where we have used the fact that the wave vector $\boldsymbol{Q}$ of the spiral only has an x-component, compare Fig. 4.2. We finally set $\hat{\boldsymbol{k}}=(1,0)$ for the c_{22}-mode and $\hat{\boldsymbol{k}}=(0,1)$ for the c_{33}-mode and calculate the total velocity shift according to Eq. (4.114).

Fig. 4.8 shows a comparison of our theoretical results for the magnetic field dependence of the velocity shifts of the two longitudinal phonon modes in

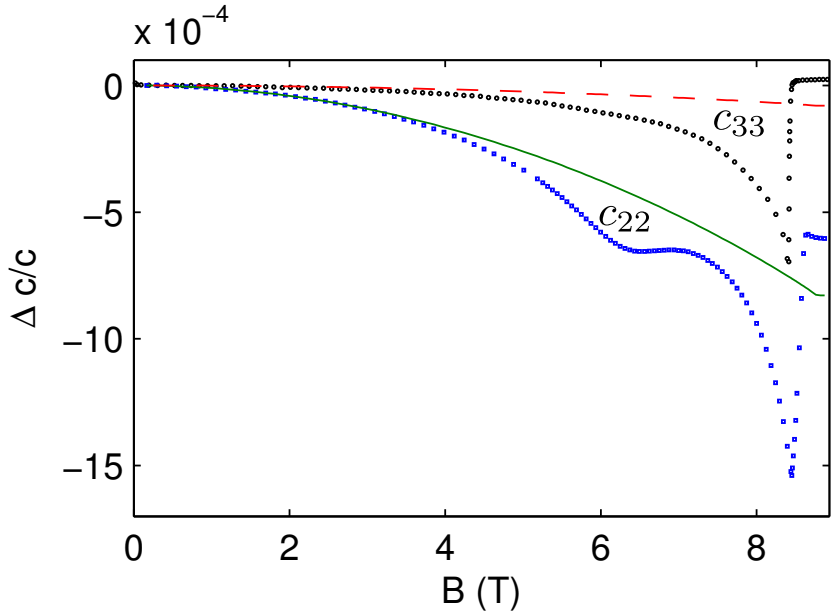

Figure 4.8: *The points are the measured velocity shifts of the longitudinal c_{22} (blue squares) and c_{33} (black circles) phonon modes in Cs_2CuCl_4 as a function of the magnetic induction B at low temperature. The data for the c_{22}-mode was measured at $T = 52$ mK, while the data for the c_{33}-mode was taken at $T = 48$ mK. The solid green line is a fit of our corresponding theoretical results at zero temperature given in Eqs. (4.83, 4.102, 4.113, 4.114) to the data for the c_{22}-mode. Having fixed the parameters $|\kappa| \approx 15$ and $|\kappa'| \approx 51$ from the fit to the c_{22}-mode, we can use the same parameters for our theoretical prediction for the c_{33}-mode (red dashed line). Features near the critical field $B_c \approx 8.5$ Tesla might have a different physical origin than magnon excitations, data taken from [P8]*

.

the plane with experimental data measured at low temperatures $T \approx 50$ mK. The parameters $|\kappa| \approx 15$ and $|\kappa'| \approx 51$ were determined by a fit to the data of the c_{22}-mode. Inserting κ' back into our expression for the c_{33}-mode, we have calculated our prediction for the velocity shift such that our theoretical curve does not contain any adjustable parameters. Note that the bare velocity c_λ is taken at vanishing magnetic field, such that the shift is zero at $h = 0$. Observing Fig. 4.9 it is obvious that the velocity shift is well described by our theoretical results. Deviations between experimental data and our calculations indicate a breakdown of our approach. We neglected higher order fluctuation corrections that are supposed to play an important role in the vicinity of the critical magnetic field. For large fields the magnetic order vanishes and other excitations than spin waves might give larger contributions to observables.

Having fixed the fit parameters κ and κ' from the velocity shift, we can calculate the ultrasonic attenuation rate given in Eqs. (4.142) and (4.151). Our prediction has no further adjustable parameters except for a constant shift

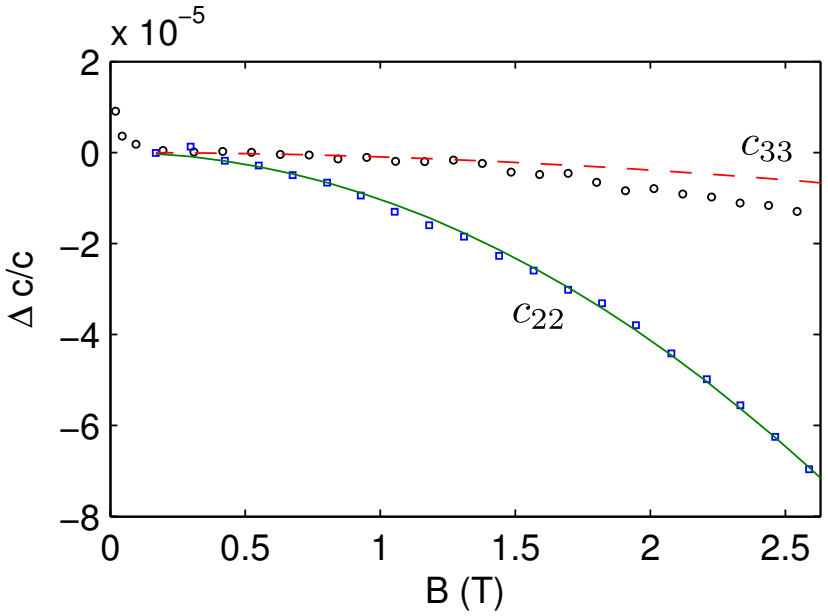

Figure 4.9: *Enlarged details of the plot shown in Fig. 4.8 for small magnetic fields where the fit has been made to obtain the parameters $|\kappa|$ and $\kappa'|$. Our spin-wave approach should be most accurate in the small field regime $B \lesssim 2.5$ Tesla, data taken from [P8]*

.

because experimentally it is only possible to determine the relative attenuation rate. Fig. 4.10 shows a comparison between the results of our calculations and the measurements of the attenuation rate of the c_{22} and c_{33} phonon modes in Cs_2CuCl_4. It turns out that the attenuation rates do not change significantly as a function of the magnetic field for fields in the range $h \lesssim 0.8h_c$. On approaching the critical field h_c there is a strong enhancement as expected in the vicinity of a phase transition. This feature is also described by our theoretical curves, but the spin-wave approach used in our work was not able to reproduce the shoulder in the attenuation rate for the c_{22}-mode, the exact shape near the critical field, nor the double peak structure[5] that is detected experimentally below a temperature of 0.3 K. Considering our result in Eq. (4.142) for the dominant contribution we may approximate the attenuation rate in the vicinity of the critical field by

$$\gamma_{\boldsymbol{k}\lambda} \approx \frac{\pi^2}{64}\left(\frac{\boldsymbol{k}^2}{2M}\right)\left(\frac{S^2 c_\lambda^2 \boldsymbol{k}^2}{V_{\mathrm{BZ}} v_x v_y}\right)\frac{\left[\boldsymbol{f}_1^{X\beta}(\hat{\boldsymbol{k}})\cdot \boldsymbol{e}_{\boldsymbol{k}\lambda}\right]^2}{(1-h/h_c)^2}\,, \tag{4.157}$$

where we have used that $\sin\theta \approx 1$ and $\cos\theta \approx [2(1-h/h_c)]^{1/2}$ for h close to h_c and only considered the terms to leading order in $r_{\boldsymbol{k}\lambda} = v(\hat{\boldsymbol{k}})/c_\lambda \ll 1$. The total attenuation rate is dominated by the factor $1/(1-h/h_c)^2$ in Eq. (4.157)

[5] B. Wolf, private communication.

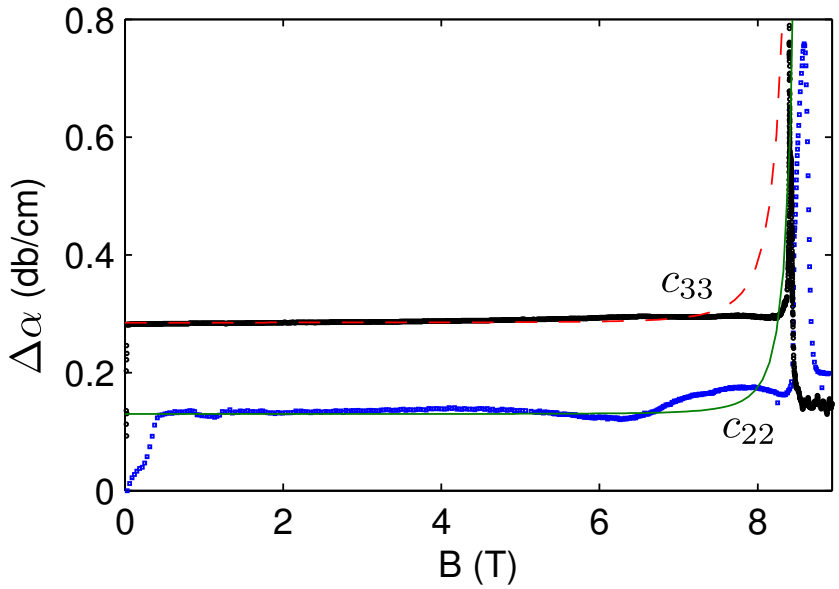

Figure 4.10: *The dots are experimental results from Ref. [P8] for the relative ultrasonic attenuation rates $\Delta\alpha$ of the longitudinal c_{22} (blue squares) and c_{33} (black circles) phonon modes in in Cs_2CuCl_4 at low temperatures ($T = 52$ mK for the c_{22}-mode and $T = 48$ mK for the c_{33}-mode). The solid green line is our theoretical result given in Eqs. (4.142) and (4.143) for the c_{22}-mode, while the red dashed line is the result for the c_{33}-mode. The attenuation rates have been calculated using the same values $|\kappa| = 15$ and $|\kappa'| = 51$ for the fit parameters as in Figs. 4.8 and 4.9. Note that a constant offset appears since it is only possible to measure the relative attenuation rate. Note that for very small fields the data approaches $\Delta\alpha = 0$; at this point we cannot comment on the reason that leads to the change of the attenuation rates at small fields.*

and qualitatively matches the strong enhancement of the attenuation rate in the vicinity of the critical field. In this regime higher order fluctuations which we neglected in our spin-wave expansion are supposed to become important. Thus, a quantitative calculation for this regime should take these spin-wave interactions into account.

4.8 Summary and conclusions

In this chapter a spin-wave approach was set up to calculate the magnetic field dependence of the elastic constants and the ultrasonic attenuation rate in an ordered helimagnet. The compound Cs_2CuCl_4 is a realization of such a frustrated antiferromagnet on the triangular lattice. Our results can therefore be compared to experimental data at low temperatures where the so-called cone state is stable. In our calculation we used the $1/S$ expansion in combination with an expansion of the exchange couplings in powers of

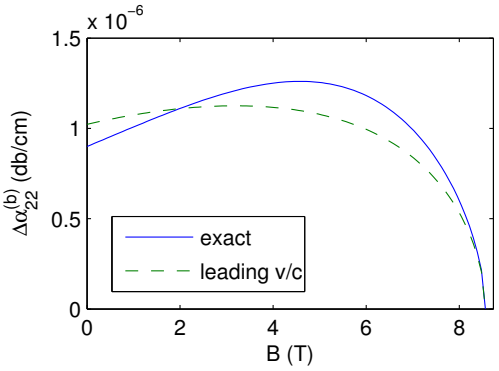

Figure 4.11: *Comparison of the contribution Eq. (4.146) to the phonon damping $\gamma_{\boldsymbol{k}}^{(b)}$ calculated with the analytical formula Eq. (4.151) that is only leading order in $r_{\boldsymbol{k}\lambda}$, and a numerical solution of the integral using a triangular method [100]. This contribution $\Delta\alpha_{22}^{(b)}$ to the total ultrasonic attenuation rate $\Delta\alpha_{22}$ of the c_{22}-mode shown in Fig. 4.10 is small.*

phonon operators to derive a model of coupled magnons and phonons. In the next step we applied perturbative many-body techniques to calculate the renormalization of the lattice vibrations in presence of magnons. Using a simple phenomenological parametrization of the spatial variations of the exchange couplings we have introduced two adjustable parameters to fit our theoretical results to experimental data of the magnetic field dependence of the sound velocity for the longitudinal c_{22} phonon mode. Especially at small fields $B \lesssim 2.5$ Tesla the observed behavior could be described quite accurately, see Fig. 4.9.

Once the parameters were fixed we also compared our result for the sound velocity of the c_{33}-mode and found a good agreement in the weak field regime. Our theoretical result for the ultrasonic attenuation rate finally reproduced the strong enhancement close to the critical field, although our spin-wave approach is believed to break down close to the quantum critical point. In our calculation we found that the phonon damping is proportional to $\boldsymbol{k}^4$ such that the spin-phonon coupling does not destroy the properties of the acoustic phonons at long wavelengths. For our frustrated magnet including Dzyaloshinsky-Moriya anisotropy in conjunction with a finite magnetic field it was necessary to take the magnon-phonon hybridization into account. The interactions between spin waves then renormalize the one-phonon two-magnon interactions such that the phonons are still valid quasiparticles.

The predicted $\boldsymbol{k}^4$-dependence of the attenuation rate on the phonon momentum has not been observed experimentally so far[6]. A possible reason is that the contribution to the phonon damping from the spin-phonon coupling

[6]P. T. Cong, private communication.

is small compared to the background which luckily does not depend on the magnetic field[7]. A detailed investigation in the vicinity of the critical field does not help to clarify this point, because it is questionable whether our calculation is still valid in this regime.

The whole theoretical investigation presented here is restricted to the cone state of Cs_2CuCl_4, because our spin-wave approach is only well justified in the magnetically ordered phase. From an experimental point of view an investigation on this cone state is most challenging, because very low temperatures are needed. Detailed experimental studies in the vicinity of the quantum critical point and in other phases of Cs_2CuCl_4 such as the spin-liquid phase or the ferromagnetic phase have been carried out, while the theoretical counterpart is left for future work. Strongly fluctuating magnons in frustrated magnets can have anomalous properties for example strong damping [28, 29] due to interactions. Therefore it is an interesting task to examine the interactions between spin waves in the cone state especially in the vicinity of the quantum critical point where also features from a Bose-Einstein condensation of magnons have been reported [142, 160–163, 178, 204, 210]. Whether a resummation of the $1/S$ expansion also retaining interaction processes could improve the agreement with experiments is still an open question. In general, spin-wave calculations including interaction effects show that the corrections from the $1/S$ expansion are large for frustrated magnets [129, 130]. Also field theoretical approaches for quantum helimagnets suffer from divergencies of quantum corrections [143]. A modified spin-wave theory with ordering-vector optimization [88, 89] could help to gain new insights on the renormalized magnons. From the experimental side, investigations on the mixed systems $Cs_2CuCl_{4-x}Br_x$ are currently running [41, 118]. The goal is to observe the possible crossover from the frustrated antiferromagnet to a magnet with plateaux in the magnetization curve [154].

[7] B. Wolf, private communication.

Appendix A

QAFM in a magnetic field

A.1 Experimental methods on quantum magnets

At this point we will give a short overview of experimental techniques and the accessible physical observables. One milestone of experimental investigations on quantum magnetism is the realization of the electron parametric resonance (EPR) [230]. Similar to the ferromagnetic resonance (FMR) technique [80] one can determine the spin and orbital contributions to magnetic properties and determine effective g-factors of the spins in condensed matter systems. The nuclear magnetic resonance (NMR) method was developed later on [17, 159] and measures the energy splitting of the nuclear spins in the internal field of magnetic materials.

On the other hand, measurements of the magnetic susceptibility as a response quantity to magnetic fields allow a distinction between classes of materials (ferromagnets, antiferromagnets, etc.) and fixes the relevant energy scales of the system. Conclusions about the microscopic model alone from the magnetic susceptibility are risky, but magnetic phase transitions can barely be extracted from susceptibility data.

Neutron scattering is the most powerful method to characterize magnetic materials because it is directly sensitive to the magnetic moments. The central quantity deduced in the experiments is the dynamical structure factor which includes all information about the magnetic ordering and the magnetic excitations. Energies of quasiparticles and their lifetime can be read off from the structure factor. In combination with the variation of external parameters as temperature and magnetic field one can explore the magnetic phase diagram and even deduce the microscopic model [37]. For more details on this experimental technique, the reader is referred to the pioneering works [16, 183] and standard textbooks [B36, B47, B7].

The investigation of the specific heat is a more indirect tool, which can reveal fingerprints of magnetic excitations or help to deduce the phase diagram. Moreover it is rather difficult to clarify the physical origin of the signatures because different types of excitations, for example magnons and spinons, can give rise to the same contributions to the specific heat. Large anomalies will however be a clear signature of magnetic phase transitions. Also investigations on thermal expansion with a magnetic field as an external control parameter and supersonic experiments [128, 223] can give important insights into quantum magnetism. They are considered as standard techniques to explore the magnetic phase diagram. The supersonic technique measures the phonon velocity and its damping with high accuracy. Details have been explained in Chapter 4 where also spin-phonon interactions are discussed. Finally, we mention Refs. [42, 122, 138, 207, 224] that describe possible compounds where the two-dimensional QAFM is realized and the energy scales of the coupling constants also allow investigations under constant magnetic fields comparable to the critical field h_c.

A.2 Quartic spin-wave interaction in Hermitian parametrization

For completeness the quartic part of the Hamiltonian $\hat{H}_4'$ for a QAFM in a uniform magnetic field defined in Eqs. (2.62, 2.63) in the Hermitian field parameterization is cited below. In order to account for the symmetrization of non-commuting operators we have used the symmetrized product

$$\left\{\hat{P}_1\hat{P}_2\hat{X}_3\hat{X}_4\right\} = \frac{1}{2}\left[\hat{P}_1\hat{P}_2, \hat{X}_3\hat{X}_4\right]_+ + \frac{1}{4}\left(\delta_{1+3,0}\delta_{2+4,0} + \delta_{1+4,0}\delta_{2+3,0}\right) , \qquad \text{(A.1)}$$

where the symmetrization symbol $\{\ldots\}$ is defined in Eq. (1.82). With these conventions this part of the Hamiltonian reads

$$\begin{aligned}
\hat{H}_4' = \frac{2}{N} \sum_{\boldsymbol{k}_1\boldsymbol{k}_2\boldsymbol{k}_3\boldsymbol{k}_4} \delta_{\boldsymbol{k}_1+\boldsymbol{k}_2+\boldsymbol{k}_3+\boldsymbol{k}_4,0} \\
\times \Bigg[\frac{1}{4!} \Big(\Gamma^{PPPP}_{++++}(\boldsymbol{k}_1,\boldsymbol{k}_2,\boldsymbol{k}_3,\boldsymbol{k}_4) \hat{P}_{\boldsymbol{k}_1+} \hat{P}_{\boldsymbol{k}_2+} \hat{P}_{\boldsymbol{k}_3+} \hat{P}_{\boldsymbol{k}_4+} \\
+ \Gamma^{PPPP}_{----}(\boldsymbol{k}_1,\boldsymbol{k}_2,\boldsymbol{k}_3,\boldsymbol{k}_4) \hat{P}_{\boldsymbol{k}_1-} \hat{P}_{\boldsymbol{k}_2-} \hat{P}_{\boldsymbol{k}_3-} \hat{P}_{\boldsymbol{k}_4-} \Big) \\
+ \frac{1}{4!} \Big(\Gamma^{XXXX}_{----}(\boldsymbol{k}_1,\boldsymbol{k}_2,\boldsymbol{k}_3,\boldsymbol{k}_4) \hat{X}_{\boldsymbol{k}_1-} \hat{X}_{\boldsymbol{k}_2-} \hat{X}_{\boldsymbol{k}_3-} \hat{X}_{\boldsymbol{k}_4-} \\
+ \Gamma^{XXXX}_{++++}(\boldsymbol{k}_1,\boldsymbol{k}_2,\boldsymbol{k}_3,\boldsymbol{k}_4) \hat{X}_{\boldsymbol{k}_1+} \hat{X}_{\boldsymbol{k}_2+} \hat{X}_{\boldsymbol{k}_3+} \hat{X}_{\boldsymbol{k}_4+} \Big) \\
+ \frac{1}{(2!)^2} \Big(\Gamma^{PPPP}_{++--}(\boldsymbol{k}_1,\boldsymbol{k}_2;\boldsymbol{k}_3,\boldsymbol{k}_4) \hat{P}_{\boldsymbol{k}_1+} \hat{P}_{\boldsymbol{k}_2+} \hat{P}_{\boldsymbol{k}_3-} \hat{P}_{\boldsymbol{k}_4-} \\
+ \Gamma^{XXXX}_{--++}(\boldsymbol{k}_1,\boldsymbol{k}_2;\boldsymbol{k}_3,\boldsymbol{k}_4) \hat{X}_{\boldsymbol{k}_1-} \hat{X}_{\boldsymbol{k}_2-} \hat{X}_{\boldsymbol{k}_3+} \hat{X}_{\boldsymbol{k}_4+} \Big) \\
+ \frac{1}{(2!)^2} \Big(\Gamma^{PPXX}_{++--}(\boldsymbol{k}_1,\boldsymbol{k}_2;\boldsymbol{k}_3,\boldsymbol{k}_4) \hat{P}_{\boldsymbol{k}_1+} \hat{P}_{\boldsymbol{k}_2+} \hat{X}_{\boldsymbol{k}_3-} \hat{X}_{\boldsymbol{k}_4-} \\
+ \Gamma^{PPXX}_{--++}(\boldsymbol{k}_1,\boldsymbol{k}_2;\boldsymbol{k}_3,\boldsymbol{k}_4) \hat{P}_{\boldsymbol{k}_1-} \hat{P}_{\boldsymbol{k}_2-} \hat{X}_{\boldsymbol{k}_3+} \hat{X}_{\boldsymbol{k}_4+} \Big) \\
+ \frac{1}{(2!)^2} \Big(\Gamma^{PPXX}_{++++}(\boldsymbol{k}_1,\boldsymbol{k}_2;\boldsymbol{k}_3,\boldsymbol{k}_4) \big\{ \hat{P}_{\boldsymbol{k}_1+} \hat{P}_{\boldsymbol{k}_2+} \hat{X}_{\boldsymbol{k}_3+} \hat{X}_{\boldsymbol{k}_4+} \big\} \\
+ \Gamma^{PPXX}_{----}(\boldsymbol{k}_1,\boldsymbol{k}_2;\boldsymbol{k}_3,\boldsymbol{k}_4) \big\{ \hat{P}_{\boldsymbol{k}_1-} \hat{P}_{\boldsymbol{k}_2-} \hat{X}_{\boldsymbol{k}_3-} \hat{X}_{\boldsymbol{k}_4-} \big\} \Big) \\
+ \Gamma^{PXPX}_{++--}(\boldsymbol{k}_1;\boldsymbol{k}_2;\boldsymbol{k}_3;\boldsymbol{k}_4) \big\{ \hat{P}_{\boldsymbol{k}_1+} \hat{X}_{\boldsymbol{k}_2+} \big\} \big\{ \hat{P}_{\boldsymbol{k}_3-} \hat{X}_{\boldsymbol{k}_4-} \big\} \Bigg] . \qquad \text{(A.2)}
\end{aligned}$$

For convenience we now introduce the shorthand notation $\gamma_{\boldsymbol{k}_1} \equiv \gamma_{\mathbf{1}}$, $\gamma_{\boldsymbol{k}_2} \equiv \gamma_{\mathbf{2}}$ (and similarly for the other labels) and symmetrize the vertices whenever the interaction is symmetric with respect to the exchange of the field labels. For the vertices involving four fields of the same type we obtain

$$\begin{aligned}
\Gamma^{XXXX}_{----}(\boldsymbol{k}_1,\boldsymbol{k}_2,\boldsymbol{k}_3,\boldsymbol{k}_4) = \frac{h_c}{16S} \Big[\gamma_{\mathbf{1}} + \gamma_{\mathbf{2}} + \gamma_{\mathbf{3}} + \gamma_{\mathbf{4}} - 2\alpha(\gamma_{\mathbf{1+2}} + \gamma_{\mathbf{3+4}}) \\
+ (\mathbf{2} \leftrightarrow \mathbf{3}) + (\mathbf{2} \leftrightarrow \mathbf{4}) \Big] , \qquad \text{(A.3a)} \\
\Gamma^{XXXX}_{++++}(\boldsymbol{k}_1,\boldsymbol{k}_2,\boldsymbol{k}_3,\boldsymbol{k}_4) = \frac{h_c}{16S} \Big[\alpha(\gamma_{\mathbf{1}} + \gamma_{\mathbf{2}} + \gamma_{\mathbf{3}} + \gamma_{\mathbf{4}}) - 2\alpha(\gamma_{\mathbf{1+2}} + \gamma_{\mathbf{3+4}}) \\
+ (\mathbf{2} \leftrightarrow \mathbf{3}) + (\mathbf{2} \leftrightarrow \mathbf{4}) \Big] , \qquad \text{(A.3b)} \\
\Gamma^{PPPP}_{++++}(\boldsymbol{k}_1,\boldsymbol{k}_2;\boldsymbol{k}_3,\boldsymbol{k}_4) = \frac{h_c}{16S} \Big[-\gamma_{\mathbf{1}} - \gamma_{\mathbf{2}} - \gamma_{\mathbf{3}} - \gamma_{\mathbf{4}} - 2\alpha(\gamma_{\mathbf{1+2}} + \gamma_{\mathbf{3+4}}) \\
+ (\mathbf{2} \leftrightarrow \mathbf{3}) + (\mathbf{2} \leftrightarrow \mathbf{4}) \Big] , \qquad \text{(A.3c)}
\end{aligned}$$

$$\Gamma^{PPPP}_{----}(\boldsymbol{k}_1,\boldsymbol{k}_2,\boldsymbol{k}_3,\boldsymbol{k}_4) = \frac{h_c}{16S}\Big[-\alpha(\gamma_{\mathbf{1}}+\gamma_{\mathbf{2}}+\gamma_{\mathbf{3}}+\gamma_{\mathbf{4}}) - 2\alpha(\gamma_{\mathbf{1+2}}+\gamma_{\mathbf{3+4}}) + (\mathbf{2}\leftrightarrow\mathbf{3}) + (\mathbf{2}\leftrightarrow\mathbf{4})\Big]\,. \tag{A.3d}$$

The vertices involving two pairs of fields of the same type can be written as

$$\Gamma^{XXXX}_{--++}(\boldsymbol{k}_1,\boldsymbol{k}_2;\boldsymbol{k}_3,\boldsymbol{k}_4) = \frac{h_c}{16S}\Big[\gamma_{\mathbf{1}}+\gamma_{\mathbf{2}}+\alpha(\gamma_{\mathbf{3}}+\gamma_{\mathbf{4}}) - 2\alpha(\gamma_{\mathbf{1+2}}+\gamma_{\mathbf{3+4}})\Big]\,, \tag{A.3e}$$

$$\Gamma^{PPPP}_{++--}(\boldsymbol{k}_1,\boldsymbol{k}_2;\boldsymbol{k}_3,\boldsymbol{k}_4) = \frac{h_c}{16S}\Big[-\gamma_{\mathbf{1}}-\gamma_{\mathbf{2}}-\alpha(\gamma_{\mathbf{3}}+\gamma_{\mathbf{4}}) - 2\alpha(\gamma_{\mathbf{1+2}}+\gamma_{\mathbf{3+4}})\Big]\,, \tag{A.3f}$$

$$\Gamma^{PPXX}_{++--}(\boldsymbol{k}_1,\boldsymbol{k}_2;\boldsymbol{k}_3,\boldsymbol{k}_4) = \frac{h_c}{16S}\Big[3(-\gamma_{\mathbf{1}}-\gamma_{\mathbf{2}}+\gamma_{\mathbf{3}}+\gamma_{\mathbf{4}}) - 2\alpha\left(\gamma_{\mathbf{1+2}}+\gamma_{\mathbf{3+4}}-\gamma_{\mathbf{1+3}}-\gamma_{\mathbf{2+4}}-\gamma_{\mathbf{2+3}}-\gamma_{\mathbf{1+4}}\right)\Big]\,, \tag{A.3g}$$

$$\Gamma^{PPXX}_{--++}(\boldsymbol{k}_1,\boldsymbol{k}_2;\boldsymbol{k}_3,\boldsymbol{k}_4) = \frac{h_c}{16S}\Big[3\alpha(-\gamma_{\mathbf{1}}-\gamma_{\mathbf{2}}+\gamma_{\mathbf{3}}+\gamma_{\mathbf{4}}) - 2\alpha\left(\gamma_{\mathbf{1+2}}+\gamma_{\mathbf{3+4}}-\gamma_{\mathbf{1+3}}-\gamma_{\mathbf{2+4}}-\gamma_{\mathbf{2+3}}-\gamma_{\mathbf{1+4}}\right)\Big]\,, \tag{A.3h}$$

$$\Gamma^{PPXX}_{++++}(\boldsymbol{k}_1,\boldsymbol{k}_2;\boldsymbol{k}_3,\boldsymbol{k}_4) = \frac{h_c}{16S}\Big[-\gamma_{\mathbf{1}}-\gamma_{\mathbf{2}}+\alpha(\gamma_{\mathbf{3}}+\gamma_{\mathbf{4}}) - 2\alpha(\gamma_{\mathbf{1+2}}+\gamma_{\mathbf{3+4}})\Big]\,, \tag{A.3i}$$

$$\Gamma^{PPXX}_{----}(\boldsymbol{k}_1,\boldsymbol{k}_2;\boldsymbol{k}_3,\boldsymbol{k}_4) = \frac{h_c}{16S}\Big[-\alpha(\gamma_{\mathbf{1}}+\gamma_{\mathbf{2}})+\gamma_{\mathbf{3}}+\gamma_{\mathbf{4}} - 2\alpha(\gamma_{\mathbf{1+2}}+\gamma_{\mathbf{3+4}})\Big]\,. \tag{A.3j}$$

And finally, to complete the eleven vertices appearing in interacting spin-wave theory, there is one vertex without permutation symmetry connecting four different field types[1],

$$\Gamma^{PXPX}_{++--}(\boldsymbol{k}_1;\boldsymbol{k}_2;\boldsymbol{k}_3;\boldsymbol{k}_4) = \frac{h_c}{16S}\Big[\gamma_{\mathbf{1}}+\alpha(-\gamma_{\mathbf{2}}+\gamma_{\mathbf{3}})-\gamma_{\mathbf{4}} - 2\alpha(\gamma_{\mathbf{1+4}}+\gamma_{\mathbf{2+3}})\Big]\,. \tag{A.3k}$$

Note that the above expressions contain quantities defined in chapter 2, for example Eq. (2.6a). Let us finally stress that the vertices are analytic functions of the external momenta and analytic functions of the square h^2 of the magnetic field. On the other hand, if we express $\hat{H}'_4$ in terms of the usual magnon creation and annihilation operators, we obtain vertices which are singular for certain combinations of external momenta [85, 87, 114].

[1]There is a mistake in Eq. (13e) of Ref. [86]: The term $\gamma_{\mathbf{1}}-\gamma_{\mathbf{2}}-\gamma_{\mathbf{3}}+\gamma_{\mathbf{4}}$ should be multiplied by a factor of 2. Taking into account the different labeling of the fields in that work as compared with the labeling in Eq. (A.2) [so that we should rename $\mathbf{3}\leftrightarrow\mathbf{4}$], in the limit of vanishing magnetic field the vertices in Eqs. (A.3a–A.3k) are then equivalent to the vertices given in Ref. [86].

Appendix B

Microscopic spin-wave theory for yttrium-iron garnet films

B.1 Material properties of YIG

In order to motivate the microscopic model Eq. (3.2), used in Chapter 3, it is necessary to examine the material properties of the compound YIG with stoichiometric formula $Y_3Fe_2(FeO_4)_3$. Crystals of YIG and related materials were fabricated more than 50 years ago [75, B37]. It turned out that this compound forms crystals of the cubic space group $Ia3d$ where the primitive elementary

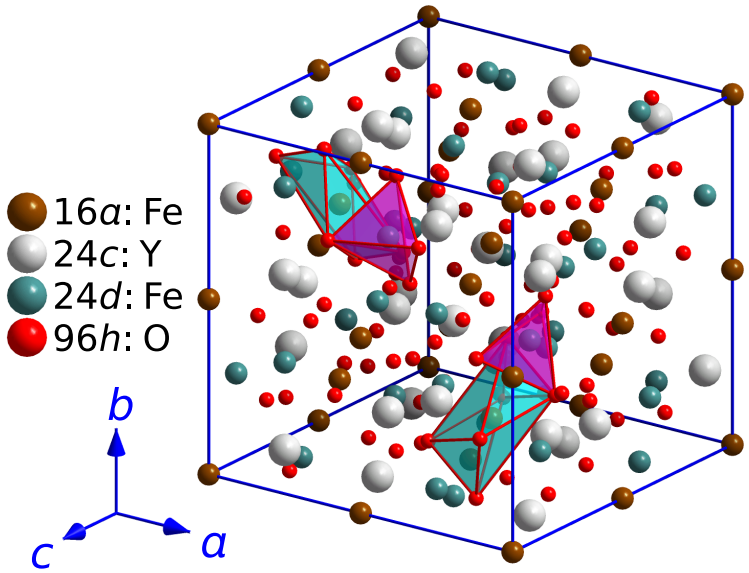

Figure B.1: *Elementary cell of YIG with 160 atoms. The spins of the 16 iron atoms at the a positions are coupled antiferromagnetically to the spins of the 24 iron atoms at the d positions and cause the ferrimagnetic ordering, taken from [P4]*

.

cell contains 160 atoms [26, 75, B46]. Concerning the magnetic properties of this insulating material one has to rely on experimental investigations because first principle investigations are quite challenging [226], and cannot explain the magnetic properties at low energies. Observing the ions in the elementary cell, it is evident that the magnetic moments are carried by the Fe ions which occupy the 16 octahedral sites a and the 24 tetrahedral sites d, compare Fig. B.1. Thermodynamic and microwave measurements as well as neutron scattering data have determined the 20 magnon bands of YIG [26, 157]. It turned out that YIG is a ferrimagnet at experimentally accessible static magnetic fields below the temperature $T \approx 560$ K of the phase transition to the paramagnetic phase [52, B43]. Since the ferromagnetic and the antiferromagnetic magnon bands are well separated in energy at the center of the Brillouin zone, our assumption of chapter 3 to only consider the lowest (ferromagnetic) band is justified.

B.2 Wave-vector resolved Brillouin light scattering spectroscopy

Since the second part of this thesis, chapter 3, was mainly motivated by experimental investigations on thin-film magnets, we will briefly describe an experimental setup that was build up recently [170, P6]. The basic idea is to use the magneto-optical coupling to observe spin waves using Brillouin light scattering spectroscopy (BLS). In the experiment a probing light beam, usually a laser beam of fixed momentum k_0, is shone onto a thin-film sample while the reflected light is analyzed in a tandem Fabry-Pérot interferometer. The desired information is contained in the inelastically scattered fraction of the light: From the diffraction on the grating of the spin waves, the frequency of the light and its momentum is changed. The first is extracted in the interferometer and corresponds to the energy of the spin waves under observation, while the momentum $\boldsymbol{k}_{\mathrm{SW}}$ of the spin waves is determined by the geometry. Wave vectors which are oriented parallel to the external magnetic field are analyzed by turning the entire setup. This is an improvement to the setup where the wave numbers are selected utilizing a diaphragm [225]. Using metalized samples, it is possible to use the same optical assembly for the incoming and the scattered light. For a fixed source of laser light, the angle of incidence Θ_B is varied by turning the sample together with the magnet that provides the external magnetic field in the range of 1300 to 2100 Oe. In the setup described in Ref. [P6] spin waves with wave vectors up to $|\boldsymbol{k}_{\mathrm{SW}}| \approx 2 \cdot 10^5 \mathrm{cm}^{-1}$ with all orientations in the plane of the film are accessible. The momentum resolution is then given by the resolution of the determination of the angle Θ_B via

$$\Delta k = 2k_0 \cos(\Theta_B)\, \Delta\Theta_B \,, \tag{B.1}$$

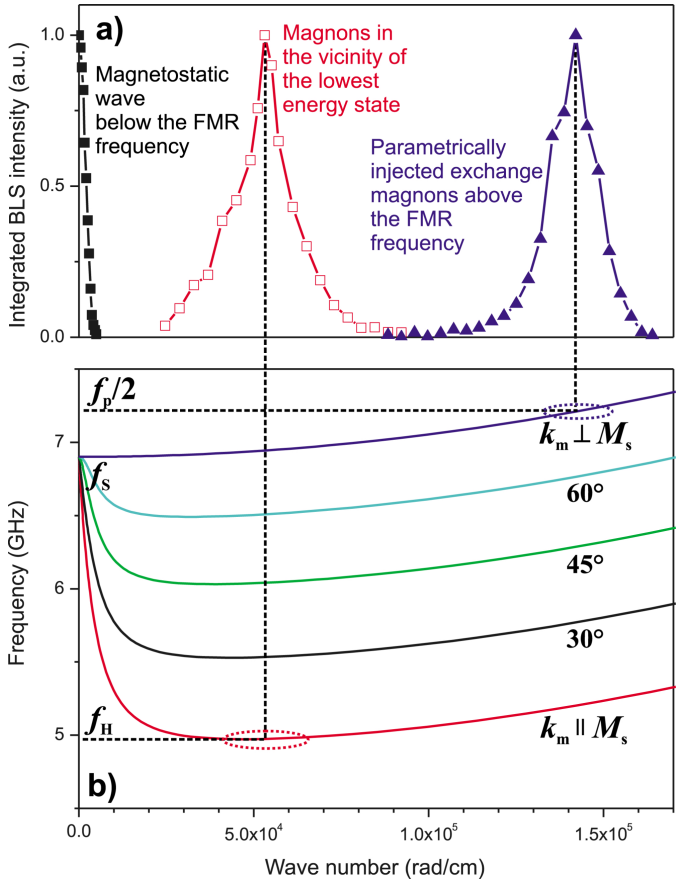

Figure B.2: *(a) Result of the measurements using the BLS technique in YIG films of different spectral areas: Magnetostatic waves below the FMR, directly injected exchange magnons at* $(f_\mathrm{p}/2, k_\perp) = (7.2\ \mathrm{GHz},\ 1.42 \cdot 10^5\ \mathrm{rad/cm})$*, and magnons accumulated in the vicinity of the lowest energy state* $(f_H, k_\parallel) = (5\ \mathrm{GHz},\ 5.2 \cdot 10^4\ \mathrm{rad/cm})$*. (b) Spin-wave dispersion relation and spectral positions of the excited magnons. The calculated spectral positions of both magnon groups using our numerical approach from chapter 3 agree with the measured positions. Additionally, the calculated dispersion branches for an angle of* 30°, 45°, 60° *between the wave vector of the spin waves and the magnetization are shown, taken from [P6].*

where $\Delta\Theta_B$ is the error of the angle Θ_B. Thus, the minimal resolution is realized in the vicinity of $\boldsymbol{k}_\mathrm{SW} \approx 0$ for spin waves near the ferromagnetic resonance Eq. (3.24). On the other hand, the energy resolution is determined by the corresponding resolution of the interferometer, which is estimated by the error of a fit to the maxima of the intensity, see Fig. B.2. The two advantages of this setup are the wide range of observable wave vectors and the two-dimensional momentum sensitivity.

Appendix C

Deutsche Zusammenfassung

Die vorliegende Arbeit beschäftigt sich mit der theoretischen Untersuchung von Modellsystemen, die zu Beschreibung von magnetischen Materialien geeignet sind. Magnetismus als solcher ist einerseits ein Phänomen, das wir durchaus aus dem heutigen Lebensalltag kennen. Das Phänomen ist aber andererseits theoretisch nur mit Hilfe der Quantentheorie erklärbar. Ohne hier auf die Ansätze dieser Erklärungen einzugehen, nehmen wir in dieser Arbeit an, dass die Spinzustände der Elektronen in den betrachteten Festkörpern energetisch derart aufgespalten sind, dass diese durch ein effektives Modell, das sogenannte *Heisenberg-Modell*, beschrieben werden können. Der entsprechende Hamilton-Operator als mathematische Formulierung des Modells lautet

$$\hat{H} = \sum_{ij} J_{ij} \boldsymbol{S}_i \cdot \boldsymbol{S}_j \ , \tag{C.1}$$

wobei $\boldsymbol{S}_i$ und $\boldsymbol{S}_j$ Spinoperatoren an den Gitterpunkten i und j sind, die lokalisierte magnetische Momente beschreiben. J_{ij} ist die dem Skalarprodukt zugeordnete Energie, die sogenannte Austauschkopplung.

Das Heisenberg-Modell weist die sogenannte $SU(2)$-Spinsymmetrie auf und wurde seit der Aufstellung des Modells durch Heisenberg [93] bereits intensiv untersucht. Als herausragende Methode sei an dieser Stelle der Bethe-Ansatz [B8] für eindimensionale Quanten-Antiferromagnete (QAFM) zu nennen, für die insbesondere keine langreichweitige Ordnung besteht. In diesem Zusammenhang ist auch das Mermin-Wagner Theorem wichtig, welches voraussagt, dass es in Heisenberg-Magneten in zwei oder weniger Dimensionen mit endlicher Reichweite der Spin-Wechselwirkungen bei endlichen Temperaturen keine Magnetisierung gibt [141]. Existiert dagegen eine endliche Magnetisierung, so kann man mit der Spinwellentheorie die Energiedispersion der elementaren Quantenanregungen (Spinwellen) berechnen und thermodynamische Größen wie zum Beispiel die Magnetisierung bestimmen [B21]. Diese Methode wird auch im Folgenden benutzt, um geordnete Heisenberg Magnete zu untersuchen. Da ebenfalls zweidimensionale Systeme untersucht werden, muss man sich in der gewöhnlichen Formulierung entweder auf den

Fall des absoluten Temperaturnullpunktes beschränken, oder eine geordnete Phase durch zusätzliche Energiebeiträge im Hamilton-Operator begründen. In den drei in der Arbeit diskutierten Anwendungen der Spinwellentheorie auf Modellsysteme handelt es sich um Systeme, deren Symmetrie durch ein externes Magnetfeld, sowie zusätzlicher Terme niedriger Symmetrie, reduziert sind.

Dazu wird zunächst im ersten Kapitel eine Einführung in die verwendeten Methoden dargestellt: Die mathematischen Grundlagen der *Spinwellentheorie* als Entwicklung des Heisenberg-Hamilton-Operators in Quantenfluktuationen um den klassischen Grundzustand mittels der Holstein-Primakoff Transformation [96] werden in den drei verschiedenen Anwendungen verwendet. Wir bilden dabei den Hamilton-Operator, der ursprünglich mit den Spinoperatoren formuliert ist, auf ein Modellsystem (wechselwirkender) Bosonen ab. Mathematisch handelt es sich um eine Entwicklung in inversen Potenzen des Gesamtspins S, die im Grenzfall $S \to \infty$ exakt wird. Üblicherweise lässt man die höheren Terme auch für endliche S weg. In der vorliegenden Arbeit betrachten wir nur die führenden Korrekturterme in $1/S$ in der Annahme, dass der Gesamtspin groß ist. Die Spinwellentheorie liefert insbesondere eine Theorie freier Bosonen, wenn man nur die führenden quadratischen Korrekturen berücksichtigt (lineare Spinwellentheorie). Die Terme in höherer Ordnung in $1/S$ sind dann Wechselwirkungen zwischen diesen Bosonen. Die Frage, ob diese als schwach betrachtet werden können, hängt vom Modellsystem ab. Im QAFM sind die Wechselwirkungen für bestimmte Konstellationen stark, so dass Quantenkorrekturen, die im Kapitel 2 betrachtet werden, einen großen Einfluss haben. In der Praxis handelt es sich häufig um Spinsysteme mit $S = 1/2$, so dass die Entwicklung eigentlich schlecht sein sollte, aber dennoch gute Ergebnisse liefert. Im Hinblick auf Beiträge zum Hamilton-Operator, die die Symmetrie des Systems reduzieren, sei auf die *Dzyaloshinsky-Moriya Anisotropie* [56, 144],

$$\hat{H}_{\mathrm{DM}} = \sum_{ij} \boldsymbol{D}_{ij} \cdot (\boldsymbol{S}_i \times \boldsymbol{S}_j) \ , \tag{C.2}$$

hingewiesen, die in Materialien mit fehlender Inversionssymmetrie der Elementarzelle auftreten kann. Im Kapitel 3 werden Rechnungen für einen Quantenmagneten mit großem effektiven Spin $S \approx 14.3$ durchgeführt, bei dem darüber hinaus noch die klassische *Dipol-Dipol Wechselwirkung*,

$$\hat{H}_{\mathrm{dd}} = -\frac{1}{2} \sum_{ij, i \neq j} \frac{\mu^2}{|\boldsymbol{R}_{ij}|^3} \left[3(\boldsymbol{S}_i \cdot \hat{\boldsymbol{R}}_{ij})(\boldsymbol{S}_j \cdot \hat{\boldsymbol{R}}_{ij}) - \boldsymbol{S}_i \cdot \boldsymbol{S}_j \right] \ , \tag{C.3}$$

eine entscheidende Rolle spielt. Dieser Zusatzterm bricht die Spin-Rotationssymmetrie des Hamilton-Operators explizit, so dass wir einerseits eine Stabilisierung der Magnetisierung erhalten und andererseits keine sogenannte Goldstone-Mode ohne Anregungslücke mehr vorfinden.

Weitere Techniken, die kurz im einleitenden Kapitel besprochen werden, sind die benutzten Transformationen, um die Freiheitsgrade der magnetischen Anregungen adäquat darzustellen und die physikalisch interessanten Wechselwirkungen zu vereinfachen: Neben der Bogoliubov Transformation, die den Hamilton-Operator in linearer Spinwellentheorie diagonalisiert, wird insbesondere die *hermitesche Parametrisierung* eine wichtige Rolle bei der Identifikation relevanter Freiheitsgrade spielen. Weiterhin behandelt das einleitende Kapitel noch die Formulierung der Vielteilchentheorie mittels feldtheoretischer Methoden und die störungstheoretische Berechnung von Wechselwirkungskorrekturen über die sogenannte Selbstenergie, die auch eine grafische Veranschaulichung über Feynman Diagramme hat [B22].

Was die Anwendung der Ergebnisse angeht, haben wir keine spezielle technologische Verwendung der Resultate im Blick. Jedoch ist unbestreitbar, dass magnetische Werkstoffe in der Vergangenheit wichtige Entwicklungen erst ermöglichten, z.B. im Bereich Elektrotechnik. Für die Datenspeicherung ist derzeit die Verwendung magnetischer Materialien sowie damit verbundene physikalische Effekte zum Beschreiben und Auslesen nicht mehr wegzudenken. Die im dritten Kapitel behandelten dünnen ferromagnetischen Filme wurden vor kurzem für Anwendungen in der Spintronik vorgeschlagen [102]. Ein Verständnis der Grundlagen mittels vereinfachter Modellsysteme wie in dieser Arbeit ausgeführt, kann später sicherlich zu technologischen Weiterentwicklungen führen.

C.1 Quanten-Antiferromagnet in einem Magnetfeld

Als erstes Modellsystem betrachten wir einen Heisenberg Antiferromagneten in zwei oder drei Dimensionen mit nächster Nachbar Wechselwirkung im externen Magnetfeld, dessen Hamilton-Operator durch

$$\hat{H} = \frac{1}{2}\sum_{ij} J_{ij}\boldsymbol{S}_i \cdot \boldsymbol{S}_j - \boldsymbol{h}\cdot\sum_i \boldsymbol{S}_i \tag{C.4}$$

gegeben ist. Hierbei sind $J_{ij} = J > 0$ die Austauschkopplungen und $\boldsymbol{h} = h\boldsymbol{e}_z$ das Magnetfeld in Einheiten der Energie. Dieses Modellsystem wurde schon eingehend analysiert; hier sind Arbeiten unter Verwendung der Spinwellentheorie mit konventioneller Parametrisierung [137, 233] und unter Verwendung der effektiven Theorie im *nichtlinearen Sigma-Modell* (NLSM) besonders herauszustellen [25]. Beide Methoden lieferten experimentell überprüfbare Ergebnisse zum Anregungsspektrum und zu den Eigenschaften möglicher Phasen, haben jedoch auch konzeptionelle Nachteile: Die Spinwellentheorie liefert im Falle des QAFM ein Modellsystem wechselwirkender Bosonen, die

antiferromagnetischen Magnonen. Die entsprechenden Wechselwirkungsvertizes divergieren aber für bestimmte Kombinationen externer Impulse, sodass eine störungstheoretische Analyse diese divergenten Terme korrekt kombinieren muss, um aussagekräftige Ergebnisse zu erhalten [86]. Aufgrund der Symmetrie des Heisenberg-Modells ist der Gesamtspin in jedem Fall erhalten, woraus man folgern kann, dass die Ergebnisse für Observablen endlich sein müssen [134] und divergente Ergebnisse der Spinwellentheorie somit falsch sind. Der Ansatz über das NLSM geht dagegen von einer effektiven Theorie für die antiferromagnetischen Fluktuationen bei langen Wellenlängen aus. In diesem Fall sind die Wechselwirkungsvertizes nicht divergent und machen eine störungstheoretische Behandlung mittels Vielteilchenmethoden praktikabel. Das NLSM kann die Phasen von Quantenmagneten, insbesondere kritische Phänomene, gut beschreiben, benötigt aber einen nicht-physikalischen Cutoff Parameter zur Regularisierung der entsprechenden Feldtheorie. Da der Wert dieses Parameters nicht eindeutig festliegt, können numerische Werte für Observablen mit dieser Theorie allein nicht berechnet werden.

Um die beiden eben genannten Herangehensweisen zu kombinieren, werden im Folgenden die relevanten Freiheitsgrade des Quantenantiferromagneten geeignet parametrisiert und anschließend das Magnonenspektrum untersucht. Unser Hybridansatz, der die Vorteile der Spinwellentheorie und des NLSM vereinigt, erlaubt es Korrekturen zur Spinwellengeschwindigkeit durch das angelegte Magnetfeld sowie das Quasiteilchenresiduum und die Dämpfung der Magnonen zu berechnen. Das durch Gleichung (C.4) beschriebene Modellsystem hat einen sogenannten Néel-Grundzustand, bei dem jeder zweite Spin geflippt ist. Solange das externe Magnetfeld kleiner ist als das kritische Feld $h_c = 4DJS$, sind die Spins um den Winkel ϑ_0 verkippt, siehe Abbildung C.1. Die Holstein-Primakoff Transformation erlaubt es, Quantenfluktuationen um diesen klassischen Grundzustand einzuführen. Betrachtet man diese bis zur quadratischen Ordnung in den bosnonischen Operatoren, so stellt sich heraus, dass in $D > 1$ Dimensionen zwei Spezies antiferromagnetischer Magnonen als elementare Quantenanregungen existieren. In *linearer Spinwellentheorie* können wir die Magnonen im Antiferromagneten durch den Hamilton-Operator

$$\hat{H}_2 = \sum_{\boldsymbol{k}\sigma} E_{\boldsymbol{k}\sigma} \left[\hat{\Psi}^\dagger_{\boldsymbol{k}\sigma} \hat{\Psi}_{\boldsymbol{k}\sigma} + \frac{1}{2} \right] + E^{(1)}_{0\|} \tag{C.5}$$

beschreiben, wobei $\hat{\Psi}^\dagger_{\boldsymbol{k}\sigma}$ und $\hat{\Psi}_{\boldsymbol{k}\sigma}$ die Erzeugungs- und Vernichtungsoperatoren in der sogenannten Bogoliubov Basis mit $\sigma = \pm$ sind. Die beiden Energiedispersionen haben im Zentrum der antiferromagnetischen Brillouinzone für lange Wellenlängen die folgenden Entwicklungen,

$$E_{\boldsymbol{k}+} = h + \mathcal{O}(\boldsymbol{k}^2) \,, \tag{C.6a}$$

$$E_{\boldsymbol{k}-} = c_- \, |\boldsymbol{k}| + \mathcal{O}(|\boldsymbol{k}|^3) \,. \tag{C.6b}$$

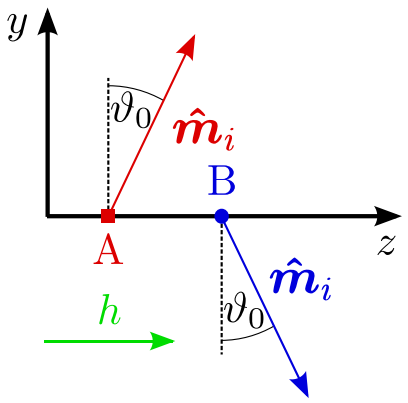

Abbildung C.1: *Spinkonfiguration $\langle \boldsymbol{S}_i \rangle = S\hat{\boldsymbol{m}}_i$ des Antiferromagneten im klassischen Grundzustand. Das hyperkubische Gitter kann so in die zwei mit A und B bezeichneten Untergitter unterteilt werden, dass jeweils benachbarte Spins zum jeweilig anderen Untergitter gehören. Durch das Magnetfeld $\boldsymbol{h} = h\boldsymbol{e}_z$ in z-Richtung ist die lokale Spinrichtung $\hat{\boldsymbol{m}}_i$ um den klassischen Kippwinkel ϑ_0 gedreht.*

Eine Mode erhält durch das Magnetfeld eine Anregungslücke der Größe $E_{0+} = h$, während die zweite Mode ein lineares Spektrum ohne Anregungslücke hat und die entsprechende Goldstone-Mode im System mit spontan gebrochener Symmetrie ist. Im Spektrum vorkommende Größen wie die Spinwellengeschwindigkeit c_- sind analytische Funktionen des Quadrates h^2 des angelegten Magnetfeldes. Wie die folgende Berechnung zeigt, wird sich das ändern, sobald man Korrekturen durch Wechselwirkungen zwischen den Spinwellen berücksichtigt. Dazu verwenden wir zunächst die eingangs erwähnte hermitesche Parametrisierung der bosonischen Freiheitsgrade,

$$\hat{\Psi}_{\boldsymbol{k}\sigma} = p_\sigma \left[\sqrt{\frac{\nu_{\boldsymbol{k}\sigma}}{2}} \hat{X}_{\boldsymbol{k}\sigma} + \frac{i}{\sqrt{2\nu_{\boldsymbol{k}\sigma}}} \hat{P}_{\boldsymbol{k}\sigma} \right] , \tag{C.7}$$

die longitudinale und transversale Anregungen des Quantenmagneten trennt und durch die Operatoren $\hat{X}_{\boldsymbol{k}\sigma}$ und $\hat{P}_{\boldsymbol{k}\sigma}$ repräsentiert. Im Zuge einer Formulierung der Theorie mittels eines Funktionalintegral-Zugangs [B23] stellen wir die Zustandssumme als

$$\mathcal{Z} = \int \mathcal{D}[P_\sigma, X_\sigma]\, e^{-S[P_\sigma, X_\sigma]} \tag{C.8}$$

dar, wobei über die im Impuls- und Frequenzraum $K = (\boldsymbol{k}, i\omega)$ definierten Felder P_σ und X_σ integriert wird und die Quantendynamik in der Euklidischen Wirkung $S[P_\sigma, X_\sigma]$ enthalten ist. Diese Wirkung $S[P_\sigma, X_\sigma]$ wird analog zum Pfadintegral-Formalismus im Phasenraum aus dem entsprechenden Hamilton-Operator hergeleitet, wobei im Spezialfall der Magnonen des QAFM insbesondere der Wechselwirkungsterm der 3-Magnonen Streuung berücksichtigt werden muss. Er ist einerseits der Wechselwirkungsterm mit niedrigster Ordnung in $1/S$ und ruft andererseits wichtige Quasiteilchenkorrekturen hervor.

Der Vorteil unserer Parametrisierung besteht nun darin, dass wir die für die Quantendynamik bei langen Wellenlängen irrelevanten Freiheitsgrade durch approximatives Lösen der Integrale über die Feldvariablen P_σ eliminieren können. Wir definieren eine *effektive Wirkung*

$$S_{\text{eff}}[X_\sigma] = S_0 + S_{\text{eff}}^{(0)}[X_\sigma] + S_{\text{eff}}^{\text{int}}[X_\sigma] \,, \tag{C.9}$$

die nur noch von den Variablen X_σ abhängt und sich über die Rechenvorschrift

$$e^{-S_{\text{eff}}[X_\sigma]} = \int \mathcal{D}[P_\sigma]\, e^{-S[P_\sigma, X_\sigma]} \tag{C.10}$$

aus der bekannten Wirkung $S[P_\sigma, X_\sigma]$ berechnen lässt. Die einzelnen Terme der rechten Seite der Gleichung (C.9) sind ein feldunabhängiger Term S_0, ein Term $S_{\text{eff}}^{(0)}[X_\sigma]$, der quadratisch in den Feldern ist sowie ein Term, $S_{\text{eff}}^{\text{int}}[X_\sigma]$, der Wechselwirkungen zwischen den durch X_σ definierten Freiheitsgraden vermittelt. Der Letztere wird im Rahmen der $1/S$-Entwicklung perturbativ berechnet und auf Gaußsche Integrale zurückgeführt. Ohne auf die explizite Form von $S_{\text{eff}}[X_\sigma]$ einzugehen, sei angemerkt, dass diese Wirkung eine analoge Form hat wie die Wirkung, die man in der Beschreibung des QAFM mittels des NLSM verwendet. Üblicherweise wird in diesem Zusammenhang das Magnetfeld dadurch eingeführt, dass die Ableitung nach der Imaginärzeit ∂_τ in der Euklidischen Wirkung durch die kovariante Ableitung mit dem Magnetfeld ersetzt wird, d.h. $\partial_\tau \to \partial_\tau - i\boldsymbol{h}\times$ [66]. Gleichzeitig geht man davon aus, dass die Parameter des NLSM nun durch effektive Parameter beschrieben werden, die den Einfluss des Magnetfeldes enthalten. Beim genaueren Vergleich mit der in dieser Arbeit berechneten Wirkung $S_{\text{eff}}[X_\sigma]$, fällt jedoch auf, dass das theoretische Modell nicht mehr durch den Parameter einer Spinwellengeschwindigkeit charakterisiert wird, sondern stattdessen zwei verschiedene Spinwellengeschwindigkeiten c_- und c_+ der beiden Moden zu berücksichtigen sind.

Ausgehend von der effektiven Wirkung in Gleichung (C.9) berechnen wir nun die Korrekturen zum Anregungsspektrum der antiferromagnetischen Mode X_-, die als Goldstone-Mode des Systems die Eigenschaften des Quantenmagneten bei tiefen Temperaturen maßgeblich bestimmt. Dazu werden die Korrelationsfunktionen bzw. Propagatoren in Gaußscher Näherung (lineare Spinwellentheorie) definiert,

$$G_{0,\sigma}(K) = \frac{\Delta_{\boldsymbol{k}\sigma}}{E_{\boldsymbol{k}\sigma}^2 + \omega^2} \,. \tag{C.11}$$

Die Korrekturen ergeben sich nun durch eine Resummation der Wechselwirkung mittels der Dyson-Gleichung

$$G_\sigma^{-1}(K) = G_{0,\sigma}^{-1}(K) + \Sigma_\sigma(K) \,, \tag{C.12}$$

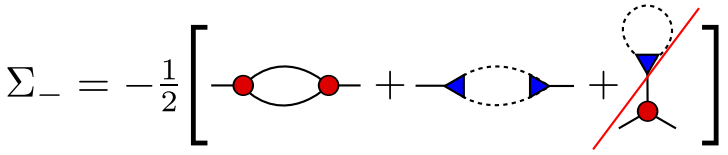

Abbildung C.2: *Darstellung der Selbstenergiekorrektur in 2. Ordnung der 3-Magnon Vertizes des Goldstone-Magnons $\Sigma_{\boldsymbol{k}-}$ durch Feynman-Diagramme. Das durchgestrichene Diagramm entspricht einem frequenzunabhängigen Term. Dieser ergibt nur Beiträge, die analytisch im Magnetfeld sind und somit nicht berücksichtigt werden.*

die den renormierten Propagator $G_\sigma(K)$ durch den freien Propagator $G_{0,\sigma}(K)$ und eine sogenannte *Selbstenergie* $\Sigma_\sigma(K)$ parametrisiert. Diese enthält Korrekturen aufgrund der Wechselwirkungen und wird im Rahmen unseres Spinwellen-Ansatzes in führender Ordnung in $1/S$ berechnet. Die bei dieser Berechnung auftretenden Terme sind in Abbildung C.2 grafisch dargestellt. Hierbei sei zu beachten, dass die roten Punkte und blauen Dreiecke die Wechselwirkungsvertizes darstellen, die bei der Herleitung von $S_{\text{eff}}[X_\sigma]$ mittels Gleichung (C.10) berechnet wurden. Das durchgestrichene Diagramm muss für die Berechnung der Spinwellengeschwindigkeit $\tilde{c}_-$, des Quasiteilchenresiduums Z_- und der Magnonendämpfung $\Gamma_{\boldsymbol{k}-}$ nicht ausgewertet werden, da es einen frequenzunabhängigen Beitrag zur Selbstenergie liefert. Die Selbstenergie wird nun analytisch im Bereich langer Wellenlängen berechnet und die Entwicklungskoeffizienten f_0 bis f_4 der Entwicklung

$$\Sigma_-(\boldsymbol{k}, i\omega) = f_0\omega^2 + f_1\omega_{\boldsymbol{k}}^2 + f_2\omega^4 + f_3\omega^2\omega_{\boldsymbol{k}}^2 + f_4\omega_{\boldsymbol{k}}^4 + O(\omega^6) \tag{C.13}$$

bestimmt. Über die Parametrisierung des Propagators

$$G_-(\boldsymbol{k}, i\omega) = \frac{Z_- h_c n^2}{\omega^2 + \tilde{c}_-^2 \boldsymbol{k}^2} \tag{C.14}$$

führen wir die *renormierte Spinwellengeschwindigkeit* $\tilde{c}_-$ und das *Quasiteilchenresiduum* Z_- ein. Nach Auswertung der auftretenden Integrale erhält man für die Spinwellengeschwindigkeit das Ergebnis

$$\frac{\tilde{c}_-^2}{c_0^2} \approx \begin{cases} 1 - \dfrac{2}{\pi S}\dfrac{|\boldsymbol{h}|}{h_c}\,, & D = 2 \\ 1 - \dfrac{6\sqrt{3}}{\pi^2 S}\dfrac{\boldsymbol{h}^2}{h_c^2}\ln\left(\dfrac{h_c}{|\boldsymbol{h}|}\right)\,, & D = 3 \end{cases} \tag{C.15}$$

und für das Quasiteilchenresiduum

$$Z_{\boldsymbol{k}-} \equiv Z_-(i\omega \to \tilde{c}_-|\boldsymbol{k}|) = 1 - \frac{1}{S}\left(\frac{2\sqrt{D}h}{h_c}\right)^{D-1}\left[\tilde{\alpha}_D - \tilde{\beta}_D \boldsymbol{k}^2 \frac{a^2}{4D}\left(\frac{h_c}{h}\right)^2\right]\,, \tag{C.16}$$

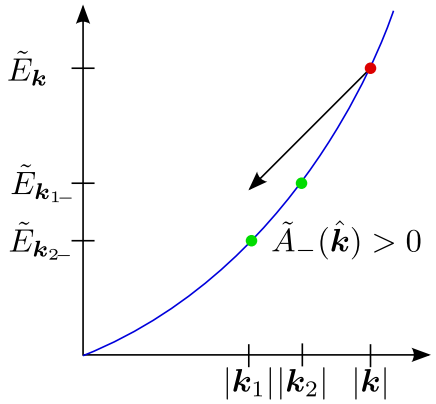

Abbildung C.3: *Aufgrund Energie-Impulserhaltung kann ein Magnon der Energie $E_{\boldsymbol{k}}$ (roter Punkt) durch die 3-Magnon-Wechselwirkung nur in zwei Magnonen (grüne Punkte) zerfallen, wenn der Koeffizient $A_-(\hat{\boldsymbol{k}})$ der Entwicklung (C.17) positiv ist.*

wobei das Magnetfeld mit dem kritischen Feld h_c in Relation gesetzt wird, a die Gitterkonstante ist, und $\tilde{\alpha}_D$ sowie $\tilde{\beta}_D$ numerische Konstanten sind. Man beachte, dass beide Größen die führenden Korrekturterme in der $1/S$-Entwicklung enthalten und sowohl in zwei Dimensionen ($D = 2$) als auch in drei Dimensionen ($D = 3$) nicht-analytische Funktionen des Magnetfeldes sind. Wie schon vorher erwähnt, sind diese Größen in linearer Spinwellentheorie wie auch die Wechselwirkungsvertizes analytische Funktionen von h^2, so dass die Gleichungen (C.15) und (C.16) nichttriviale Ergebnisse darstellen. Das Auftreten der nicht-analytischen Korrekturen steht in engem Zusammenhang mit den Eigenschaften des wechselwirkenden Bose Gases in der kondensierten Phase. Insbesondere ist $D = 3$ in beiden Fällen eine kritische Dimension, für die gerade noch logarithmische Korrekturen auftreten. Im Falle des Magnonengases lassen sich die Auswirkungen der Nichtanalytizitäten in Observablen wie der Spinwellengeschwindigkeit nachweisen.

Abschließend wird die *Spinwellendämpfung* $\gamma_{\boldsymbol{k}-}$ betrachtet. Wie aus geometrischen Überlegungen zur Streuoberfläche ersichtlich wird, kann der dominierende Zerfallsprozess eines Magnons in zwei Magnonen nur stattfinden, wenn der Koeffizient $A_-(\hat{\boldsymbol{k}})$ in der Entwicklung,

$$E_{\boldsymbol{k}-}^2 = c_-^2 \boldsymbol{k}^2 \left[1 + A_-(\hat{\boldsymbol{k}})\boldsymbol{k}^2 + O(\boldsymbol{k}^4)\right], \tag{C.17}$$

der Dispersion des Goldstone-Magnons positiv ist, vergleiche Abbildung C.3. Die Zerfallsrate lässt sich aus der Selbstenergie wie folgt berechnen,

$$\gamma_{\boldsymbol{k}-} = -\frac{\Delta_{\boldsymbol{k}-}}{2E_{\boldsymbol{k}-}} \mathrm{Im}\Sigma_-(\boldsymbol{k}, \tilde{E}_{\boldsymbol{k}-} + i0^+) \,, \tag{C.18}$$

und liefert das Ergebnis

$$\frac{\gamma_{\boldsymbol{k}-}}{E_{\boldsymbol{k}-}} = \frac{\gamma_D}{S}\left(\frac{h}{h_c}\right)^2 \left(\sqrt{3\bar{A}_-}\right)^{D-3} a^{D+1}|\boldsymbol{k}|^{2D-2} \,. \tag{C.19}$$

Hierbei ist γ_D eine numerische Konstante und der Einfachheit halber wurde ein Mittelwert $\bar{A}_-$ des Koeffizienten $A_-(\hat{\boldsymbol{k}})$ eingeführt. Das Ergebnis spiegelt das Verhalten der Dämpfung als Funktion des Impulses wieder, wie es auch für die Dämpfung des wechselwirkenden Bose Gases gefunden wurde [185]. Bemerkenswert ist weiterhin, dass der Koeffizient $\bar{A}_-$ zwar nicht-analytische Korrekturen enthält, die Beiträge aus der linearen Spinwellentheorie jedoch dominieren. Somit tritt der Magnonenzerfall oberhalb des kritischen Magnetfeldes $h_* = 2h_c/\sqrt{7}$ ein.

Zusammenfassend lässt sich festhalten, dass die führenden Korrekturen der Selbstenergie im QAFM mit externem Magnetfeld $\boldsymbol{h}$ nicht-analytisch in h^2 sind. Explizit wurden diese Korrekturen anhand der Berechnung von Observablen des Magnonenspektrums der Goldstone-Mode demonstriert. Dazu wurde der Spinwellenformalismus mit dem Formalismus des NLSM kombiniert, um Vorteile beider Methoden auszunutzen.

C.2 Mikroskopische Spinwellentheorie für dünne Filme von Yttrium-Eisengranat

Um Dünnschicht-Ferromagnete mittels eines mikroskopischen Modells einigermaßen realistisch zu beschreiben, ist es notwendig das Heisenberg-Modell um den Energiebeitrag der Dipol-Dipol Wechselwirkungen zu ergänzen. Der Hamilton-Operator im externen Magnetfeld $\boldsymbol{H}_e$ lautet dann[1]

$$\begin{aligned}\hat{H} = &-\frac{1}{2}\sum_{ij} J_{ij}\boldsymbol{S}_i\cdot\boldsymbol{S}_j - \mu\boldsymbol{H}_e\cdot\sum_i \boldsymbol{S}_i \\ &-\frac{1}{2}\sum_{ij,i\neq j}\frac{\mu^2}{|\boldsymbol{R}_{ij}|^3}\left[3(\boldsymbol{S}_i\cdot\hat{\boldsymbol{R}}_{ij})(\boldsymbol{S}_j\cdot\hat{\boldsymbol{R}}_{ij}) - \boldsymbol{S}_i\cdot\boldsymbol{S}_j\right] \,.\end{aligned} \tag{C.20}$$

Hierbei sind die ferromagnetischen Kopplungen $J_{ij} > 0$ auf die nächste Nachbarn des kubischen Gitters mit der Gitterkonstante a beschränkt und die Stärke der Dipol-Dipol Wechselwirkung wird durch μ festgelegt. $\boldsymbol{R}_{ij}$ sind die Verbindungsvektoren zwischen den bei $\boldsymbol{R}_i$ und $\boldsymbol{R}_j$ lokalisierten Spins, sowie $\hat{\boldsymbol{R}}_{ij} = \boldsymbol{R}_{ij}/|\boldsymbol{R}_{ij}|$.

Die theoretische Untersuchung des Hamilton-Operator von Gleichung (C.20) ist sowohl theoretisch als auch experimentell motiviert: Durch die

[1] Üblicherweise werden die Austauschkopplungen J_{ij} positiv definiert, sodass für ferromagnetische Modelle ein zusätzliches Minuszeichen im Hamiltonian auftritt.

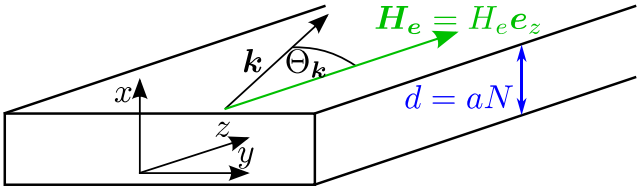

Abbildung C.4: *Wahl des Koordinatensystems für den Dünnschicht-Ferromagneten der Dicke d. Für die Berechnungen wird angenommen, dass das Magnetfeld* $\boldsymbol{H}_e = H_e \boldsymbol{e}_z$ *parallel zur z-Achse ist und mit dem Wellenvektor* $\boldsymbol{k}$ *den Winkel* $\Theta_{\boldsymbol{k}}$ *einschließt.*

Berücksichtigung des letzten Terms, der Dipol-Dipol Wechselwirkung, ergeben sich neue Eigenschaften des Spinwellenspektrums in Heisenberg-Ferromagneten bei langen Wellenlängen. Üblicherweise wird davon ausgegangen, dass dieser Term klein ist und damit vernachlässigt werden kann; die Energiebeiträge fallen ja ohnehin mit der dritten Potenz des Abstandes der Spins ab. Effekte wie starke Renormierung der Magnonen, induzierte Dämpfung durch die anisotrope Dipol-Dipol Wechselwirkungen sowie das Fehlen einer Goldstone-Mode ohne Anregungslücke können mit dem reinen Heisenberg-Modell nicht erklärt werden [194]. An dieser Stelle sollen jedoch die eben genannten Konsequenzen der Dipol-Dipol Wechselwirkung nicht im Vordergrund stehen, sondern die realistische Berechnung des Spinwellenspektrums für das Material Yttrium-Eisengranat (YIG). Hintergrund ist der experimentelle Nachweis von Kondensationsphänomenen in dünnen Filmen dieses ferromagnetischen Werkstoffs. Mittels Mikrowellentechnik lassen sich in speziell hergestellten epitaxischen Filmen von YIG verschiedene Moden der Spinwellen anregen. Aufgrund der Reinheit der Proben zeigen diese Magnonen eine geringe Dämpfung und werden in Pump-Probe Experimenten untersucht. Die Brillouin-Lichtstreuung erlaubt es zum Beispiel, das Spinwellenspektrum energie- und wellenvektoraufgelöst zu bestimmen und so die Verteilungsfunktion $\langle n_{\boldsymbol{k}}(t) \rangle$ unter Bedingungen des stationären oder nicht-stationären Nichtgleichgewichts zu messen [P6]. Es zeigt sich, dass das Spinwellenspektrum ein Minimum bei endlichem Wellenvektor aufweist und somit Magnonen-Kondensate bei endlichem Impuls realisiert werden können [48]. Auf dem Weg zur Beschreibung der Experimente an gepumpten Magnonensystemen im Nicht-Gleichgewicht braucht man für eine mikroskopische Herangehensweise zunächst eine fundierte Theorie über das Anregungsspektrum und die Wechselwirkungen. Die Spinwellentheorie liefert diese bei Berücksichtigung der Austauschwechselwirkung, der Dipol-Dipol Wechselwirkung sowie der endlichen Dicke der betrachteten Filme.

Im Zuge der Spinwellentheorie starten wir von der in Abbildung C.4 gezeigten Geometrie eines dünnen Films, der in zwei Raumrichtungen praktisch als unendlich ausgedehnt angesehen werden kann und die Dicke $d = Na$ hat. Betrachtet man die Materialparameter von YIG für unser mikroskopisches

Modell, so stellt sich heraus, dass der effektive Spin S als Quotient der Sättigungsmagnetisierung M_S, der Gitterkonstanten a sowie dem magnetischen Moment μ geschrieben werden kann,

$$S = \frac{M_S a^3}{\mu} \approx 14.2 \; . \tag{C.21}$$

Wegen des großen effektiven Spins S kann die Spinwellenentwicklung um den klassischen Grundzustand, einem saturierten Ferromagneten mit externem Feld in der Ebene, schon nach dem quadratischen Quantenfluktuationen abgebrochen werden. Nach einer partiellen Fouriertransformation werden die Freiheitsgrade durch die bosonischen Operatoren $b^\dagger_{\boldsymbol{k}}$ und $b_{\boldsymbol{k}}$ ausgedrückt, die neben dem zweidimensionalen Impuls $\boldsymbol{k}$ noch einen Index x_i im Ortsraum tragen. Der Hamilton-Operator in *linearer Spinwellentheorie* lautet nun

$$\begin{aligned}\hat{H}_2 = \sum_{\boldsymbol{k}} \sum_{x_i, x_j} \Big[& A_{\boldsymbol{k}}(x_{ij}) b^\dagger_{\boldsymbol{k}}(x_i) b_{\boldsymbol{k}}(x_j) + \frac{B_{\boldsymbol{k}}(x_{ij})}{2} b_{\boldsymbol{k}}(x_i) b_{-\boldsymbol{k}}(x_j) \\ & + \frac{B^*_{\boldsymbol{k}}(x_{ij})}{2} b^\dagger_{\boldsymbol{k}}(x_i) b^\dagger_{-\boldsymbol{k}}(x_j) \Big] \; ,\end{aligned} \tag{C.22}$$

wobei $A_{\boldsymbol{k}}(x_{ij})$ und $B_{\boldsymbol{k}}(x_{ij})$ die Einträge von $N \times N$ Matrizen sind. Die Aufgabe zur Bestimmung des Magnonenspektrums besteht nun darin die Matrizen $\mathbf{A}_{\boldsymbol{k}}$ und $\mathbf{B}_{\boldsymbol{k}}$ zu bestimmen, da sie die partiellen Fouriertransformierten der Dipol-Dipol Wechselwirkungen enthalten und anschließend den Hamilton-Operator von Gleichung (C.22) zu diagonalisieren.

In einem *numerischen Ansatz* werden die Einträge der Matrizen mit der Ewald-Summationstechnik berechnet und die Diagonalisierung auf die Bestimmung der Eigenwerte der $2N \times 2N$-Matrix

$$\mathbf{F}_{\boldsymbol{k}} = \begin{pmatrix} \mathbf{A}_{\boldsymbol{k}} & \mathbf{B}_{\boldsymbol{k}} \\ \mathbf{B}^*_{-\boldsymbol{k}} & -\mathbf{A}^T_{-\boldsymbol{k}} \end{pmatrix} \tag{C.23}$$

für festen externen Impuls $\boldsymbol{k}$ zurückgeführt [168]. Die Eigenwerte der Matrix $\mathbf{F}_{\boldsymbol{k}}$ sind dann die positiven und negativen Energieeigenwerte der insgesamt N Magnonenmoden des Dünnschicht-Ferromagneten. Wird der Impuls der Magnonen über $\boldsymbol{k} = |\boldsymbol{k}| \, (\cos\Theta_{\boldsymbol{k}} \, \boldsymbol{e}_z + \sin\Theta_{\boldsymbol{k}} \, \boldsymbol{e}_y)$ parametrisiert, so ergeben sich die zwei prinzipiell zu unterscheidenden Szenarien, die in Abbildung C.5 dargestellt sind: Für parallel zum Magnetfeld propagierende Spinwellen, $\Theta_{\boldsymbol{k}} = 0°$, hat insbesondere die niedrigste Mode ein ausgeprägtes Minimum bei endlichem Wellenvektor. Dagegen haben die Spinwellen, für die $\boldsymbol{k} \perp \boldsymbol{H}_e$, d.h. $\Theta_{\boldsymbol{k}} = 90°$ gilt, eine positive Gruppengeschwindigkeit und somit eine mit dem Impuls ansteigende Dispersion und zeigen Hybridisierung mit den höheren Moden. Für beide Fälle stellt sich bei der niedrigsten Mode für $|\boldsymbol{k}| \to 0$ die ferromagnetische Resonanzenergie $E = \mu[H_e(H_e + 4\pi M_S)]^{1/2}$ ein.

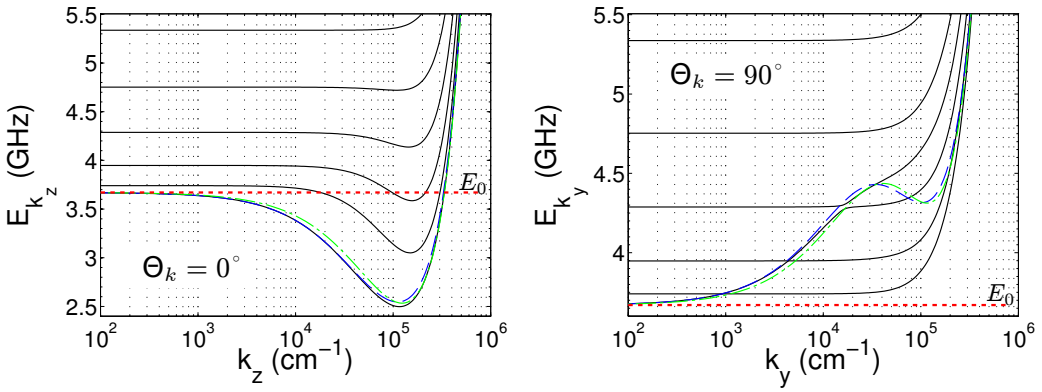

Abbildung C.5: *Spinwellendispersion eines YIG Films der Dicke* $d = 400a \approx 0.495\,\mu m$ *in einem externen Magnetfeld der Stärke* 700 Oe. *Während die Dispersion der niedrigsten Magnonenmode für Wellenvektoren parallel zum externen Feld ein Minimum aufweist (links), haben senkrecht zum Feld propagierende Moden eine positive Gruppengeschwindigkeit und die niedrigen Moden hybridisieren (rechts). In beiden Graphen sind die schwarzen Kurven die Resultate aus dem numerischen Ansatz, während die gestrichelten Kurven die Ergebnisse gemäß Gleichung (C.25) mit den Strukturfaktoren (C.26) (blau) und (C.28) (grün) darstellen. Die Energie der ferromagnetischen Resonanz* E_0 *ist mit einer roten gestrichelten Linie gekennzeichnet.*

Der volle numerische Ansatz ist für Modellrechnungen unter Berücksichtigung von Wechselwirkungen oder für Betrachtungen der Magnonendynamik im Nicht-Gleichgewicht jedoch nicht praktikabel. Daher führen wir noch zwei verschiedene analytische Näherungen für die experimentell relevante niedrigste Mode durch: In der *Uniform-Mode-Näherung* approximieren wir den bosonischen Operator durch seinen konstanten Mittelwert über alle Schichten,

$$b_{\boldsymbol{k}}(x_i) \approx \frac{1}{N}\sum_j b_{\boldsymbol{k}}(x_j) \equiv \frac{1}{\sqrt{N}} b_{\boldsymbol{k}} \,. \tag{C.24}$$

Der Hamilton-Operator enthält dann nur noch eine Mode und kann mittels Bogoliubov-Transformation diagonalisiert werden. Die Dispersion ist in diesem Fall gegeben durch

$$E_{\boldsymbol{k}} = \sqrt{[h + \rho_{\mathrm{ex}}\boldsymbol{k}^2 + 4\pi\mu M_S(1 - f_{\boldsymbol{k}})\sin^2\Theta_{\boldsymbol{k}}][h + \rho_{\mathrm{ex}}\boldsymbol{k}^2 + 4\pi\mu M_S f_{\boldsymbol{k}}]}\,, \tag{C.25}$$

wobei $\rho_{\mathrm{ex}} = JSa^2/\mu$ die Austauschsteifigkeit ist. Der Strukturfaktor

$$f_{\boldsymbol{k}} = \frac{1 - e^{-|\boldsymbol{k}|d}}{|\boldsymbol{k}|d} \tag{C.26}$$

bestimmt entscheidend die Form der Dispersion, die im Falle $\Theta_{\boldsymbol{k}} = 0°$ die Dispersion der niedrigsten Mode bis auf kleine Abweichungen in der Nähe des Minimums sehr gut beschreibt, vergleiche Abbildung C.5. Um der Anwesenheit

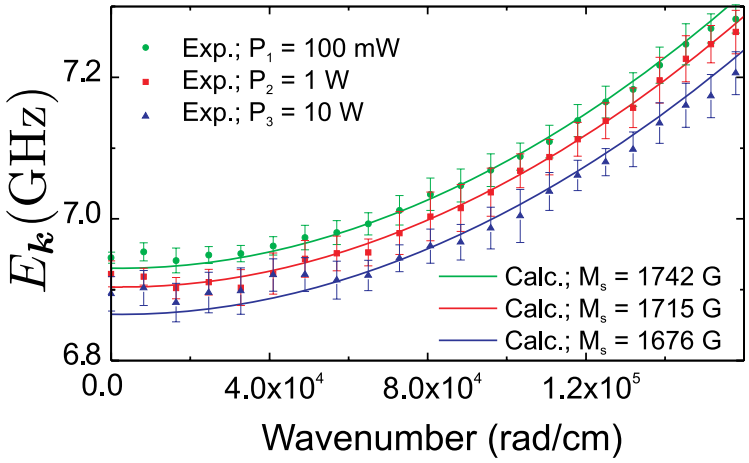

Abbildung C.6: *Vergleich des gemessenen Magnonenspektrums (Punkte) für Magnonen mit Wellenvektor senkrecht zum Magnetfeld ($\Theta_{\boldsymbol{k}} = 90°$) mit dem im numerischen Ansatz berechneten Spektrum (durchgezogene Linie) für die Pumpraten $P_1 = 0.1$W (grüne Kreise), $P_2 = 1$W (rote Quadrate) und $P_3 = 10$W (blaue Punkte).*

der Austausch-Wechselwirkung Rechnung zu tragen, haben wir die Operatoren in der *Eigenmoden-Näherung* nach den Eigenfunktionen der Austausch-Matrix entwickelt. Betrachtet man nur den führenden Term,

$$b_{\boldsymbol{k}}(x_i) \approx \sqrt{\frac{2}{N}} \cos(k_0 x_i) b_{\boldsymbol{k}} \,, \tag{C.27}$$

so ist die Dispersion der niedrigsten Mode wieder durch die Gleichung (C.25) beschrieben. Der Strukturfaktor

$$f_{\boldsymbol{k}} = 1 - |\boldsymbol{k}d| \frac{|\boldsymbol{k}d|^3 + |\boldsymbol{k}d|\pi^2 + 2\pi^2(1 + e^{-|\boldsymbol{k}d|})}{(\boldsymbol{k}^2 d^2 + \pi^2)^2} \tag{C.28}$$

weicht leicht ab, so dass mit diesem Strukturfaktor die numerischen Ergebnisse insbesondere in der Nähe des Minimums der Dispersion für experimentell relevante Filmdicken $d \approx 5$ μm besser beschrieben werden. Für Wellenvektoren in der Nähe von $\boldsymbol{k} = 0$, sollte man jedoch das Ergebnis (C.26) der Uniform-Mode-Näherung bevorzugen.

Ein *Vergleich der Ergebnisse* der numerischen Methode mit Messungen an YIG-Filmen mittels Brillouin-Lichtstreuung zeigt im Rahmen der Messungenauigkeit perfekte Übereinstimmung. Gleichzeitig lassen sich Effekte wie das Verschieben und Erweichen der Dispersion mit zunehmender Magnonendichte erklären, siehe Abbildung C.6.

Mittels der mikroskopischen Spinwellentheorie ist das Anregungsspektrum in YIG-Filmen gut beschreibbar. Sie bietet nun den Startpunkt für theoretische

Untersuchungen an gepumpten Bose-Kondensaten bei endlichen Wellenvektoren [P7], der Berechnung der Magnonendämpfung durch Magnon-Magnon Wechselwirkungen oder Berechnungen zur Nicht-Gleichgewichtsdynamik gepumpter Magnonengase [111]. Startpunkt ist hierbei die in der vorliegenden Arbeit eingeführte Spinwellenentwicklung.

C.3 Elastische Konstanten und Ultraschalldämpfung in frustrierten Antiferromagneten

Im letzten Kapitel dieser Arbeit betrachten wir ein Modellsystem, an dem in den letzten Jahren intensiv geforscht wurde: niedrigdimensionale Quantenmagnete auf frustrierten Gittern. Eine große Anzahl theoretischer und experimenteller Arbeiten hat mögliche Phasen sowie deren Phasenübergänge als Funktion externer nicht-thermischer Parameter untersucht [B16]. Neben geordneten magnetischen Phasen spielen auch ungeordnete Phasen, die durch starke Quantenfluktuationen stabilisiert werden, eine große Rolle. Um die Spinwellentheorie in einem kontrollierten Ansatz anwenden zu können, beschränken wir uns auf die *geordnete magnetische Phase*, die unter bestimmten Bedingungen bei tiefen Temperaturen stabil ist [38]. Die theoretische Untersuchung zielt hier auf das Material Cs_2CuCl_4 ab, in dem es experimentelle Hinweise auf einen quantenkritischen Punkt und damit zusammenhängende Kondensationsphänomene gibt [162]. Für ein senkrecht zu den Ebenen der Schichtstruktur des Materials angelegtes Magnetfeld wurde der Quantenphasenübergang von einer geordneten antiferromagnetischen Phase im schwachen Magnetfeld (Kegel-Zustand) hin zum saturierten Ferromagneten beobachtet. Aus den Daten von Neutronenstreuexperimenten konnte ein mikroskopisches Modell inklusive Festlegung der Modellparameter aufgestellt werden [37]. Es hat sich herausgestellt, dass eine antiferromagnetische Kopplung zwischen den auf einem Dreiecksgitter lokalisierten Spins der Cu-Ionen zusammen mit einer Dzyaloshinsky-Moriya Anisotropie die magnetischen Eigenschaften des Materials sehr gut beschreibt, vgl. Abbildung C.7. Im Magnetfeld können wir daher vom Spin-Hamilton-Operator

$$\hat{H}_{\text{spin}}^{\text{pho}} = \frac{1}{2}\sum_{ij}\left[J_{ij}\boldsymbol{S}_i\cdot\boldsymbol{S}_j + \boldsymbol{D}_{ij}\cdot(\boldsymbol{S}_i\times\boldsymbol{S}_j)\right] - \sum_i \boldsymbol{h}\cdot\boldsymbol{S}_i \tag{C.29}$$

ausgehen, wobei die Spinoperatoren $\boldsymbol{S}_i$ wie gewöhnlich Spinoperatoren zum Gesamtspin S sind, die Austauschkopplungen J_{ij} gemäß dem räumlich anisotropen Modell auf dem Dreiecksgitter gegeben sind und die Vektoren $\boldsymbol{D}_{ij}$ die Kopplung der Dzyaloshinsky-Moriya Anisotropie vermitteln. Betrachtet man die experimentell ermittelten Werte der wichtigsten Kopplungskonstanten $J \approx 0.37$ meV und $J' \approx 0.13$ meV, so bieten sich zur theoretischen Untersuchung des Modellsystems zwei verschiedene Ansätze: Wegen des kleinen

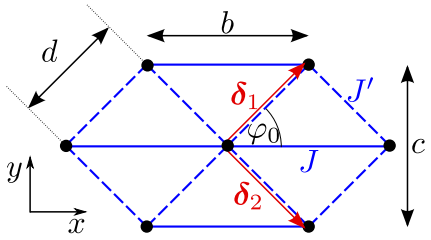

Abbildung C.7: *Modell des Antiferromagneten auf dem Dreiecksgitter mit den Gitterkonstanten b und c: Die lokalisierten Spins der Cu-Ionen befinden sich an den Ecken der Dreiecke (schwarze Punkte) und sind durch zwei verschieden starke Kopplungen J (durchgezogene Linie) und J′ (gestrichelte Linie) gekoppelt. Die Bindungslängen in der Gleichgewichtslage sind durch b und d gegeben, wobei* $\cos\varphi_0 = b/(2d)$ *und* $\sin\varphi_0 = c/(2d)$.

Verhältnisses $J'/J \approx 0.34$ lässt sich das System als schwach gekoppelte Spinketten auffassen [8]. Die Eigenschaften des antiferromagnetischen Spinsystems in einer Dimension lassen sich mit dem sogenannten Bethe-Ansatz exakt berechnen [B8], so dass Effekte aufgrund der Kopplung zwischen den einzelnen Ketten als Störung in einem Mean-Field Ansatz einfließen. Der komplementäre Ansatz der Spinwellentheorie geht von einem geordneten Zustand aus und führt Quantenfluktuationen über die Entwicklung um den klassischen Grundzustand ein [B21]. Unter der Annahme, dass der Gesamtspin S groß ist, kann man das Spinsystem auf ein System (schwach) wechselwirkender Bosonen abbilden und mit Techniken der Vielteilchentheorie lösen. Obwohl die Bedingung des großen Gesamtspins insbesondere im Falle der lokalisierten Spins mit $S = 1/2$ an den Cu-Ionen sicher nicht gut erfüllt ist, liefert die Spinwellentheorie auch im Falle frustrierter Magnete gute Ergebnisse [29]. Spinwellen-Wechselwirkungen sind im vorliegenden Modellsystem von Gleichung (C.29) sicherlich stark und wurden für den Fall ohne Magnetfeld $\boldsymbol{h} = 0$ schon eingehend untersucht [213]. An dieser Stelle sollen nicht die magnetischen Anregungen allein betrachtet werden, sondern zusammen mit der Kopplung an die Gitterschwingungen. Genau dieser Mechanismus macht es möglich, experimentell Einsichten über magnetische Eigenschaften zu gewinnen, indem mittels der sogenannten Ultraschall-Technik die Ausbreitungsgeschwindigkeit und die Dämpfung von Ultraschall gemessen wird [B15]. Zur theoretischen Beschreibung der in diesen Experimenten gemessenen Größen führen wir zunächst formal nicht-wechselwirkende *akustische Phononen* mit dem Hamilton-Operator

$$\hat{H}^{\mathrm{pho}} = \sum_{\boldsymbol{k}\lambda} \left[\frac{\hat{P}_{-\boldsymbol{k}\lambda}\hat{P}_{\boldsymbol{k}\lambda}}{2M} + \frac{M}{2}\omega_{\boldsymbol{k}\lambda}^2 \hat{X}_{-\boldsymbol{k}\lambda}\hat{X}_{\boldsymbol{k}\lambda} \right] \tag{C.30}$$

ein. Hierbei beschreibt der Operator $\hat{X}_{\boldsymbol{k}\lambda}$ die Auslenkungen der Gitterpunkte in der Mode λ im Fourier-Raum und $\hat{P}_{\boldsymbol{k}\lambda}$ ist der entsprechende kanonisch konjugierte Operator. Neben der Masse M der Elementarzelle haben wir noch die Dispersion der Phononen eingeführt, die im experimentell zugänglichen

Bereich als linear angenommen werden kann, d.h.

$$\omega_{\boldsymbol{k}\lambda} = c_\lambda(\hat{\boldsymbol{k}})|\boldsymbol{k}| \ , \tag{C.31}$$

mit der Phononengeschwindigkeit $c_\lambda(\hat{\boldsymbol{k}})$, die von der Richtung $\hat{\boldsymbol{k}} = \boldsymbol{k}/|\boldsymbol{k}|$ abhängt. Die Kopplung zu den magnetischen Freiheitsgraden wird nun über die Tatsache eingeführt, dass die magnetischen Kopplungskonstanten von der aktuellen Gitterdeformation abhängen. Über die Entwicklung

$$J_{ij} = J(\boldsymbol{R}_{ij}) + (\hat{\boldsymbol{X}}_{ij} \cdot \nabla_{\boldsymbol{r}})\ J(\boldsymbol{r})|_{\boldsymbol{r}=\boldsymbol{R}_{ij}} + \frac{1}{2}(\hat{\boldsymbol{X}}_{ij} \cdot \nabla_{\boldsymbol{r}})^2\ J(\boldsymbol{r})|_{\boldsymbol{r}=\boldsymbol{R}_{ij}} + \dots \tag{C.32}$$

der Austauschwechselwirkungen koppelt der Operator $\hat{\boldsymbol{X}}_{ij}$ als Darstellung der Operatoren $\hat{X}_{\boldsymbol{k}\lambda}$ im Ortsraum an den Spin-Hamilton-Operator, wobei die Richtung im Ortsraum durch den Polarisationsvektor $\boldsymbol{e}_{\boldsymbol{k}\lambda}$ der Normalmode bestimmt wird. Die Ortsabhängigkeit der Anisotropie sowie die Kopplung zwischen den Ebenen wird an dieser Stelle vernachlässigt. Damit hat unser Hamilton-Operator die Entwicklung

$$\hat{H}_{\text{spin}}^{\text{pho}} = \hat{H}_{\text{spin}} + \hat{H}_{\text{spin}}^{\text{1pho}} + \hat{H}_{\text{spin}}^{\text{2pho}} + \dots \ , \tag{C.33}$$

wobei der erste Term das Heisenberg-Modell ohne Gitterschwingungen darstellt und die Kopplungsterme gegeben sind durch

$$\hat{H}_{\text{spin}}^{n\text{pho}} = \frac{1}{2}\sum_{ij} U_{ij}^{(n)} \boldsymbol{S}_i \cdot \boldsymbol{S}_j \ . \tag{C.34}$$

Die Matrix $U_{ij}^{(n)}$ enthält n Potenzen der Phonon-Operatoren. Über die Spinwellenentwicklung für das reine Heisenberg-Modell mittels der Holstein-Primakoff Transformation ersetzen wir nun die Spinoperatoren durch bosonische Operatoren. Dazu wird der klassische Grundzustand bestimmt. Wir beschränken uns auf den einfachen Fall bei dem das externe Magnetfeld parallel zu den Vektoren der Dzyaloshinsky-Moriya Anisotropie angelegt ist, da das Phasendiagramm für diese Geometrie hinreichend einfach ist und das Magnonenspektrum aufgrund der spontanen Symmetriebrechung in der geordneten Phase ohne Anregungslücke bleibt (Goldstone Theorem) [77]. Der klassische Grundzustand ist dann der „Kegel-Zustand“ und durch den Öffnungswinkel ϑ und den Ordnungsvektor $\boldsymbol{Q}$ festgelegt. In *linearer Spinwellentheorie* können wir die magnetischen Anregungen in der sogenannten Bogoliubov-Basis durch den Hamilton-Operator [213]

$$\hat{H}_2 = \sum_{\boldsymbol{k}} \left[E_{\boldsymbol{k}} \beta_{\boldsymbol{k}}^\dagger \beta_{\boldsymbol{k}} + \frac{\epsilon_{\boldsymbol{k}} - A_{\boldsymbol{k}}^+}{2} \right] \tag{C.35}$$

angeben. Die Magnonen-Quasiteilchen mit der Energie-Impuls Beziehung (Dispersionsrelation)

$$E_{\boldsymbol{k}} = \sqrt{(A_{\boldsymbol{k}}^+)^2 - B_{\boldsymbol{k}}^2} + A_{\boldsymbol{k}}^- \tag{C.36}$$

werden mathematisch durch die Operatoren $\beta_{\boldsymbol{k}}^{\dagger}$ und $\beta_{\boldsymbol{k}}$ beschrieben. Die auftretenden Koeffizienten haben die Symmetrie-Eigenschaften $A_{\boldsymbol{k}}^{\pm} = \pm A_{-\boldsymbol{k}}^{\pm}$ und $B_{\boldsymbol{k}} = B_{-\boldsymbol{k}}$, so dass die Dispersion $E_{\boldsymbol{k}}$ keine einheitliche Symmetrie unter der Operation $\boldsymbol{k} \to -\boldsymbol{k}$ hat. Dies ist ein Resultat der Dzyaloshinsky-Moriya Anisotropie, die nur bei fehlender Inversionssymmetrie auftritt. Die Spinwellengeschwindigkeit $v(\hat{\boldsymbol{k}})$ als Entwicklungskoeffizient der Dispersion bei langen Wellenlängen, d.h. $E_{\boldsymbol{k}} \approx v(\hat{\boldsymbol{k}})|\boldsymbol{k}|$, hängt zwar von der Ausbreitungsrichtung ab, ist aber symmetrisch bezüglich $\hat{\boldsymbol{k}} \leftrightarrow -\hat{\boldsymbol{k}}$. Die Anwendung der Spinwellenentwicklung auf die Terme aus Gleichung (C.34) erzeugt nun eine kombinierte Entwicklung, bei der alle Terme mit n Potenzen von Phononoperatoren und m Potenzen von Magnonenoperatoren auftauchen. Der Abbruch der Entwicklung für die Magnonen erfolgt nun durch Berücksichtigung der Potenz von $1/S$, während bei den Gitterschwingungen angenommen wird, dass diese kleine Abweichungen vom Gleichgewichtszustand sind und somit Terme bis zur zweiten Ordnung in $\hat{\boldsymbol{X}}_{\boldsymbol{k}}$ berücksichtigt werden [133]. Zur Analyse der Magnon-Phonon-Wechselwirkungen machen wir die vereinfachte Annahme, dass die Austauschkopplungen nur über

$$\frac{\partial J'}{\partial x} = \cos\varphi_0 \frac{\partial J'}{\partial r} \ , \quad \frac{\partial J'}{\partial y} = \sin\varphi_0 \frac{\partial J'}{\partial r} \ , \tag{C.37}$$

von den aktuellen Bindungslängen abhängen, vergleiche Abbildung C.7. Ohne auf die technische Herleitung der gemischten Entwicklung einzugehen, die die einzelnen Terme $\hat{H}_{m\,\mathrm{mag}}^{n\,\mathrm{pho}}$ des gekoppelten Magnon-Phonon-Systems liefert, sei an dieser Stelle auf die Verschiebung durch *Magnonen-Phononen Hybridisierung* hingewiesen. Berechnet man Eigenschaften der Phononen unter Verwendung der hier vorgestellten Spinwellentheorie, so ergeben sich unphysikalische Ergebnisse, sobald die Dzyaloshinsky-Moriya Anisotropie und das Magnetfeld ungleich Null sind. Grund dafür ist die Hybridisierung zwischen Magnonen und Phononen, die indirekt berücksichtigt werden kann, indem die Magnon-Operatoren in der sogenannten Holstein-Primakoff Basis nach der Vorschrift

$$b_{\boldsymbol{k}} = \tilde{b}_{\boldsymbol{k}} + \boldsymbol{\lambda}_{\boldsymbol{k}} \cdot \hat{\boldsymbol{X}}_{\boldsymbol{k}} \tag{C.38}$$

verschoben werden. Mittels der bereits im Abschnitt C.1 verwendeten hermiteschen Parametrisierung der Magnon-Freiheitsgrade in die Operatoren $\hat{\Phi}_{\boldsymbol{k}}$ und $\hat{\Pi}_{\boldsymbol{k}}$,

$$b_{\boldsymbol{k}} = \sqrt{\frac{\Delta_{\boldsymbol{k}}}{2}}\hat{\Phi}_{\boldsymbol{k}} + \frac{i}{\sqrt{2\Delta_{\boldsymbol{k}}}}\hat{\Pi}_{\boldsymbol{k}} \ , \tag{C.39}$$

wobei $\Delta_{\boldsymbol{k}} = A_{\boldsymbol{k}}^{+} - B_{\boldsymbol{k}}$ eine Energie ist, lässt sich zeigen, dass die verschobenen Operatoren $\tilde{b}_{\boldsymbol{k}}$ zum gleichen Spektrum (C.36) führen und die Kopplung $\boldsymbol{\Gamma}_{\boldsymbol{k}}^{X\Pi}$ zwischen den Phonon-Koordinaten $\hat{\boldsymbol{X}}_{\boldsymbol{k}}$ und den Magnon-Operatoren $\hat{\Pi}_{\boldsymbol{k}}$ verschwindet, wenn man die Verschiebung als

$$\boldsymbol{\lambda}_{\boldsymbol{k}} = \frac{i}{\sqrt{2\Delta_{\boldsymbol{k}}}}\boldsymbol{\Gamma}_{\boldsymbol{k}}^{X\Pi} \tag{C.40}$$

wählt. Mathematisch führt dies zu einer Renormierung der Wechselwirkungen $\hat{H}^{n\,\mathrm{pho}}_{m-1\,\mathrm{mag}}$ zwischen Magnonen und Phononen aufgrund der reinen Spinwellen-Wechselwirkungen $\hat{H}_{m\,\mathrm{mag}}$. Ohne auf die Details einzugehen, sei angemerkt, dass diese Renormierung Singularitäten in der sich nun anschließenden Störungsrechnung beseitigt. So renormierte Größen werden im Folgenden mit einer Tilde gekennzeichnet.

Wie im Abschnitt C.1 wird nun eine *effektive Wirkung* der relevanten Freiheitsgrade hergeleitet, indem in einem Funktionalintegral-Zugang über die konjugierten Felder $\boldsymbol{P_k}$ der Phononen integriert wird, so dass die Zustandssumme durch

$$\mathcal{Z} = \int \mathcal{D}[\boldsymbol{X}, \beta, \bar{\beta},] e^{-S_2[\boldsymbol{X},\beta,\bar{\beta},]} \,, \tag{C.41}$$

geben ist. Die effektive Wirkung $S_2[\boldsymbol{X}, \beta, \bar{\beta},]$ enthält alle Terme $S^{n\,\mathrm{pho}}_{m\,\mathrm{mag}}$ der kombinierten Entwicklung, d.h.

$$\begin{aligned} S_2[\boldsymbol{X}, \bar{\beta}, \beta] = S^{2\mathrm{pho}}[\boldsymbol{X}] + S_{2\mathrm{mag}}[\bar{\beta}, \beta] + S^{1\mathrm{pho}}_{1\mathrm{mag}}[\boldsymbol{X}, \bar{\beta}, \beta] \\ + S^{1\mathrm{pho}}_{2\mathrm{mag}}[\boldsymbol{X}, \bar{\beta}, \beta] + S_{3\mathrm{mag}}[\bar{\beta}, \beta] + \dots \,. \end{aligned} \tag{C.42}$$

Die *Änderung der elastischen Konstanten* und somit die Änderung der Ultraschallgeschwindigkeit lässt sich direkt aus dem Gaußschen Propagator der Phononen ablesen, wenn man die Freiheitsgrade $\bar{\beta}$ und β in Gleichung (C.41) approximativ in Gaußscher Näherung ausintegriert. Es stellt sich heraus, dass die relative Verschiebung zwei Beiträge enthält, die formal von gleicher Ordnung in $1/S$ sind,

$$\frac{\Delta c_\lambda}{c_\lambda} = \frac{(\Delta c_\lambda)_0 + (\Delta c_\lambda)_1}{c_\lambda} \,. \tag{C.43}$$

Der erste Term hängt mit der Energieverschiebung $\Sigma^{\mathrm{pho}}_0(\boldsymbol{k}, \lambda)$ der Phononenenergie aufgrund der Bewegung unter dem Einfluss von klassischen Spins über den folgenden Grenzwert zusammen

$$\frac{(\Delta c_\lambda)_0}{c_\lambda} = \sqrt{1 - \lim_{|\boldsymbol{k}|\to 0} \frac{\Sigma^{\mathrm{pho}}_0(\boldsymbol{k}, \lambda)}{\omega^2_{\boldsymbol{k}\lambda}}} - 1 \,. \tag{C.44}$$

Der zweite Term

$$\frac{(\Delta c_\lambda)_1}{c_\lambda} = \lim_{|\boldsymbol{k}|\to 0} \frac{\left|\boldsymbol{\Gamma}^{X\beta}_{\boldsymbol{k}} \cdot \boldsymbol{e}_{\boldsymbol{k}\lambda}\right|^2}{2M\omega^3_{\boldsymbol{k}\lambda}} \tag{C.45}$$

ist von gleicher Ordnung in $1/S$ und ein Hybridisierungseffekt, der von der Ein-Magnon Ein-Phonon Wechselwirkung $\boldsymbol{\Gamma}^{X\beta}_{\boldsymbol{k}}$ in der Bogoliubov-Basis bestimmt wird. Ohne auf die explizite funktionelle Abhängigkeit einzugehen merken wir an, dass dieser Term sich in niedrigster Ordnung aus dem Koeffizient $U^{(1)}_{ij}$ in Gleichung (C.34) ergibt, wenn man alle nötigen Transformationen ausführt.

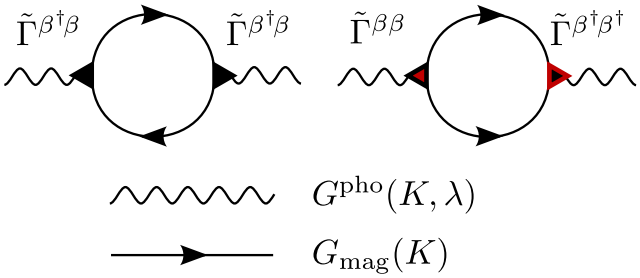

Abbildung C.8: *Feynman Diagramme für die Phononenselbstenergie, die den dominanten Beitrag zur Ultraschalldämpfung in der führenden Ordnung in* $1/S$ *ergeben: Aufgrund der weichen Magnonen mit kleiner Spinwellengeschwindigkeit* $v(\hat{\boldsymbol{k}})$ *im Vergleich zur Phononengeschwindigkeit* c_λ *dominieren die Ein-Phononen Zwei-Magnonen Prozesse (oben). Die Propagatoren* $G^{\mathrm{pho}}(i\omega, \boldsymbol{k}, \lambda)$ *der Phononen sind durch ungerichtete geschlängelte Linien dargestellt und die Magnonen Green Funktionen* $G_{\mathrm{mag}}(i\omega, \boldsymbol{k})$ *durch gerichtete Linien (unten).*

Für die Berechnung der *Phononendämpfung* müssen wir die oben beschriebene Hybridisierung berücksichtigen und starten mit der Euklidischen Wirkung

$$S_2[\boldsymbol{X}, \bar{\beta}, \beta] = S^{2\mathrm{pho}}[\boldsymbol{X}] + S_{2\mathrm{mag}}[\bar{\beta}, \beta] + \tilde{S}^{1\mathrm{pho}}_{2\mathrm{mag}}[\boldsymbol{X}, \bar{\beta}, \beta] + S^{2\mathrm{pho}}_{1\mathrm{mag}}[\boldsymbol{X}, \bar{\beta}, \beta] \ , \quad \text{(C.46)}$$

im Funktionalintegral von Gleichung (C.41). Mittels Methoden der Vielteilchentheorie lässt sich die Selbstenergie der Phononen $\Sigma_2^{\mathrm{pho}}(i\omega, \boldsymbol{k}, \lambda)$ berechnen. In führender Ordnung in $1/S$ tragen die in Abbildung C.8 gezeigten Diagramme zur Selbstenergie maßgeblich bei. Andere mögliche mikroskopische Prozesse gleicher Ordnung in $1/S$, die auch durch die Wirkung von Gleichung (C.46) beschrieben werden, können sicherlich vernachlässigt werden, da im betrachteten Material Cs_2CuCl_4 die Spinwellengeschwindigkeit $v(\hat{\boldsymbol{k}})$ viel kleiner ist als die Schallgeschwindigkeit c_λ. Die im Experiment gemessene Ultraschalldämpfung lässt sich in unserem theoretischen Ansatz aus der Selbstenergie durch die Formel

$$\gamma_{\boldsymbol{k}\lambda} = -\frac{\mathrm{Im}\Sigma_2^{\mathrm{pho}}(\omega_{\boldsymbol{k}\lambda} + i0^+, \boldsymbol{k}, \lambda)}{2\omega_{\boldsymbol{k}\lambda}} \quad \text{(C.47)}$$

berechnen. Eine Auswertung dieser Formel für $T = 0$ ergibt schließlich

$$\gamma_{\boldsymbol{k}\lambda} = \frac{\pi}{2\omega_{\boldsymbol{k}\lambda}} \frac{1}{N} \sum_{\boldsymbol{k}'} \frac{|\tilde{\boldsymbol{\Gamma}}^{\beta^\dagger\beta^\dagger}_{\boldsymbol{k}',\boldsymbol{k}-\boldsymbol{k}'} \cdot \boldsymbol{e}_{\boldsymbol{k}\lambda}|^2}{2M} \delta(\omega_{\boldsymbol{k}\lambda} - E_{\boldsymbol{k}'} - E_{\boldsymbol{k}-\boldsymbol{k}'}) \ . \quad \text{(C.48)}$$

Hierbei ist $\tilde{\boldsymbol{\Gamma}}^{\beta^\dagger\beta^\dagger}_{\boldsymbol{k}',\boldsymbol{k}-\boldsymbol{k}'}$ die in Abbildung C.8 durch Dreiecke symbolisierte Wechselwirkungsstärke zwischen einem Phonon und zwei Magnonen. Die Dämpfung hat im Bereich langer Wellenlängen die Impulsabhängigkeit $\gamma_{\boldsymbol{k}\lambda} \sim \boldsymbol{k}^4$, d.h. die Phononen sind auch in Anwesenheit der Magnonen noch wohldefinierte Quasiteilchen.

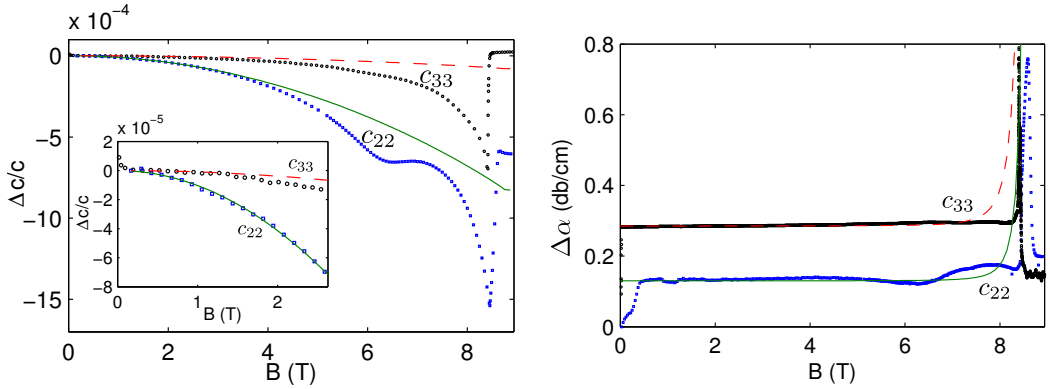

Abbildung C.9: *Vergleich der theoretischen Ergebnisse (Linien) mit experimentellen Messdaten (Punkte) für die Verschiebung der Schallgeschwindigkeit (links) und die Ultraschalldämpfung (rechts) in Cs_2CuCl_4 bei tiefen Temperaturen $T \approx 50$ mK als Funktion des externen Magnetfeldes B. Die theoretische Kurve für die longitudinale c_{22}-Mode (grün) wurde durch die Wahl der Parameter κ und κ' an die experimentellen Daten (blaue Quadrate) angepasst. Die theoretische Kurve für die c_{33}-Mode (rot gestrichelt) enthält dann keine zusätzlichen anpassbaren Parameter und gibt den Verlauf der Messwerte (schwarze Punkte) für kleine Magnetfelder $B \leq 2.5$ T recht gut wieder (kleine Grafik links). Die theoretische Vorhersage für die Änderung der Ultraschalldämpfung $\Delta\alpha$ aus Gleichung (C.48) wurde mit den ermittelten Parametern berechnet (Linien) und beschreibt das experimentell gefundene Verhalten qualitativ (rechts).*

Für einen *Vergleich unserer theoretischen Ergebnisse mit experimentellen Daten* aus einem Experiment, das von P. T. Cong durchgeführt wurde, nehmen wir folgende phänomenologische Ortsabhängigkeit der Austauschkopplungen an:

$$J(x) = J(b)e^{-\kappa(x-b)/b}\,, \tag{C.49a}$$

$$J'(r) = J'(d)e^{-\kappa'(r-d)/d}\,. \tag{C.49b}$$

Die theoretischen Kurven für die Geschwindigkeitsverschiebung der akustischen Phononenmode in x-Richtung (c_{22}-Mode) wurden durch Wahl der dimensionslosen Parameter κ und κ' an die experimentellen Daten angepasst, siehe Abbildung C.9. Mit den gleichen Werten wurde anschließend die Verschiebung der Geschwindigkeit für Phononen, die in y-Richtung propagieren (c_{33}-Mode) berechnet. Es zeigt sich, dass das Verhalten für kleine Magnetfelder korrekt wiedergegeben wird, während in der Nähe des kritischen Magnetfeldes für den Phasenübergang $B \approx 8.4$ Tesla zum saturierten Ferromagneten eine klare Abweichung zu sehen ist. Offensichtlich tragen hier Quantenfluktuationen der Magnonen höherer Ordnung oder ganz andere Arten von magnetischen Anregungen massiv bei. Mit den gewonnenen Parametern κ und κ' lässt sich auch die Dämpfung gemäß Formel (C.48) auswerten und mit experimentellen Daten vergleichen. Berücksichtigt man, dass man experimentell nur die relative

Dämpfung bestimmen kann, so geben die theoretischen Kurven ohne weitere anpassbare Parameter das Verhalten qualitativ wieder: Die Dämpfung bleibt für weite Bereiche konstant, bis sie bei steigendem Magnetfeld in der Nähe des kritischen Feldes stark zunimmt, siehe Abbildung C.9 (rechts).

Abschließend lässt sich feststellen, dass der hier verwendete Spinwellenansatz die experimentellen Ergebnisse für die Änderung der Schallgeschwindigkeit und die Dämpfung der betrachteten Phononenmoden gut beschreibt, solange man sich auf den Bereich kleiner Magnetfelder beschränkt. Mit unserem einfachen Ansatz zweier anpassbarer Parameter können essentielle Eigenschaften der Phononen berechnet werden, während die beobachteten Doppelpeakstrukturen[2] in der Nähe des kritischen Feldes nicht beschrieben werden können. Dies liegt wohl daran, dass der Spinwellenansatz in der Nähe des quantenkritischen Punktes unter starken Wechselwirkungen zwischen den Spinwellen leidet. Es ist bekannt, dass Magnonen in frustrierten Quantenantiferromagneten durch starke Fluktuationen anomale Eigenschaften wie zum Beispiel starke Dämpfung zeigen [29]. Untersuchungen des hier vorgestellten Quantenmagneten auf dem Dreiecksgitter in der ungeordneten Phase oder in der ferromagnetischen Phase im starken Magnetfeld sind interessante Fortführungen dieser Arbeit auch im Hinblick auf die vorgeschlagene Beschreibung des Quantenphasenübergangs mittels einer Bose-Einstein Kondensation von Magnonen [162].

[2] B. Wolf, private Kommunikation, [P8].

Appendix D

Bibliography

D.1 Publications

[P1] A. Kreisel, N. Hasselmann, and P. Kopietz, *Probing Anomalous Longitudinal Fluctuations of the Interacting Bose Gas via Bose-Einstein Condensation of Magnons*, Phys. Rev. Lett. **98**, 067203 (2007).

[P2] A. Kreisel, F. Sauli, N. Hasselmann, and P. Kopietz, *Quantum Heisenberg antiferromagnets in a uniform magnetic field: Nonanalytic magnetic field dependence of the magnon spectrum*, Phys. Rev. B **78**, 035127 (2008).

[P3] A. Kreisel, F. Sauli, L. Bartosch, and P. Kopietz, *Microscopic spin-wave theory for yttrium-iron garnet films*, Eur. Phys. J. B **71**, 59 (2009).

[P4] A. Kreisel, F. Sauli, L. Bartosch, and P. Kopietz, *Spin-waves in Yttrium-iron garnet*, Europhysics News **40/6**, 18 (2009).

[P5] T. Kloss, A. Kreisel, and P. Kopietz, *Parametric pumping and kinetics of magnons in dipolar ferromagnets*, Phys. Rev. B **81**, 104308 (2010).

[P6] C. W. Sandweg, M. B. Jungfleisch, V. I. Vasyuchka, A. A. Serga, P. Clausen, H. Schultheiss, B. Hillebrands, A. Kreisel, and P. Kopietz, *Wide-range wavevector selectivity of magnon gases in Brillouin light scattering spectroscopy*, Rev. Sci. Instrum. **81**, 073902 (2010).

[P7] J. Hick, F. Sauli, A. Kreisel, and P. Kopietz, *Bose-Einstein condensation at finite momentum and magnon condensation in thin film ferromagnets*, Eur. Phys. J. B **78**, 429 (2010).

[P8] A. Kreisel, P. Kopietz, P. T. Cong, B. Wolf, and M. Lang, *Elastic constants and ultrasonic attenuation in the cone state of the frustrated antiferromagnet* Cs_2CuCl_4, Phys. Rev. B **84**, 024414 (2011).

D.2 References from books

[B1] A. A. Abrikosov, L. P. Gor'kov, and I. E. Dzyaloshinsky, *Quantum field theoretical methods in statistical physics*, International series of monographs in natural philosophy; 4, Pergamon Press, London (1965).

[B2] A. I. Akhiezer, V. G. Bar'yakhtar, and S. V. Peletminskii, *Spin Waves*, North Holland, Amsterdam (1968).

[B3] A. Auerbach, *Interacting electrons and quantum magnetism*, Springer, New York (1994).

[B4] H. T. Diep, *Magnetic systems with competing interactions: frustrated spin systems*, World Scientific, Singapore (2005).

[B5] P. Fazekas, *Lecture Notes on Electron Correlation and Magnetism (Series in Modern Condensed Matter Physics)*, World Scientific, Singapore (1999).

[B6] A. L. Fetter and J. D. Walecka, *Quantum theory of many-particle systems*, McGraw-Hill, New York, NY (1971).

[B7] A. Furrer, J. Mesot, and T. Strassle, *Neutron scattering in condensed matter physics*, World Scientific, Singapore (2009).

[B8] M. Gaudin, *La Fonction d'onde de Bethe*, Masson, Paris (1983).

[B9] J. B. Goodenough, *Magnetism and the chemical bond*, Interscience Publications, New York, NY (1963).

[B10] A. G. Gurevich and G. A. Melkov, *Magnetization Oscillations and Waves*, CRC Press, Boca Raton, FL (1996).

[B11] B. Heinrich and J. A. C. Bland, *Ultrathin Magnetic Structures IV*, Springer, Berlin (2005).

[B12] J. I. Kapusta and C. Gale, *Finite temperature field theory*, Cambridge University Press, Cambridge (2006).

[B13] P. Kopietz, L. Bartosch, and F. Schütz, *Introduction to the Functional Renormalization Group*, Lecture Notes in Physics; 798, Springer, Berlin (2010).

[B14] V. S. L'vov, *Wave turbulence under parametric excitation*, Springer, Berlin (1994).

[B15] B. Lüthi, *Physical Acoustics in the Solid State*, Springer, Berlin (2005).

[B16] C. Lacroix, P. Mendels, and F. Mila, *Introduction to Frustrated Magnetism*, Springer Series in Solid-State Sciences; 164, Springer, Berlin (2011).

[B17] M. Le Bellac, *Thermal field theory*, Cambridge University Press, Cam-

bridge (2004).

[B18] E. M. Lifshitz and L. P. Pitaevskii, *Statistical Physics II*, Pergamon Press, London (1980).

[B19] G. D. Mahan, *Many particle physics*, Kluwer Academic / Plenum Press, New York, NY (2000).

[B20] N. Majlis, *The quantum theory of magnetism*, World Scientific, Singapore (2000).

[B21] D. C. Mattis, *The theory of magnetism made simple*, World Scientific, Singapore (2006).

[B22] R. D. Mattuck, *A guide to Feynman diagrams in the many-body problem*, McGraw-Hill, New York, NY (1967).

[B23] J. W. Negele and H. Orland, *Quantum many particle systems*, Frontiers in physics; 68, Addison-Wesley, Redwood City, CA (1988).

[B24] W. Nolting, *Viel-Teilchen-Theorie*, Springer-Lehrbuch, Springer, Berlin (2009).

[B25] W. Nolting, *Grunkurs Theoretische Physik: 5. Quantenmechanik 1*, Springer-Lehrbuch, Springer, Berlin (2009).

[B26] W. Nolting and A. Ramakanth, *Quantum theory of magnetism*, Springer, Berlin (2009).

[B27] A. Perelomov, *Generalized Coherent States and Their Applications*, Springer, Berlin (1986).

[B28] J. Rammer, *Quantum field theory of non-equilibrium states*, Cambridge University Press, Cambridge (2007).

[B29] R. J. Rivers, *Path integral methods in quantum field theory*, Cambridge University Press, Cambridge (1987).

[B30] D. Royer and E. Dieulesaint, *Elastic Waves in Solids I, Free and Guided Propagation*, Springer, Berlin (2000).

[B31] L. H. Ryder, *Quantum field theory*, Cambridge University Press, Cambridge (1985).

[B32] S. Sachdev, *Quantum phase transitions*, Cambridge University Press, Cambridge (2001).

[B33] U. H. Schollwöck, *Quantum magnetism*, Lecture notes in physics; 645, Springer, Berlin (2004).

[B34] L. S. Schulman, *Techniques and applications of path integration*, Wiley, New York, NY (1996).

[B35] K. P. Sinha and N. Kumar, *Interactions in magnetically ordered solids*, Oxford University Press, Oxford (1980).

[B36] G. L. Squires, *Introduction to the theory of thermal neutron scattering*, Cambridge University Press, Cambridge (1978).

[B37] G. Winkler, *Magnetic garnets*, Vieweg, Braunschweig (1981).

[B38] K. Yosida, *Theory of magnetism*, Springer series in solid state sciences; 122, Springer, Berlin (1998).

[B39] H. J. Zeiger and G. W. Pratt, *Magnetic interactions in solids*, Clarendon Press, Oxford (1973).

[B40] J. M. Ziman, *Principles of the Theory of Solids*, Cambridge University Press, Cambridge (1979).

[B41] J. Zinn-Justin, *Quantum field theory and critical phenomena*, International series of monographs on physics; 77, Clarendon Press, Oxford (1989).

[B42] C. Bland and B. Heinrich, editors, *Ultrathin Magnetic Structures*, Springer-Verlag, Berlin (1994).

[B43] K. Buschow, editor, *Handbook of magnetic materials*, volume 9, North Holland, Amsterdam (1995).

[B44] M. G. Cottam, editor, *Linear and nonlinear spin waves in magnetic films and superlattices*, World Scientific, Singapore (1994).

[B45] P. E. Wigen, editor, *Nonlinear phenomena and chaos in magnetic materials*, World Scientific, Singapore (1994).

[B46] E. Wolfarth, editor, *Ferromagnetic materials/2 (1980)*, volume 2 (1980), North Holland, Amsterdam (1980).

[B47] Y. Zhu, editor, *Modern Techniques for Characterizing Magnetic Materials*, Springer, Berlin (2005).

D.3 References from articles

[1] P. W. Anderson, *Resonating valence bonds: A new kind of insulator?*, Mater. Res. Bull. **8**, 153 (1973).

[2] P. W. Anderson, *New Approach to the Theory of Superexchange Interactions*, Phys. Rev. **115**, 2 (1959).

[3] P. W. Anderson, *An Approximate Quantum Theory of the Antiferromagnetic Ground State*, Phys. Rev. **86**, 694 (1952).

[4] M. Andres, *Korrelationen in niedrigdimensionalen Spinsystemen*, Ph.D.

thesis, Technische Universität Kaiserslautern (2008).

[5] S. Aplesnin, *Two-dimensional quantum spin liquid with S=1/2 spins interacting with acoustic phonons*, Phys. Lett. A **333**, 446 (2004).

[6] S. Bailleul, J. Hölsä, and P. Porcher, *Simulation of energy level scheme and some magnetic properties of cesium copper cloride, Cs_2CuCl_4*, Eur. J. Sol. State Inor. **31**, 431 (1994).

[7] S. Bailleul, D. Svoronos, P. Porcher, and A. Tomas, *Précisions sur la structure de Cs_2CuCl_4*, C. R. Acad. Sci. (Paris), Ser. II **313**, 1149 (1991).

[8] L. Balents, *Spin liquids in frustrated magnets*, Nature (London) **464**, 199 (2010).

[9] W. Baltensperger and J. S. Helman, *Influence of Magnetic Order in Insulators on the Optical Phonon Frequency*, Helv. Phys. Acta **41**, 668 (1968).

[10] L. Bartosch, L. Balents, and S. Sachdev, *Detecting the quantum zero-point motion of vortices in the cuprate superconductors*, Ann. Phys. (N. Y.) **321**, 1528 (2006).

[11] C. Becchi and O. Piguet, *On the renormalization of two-dimensional chiral models*, Nucl. Phys. B **315**, 153 (1989).

[12] H. Benson and D. L. Mills, *Spin Waves in Thin Films; Dipolar Effects*, Phys. Rev. **178**, 839 (1969).

[13] S. Bhattacharjee, S. Zherlitsyn, O. Chiatti, A. Sytcheva, J. Wosnitza, R. Moessner, M. E. Zhitomirsky, P. Lemmens, V. Tsurkan, and A. Loidl, *Interplay of spin and lattice degrees of freedom in the frustrated antiferromagnet $CdCr_2O_4$: High-field and temperature-induced anomalies of the elastic constants*, Phys. Rev. B **83**, 184421 (2011).

[14] U. Bhaumik and I. Bose, *Collinear Néel-type ordering in partially frustrated lattices*, Phys. Rev. B **58**, 73 (1998).

[15] D. Bitko, T. F. Rosenbaum, and G. Aeppli, *Quantum Critical Behavior for a Model Magnet*, Phys. Rev. Lett. **77**, 940 (1996).

[16] F. Bloch, *On the Magnetic Scattering of Neutrons*, Phys. Rev. **50**, 259 (1936).

[17] F. Bloch, W. W. Hansen, and M. Packard, *The Nuclear Induction Experiment*, Phys. Rev. **70**, 474 (1946).

[18] L. Bonsall and A. A. Maradudin, *Some static and dynamical properties of a two-dimensional Wigner crystal*, Phys. Rev. B **15**, 1959 (1977).

[19] E. Brézin and J. Zinn-Justin, *Renormalization of the Nonlinear σ Model in $2 + \epsilon$ Dimensions—Application to the Heisenberg Ferromagnets*, Phys.

Rev. Lett. **36**, 691 (1976).

[20] E. Brézin, J. Zinn-Justin, and J. C. Le Guillou, *Renormalization of the nonlinear σ model in $2 + \epsilon$ dimensions*, Phys. Rev. D **14**, 2615 (1976).

[21] P. Bruno, *Spin-wave theory of two-dimensional ferromagnets in the presence of dipolar interactions and magnetocrystalline anisotropy*, Phys. Rev. B **43**, 6015 (1991).

[22] E. Burzurí, F. Luis, B. Barbara, R. Ballou, E. Ressouche, O. Montero, J. Campo, and S. Maegawa, *Magnetic Dipolar Ordering and Quantum Phase Transition in an Fe_8 Molecular Magnet*, Phys. Rev. Lett. **107**, 097203 (2011).

[23] C. Castellani, C. Di Castro, F. Pistolesi, and G. C. Strinati, *Infrared Behavior of Interacting Bosons at Zero Temperature*, Phys. Rev. Lett. **78**, 1612 (1997).

[24] K. Chakraborty and J. Tucker, *Diagrammatic theory of spin excitations in an anisotropic ferromagnet with spin-phonon interactions*, Physica A **146**, 582 (1987).

[25] S. Chakravarty, B. I. Halperin, and D. R. Nelson, *Two-dimensional quantum Heisenberg antiferromagnet at low temperatures*, Phys. Rev. B **39**, 2344 (1989).

[26] V. Cherepanov, I. Kolokolov, and V. L'vov, *The Saga of YIG: Spectra, Thermodynamics, Interaction an Relaxation of Magnons in a Complex Magnet*, Phys. Reports **229**, 81 (1993).

[27] A. L. Chernyshev and M. E. Zhitomirsky, *Hydrodynamic relation in a two-dimensional Heisenberg antiferromagnet in a field*, Phys. Rev. B **79**, 174402 (2009).

[28] A. L. Chernyshev and M. E. Zhitomirsky, *Spin waves in a triangular lattice antiferromagnet: Decays, spectrum renormalization, and singularities*, Phys. Rev. B **79**, 144416 (2009).

[29] A. L. Chernyshev and M. E. Zhitomirsky, *Magnon Decay in Noncollinear Quantum Antiferromagnets*, Phys. Rev. Lett. **97**, 207202 (2006).

[30] O. Chiatti, A. Sytcheva, J. Wosnitza, S. Zherlitsyn, A. A. Zvyagin, V. S. Zapf, M. Jaime, and A. Paduan-Filho, *Character of magnetic excitations in a quasi-one-dimensional antiferromagnet near the quantum critical points: Impact on magnetoacoustic properties*, Phys. Rev. B **78**, 094406 (2008).

[31] A. V. Chumak, A. A. Serga, B. Hillebrands, G. A. Melkov, V. Tiberkevich, and A. N. Slavin, *Parametrically stimulated recovery of a microwave signal using standing spin-wave modes of a magnetic film*, Phys. Rev. B **79**,

014405 (2009).

[32] C. H. Chung, J. B. Marston, and R. H. McKenzie, *Large-N solutions of the Heisenberg and Hubbard-Heisenberg models on the anisotropic triangular lattice: application to Cs_2CuCl_4 and to the layered organic superconductors κ-(BEDT-TTF)$_2X$ (BEDT-TTF≡bis(ethylene-dithio)tetrathiafulvalene); X≡anion)*, J. Phys. C **13**, 5159 (2001).

[33] C.-H. Chung, K. Voelker, and Y. B. Kim, *Statistics of spinons in the spin-liquid phase of Cs_2CuCl_4*, Phys. Rev. B **68**, 094412 (2003).

[34] M.-C. Chung and A. B. Bhattacherjee, *Damping in 2D and 3D dilute Bose gases*, New J. Phys. **11**, 123012 (2009).

[35] R. Coldea, D. A. Tennant, R. A. Cowley, D. F. McMorrow, B. Dorner, and Z. Tylczynski, *Quasi-1D $S = 1/2$ Antiferromagnet Cs_2CuCl_4 in a Magnetic Field*, Phys. Rev. Lett. **79**, 151 (1997).

[36] R. Coldea, D. A. Tennant, R. A. Cowley, D. F. McMorrow, B. Dorner, and Z. Tylczynski, *Neutron scattering study of the magnetic structure of Cs_2CuCl_4*, J. Phys. C **8**, 7473 (1996).

[37] R. Coldea, D. A. Tennant, K. Habicht, P. Smeibidl, C. Wolters, and Z. Tylczynski, *Direct Measurement of the Spin Hamiltonian and Observation of Condensation of Magnons in the 2D Frustrated Quantum Magnet Cs_2CuCl_4*, Phys. Rev. Lett. **88**, 137203 (2002).

[38] R. Coldea, D. A. Tennant, and Z. Tylczynski, *Extended scattering continua characteristic of spin fractionalization in the two-dimensional frustrated quantum magnet Cs_2CuCl_4 observed by neutron scattering*, Phys. Rev. B **68**, 134424 (2003).

[39] J. H. P. Colpa, *Diagonalization of the quadratic boson Hamiltonian with zero modes: I. Mathematical*, Physica A **134**, 377 (1986).

[40] J. H. P. Colpa, *Diagonalization of the quadratic boson hamiltonian*, Physica A **93**, 327 (1978).

[41] P. T. Cong, B. Wolf, M. de Souza, N. Krüger, A. A. Haghighirad, S. Gottlieb-Schoenmeyer, F. Ritter, W. Assmus, I. Opahle, K. Foyevtsova, H. O. Jeschke, R. Valentí, L. Wiehl, and M. Lang, *Distinct magnetic regimes through site-selective atom substitution in the frustrated quantum antiferromagnet $Cs_2CuCl_{4-x}Br_x$*, Phys. Rev. B **83**, 064425 (2011).

[42] F. C. Coomer, V. Bondah-Jagalu, K. J. Grant, A. Harrison, G. J. McIntyre, H. M. Rønnow, R. Feyerherm, T. Wand, M. Meißner, D. Visser, and D. F. McMorrow, *Neutron diffraction studies of nuclear and magnetic structures in the $S = 1/2$ square Heisenberg antiferromagnets $(d_6 - 5CAP)_2CuX_4$ ($X = Br$ and Cl)*, Phys. Rev. B **75**, 094424 (2007).

[43] R. N. Costa Filho, M. G. Cottam, and G. A. Farias, *Microscopic theory of dipole-exchange spin waves in ferromagnetic films: Linear and nonlinear processes*, Phys. Rev. B **62**, 6545 (2000).

[44] R. N. Costa Filho, M. G. Cottam, and G. A. Farias, *Spin-wave interactions in ultrathin ferromagnetic films: The dipole-exchange regime*, Solid State Commun. **108**, 439 (1998).

[45] D. Dalidovich, R. Sknepnek, A. J. Berlinsky, J. Zhang, and C. Kallin, *Spin structure factor of the frustrated quantum magnet* Cs_2CuCl_4, Phys. Rev. B **73**, 184403 (2006).

[46] K. De'Bell, A. B. MacIsaac, and J. P. Whitehead, *Dipolar effects in magnetic thin films and quasi-two-dimensional systems*, Rev. Mod. Phys. **72**, 225 (2000).

[47] V. E. Demidov, O. Dzyapko, M. Buchmeier, T. Stockhoff, G. Schmitz, G. A. Melkov, and S. O. Demokritov, *Magnon Kinetics and Bose-Einstein Condensation Studied in Phase Space*, Phys. Rev. Lett. **101**, 257201 (2008).

[48] V. E. Demidov, O. Dzyapko, S. O. Demokritov, G. A. Melkov, and A. N. Slavin, *Observation of Spontaneous Coherence in Bose-Einstein Condensate of Magnons*, Phys. Rev. Lett. **100**, 047205 (2008).

[49] V. E. Demidov, O. Dzyapko, S. O. Demokritov, G. A. Melkov, and A. N. Slavin, *Thermalization of a Parametrically Driven Magnon Gas Leading to Bose-Einstein Condensation*, Phys. Rev. Lett. **99**, 037205 (2007).

[50] S. O. Demokritov, V. E. Demidov, O. Dzyapko, G. A. Melkov, A. A. Serga, B. Hillebrands, and A. N. Slavin, *Bose-Einstein condensation of quasi-equilibrium magnons at room temperature under pumping*, Nature (London) **443**, 430 (2006).

[51] S. O. Demokritov, V. E. Demidov, O. Dzyapko, G. A. Melkov, and A. N. Slavin, *Quantum coherence due to Bose-Einstein condensation of parametrically driven magnons*, New J. Phys. **10**, 045029 (2008).

[52] V. Druzhinin, A. Pavlovskii, G. Krinchik, O. Tasenko, M. Dolotenko, N. Kolokol'chikov, and A. Bykov, *Investigation of the phase diagram of yttrium garnets in fields of up to 10MG*, Sov. Phys. Solid State **23**, 2018 (1981).

[53] N. Dupuis, *Infrared behavior and spectral function of a Bose superfluid at zero temperature*, Phys. Rev. A **80**, 043627 (2009).

[54] F. J. Dyson, *General Theory of Spin-Wave Interactions*, Phys. Rev. **102**, 1217 (1956).

[55] F. J. Dyson, *Thermodynamic Behavior of an Ideal Ferromagnet*, Phys.

Rev. **102**, 1230 (1956).

[56] I. Dzyaloshinsky, *A thermodynamic theory of weak ferromagnetism of antiferromagnetics*, J. Phys. Chem. Solids. **4**, 241 (1958).

[57] O. Dzyapko, V. E. Demidov, S. O. Demokritov, G. A. Melkov, and A. N. Slavin, *Direct observation of Bose-Einstein condensation in a parametrically driven gas of magnons*, New J. Phys. **9**, 64 (2007).

[58] S. Eggert, O. F. Syljuåsen, F. Anfuso, and M. Andres, *Universal Alternating Order around Impurities in Antiferromagnets*, Phys. Rev. Lett. **99**, 097204 (2007).

[59] R. P. Erickson, *Long-range dipole-dipole interactions in a two-dimensional Heisenberg ferromagnet*, Phys. Rev. B **46**, 14194 (1992).

[60] R. P. Erickson and D. L. Mills, *Thermodynamics of thin ferromagnetic films in the presence of anisotropy and dipolar coupling*, Phys. Rev. B **44**, 11825 (1991).

[61] R. P. Erickson and D. L. Mills, *Microscopic theory of spin arrangements and spin waves in very thin ferromagnetic films*, Phys. Rev. B **43**, 10715 (1991).

[62] J. R. Eshbach and R. W. Damon, *Surface Magnetostatic Modes and Surface Spin Waves*, Phys. Rev. **118**, 1208 (1960).

[63] P. P. Ewald, *Die Berechnung optischer und elektrostatischer Gitterpotentiale*, Annalen der Physik **369**, 253 (1921).

[64] P. Fazekas and P. W. Anderson, *On the ground state properties of the anisotropic triangular antiferromagnet*, Philos. Mag. **30**, 423 (1974).

[65] J. D. Feldmann, G. J. Kalman, P. Hartmann, and M. Rosenberg, *Ground State of Magnetic Dipoles on a Two-Dimensional Lattice: Structural Phases in Complex Plasmas*, Phys. Rev. Lett. **100**, 085001 (2008).

[66] D. S. Fisher, *Universality, low-temperature properties, and finite-size scaling in quantum antiferromagnets*, Phys. Rev. B **39**, 11783 (1989).

[67] J. O. Fjærestad, W. Zheng, R. R. P. Singh, R. H. McKenzie, and R. Coldea, *Excitation spectra and ground state properties of the layered spin-1/2 frustrated antiferromagnets Cs_2CuCl_4 and Cs_2CuBr_4*, Phys. Rev. B **75**, 174447 (2007).

[68] K. Foyevtsova, *Investigation of microscopic behavior of Mott insulators by means of the density functional theory and many-body methods*, Ph.D. thesis, Universtität Frankfurt (in preparation).

[69] K. Foyevtsova, I. Opahle, Y.-Z. Zhang, H. O. Jeschke, and R. Valentí, *Determination of effective microscopic models for the frustrated antifer-*

romagnets Cs2CuCl4 and Cs2CuBr4 by density functional methods, Phys. Rev. B **83**, 125126 (2011).

[70] K. Foyevtsova, Y. Zhang, H. O. Jeschke, and R. Valenti, *First principles perspective on the microscopic model for Cs_2CuCl_4 and Cs_2CuBr_4*, J. Phys. Conf. Ser. **145**, 012038 (2009).

[71] D. Friedan, *Nonlinear Models in $2+\epsilon$ Dimensions*, Phys. Rev. Lett. **45**, 1057 (1980).

[72] N. M. Fujiki, K. De'Bell, and D. J. W. Geldart, *Lattice sums for dipolar systems*, Phys. Rev. B **36**, 8512 (1987).

[73] M. Gell-Mann and F. Low, *Bound States in Quantum Field Theory*, Phys. Rev. **84**, 350 (1951).

[74] S. Geller, G. P. Espinosa, and P. B. Crandall, *Thermal expansion of yttrium and gadolinium iron, gallium and aluminum garnets*, J. Appl. Crystallogr. **2**, 86 (1969).

[75] M. A. Gilleo and S. Geller, *Magnetic and Crystallographic Properties of Substituted Yttrium-Iron Garnet, $3Y_2O_3 \cdot xM_2O_3 \cdot (5-x)Fe_2O_3$*, Phys. Rev. **110**, 73 (1958).

[76] J. Goldstone, *Field theories with Superconductor solutions*, Il Nuovo Cimento **19**, 154 (1961).

[77] J. Goldstone, A. Salam, and S. Weinberg, *Broken Symmetries*, Phys. Rev. **127**, 965 (1962).

[78] T. Gollisch and C. Wetterich, *Unique Translation between Hamiltonian Operators and Functional Integrals*, Phys. Rev. Lett. **86**, 1 (2001).

[79] A. Grechnev, V. Y. Irkhin, M. I. Katsnelson, and O. Eriksson, *Thermodynamics of a two-dimensional Heisenberg ferromagnet with dipolar interaction*, Phys. Rev. B **71**, 024427 (2005).

[80] J. Griffiths, *Anomalous high-frequency resistance of ferromagnetic metals*, Nature (London) **158**, 670 (1946).

[81] S. C. Guerreiro and S. M. Rezende, *Quantum Theory of the Magnon-Phonon Interaction in a Time-Dependent Magnetic Field*, Rev. Bras. Fís. **1**, 207 (1971).

[82] F. D. M. Haldane, *Nonlinear Field Theory of Large-Spin Heisenberg Antiferromagnets: Semiclassically Quantized Solitons of the One-Dimensional Easy-Axis Néel State*, Phys. Rev. Lett. **50**, 1153 (1983).

[83] F. D. M. Haldane, *Continuum dynamics of the 1-D Heisenberg antiferromagnet: Identification with the O(3) nonlinear sigma model*, Phys. Lett. A **93**, 464 (1983).

[84] C. J. Hamer, Z. Weihong, and J. Oitmaa, *Spin-wave stiffness of the Heisenberg antiferromagnet at zero temperature*, Phys. Rev. B **50**, 6877 (1994).

[85] A. B. Harris, D. Kumar, B. I. Halperin, and P. C. Hohenberg, *Dynamics of an Antiferromagnet at Low Temperatures: Spin-Wave Damping and Hydrodynamics*, Phys. Rev. B **3**, 961 (1971).

[86] N. Hasselmann and P. Kopietz, *Spin-wave interactions in quantum antiferromagnets*, Europhys. Lett. **74**, 1067 (2006).

[87] N. Hasselmann, F. Schütz, I. Spremo, and P. Kopietz, *Effective spin-wave action for ordered Heisenberg antiferromagnets in a magnetic field*, C. R. Chim. **10**, 60 (2007).

[88] P. Hauke, T. Roscilde, V. Murg, J. I. Cirac, and R. Schmied, *Modified spin-wave theory with ordering vector optimization: spatially anisotropic triangular lattice and J 1 J 2 J 3 model with Heisenberg interactions*, New Journal of Physics **13**, 075017 (2011).

[89] P. Hauke, T. Roscilde, V. Murg, J. I. Cirac, and R. Schmied, *Modified spin-wave theory with ordering vector optimization: frustrated bosons on the spatially anisotropic triangular lattice*, New J. Phys. **12**, 053036 (2010).

[90] Y. Hayashi and M. Ogata, *Finite temperature RVB mean-field analysis of the anisotropic triangular lattice spin system*, J. Phys. Conf. Ser. **150**, 042053 (2009).

[91] D. Heidarian, S. Sorella, and F. Becca, *Spin*-1/2 *Heisenberg model on the anisotropic triangular lattice: From magnetism to a one-dimensional spin liquid*, Phys. Rev. B **80**, 012404 (2009).

[92] J. Heil, I. Kouroudis, B. Luthi, and P. Thalmeier, *Surface acoustic waves in metals*, J. Phys. C **17**, 2433 (1984).

[93] W. Heisenberg, *Zur Theorie des Ferromagnetismus*, Z. Phys. A **49**, 619 (1928).

[94] L. Helmholz and R. F. Kruh, *The Crystal Structure of Cesium Chlorocuprate, Cs_2CuCl_4, and the Spectrum of the Chlorocuprate Ion*, J. Am. Chem. Soc. **74**, 1176 (2002).

[95] P. C. Hohenberg, *Existence of Long-Range Order in One and Two Dimensions*, Phys. Rev. **158**, 383 (1967).

[96] T. Holstein and H. Primakoff, *Field Dependence of the Intrinsic Domain Magnetization of a Ferromagnet*, Phys. Rev. **58**, 1098 (1940).

[97] J. Igarashi, *1/S expansion for thermodynamic quantities in a two-dimensional Heisenberg antiferromagnet at zero temperature*, Phys. Rev.

B **46**, 10763 (1992).

[98] S. V. Isakov, T. Senthil, and Y. B. Kim, *Ordering in $Cs_2 Cu\, Cl_4$: Possibility of a proximate spin liquid*, Phys. Rev. B **72**, 174417 (2005).

[99] J. J. M. Pereira and M. G. Cottam, *Theory of dipole-exchange spin waves in ultrathin antiferromagnetic films*, J. Appl. Phys. **85**, 4949 (1999).

[100] O. Jepsen, J. Madsen, and O. K. Andersen, *Band structure of thin films by the linear augmented-plane-wave method*, Phys. Rev. B **18**, 605 (1978).

[101] M. Johnson and R. H. Silsbee, *Interfacial charge-spin coupling: Injection and detection of spin magnetization in metals*, Phys. Rev. Lett. **55**, 1790 (1985).

[102] Y. Kajiwara, K. Harii, S. Takahashi, J. Ohe, K. Uchida, M. Mizuguchi, H. Umezawa, H. Kawai, K. Ando, K. Takanashi, S. Maekawa, and E. Saitoh, *Transmission of electrical signals by spin-wave interconversion in a magnetic insulator*, Nature (London) **464**, 262 (2010).

[103] B. A. Kalinikos and A. N. Slavin, *Theory of dipole-exchange spin wave spectrum for ferromagnetic films with mixed exchange boundary conditions*, J. Phys. C. **19**, 7013 (1986).

[104] A. A. Katanin and V. Y. Irkhin, *Magnetic order and spin fluctuations in low-dimensional insulating systems*, Phys.-Usp. **50**, 613 (2007).

[105] A. Katanin and O. P. Sushkov, *Quasielastic neutron scattering from two-dimensional antiferromagnets at a finite temperature*, Phys. Rev. B **83**, 094426 (2011).

[106] H. Kawamura, *Universality of phase transitions of frustrated antiferromagnets*, J. Phys. C **10**, 4707 (1998).

[107] A. Khitun, D. E. Nikonov, M. Bao, K. Galatsis, and K. L. Wang, *Feasibility study of logic circuits with a spin wave bus*, Nanotechnology **18**, 465202 (2007).

[108] A. Khitun, R. Ostroumov, and K. L. Wang, *Spin-wave utilization in a quantum computer*, Phys. Rev. A **64**, 062304 (2001).

[109] J. H. Kim and J. H. Han, *Coupling of phonons and spin waves in a triangular antiferromagnet*, Phys. Rev. B **76**, 054431 (2007).

[110] C. Kittel, *On the Theory of Ferromagnetic Resonance Absorption*, Phys. Rev. **73**, 155 (1948).

[111] T. Kloss and P. Kopietz, *Nonequilibrium time evolution of bosons from the functional renormalization group*, Phys. Rev. B **83**, 205118 (2011).

[112] M. Kohno, *Quasiparticles of Spatially Anisotropic Triangular Antiferromagnets in a Magnetic Field*, Phys. Rev. Lett. **103**, 197203 (2009).

[113] M. Kohno, O. A. Starykh, and B. Leon, *Spinons and triplons in spatially anisotropic frustrated antiferromagnets*, Nat. Phys. **3**, 790 (2007).

[114] P. Kopietz, *Magnon damping in the two-dimensional quantum Heisenberg antiferromagnet at short wavelengths*, Phys. Rev. B **41**, 9228 (1990).

[115] P. Kopietz, P. Scharf, M. S. Skaf, and S. Chakravarty, *The Magnetic Properties of Solid ^{3}He in Two Dimensions*, Europhys. Lett. **9**, 465 (1989).

[116] D. L. Kovrizhin, V. Yushankhai, and L. Siurakshina, *Bose-Einstein condensation of magnons in Cs_2CuCl_4: A dilute gas limit near the saturation magnetic field*, Phys. Rev. B **74**, 134417 (2006).

[117] V. V. Kruglyak, S. O. Demokritov, and D. Grundler, *Magnonics*, J. Phys. D **43**, 264001 (2010).

[118] N. Krüger, S. Belz, F. Schossau, A. A. Haghighirad, P. T. Cong, B. Wolf, S. Gottlieb-Schoenmeyer, F. Ritter, and W. Assmus, *Stable Phases of the $Cs_2CuCl_{4-x}Br_x$ Mixed Systems*, Cryst. Growth. Des. **10**, 4456 (2010).

[119] R. Kubo, *The Spin-Wave Theory of Antiferromagnetics*, Phys. Rev. **87**, 568 (1952).

[120] A. Lüscher and A. M. Läuchli, *Exact diagonalization study of the antiferromagnetic spin-1/2 Heisenberg model on the square lattice in a magnetic field*, Phys. Rev. B **79**, 195102 (2009).

[121] T. D. Ladd, F. Jelezko, R. Laflamme, Y. Nakamura, C. Monroe, and J. L. O/'Brien, *Quantum computers*, Nature (London) **464**, 45 (2010).

[122] T. Lancaster, S. J. Blundell, M. L. Brooks, P. J. Baker, F. L. Pratt, J. L. Manson, M. M. Conner, F. Xiao, C. P. Landee, F. A. Chaves, S. Soriano, M. A. Novak, T. P. Papageorgiou, A. D. Bianchi, T. Herrmannsdörfer, J. Wosnitza, and J. A. Schlueter, *Magnetic order in the $S = 1/2$ two-dimensional molecular antiferromagnet copper pyrazine perchlorate $Cu(Pz)_2(ClO_4)_2$*, Phys. Rev. B **75**, 094421 (2007).

[123] M. Lang, R. Steinberg, H. J. Schmidt, and J. Michaelis, *Application for the 1. Founding Period of the Transregional Collaborative Research Centre SFB/TR 49*, (unpublished) (2007).

[124] R. Liang and F. Liu, *Measurement of thermal expansion coefficient of substrate GGG and its epitaxial layer YIG*, Powder Diffr. **14**, 2 (1999).

[125] A. R. Lim and J. K. Jung, *Phonon processes and the spin-lattice relaxation of two inequivalent Cs sites in Cs_2CuCl_4 and Cs_2CoCl_4 single crystals*, Solid State Commun. **132**, 393 (2004).

[126] A. R. P. Lima, *Hydrodynamic studies of dipolar quantum gases*, Ph.D. thesis, Freie Universität Berlin (2011).

[127] F. Luis, J. Campo, J. Gómez, G. J. McIntyre, J. Luzón, and D. Ruiz-Molina, *Long-Range Ferromagnetism of Mn_{12} Acetate Single-Molecule Magnets under a Transverse Magnetic Field*, Phys. Rev. Lett. **95**, 227202 (2005).

[128] B. Lüthi, G. Bruls, P. Thalmeier, B. Wolf, D. Finsterbusch, and I. Kouroudis, *Electron - phonon effects in heavy fermion systems*, J. Low Temp. Phys. **95**, 257 (1994).

[129] K. Majumdar, *Magnetic phase diagram of a spatially anisotropic, frustrated spin-1/2 Heisenberg antiferromagnet on a stacked square lattice*, J. Phys. C **23**, 046001 (2011).

[130] K. Majumdar, *Spin-wave energy dispersion of a frustrated spin-1/2 Heisenberg antiferromagnet on a stacked square lattice*, J. Phys. C **23**, 116004 (2011).

[131] K. Majumdar, *Second-order quantum corrections for the frustrated spatially anisotropic spin-1/2 Heisenberg antiferromagnet on a square lattice*, Phys. Rev. B **82**, 144407 (2010).

[132] M. Malard Sales, *Sistemas Antiferromagnéticos Unidimensionais de Spin-1*, Ph.D. thesis, Departamento de Física da UFMG, Belo Horizonte (2007).

[133] M. Malard and A. S. T. Pires, *Influence of magnon-phonon coupling on the phonon dynamics of one-dimensional antiferromagnets*, Phys. Rev. B **76**, 104407 (2007).

[134] S. V. Maleyev, *Spin-Wave Interaction and Renormalization of Magnetic Anisotropy in 2D Antiferromagnets*, Phys. Rev. Lett. **85**, 3281 (2000).

[135] S. V. Maleyev, *Scattering of slow neutrons in ferromagnets*, Sov. Phys. JETP **6**, 776 (1957).

[136] S. V. Maleyev, Zh. Eksp. Teor. Fiz. **33**, 1010 (1957).

[137] E. Manousakis, *The spin-$\frac{1}{2}$ Heisenberg antiferromagnet on a square lattice and its application to the cuprous oxides*, Rev. Mod. Phys. **63**, 1 (1991).

[138] T. Masuda, S. Kitaoka, S. Takamizawa, N. Metoki, K. Kaneko, K. C. Rule, K. Kiefer, H. Manaka, and H. Nojiri, *Instability of magnons in two-dimensional antiferromagnets at high magnetic fields*, Phys. Rev. B **81**, 100402 (2010).

[139] T. Matsubara, *A New Approach to Quantum-Statistical Mechanics*, Prog. Theor. Phys. **14**, 351 (1955).

[140] J. Merino, R. H. McKenzie, J. B. Marston, and C. H. Chung, *The Heisenberg antiferromagnet on an anisotropic triangular lattice: linear spin-wave theory*, J. Phys. C **11**, 2965 (1999).

[141] N. D. Mermin and H. Wagner, *Absence of Ferromagnetism or Antiferromagnetism in One- or Two-Dimensional Isotropic Heisenberg Models*, Phys. Rev. Lett. **17**, 1133 (1966).

[142] D. L. Mills, *Comment on "Bose-Einstein Condensation of Magnons in Cs_2CuCl_4"*, Phys. Rev. Lett. **98**, 039701 (2007).

[143] A. I. Milstein and O. P. Sushkov, *Effective field theories and spin-wave excitations in helical magnets*, arXiv:**1103.2422** (2011).

[144] T. Moriya, *New Mechanism of Anisotropic Superexchange Interaction*, Phys. Rev. Lett. **4**, 228 (1960).

[145] T. Moriya, *Anisotropic Superexchange Interaction and Weak Ferromagnetism*, Phys. Rev. **120**, 91 (1960).

[146] M. Mourigal, M. E. Zhitomirsky, and A. L. Chernyshev, *Field-induced decay dynamics in square-lattice antiferromagnets*, Phys. Rev. B **82**, 144402 (2010).

[147] K. Nakajima and K. Machida, *Thermal expansion of gallium garnets and Bi-substituted iron garnet epitaxial thick films*, J. Cryst. Growth **92**, 23 (1988).

[148] A. N. Nasyrov, H. Shodiev, Z. Tylczynski, A. D. Karaev, and V. S. Kim, *Elastic properties of Cs_2CuCl_4*, Ferroelectrics **158**, 93 (1994).

[149] T. Neumann, A. A. Serga, and B. Hillebrands, *Probing of a parametrically pumped magnon gas with a nonresonant packet of traveling spin waves*, Appl. Phys. Lett. **93**, 252501 (2008).

[150] T. M. Nguyen and M. G. Cottam, *Microscopic theory of dipole-exchange spin-wave excitations in ferromagnetic nanowires*, Phys. Rev. B **71**, 094406 (2005).

[151] T. Oguchi, *Theory of Spin-Wave Interactions in Ferro- and Antiferromagnetism*, Phys. Rev. **117**, 117 (1960).

[152] T. Ohyama and H. Shiba, *Spin Dynamics and Quantum Fluctuations in Quasi-One-Dimensional Triangular Antiferromagnets: Magnetic Field Effects*, J. Phys. Soc. Jpn. **63**, 3454 (1994).

[153] T. Ohyama and H. Shiba, *Nonlinear Excitations in Quasi-One-Dimensional Triangular Antiferromagnets*, J. Phys. Soc. Jpn. **62**, 3277 (1993).

[154] T. Ono, H. Tanaka, O. Kolomiyets, H. Mitamura, T. Goto, K. Nakajima, A. Oosawa, Y. Koike, K. Kakurai, J. Klenke, P. Smeibidle, and M. Meissner, *Magnetization plateaux of the S =1/2 two-dimensional frustrated antiferromagnet Cs_2CuBr_4*, J. Phys. C **16**, S773 (2004).

[155] C. E. Patton, *Magnetic excitations in solids*, Phys. Reports **103**, 251 (1984).

[156] F. Pistolesi, C. Castellani, C. Di Castro, and G. C. Strinati, *Renormalization-group approach to the infrared behavior of a zero-temperature Bose system*, Phys. Rev. B **69**, 024513 (2004).

[157] J. S. Plant, *Spinwave dispersion curves for yttrium iron garnet*, J. Phys. C **10**, 4805 (1977).

[158] K. Y. Povarov, A. I. Smirnov, O. A. Starykh, S. V. Petrov, and A. Y. Shapiro, *Modes of Magnetic Resonance in the Spin-Liquid Phase of Cs_2CuCl_4*, Phys. Rev. Lett. **107**, 037204 (2011).

[159] E. M. Purcell, H. C. Torrey, and R. V. Pound, *Resonance Absorption by Nuclear Magnetic Moments in a Solid*, Phys. Rev. **69**, 37 (1946).

[160] T. Radu, Y. Tokiwa, R. Coldea, P. Gegenwart, Z. Tylczynski, and F. Steglich, *Field induced magnetic phase transition as a magnon Bose Einstein condensation*, Sci. Technol. Adv. Mat. **8**, 406 (2007).

[161] T. Radu, H. Wilhelm, V. Yushankhai, D. Kovrizhin, R. Coldea, Z. Tylczynski, T. Lühmann, and F. Steglich, *Radu et al. Reply:*, Phys. Rev. Lett. **98**, 039702 (2007).

[162] T. Radu, H. Wilhelm, V. Yushankhai, D. Kovrizhin, R. Coldea, Z. Tylczynski, T. Lühmann, and F. Steglich, *Bose-Einstein Condensation of Magnons in Cs_2CuCl_4*, Phys. Rev. Lett. **95**, 127202 (2005).

[163] T. Radu, H. Wilhelm, V. Yushankhai, D. Kovrizhin, R. Coldea, Z. Tylczynski, T. Luhmann, and F. Steglich, *Radu et al. Reply:*, Phys. Rev. Lett. **96**, 189704 (2006).

[164] S. M. Rezende, *Theory of coherence in Bose-Einstein condensation phenomena in a microwave-driven interacting magnon gas*, Phys. Rev. B **79**, 174411 (2009).

[165] S. M. Rezende, *Theory of microwave superradiance from a Bose-Einstein condensate of magnons*, Phys. Rev. B **79**, 060410 (2009).

[166] J. Rudnick and D. Jasnow, *Renormalization-group proof of Josephson's relation and ϵ expansion for the helicity modulus (superfluid density)*, Phys. Rev. B **16**, 2032 (1977).

[167] A. Ruppel, Master's thesis, Universtität Frankfurt (in preparation).

[168] S. Sachdev, *Kagomé- and triangular-lattice Heisenberg antiferromagnets: Ordering from quantum fluctuations and quantum-disordered ground states with unconfined bosonic spinons*, Phys. Rev. B **45**, 12377 (1992).

[169] C. Sandweg, V. I. Vasyuchka, M. B. Jungfleisch, A. A. Serga, A. Kreisel,

P. Kopietz, and B. Hillebrands, in preparation.

[170] C. W. Sandweg, *Untersuchungen parametrisch gepumpter Magnonengase*, Ph.D. thesis, Technische Universität Kaiserslautern (2011).

[171] C. W. Sandweg, Y. Kajiwara, A. V. Chumak, A. A. Serga, V. I. Vasyuchka, M. B. Jungfleisch, E. Saitoh, and B. Hillebrands, *Spin Pumping by Parametrically Excited Exchange Magnons*, Phys. Rev. Lett. **106**, 216601 (2011).

[172] F. Sauli, *Spin-Wellen und magnetische Anregungen in niedrig-dimensionalen Magneten*, Ph.D. thesis, Universtität Frankfurt (in preparation).

[173] G. A. Sawatzky, W. Geertsma, and C. Haas, *Magnetic interactions and covalency effects in mainly ionic compounds*, J. Magn. Magn. Mater. **3**, 37 (1976).

[174] F. Schütz, *Aspects of strong correlations in low dimensions*, Ph.D. thesis, Universtität Frankfurt (2005).

[175] F. Schütz, M. Kollar, and P. Kopietz, *Persistent Spin Currents in Mesoscopic Heisenberg Rings*, Phys. Rev. Lett. **91**, 017205 (2003).

[176] T. Schneider, A. A. Serga, B. Leven, B. Hillebrands, R. L. Stamps, and M. P. Kostylev, *Realization of spin-wave logic gates*, Appl. Phys. Lett. **92**, 022505 (2008).

[177] S. Schäfer, A. V. Chumak, A. A. Serga, G. A. Melkov, and B. Hillebrands, *Microwave spectral analysis by means of nonresonant parametric recovery of spin-wave signals in a thin magnetic film*, Appl. Phys. Lett. **92**, 162514 (2008).

[178] S. E. Sebastian, V. S. Zapf, N. Harrison, C. D. Batista, P. A. Sharma, M. Jaime, I. R. Fisher, and A. Lacerda, *Comment on "Bose-Einstein Condensation of Magnons in Cs_2CuCl_4"*, Phys. Rev. Lett. **96**, 189703 (2006).

[179] M. Seehra and T. Castner, *The paramagnetic line width in $Cu(HCOO)_2{\cdot}4H_2O$*, Z. Phys. B **7**, 185 (1968).

[180] A. A. Serga, A. V. Chumak, A. André, G. A. Melkov, A. N. Slavin, S. O. Demokritov, and B. Hillebrands, *Parametrically Stimulated Recovery of a Microwave Signal Stored in Standing Spin-Wave Modes of a Magnetic Film*, Phys. Rev. Lett. **99**, 227202 (2007).

[181] A. A. Serga, A. V. Chumak, and B. Hillebrands, *YIG magnonics*, J. Phys. D **43**, 264002 (2010).

[182] S. Shinkevich, O. F. Syljuåsen, and S. Eggert, *Spin-wave calculation of the field-dependent magnetization pattern around an impurity in Heisenberg*

antiferromagnets, Phys. Rev. B **83**, 054423 (2011).

[183] C. G. Shull, E. O. Wollan, and W. A. Strauser, *Magnetic Structure of Magnetite and Its Use in Studying the Neutron Magnetic Interaction*, Phys. Rev. **81**, 483 (1951).

[184] A. Sinner, *Application of the functional renormalization group to Bose systems with broken symmetry*, Ph.D. thesis, Universtität Frankfurt (2009).

[185] A. Sinner, N. Hasselmann, and P. Kopietz, *Spectral Function and Quasiparticle Damping of Interacting Bosons in Two Dimensions*, Phys. Rev. Lett. **102**, 120601 (2009).

[186] A. Sinner, N. Hasselmann, and P. Kopietz, *Functional renormalization group approach to the two dimensional Bose gas*, J. Phys. Conf. Ser. **150**, 032097 (2009).

[187] A. Sinner, N. Hasselmann, and P. Kopietz, *Functional renormalization group in the broken symmetry phase: momentum dependence and two-parameter scaling of the self-energy*, J. Phys. C **20**, 075208 (2008).

[188] A. N. Slavin and B. A. Kalinikos, *Nonlinear theory of spin waves in a ferromagnetic film*, Sov. Phys. Tech. Phys. **32**, 1446 (1987).

[189] E. B. Sonin, *Spin currents and spin superfluidity*, Adv. Phys. **59**, 181 (2010).

[190] I. Spremo, *Spin-wave calculations for low-dimensional magnets*, Ph.D. thesis, Universtität Frankfurt (2006).

[191] I. Spremo, F. Schütz, P. Kopietz, V. Pashchenko, B. Wolf, M. Lang, J. W. Bats, C. Hu, and M. U. Schmidt, *Magnetic properties of a metal-organic antiferromagnet on a distorted honeycomb lattice*, Phys. Rev. B **72**, 174429 (2005).

[192] O. A. Starykh and L. Balents, *Ordering in Spatially Anisotropic Triangular Antiferromagnets*, Phys. Rev. Lett. **98**, 077205 (2007).

[193] O. A. Starykh, H. Katsura, and L. Balents, *Extreme sensitivity of a frustrated quantum magnet: Cs_2CuCl_4*, Phys. Rev. B **82**, 014421 (2010).

[194] A. V. Syromyatnikov, *Anomalously large damping of long-wavelength quasiparticles caused by long-range interaction*, Phys. Rev. B **82**, 024432 (2010).

[195] A. V. Syromyatnikov, *Spin-wave interaction in two-dimensional ferromagnets with dipolar forces*, Phys. Rev. B **77**, 144433 (2008).

[196] A. V. Syromyatnikov, *Bose-Einstein condensation of magnons in magnets with predominant ferromagnetic interactions*, Phys. Rev. B **75**, 134421

(2007).

[197] A. V. Syromyatnikov, *Renormalization of the spin-wave spectrum in three-dimensional ferromagnets with dipolar interaction*, Phys. Rev. B **74**, 014435 (2006).

[198] A. V. Syromyatnikov and S. V. Maleyev, *Spin-wave interaction in two- and three-dimensional antiferromagnets in a weak magnetic field*, Phys. Rev. B **65**, 012401 (2001).

[199] A. Sytcheva, O. Chiatti, J. Wosnitza, S. Zherlitsyn, A. A. Zvyagin, R. Coldea, and Z. Tylczynski, *Short-range correlations in quantum frustrated spin system*, Phys. Rev. B **80**, 224414 (2009).

[200] A. Sytcheva, O. Chiatti, J. Wosnitza, S. Zherlitsyn, A. Zvyagin, R. Coldea, and Z. Tylczynski, *Magnetoacoustics of the Low-Dimensional Quantum Antiferromagnet Cs_2CuCl_4 with Spin Frustration*, J. Low Temp. Phys. **159**, 109 (2009).

[201] M. Tachiki and S. Maekawa, *Effect of Magnetic Field on Sound Propagation near Magnetic Phase Transition Temperatures*, Prog. Theor. Phys. **51**, 1 (1974).

[202] M. Takahashi, *Quantum Heisenberg Ferromagnets in One and Two Dimensions at Low Temperature*, Prog. Theor. Phys. Supp. **87**, 233 (1986).

[203] B. R. Tittmann, *Possible identification of magnetostatic surface spin wave modes in ferromagnetic resonance on epitaxial yttrium-iron-garnet films*, Solid State Commun. **13**, 463 (1973).

[204] Y. Tokiwa, T. Radu, R. Coldea, H. Wilhelm, Z. Tylczynski, and F. Steglich, *Magnetic phase transitions in the two-dimensional frustrated quantum antiferromagnet Cs_2CuCl_4*, Phys. Rev. B **73**, 134414 (2006).

[205] A. E. Trumper, *Spin-wave analysis to the spatially anisotropic Heisenberg antiferromagnet on a triangular lattice*, Phys. Rev. B **60**, 2987 (1999).

[206] M. H. Tsai, *The possibility of phonon induced antiferromagnetic magnons in cuprate superconductors at low temperatures*, Physica C **191**, 108 (1992).

[207] N. Tsyrulin, T. Pardini, R. R. P. Singh, F. Xiao, P. Link, A. Schneidewind, A. Hiess, C. P. Landee, M. M. Turnbull, and M. Kenzelmann, *Quantum Effects in a Weakly Frustrated $S = 1/2$ Two-Dimensional Heisenberg Antiferromagnet in an Applied Magnetic Field*, Phys. Rev. Lett. **102**, 197201 (2009).

[208] I. S. Tupitsyn, P. C. E. Stamp, and A. L. Burin, *Stability of Bose-Einstein Condensates of Hot Magnons in Yttrium Iron Garnet Films*, Phys. Rev. Lett. **100**, 257202 (2008).

[209] Z. Tylczyński, P. Piskunowicz, A. N. Nasyrov, A. D. Karaev, K. T. Shodiev, and G. Gulamov, *Physical Properties of Cs_2CuCl_4 Crystals*, Phys. Status. Solidi A **133**, 33 (1992).

[210] H. T. Ueda and K. Totsuka, *Magnon Bose-Einstein condensation and various phases of three-dimensonal quantum helimagnets under high magnetic field*, Phys. Rev. B **80**, 014417 (2009).

[211] M. Y. Veillette and J. T. Chalker, *Commensurate and incommensurate ground states of Cs_2CuCl_4 in a magnetic field*, Phys. Rev. B **74**, 052402 (2006).

[212] M. Y. Veillette, J. T. Chalker, and R. Coldea, *Ground states of a frustrated spin-1/2 antiferromagnet: Cs_2CuCl_4 in a magnetic field*, Phys. Rev. B **71**, 214426 (2005).

[213] M. Y. Veillette, A. J. A. James, and F. H. L. Essler, *Spin dynamics of the quasi-two-dimensional spin-1/2 quantum magnet Cs_2CuCl_4*, Phys. Rev. B **72**, 134429 (2005).

[214] V. Vlaminck and M. Bailleul, *Current-Induced Spin-Wave Doppler Shift*, Science **322**, 410 (2008).

[215] O. Waldmann, *Spin dynamics of finite antiferromagnetic Heisenberg spin rings*, Phys. Rev. B **65**, 024424 (2001).

[216] L. R. Walker, *Magnetostatic Modes in Ferromagnetic Resonance*, Phys. Rev. **105**, 390 (1957).

[217] M. Q. Weng, D. N. Sheng, Z. Y. Weng, and R. J. Bursill, *Spin-liquid phase in an anisotropic triangular-lattice Heisenberg model: Exact diagonalization and density-matrix renormalization group calculations*, Phys. Rev. B **74**, 012407 (2006).

[218] C. Wetterich, *Occupation numbers from functional integral*, Nucl. Phys. B **802**, 368 (2008).

[219] M. Weyrauch and A. W. Schreiber, *Comment on "Unique Translation between Hamiltonian Operators and Functional Integrals"*, Phys. Rev. Lett. **88**, 078901 (2002).

[220] R. M. White, M. Sparks, and I. Ortenburger, *Diagonalization of the Antiferromagnetic Magnon-Phonon Interaction*, Phys. Rev. **139**, A450 (1965).

[221] S. R. White and A. L. Chernyshev, *Neél Order in Square and Triangular Lattice Heisenberg Models*, Phys. Rev. Lett. **99**, 127004 (2007).

[222] J. H. Wilson and V. Galitski, *Breakdown of the Coherent State Path Integral: Two Simple Examples*, Phys. Rev. Lett. **106**, 110401 (2011).

[223] B. Wolf, S. Zherlitsyn, S. Schmidt, and B. Lüthi, *Soundwave propagation in pulsed magnetic fields in $CsCuCl_3$*, Europhys. Lett. **48**, 182 (1999).

[224] F. M. Woodward, A. S. Albrecht, C. M. Wynn, C. P. Landee, and M. M. Turnbull, *Two-dimensional $S = 1/2$ Heisenberg antiferromagnets: Synthesis, structure, and magnetic properties*, Phys. Rev. B **65**, 144412 (2002).

[225] H. Xia, P. Kabos, H. Y. Zhang, P. A. Kolodin, and C. E. Patton, *Brillouin Light Scattering and Magnon Wave Vector Distributions for Microwave-Magnetic-Envelope Solitons in Yttrium-Iron-Garnet Thin Films*, Phys. Rev. Lett. **81**, 449 (1998).

[226] Y.-N. Xu, Z. quan Gu, and W. Y. Ching, *First-principles calculation of the electronic structure of yttrium iron garnet ($Y_3Fe_5O_{12}$)*, J. Appl. Phys. **87**, 4867 (2000).

[227] Y. Yafet, J. Kwo, and E. M. Gyorgy, *Dipole-dipole interactions and two-dimensional magnetism*, Phys. Rev. B **33**, 6519 (1986).

[228] M. Yamashita, N. Nakata, Y. Senshu, M. Nagata, H. M. Yamamoto, R. Kato, T. Shibauchi, and Y. Matsuda, *Highly Mobile Gapless Excitations in a Two-Dimensional Candidate Quantum Spin Liquid*, Science **328**, 1246 (2010).

[229] S. Yunoki and S. Sorella, *Two spin liquid phases in the spatially anisotropic triangular Heisenberg model*, Phys. Rev. B **74**, 014408 (2006).

[230] E. Zavoisky, *Relaxation of liquid solutions for perpendicular fields*, J. Phys. U.S.S.R. **9**, 211 (1945).

[231] Y.-Z. Zhang, H. O. Jeschke, and R. Valentí, *Microscopic model for transitions from Mott to spin-Peierls insulator in $TiOCl$*, Phys. Rev. B **78**, 205104 (2008).

[232] S. Zherlitsyn, S. Schmidt, B. Wolf, H. Schwenk, B. Lüthi, H. Kageyama, K. Onizuka, Y. Ueda, and K. Ueda, *Sound-wave anomalies in $SrCu_2(BO_3)_2$*, Phys. Rev. B **62**, R6097 (2000).

[233] M. E. Zhitomirsky and A. L. Chernyshev, *Instability of Antiferromagnetic Magnons in Strong Fields*, Phys. Rev. Lett. **82**, 4536 (1999).

[234] M. E. Zhitomirsky and T. Nikuni, *Magnetization curve of a square-lattice Heisenberg antiferromagnet*, Phys. Rev. B **57**, 5013 (1998).

[235] Y. Zhou and P. A. Lee, *Spinon Phonon Interaction and Ultrasonic Attenuation in Quantum Spin Liquids*, Phys. Rev. Lett. **106**, 056402 (2011).

[236] B. Zumino, *Supersymmetry and Kähler manifolds*, Phys. Lett. B **87**, 203 (1979).

Lebenslauf

Angaben zur Person

Name:	Andreas Kreisel
Geburtsdatum:	22.07.1982
Geburtsort:	Hanau
Staatsangehörigkeit:	Deutsch

Beruflicher Werdegang

07/2011	Promotion mit Auszeichnung
09/2010-10/2010	Auslandsaufenthalt (DAAD-Stipendium) Universidade Federal do Rio Grande do Norte, Natal, Brasilien
10/2009-11/2009 09/2008-10/2008	Auslandsaufenthalt (DAAD-Stipendium) Universidade de Brasília, Brasilien
10/2007-06/2011	Doktorand am Institut für Theoretische Physik an der Johann Wolfgang Goethe - Universität Frankfurt Betreuer: Prof. Dr. Peter Kopietz
10/2007	Diplom im Studiengang Physik, Note: 1.0 Diplomarbeit: Spin-Wellen-Wechselwirkungen in Quanten-Anti-Ferromagneten Betreuer: Prof. Dr. Peter Kopietz
04/2004	Vordiplom, Note: 1.0
10/2002-10/2007	Studium der Physik an der Johann Wolfgang Goethe - Universität Frankfurt
07/2001-03/2002	Wehrdienst in Bayreuth und Schöneck-Kilianstätten
06/2001	Abitur (Grimmelshausen Gymnasium Gelnhausen)

Danksagung

Am Ende möchte ich noch all denjenigen danken, die ihren Teil zum Gelingen dieser Arbeit beigetragen haben.

Meinem Betreuer Prof. Dr. Peter Kopietz möchte ich für die Ermöglichung meiner Forschung an spannenden Themen danken. Er hat mich stets bei meiner Arbeit unterstützt, mir Gelegenheit gegeben auch Wissen außerhalb der Physik anzueignen und meine Pläne zu verwirklichen. Für die Möglichkeit, einen Teil meiner Arbeit in Brasilien anzufertigen, bin ich ihm in besonderer Weise dankbar. Peter Kopietz hatte stets ein offenes Ohr für Probleme und konnte ins Stocken geratene Überlegungen und Berechnungen durch seine physikalische Intuition vorantreiben.

Prof. Dr. Sebastian Eggert danke ich für die Bereitschaft zur Übernahme des Zweitgutachtens sowie für die zahlreichen Diskussionen während der gesamten Promotionsphase. Die Zusammenarbeit im Rahmen des Graduiertenkollegs des Sonderforschungsbereichs TRR 49 war stets kollegial und eröffnete mir neue Perspektiven.

Besonders am ersten Teil meiner Arbeit war Nils Hasselmann maßgeblich beteiligt. In zahlreichen Gesprächen mit ihm kam man der Lösung von kleinen und großen Problemen durchweg einen Schritt weiter. Neben seiner fachlichen Unterstützung bin ich ihm für seine Hilfe während meiner Aufenthalte in Brasilien in besonderer Weise dankbar.

Der zweite Teil der Arbeit wurde durch eine Zusammenarbeit mit der Arbeitsgruppe Hillebrands und auch durch die finanzielle Förderung der DFG ermöglicht. Für die anregenden Diskussionen und die Erklärung experimenteller Details bin ich insbesondere Christian Sandweg, Sebastian Schäfer und Alexander Serga zu Dank verpflichtet. Einen entscheidenden Anteil an der theoretischen Arbeit wurde von Francesca Sauli erbracht. Für ihre angenehme Zusammenarbeit seit meinem Grundstudium möchte ich ihr herzlich danken. Pham Thanh Cong und Bernd Wolf danke ich für die stete Bereitschaft aktuelle Fragestellungen und experimentelle Einzelheiten zu diskutieren.

Dank gebührt auch den anderen Mitgliedern der Arbeitsgruppe Kopietz: Lorenz Bartosch war immer bereit Fragen zu beantworten, so dass ich einiges besser verstehen konnte. Die Zusammenarbeit mit Thomas Kloss, Johannes Hick und Peymann Pirooznia bei kleineren Projekten war stets erfrischend; Annika Ruppel und Casper Drukier haben mein Manuskript gewissenhaft gegengelesen und so manchen Fehler gefunden, der mir sicherlich entgangen wäre. Meinen Büropartnern Christopher Eichler und Carlo Krimphoff danke ich für die nette aufgelockerte Arbeitsatmosphäre. Aus gleichem Grund möchte

ich besonders Aldo Isidori für unsere schöne gemeinsame Zeit danken. Für die nette Arbeitsatmosphäre danke ich auch allen Mitgliedern des Instituts für Theoretische Physik sowie des SFB TRR 49.

Zuletzt möchte ich mich herzlich bei meinen Eltern und meiner Familie bedanken. Ohne die entsprechende Unterstützung wäre es mir nicht möglich gewesen, diese Arbeit anzufertigen. Vielen Dank!